Investigation of Charge-Neutral Backbone Modified Oligonucleotides for Antisense Applications

---

A Thesis submitted to the Board of Mathematical, Physical and Life Sciences Division, Department of Chemistry in partial fulfilment for the degree of

Doctor of Philosophy

Benjamin J. Lagan

New College, University of Oxford, Trinity Term 2025



Declaration

I, Benjamin Lagan, declare that the thesis titled “Investigation of Charge-Neutral Backbone Modified Oligonucleotides” and the related research presented in this thesis was performed and written by the author under the supervision of Professor Tom Brown at the University of Oxford. The research is original and has not been submitted in full or in part for any other degree at this or at any other university. The copyright of this thesis rests with the author.

ACKNOWLEDGEMENTS

The work conducted in this thesis would not have been possible without a multitude of people whose support pushed me ever onwards. The first thank you is of course to my DPhil supervisor, Professor Tom Brown. His expert guidance and endless scientific curiosity, and willingness to dedicate countless hours in support provided the framework in which this thesis was conducted. His advice on every aspect from the first experimental design to the writing of this work have had indescribable value, and so I truly say, thank you. Along these lines thanks also must go to Professor Afaf El-Sagheer. Her wisdom and support with oligonucleotide synthesis helped immensely and I cannot say thank you enough.

Next is the wonderful cast of characters I have been fortunate enough to call lab mates in the past four years. In particular I have to thank Sebastian, Brendan, Alice, Lillian, Nicolo and Chunsen. Their support came in many forms- scientific advice, fun at the pub, time on the tennis court just to name a few. All of this was necessary and without them I would not have been able to do the work I did.

I must also extend heartfelt thanks to the people in my personal life who pushed me to be where I am. Of course, I mean my lovely girlfriend Anna whose patience to listen to me when experiments did not go as planned was endless as was her encouragement at every step of the way. I also speak of my family- my parents in particular- who have nurtured my curiosity from a young age and supported my journey at every step.

I would not be where I am without any of the people mentioned above and so to all of you I say thank you, though this does not even begin to cover your invaluable support.

ABSTRACT

Antisense oligonucleotides (ASOs) are short strands of DNA or RNA that bind to complementary pre-mRNA and alter gene expression. The oligonucleotides can prevent inclusion of mutated sites and restore expression or induce mRNA degradation to silence it. Antisense oligonucleotides hold tremendous promise as therapeutic agents for genetic disorders and other diseases that are not treatable by small molecule medicines. Eleven antisense oligonucleotides have been approved by the US Food and Drug Administration but a major need still exists for the improvement of their therapeutic properties including more efficient cell uptake and targeting of specific tissues.

In this work, new chemical modifications and methods for introducing them into oligonucleotides were explored. Solid phase chemistry was used to evaluate conditions for replacing the OH group at the 5´-position of a ribose sugar with an azide. This allows the synthesis of various internucleoside triazole backbones by copper-catalysed click chemistry (CuAAC). The backbones were then tested in splice switching oligonucleotides in a HeLa cell luciferase reporter assay and compared to phosphorothioate and alkyl phosphonate backbones.

As the charge-neutral phosphonate and triazole linkages reduce the overall negative charge of the oligonucleotide, they have the potential to increase cellular uptake. In particular it was shown that a combination of a locked nucleic acid sugar and the alkyl phosphonate linkage improves the splice switching efficiency of an oligonucleotide compared to a standard 2´-O-methyl phosphorothioate control oligonucleotide. Our findings highlight the need to understand the origins of the improved activity, including the efficiency of oligonucleotide uptake into cells and intracellular trafficking and localisation.

Assay development was then started to find a method to allow for simple and effective screening of new antisense modifications. Initial results show potential pitfalls

with current techniques that employ large dye molecules attached to oligonucleotides. These molecules allow precise visualisation but were shown to influence the activity of the oligonucleotides. Method development done in this thesis gives an alternative to visualise oligonucleotides using an azide installed during solid-phase synthesis as explored in earlier sections of this thesis as handle for *in-situ* CuAAC ligation of dyes in fixed cells.

The work discussed in this thesis begins with development of modifications with potential applications in ASOs. It then tests the efficacy of these and other modifications in exon-skipping oligonucleotides, revealing patterns of use for developing more effective molecules. Finally, it advances techniques to explore the reasons behind these patterns that avoid problems associated with some current practices. These factors can help to create high performing ASO therapeutic molecules in future.

Chapter 1: Introduction 12
1.1. Nucleic Acid Structure and Synthesis 13
1.1.1 Basic Structure 13
1.1.2 Oligonucleotide Synthesis 16
1.2. Antisense Oligonucleotides 19
1.3. Chemical Modifications in Therapeutic Oligonucleotides 22
1.3.1 First Generation ASOs 23
1.3.2 Second Generation ASOs 24
1.3.3 Third Generation ASOs 24
1.3.3.1 Locked Ribsoe Sugar ASO Modifications 25
1.3.3.2 Peptide Nucleic Acid ASO Modification 25
1.3.3.3 Phosphordiamidate Morpholino ASO Modification 26
1.4. Additional Chemical Modifications to ASOs 28
1.4.1 Triazole Backbone Linkages in ASOs 29
1.4.2 Alkyl Phosphonates 31
1.5. Research Aims 33
Chapter 2: On-Resin Conversion of Oligonucleotide 5´-OH to Azide During Solid-Phase Synthesis 35
2.1 Introduction 36
2.2 Methodology for Determination of Alcohol to Azide Conversion 39
2.3 OH to Azide Conversion for Phosphodiester Oligonucleotides 44
2.3.1 Oligonucleotides Used and Chromatograms of Azide Conversions of Phosphodiesters 44
2.3.2. Analysis of Azide Conversions of Phosphodiester Oligonucleotides ... 46
2.3.2.1 Effects of the Nucleobase on Azide Conversion of Phosphodiester Oligonucleotides 48
2.3.2.2 Effects of the Ribose Sugar on Azide Conversion of Phosphodiester Oligonucleotides 49
2.4 OH to Azide Conversion of Phosphorothioate Oligonucleotides ... 51
2.4.1. Oligonucleotides Used and Chromatograms of Phosphorothioate Azide Conversions 51
2.4.2 Analysis of Azide Conversion Results with Phosphorothioate Oligonucleotides 53
2.4.3. Unintended Reactions Stemming from Phosphorothioate Backbones ... 55
2.5 Conclusion 57
Chapter 3: On-Resin Copper Click Reactions to Give Internucleoside Triazole Linkages 59
3.1 Introduction 60
3.2 Initial On-Resin Copper Click Reactions with Phopshorothioate Oligonucleotides 63
3.3 On-Resin CuAAC Reactions with Phosphodiester Oligonucleotides 66
3.3.1. Analysis of On-Resin CuAAC Reactions 68
3.3.2. Effects of the 5´ ribose sugar on CuAAC Reaction Efficiency 70
3.4 Duplex Melting Temperature of Triazole Containing Oligonucleotides 72
3.4.1 Analysis of Duplex Melting Temperature for Triazole-Containing Oligonucleotides with an RNA Compliment 74
3.4.2 Analysis of Duplex Melting Temperature for Triazole-Containing Oligonucleotides with a DNA Compliment 74
3.5 Conclusion 77
Chapter 4: Synthesis and Assessment of Splice Switching ASOs Containing Triazole-Linkages 80
4.1 Introduction 81
4.2 Luciferase-Based Assay used to Determine Splice-Switching activity of ASOs 84
4.3 Triazole Linkages in Splice-Switching ASOs 86

4.3.1 Oligonucleotides used to Evaluate Triazole Linkages in ssASOs 86
4.3.2 Results of Triazole-Containing ASOs in a Splice-Switching Assay 88
4.4 Conclusions 91
Chapter 5: Synthesis and Assessment of Splice Switching ASOs With alternate Ribose Patterns and Methoxypropyl Phosphonate-Linkages 95
5.2 Introduction 96
5.2 Ribsoe Substitutions in Splice-Switching ASOs 98
5.2.1 Oligonucleotides used to Evaluate Ribose Sugar Substitutions in ssASOs 98
5.2.2 Results of Ribose-Substituted ASOs in Splice-Switching Assays 100
5.2.3 Analysis of Results from Ribose Substituted ssASO Activity 103
5.3 Methoxypropyl Phosphonate (MOP) Backbone in Splice-Switching ASOs 106
5.3.1 Oligonucleotides used to Study LNA-PS and LNA-MOP Linkgaes in ssASOs 106
5.3.2 Results of ssASOs with LNA-PS and LNA-MOP linkages 108
5.3.3 Analysis of Results of ssASOs Containing LNA-PS and LNA-MOP Linkages 109
5.4 Additional Investigations of Splice Switching ASOs with LNA-PS and LNA-MOP Modifications 110
5.4.1 Oligonucleotides Used to Study the Effects of Additional LNA Sugars 110
5.4.2 Results of ssASOs Containing clustered LNA riboses with PS, MOP-PS and MOP-PO linkages 112
5.4.3 Analysis of Results of ssASOs with LNA-PS and LNA-MOP-PS Linkages 114
5.5 Generalisations on ASOs modified with LNA-PS and LNA-MOP-PS Linkages 116
5.6 Conclusions 119
Chapter 6: Alternative Splice Switching Assays and Methods for Imaging Oligonucleotides in Cells 123
6.1 Introduction 124
6.2: H2K Exon-skipping Assay 126
6.2.1: Methods for and Results from a Splice-Switching Assay in H2K Cells 126
6.2.2: Analysis of Results from a splice-switching assay in H2K Cells 128
6.3 Imaging of RNaseH-Dependent Knockdown ASOs in HeLa Cells 129
6.3.1 Effects of Dyes on Pre-Labelled ASOs 129
6.3.2 Fixed Cell, In-Situ Labelling of ASOs using Click Chemistry 132
6.3.3 Optimisation of Blocking Conditions for Fixed Cell Clicks 133
6.3 Conclusions 137
Chapter 7: Conclusions and Future Directions 139
7.1 Results and Conclusions 140
7.2 Future Directions 144
Chapter 8: Experimental 147
8.1 Oligonucleotides 148
8.8.1 Synthesis 148
8.1.2 Deprotection 148
8.1.3 Purification and Desalting 149
8.1.4. Analysis of Oligonucleotides 149
8.2 Organic Synthesis 150
8.3 UV Melting Studies 151
8.4 Cell Culture and Assays 152

8.4.1 Culture Conditions 152
8.4.2 HeLa pLuc 705 Assays 153
8.4.3 qPCR Based Assays 153
8.5 Data for Chapter 2 155
8.5.1 LC-MS Data for Oligonucleotides ON-2.1 to ON-2.24 156
8.5.2 LC-MS Data for Oligonucleotides ON-2.25 to ON-2.48 161
8.6 Data for Chapter 3 166
8.6.1 LC-MS Data for Oligonucleotides ON-3.1 to ON-3.4 167
8.6.2 LC-MS Data for ON-3.5 to ON-3.28 168
8.6.3 LC-MS Data for Oligonucleotides ON-3.29 to ON-3.33 172
8.6.4 Organic Chemistry for Compounds of Chapter 3 175
8.7 Data for Chapter 4 177
8.7.1 LC-MS Data for Oligonucleotides ON-4.1 to ON-4.8 178
8.7.2 Data for Luciferase Intron-Skipping Assays in Chapter 4 179
8.7.3 Organic Chemistry Data for Compounds of Chapter 4 181
8.8 Data for Chapter 5 184
8.8.1 LC-MS Data for Oligonucleotides ON-5.1 to ON-5.16 184
8.8.2 Data for Luciferase Intron-Skipping Assays in Chapter 5 187
8.8.3 Organic Chemistry for Compounds of Chapter 5 191
8.9 Data for Chapter 6 195
8.9.1 LC-MS Data for Oligonucleotides ON-6.1 to ON-6.13 195
8.9.2 Data for Assays of Chapter 6 198
8.9.3 Click Background Data Collection Parameters 201
9. References 203

ABBREVIATIONS

Å	Angstom
A	Adenine
Abs	Absorbance
Ac	Acetal
ACN	Acetonitrile
Ar	Aryl
ASO	Antisense Oligonucleotide
a.u.	arbitrary units
bp	Base Pair
Bz	Benzoyl
C	Cytidine
˚C	Degree Celsius
Calc.	Calculated
CPG	Controlled Pore Glass
CuAAC	Copper-catalysed Azide-Alkyne Cycloaddition
d	Doublet (NMR)
Da	Dalton
DCM	Dichloro Methane
dd	doublet of doublets (NMR)
DMF	*N,N'*-dimethylformamide
dmf	*N,N'*-dimethylformamidyl protecting group
DMSO	Dimethyl Sulfoxide
DMT	Dimethoxytrityl
DNA	Deoxyribose Nucleic Acid
eq.	Equivalent
ESI	Electrospray ionization
EtOAc	Ethyl Acetate
Et_2O	Diethyl Ether
FDA	Food and Drug Administration
2'Fluoro	2' Fluoro Nucleic Acid
Fmoc	9-fluorenylmethyl
G	Guanine
g	gram

HPLC	High Performance Liquid Chromatography
HRMS	High Resolution Mass Spectrometry
Hz	Hertz
iBu	isobutyryl
LCMS	Liquid Chromatography Mass Spectrometry
LNA	Locked Nucleic Acid
LRMS	Low Resolution Mass Spectrometry
M	Molar (concentration)
m	multiplet (NMR)
mg	milligram
mL	millilitre
MeC	5-methylcytidine
2'MOE	2'-O-Methoxyethyl Nucleic Acid
mRNA	messenger RNA
MS	Mass Spectrometry
MW	Molecular Weight
M/Z	Mass to Charge Ratio
NHS	*N*-hydroxysuccinimide
nm	nanometer
nM	nano Molar
NMR	Nuclear Magnetic Resonance
2'OMe	2'Methoxy Nucleic Acid
PCR	Polymerase Chain Reaction
pH	potential of Hydrogen
PMO	Phosphorodiamidate Morpholino Oligonucleotide
PNA	Peptide Nucleic Acid
PO	Phosphodiester
ppm	parts per million
PS	Phosphorothioate
q	quartet (NMR)
qPCR	quantitative PCR
rt	room temperature
RNA	Ribose Nucleic Acid
s	singlet (NMR)

T	Thymine
t	Triplet (NMR)
TC	1,1-dioxo-λ6-thiomorpholine-4-carbothioate
TCA	Trichloro Acetic Acid
THF	Tetrahydrofuran
TEA	Triethylamine
TLC	Thin Layer Chromatography
U	Uridine

Chapter 1: Introduction

1.1. Nucleic Acid Structure and Synthesis

1.1.1 Basic Structure

Nucleic acids exist in every organism and make up the basis of genetic code. They are composed of the polymers Ribose Nucleic Acid (RNA) and Deoxyribose Nucleic Acid (DNA) which each contain four aromatic nitrogenous nucleobases. These are Adenine (A), Cytosine (C), Guanine (G) and Thymine (for DNA) and Adenine (A), Cytosine (C), Guanine (G) and Uracil (U) for RNA, As well as a ribose sugar for RNA, a 2´-deoxyribose sugar for DNA, and a phosphodiester linkage between the sugars (Figure 1.1).

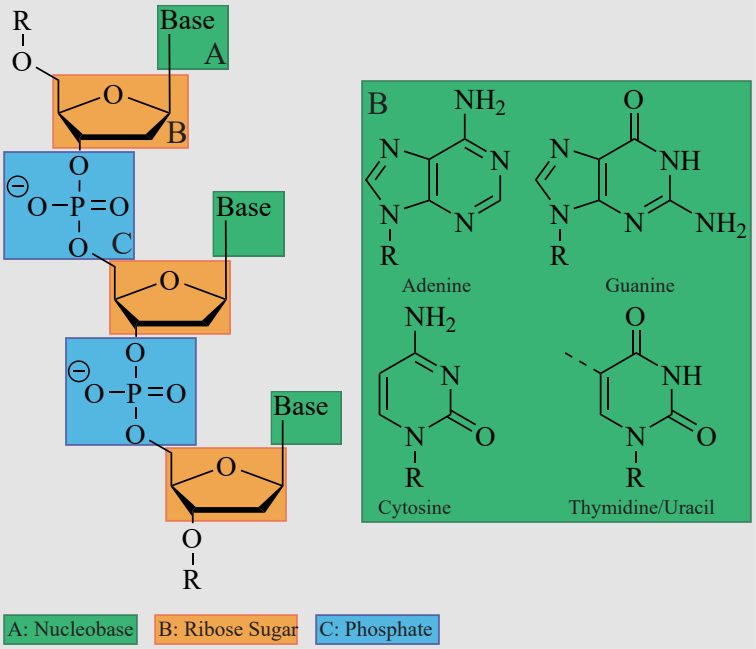


Figure 1.1: Structure of DNA and the nucleobases found in DNA and RNA.

The nucleobases can be further partitioned into the purines (A and G) which contain a five and six membered fused ring and the pyrimidines (C and T/U) which have a six membered ring. These nucleobases are connected to the ribose sugar through the glycosidic bond. Rotation of this bond allows the nucleobase to adopt various conformations, with the extremes being *syn* and *anti*. For largely steric reasons the *anti* conformation is more abundant.[1] Single strands of DNA and RNA interact with each other through base-pairing (A:U, A:T, T:U and C:G), stabilised by hydrogen bonds and base

stacking. Base pairing is by a Watson-Crick arrangement, although in some special cases Hoogsteen base pairing is observed[2] (Figure 1.2).

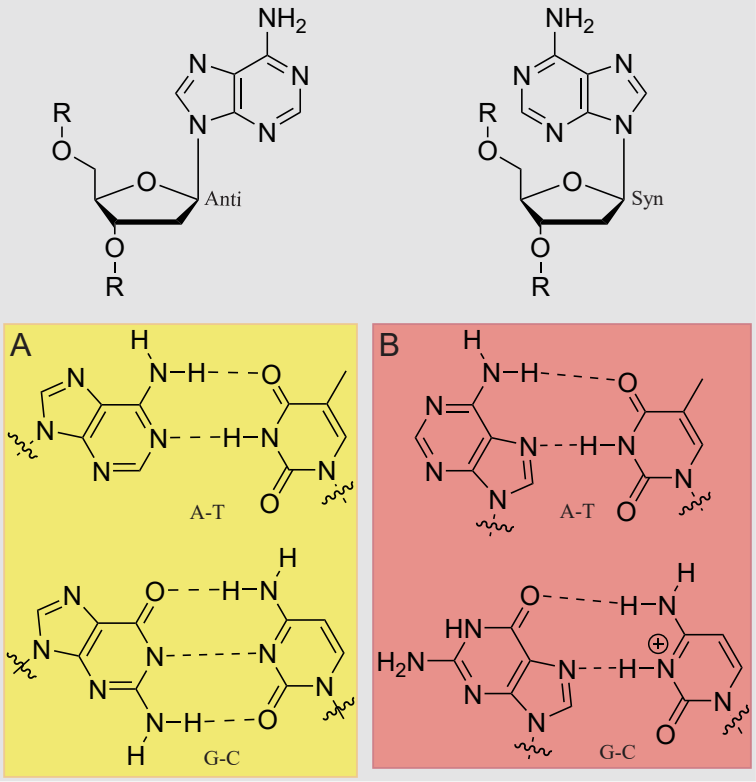


Figure 1.2: Depiction of *anti* and *syn* nucleobase conformations as well as **A:** Watson Crick and **B:** Hoogsteen base pairing.

In addition to the nucleobase, the ring can adopt several conformations influenced largely by the chemical composition of the ring. These can be represented in a pseudo-rotation wheel where the four extremes are represented by the four cardinal directions. The ribose sugar positions are labelled 1´ to 5´, where 1´ is at the glycosidic bond and 5´ is the CH_2 group attached to the furanose sugar ring. Here *endo* indicates positioning above the plane of the sugar ring and *exo* indicates positioning below. North represents C3´ in the *endo*-position (and C2´ in the *exo*-position), West the oxygen in an *endo*-position, South C2´ in the *endo*-position (and C3´ in the *exo*-position) and East the oxygen in the *exo*-position (Figure 1.3).

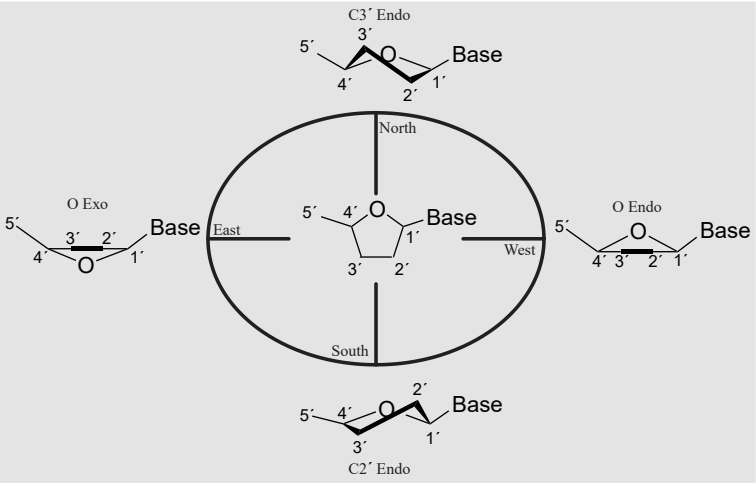


Figure 1.3: Ribose sugar labelling and the pseudo-rotation wheel adapted from.[3]

The conformation of the ribose sugar then influences the structure of the duplex, with C3´-*endo* sugars such as ribose favouring an A-form helix, and C2´-*endo* sugars like DNA favouring the less thermally stable B-form helix (Figure 1.4).

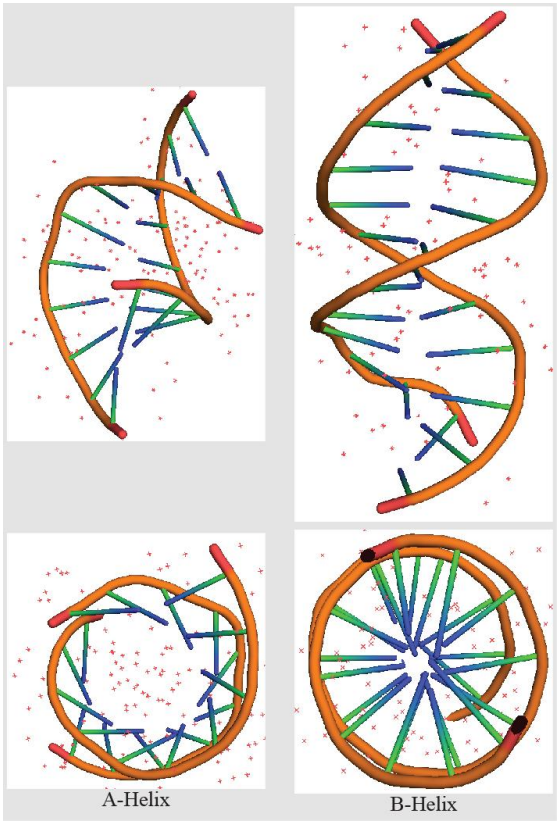


Figure 1.4: The A-form double helix (left) and the B-form double helix (right) viewed from the top and side. The A-form[4] and B-form[5] images were generated from PDB flies using PyMol.[6]

The A-form has11 base pairs(bp) per helical turn whereas the B-form has 10.5 bp). The A-form also has a narrower angle of turn (25.3° vs. 35. 4°), less rise per base (2.3 Å vs. 3.4 Å) and a wider diameter (25.5 Å vs. 23.7 Å) than the B-form. The A-form duplex is also associated with increased thermal stability, leading to a higher duplex melting temperature.[7]

1.1.2 Oligonucleotide Synthesis

Pioneering advances in the synthesis of nucleic acids were made by Michelson and Todd in 1955 using phosphorus (V) building blocks.[8] Another major advancement was made by Lestinger in 1966 when oligonucleotides were first synthesised on a solid support.[9] This strategy is extremely useful as it allows reagents to be added in large excesses and removed quickly and making the methodology suitable for automation. By far the most widely used current method is the solid-phase phosphorus (III) based phosphoramidite approach developed by Caruthers et al[10] where synthesis proceeds in a 3´ to 5´ direction. In this approach, the first nucleoside is attached to a resin, generally Controlled Pore Glass (CPG) via its 3´-hydroxyl group. Subsequent nucleotides (phosphoramidites) are then coupled to the resin-bound oligonucleotide. These phosphoramidites have a 4,4´-dimethoxytrityl (DMT) 5´-hydroxyl protecting group while the 3´-OH is functionalised with a bis(diisopropyl)amino cyanoethyl group (phosphoramidite).

The synthesis cycle starts with the DMT group of the resin bound nucleoside being removed with trichloroethanoic acid (trichloroacetic acid, TCA), Figure 1.5. The next nucleoside phosphoramidite monomer is then added with mild acid catalysis using an activator which protonates the bis(diisopropyl)amino group, allowing it to be displaced by the newly exposed 5´-hydroxyl group on the resin. The catalyst (activator) is normally a tetrazole derivative, usually 5-ethylthio-1H-tetrazole (ETT) or 5-benzylthio-1H-tetrazole (BTT). Nucleotides on the solid-support that fail to couple to the activated

phosphoramidite are then capped using acetic anhydride catalysed by N-methylimidizole (NMI). Acetyl capping allows for easier oligonucleotide purification as it minimises the percentage of 'failure' sequences that are only one nucleotide shorter (N-1) than the target sequence, producing a more even distribution of failure sequences. Next, the phosphorus (III) group on the growing oligonucleotide is oxidised to phosphorus (V) by a solution of I_2 in a mixture of water, THF and pyridine to give a cyanoethyl phosphotriester (protected phosphodiester). Oligonucleotide synthesis is continued by detritylation of the coupled nucleotide on the resin and repeating the process many times until the full-length oligonucleotide has been assembled. An excess of reagents is used to ensure rapid chemical reactions. The reagents are quickly and efficiently washed away multiple times during the synthesis cycle. The overall process is highly efficient, > 99.5% per cycle, with automation employed to ensure consistency. Several DNA/RNA synthesis instruments are available to make oligonucleotides on small and large scale, and to assemble large numbers of oligonucleotides simultaneously.

When solid-phase oligonucleotide assembly is complete the oligonucleotide is cleaved from the solid support and deprotected in aqueous ammonia which removes the cyanoethyl protecting groups (as acrylonitrile) from the phosphotriesters as well as cleaving the protecting groups from the nucleobases. The primary amines of the nucleobases are typically protected with benzoyl (Bz) for adenine, Bz or acetyl (Ac) for cytosine, and isobutyryl (iBu) or dimethylformamidine (DMF) for guanine.

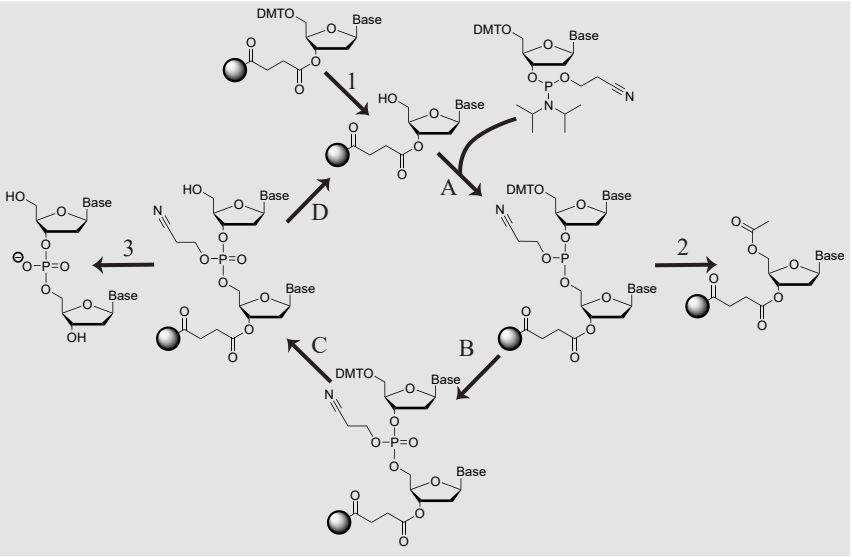


Figure 1.5: Solid-phase oligonucleotide synthesis cycle, the conditions described and figure are adapted from the literature.[11] **A.** Activation and coupling of a phosphoramidite with ETT or ETT. **B.** Oxidation step to create the phosphotriester bond with I_2/THF/H_2O/Pyridine. **C.** Detritylation of added nucleotide with TCA. **D.** Repetition of the cycle. **1.** Detritylation of the initial CPG bound nucleotide. **2.** Capping of uncoupled 5´-OH groups with acetic anhydride/NMI. **3.** Oligonucleotide cleavage and deprotection with ammonium hydroxide in water.

This method offers a large amount of flexibility both in terms of synthesis scale and in modifications available. Scales can be as small as 25 nmole[12] or as large as 150 mmole[13] for applications ranging from PCR primers to therapies. Commercially available catalogues offer phosphoramidites and CPGs such as standard nucleobases, dyes, carbon spacers, amine linkers and more that support a diverse array of easily accessible oligonucleotide chemistry.[14, 15]

1.2. Antisense Oligonucleotides

Antisense Oligonucleotides (ASOs) are a class of chemically modified single stranded oligonucleotides (~18-30 nucleotides in length) that are designed to interact with endogenous messenger RNA (mRNA). They are used to treat genetic disorders and other diseases[16] with eleven ASOs currently approved by the FDA.[17]

Genetic diseases can stem from mutations that are inherited from one or both parents or from a novel change that disrupts normal mRNA function, altering protein expression. These genetic changes can result in different outcomes. In some diseases, such as Duchenne's Muscular Dystrophy (DMD), mutations in pre-mRNA lead to a shift in reading frame that prevents the production of essential proteins, or results in a non-functional protein. In other occurrences like Familial Hypercholesterolemia (FH), a build-up of lipoproteins leads to toxicity. Both are amenable to treatment with ASOs via different mechanisms.

One therapeutic strategy is to create an ASO that is complementary to a splice site in the mutant pre-mRNA (Figure 1.6 (3)). The oligonucleotide disrupts the function of spliceosomes and prevents a particular exon or intron from being incorporated. This process was first reported by Kole et al in 1993.[18] This strategy is used to treat DMD where one of several exons can be skipped to restore the correct mRNA reading frame. Although this leads to a truncated final protein, the protein is functional. Without such an intervention a premature stop codon is present in the mRNA preventing any functional protein from being produced.[19] Several oligonucleotides using this approach are approved for clinical use including Eteplirsen, Golodirsen and Casimersen from Sarepta Therapeutics and Vitolanersen from Nippon Shinyaku.[20]

Another mechanism by which ASOs act as therapeutic agents is in gene silencing by recruitment of the nuclease enzyme ribonuclease H (RNase H). In this strategy (Figure

1.6 (2)) an oligonucleotide binds to a complementary section of the target mRNA, creating a heteroduplex which is rapidly recognised by RNase H which degrades the mRNA of the heteroduplex, preventing the targeted gene from being expressed.[21] The FDA-approved drug Mipomersen from Ionis acts by this mechanism to treat familial Hypercholesterolemia (FH).[22] This genetic disease is characterised by elevated levels of cholesterol in the blood caused by mutations that prevent clearing of Low-Density Lipoprotein Cholesterol (LDL-C). Several genes can be responsible for this condition which leads to an increase in cardiovascular issues and other problems.[23] Mipomersen targets Apolipoprotein B, a significant component of LDL-C and reduces its abundance in circulation.[24] The mechansims of action discussed can be seen in Figure 1.6.

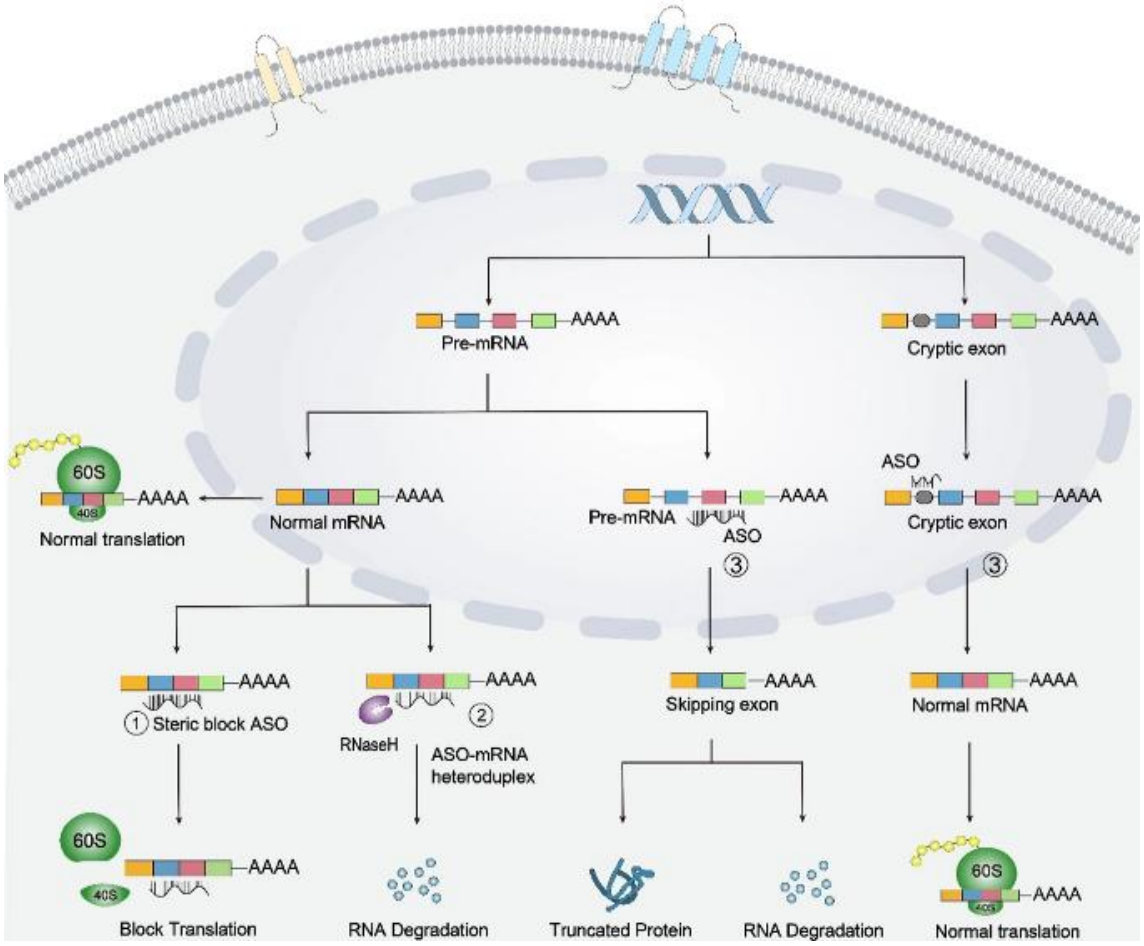


Figure 1.6: Mechanisms steric blocking (1), RNaseH dependent knockdown (2) and Exon skipping (3) reproduced from literature[25] with permission.

Figure 1.6 depicts two additional strategies, one of gene silencing and one for splice modulation. Figure 1.6 (1) shows prevention of translation via steric blocking. In this case the end result is the same as with RNAseH dependent ASOs however they function simply by occupying space and preventing ribosomes from reading through the mRNA. Figure 1.6 (3) shows prevention of cryptic exon inclusion as well as exon skipping. This case is the same as discussed with the work from Kole et al. where introns that are aberrantly included are subsequently excluded to restore the normal transcript.

1.3. Chemical Modifications in Therapeutic Oligonucleotides

Regardless of the therapeutic mechanism of action, it is necessary to change the chemical structure of ASOs. This is because naturally occurring unmodified nucleic acids are unstable *in vivo*[26]. They are rapidly degraded by nuclease enzymes[27, 28] resulting in very poor biological activity. Chemical modifications have evolved over the years to address this problem, with three distinct 'generations' used to classify the history of ASO chemistry. Some of the most popular modifications as well as examples of their substitution patterns in ASOs are shown in Figure 1.7.

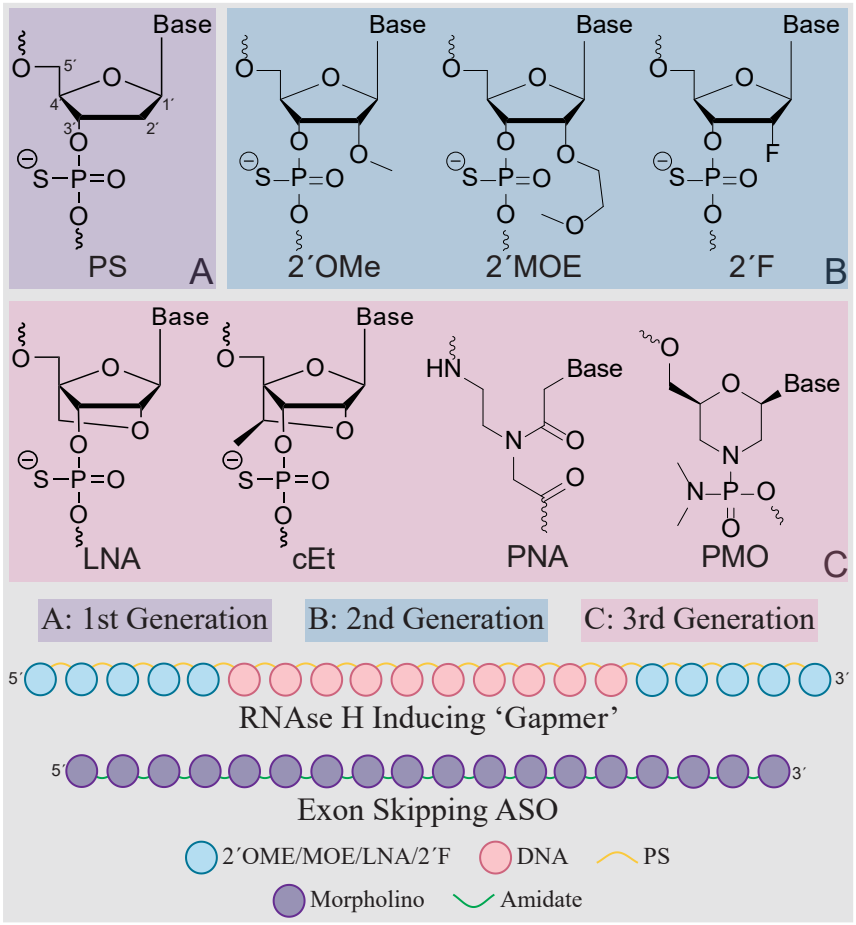


Figure 1.7: Chemical modifications divided **A:** First Generation **B:** Second generation and **C:** Third Generation and substitution patterns. Abbreviations used are as follows: Phosphorothioate (PS), 2´-Methoxy RNA (2´-OMe), 2´-Methoxyoethyl DNA (2´-MOE), 2´-Fluoro RNA (2´-F), Locked Nucleic Acid (LNA), Constrained Ethyl Nucleic Acid (cEt), Peptide Nucleic Acid (PNA) and Phosphoramidate Morpholino Oligonucleotide (PMO)

1.3.1 First Generation ASOs

The first generation of modified ASOs incorporate the phosphorothioate (PS) modification in which one of the non-bridging oxygens of the phosphodiester linkage is replaced by sulfur. Phosphorothioates were first described in the mid-1960s as nucleoside phosphate derivatives[29] and then as dinucleotides by Eckstein et al. where they were found to confer stability against phosphatase enzymes.[30] Introduction of the sulfur creates a chiral centre at each phosphothiodiester linkage, giving rise to Sp and Rp phosphorothioate configurations. It was later found that the enhanced nuclease stability conferred by the phosphorothioate modification largely comes from the Sp isomer as it displaces metal ions key to the function of nucleases. While the Rp isomer does confer some stability it is not of the same magnitude as the Sp isomer.[31] Critically, the stabilising effect can be achieved without interfering with the ability of an ASO-mRNA duplex to be recognised by RNase H. This makes it an extremely important modification for ASOs which was first used to target cytomegalovirus (CMV)[32, 33] in AIDS patients in the first FDA approved ASO, Fomivirsen.[34]

In addition to enzymatic stability, phosphorothioates give rise to other effects, both positive and negative. The PS modification destabilises the ASO-RNA duplex, though usually by less than 1°C per modification.[35] Additionally phosphorothioates are known to have a number of sequence-independent ASO-protein interactions including albumin binding, and interactions with immunoglobulin G and transferrin.[36] Some of these protein-ASO interactions may contribute to the *in vivo* slowing down of PS-ASO clearance by filtration. They also have an impact on nearly all aspects of the biological properties of ASOs. These can be positive, like increased affinity for intracellular trafficking proteins[37] and internalisation of ASOs by thiol-mediated uptake.[38] Negative effects mostly relate to safety, as phosphorothioates have been shown to be associated with toxicity.[39-44] The phosphorothioate modification remains one of the most enduring,

and all ASOs in the clinic, with the exception of PMOs, contain PS backbone linkages. Interestingly, the biophysical and biological effects of controlling phosphorothioate stereochemistry is the subject of much current research.[45-47]

1.3.2 Second Generation ASOs

After the phosphorothioate, a new generation of modifications was created with a focus on modifications at the 2´-position of the ribose sugar. In particular the 2´-OMe and 2´-MOE modifications were introduced. Modifying the 2´-position gives strong nuclease resistance[48-51] and can increase the thermal stability of duplexes.[52, 53] These modifications are used in conjunction with the phosphorothioate linkage synergistically; the duplex melting temperature is raised by the 2´-modification and the nuclease resistance of the phosphorothioate linkage is maintained. A downside to these 2´-sugar modifications is that they are not compatible with RNase H degradation of complementary mRNA[54-56], meaning that although splice switching ASOs can be fully modified at the 2´-position, any ASOs intended for use in RNase H dependent gene knockdown must employ the 'gapmer' strategy as depicted in Figure 1.7. In these designs, the ASO is constructed with 'wings' of modified ribose sugars (typically 5 nucleotides in length) with a 'gap' of unmodified deoxyribose sugars (~10 nucleotides) in the central region with phosphorothioate linkages throughout. This allows RNase H function, gives good affinity of the ASO for its complementary RNA target, and strongly protects the ASO from degradation by exonucleases.[57]

1.3.3 Third Generation ASOs

As the therapeutic oligonucleotide field developed, more nucleotide analogues were created in the 'third generation', departing further from the naturally occurring DNA and RNA structures.

1.3.3.1 Locked Ribsoe Sugar ASO Modifications

A major advancement was the 'locked' sugars such as locked nucleic acid (LNA)[58] and closely related constrained ethyl (cEt)as shown in Figure 1.7.[59] In this class of ribose sugar analogues, the 2´ and 4´ positions are linked by an oxymethylene linker, creating bicyclic LNA with the ability to significantly increase duplex thermal stability, raising the melting temperature by as much as 9°C per LNA modification.[60] This effect stems from the conformation of the locked sugar, which is forced into a 3´-*endo* (north) conformation.[61] In addition to this increased duplex stability, LNA maintains good mismatch discrimination[62] and is resistant to nucleases.[63] All of this would seem to make it a very useful modification, however it is associated with toxicity.[64-70] Derivatives of LNA such as constrained ethyl and constrained 2′-O-methoxyethyl show even more nuclease resistance[71, 72] but fail to solve this core toxicity issue. This is thought to be derived from protein-ASO interactions that are promoted by the locked sugars, leading to hepatotoxicity.[73]

1.3.3.2 Peptide Nucleic Acid ASO Modification

Peptide Nucleic Acid (PNA) as shown in Figure 1.7 is a completely charge-neutral analogue of DNA where the ribose sugar and phosphate linkage are both replaced by a polyamide chain.[74] PNA is synthesised using solid phase peptide methods and the building blocks are Fmoc and tBoc protected amines rather than the DMT-protected alcohols used in standard oligonucleotide synthesis.[75] PNA is also known to form very thermally stable duplexes through Watson-Crick base pairing[76] and has been employed in ASOs.[77-79] PNA suffers from a few key issues, however. The lack of a negatively charged backbone means that PNA does not complex with serum proteins, so is rapid cleared *in vivo*. Additionally, there are solubility issues in aqueous solution and PNA has poor cell uptake properties.[80, 81] Conjugation of PNA to peptides has been shown to

increase cell uptake and circulation time but no PNA analogues have so far reached the clinic.

1.3.3.3 Phosphordiamidate Morpholino ASO Modification

Phosphordiamidate morpholino oligonucleotides (PMOs) as seen in Figure 1.7, like PNA, are completely charge-neutral. The ribose sugar is replaced by a morpholine ring and the phosphodiesters are replaced by phosphorodiamidate groups.[82] PMOs are the most widely used and successful modifications in exon-skipping oligonucleotides as they constitute the entirety of DMD targeting exon skipping ASOs approved by the FDA and two thirds of all approved splice modulating oligonucleotides.[83] Synthesis of PMOs can be carried out by phosphoramidite chemistry[84], however it is often done as originally described, using chlorophosphoramidate[85] method which differs in two key ways.

Firstly, the coupling is done using phosphorus (V) where the secondary amine of the morpholine displaces a chlorine atom to form the backbone linkage. Secondly synthesis proceeds in the opposite direction to standard oligonucleotide synthesis, starting with the 6- position on the morpholine attached to a solid support then adding the next nucleotide to the 3´-site. Although PMOs are charge-neutral like PNA, they show excellent solubility in water due to base-stacking which shields the hydrophobic nucleobases.[86, 87] They also show moderate duplex stability (similar to that of DNA-RNA duplexes) and are highly resistant to nuclease and other enzymes *in vivo*.[88] As with PNAs, they do not bind strongly to serum proteins[84] which perhaps accounts for the relatively short (about 1-4 hours) half-life observed in patients.[89, 90] They have a good safety profile[91] which is partly why they are used so extensively in the clinic.

These three generations of modifications provide a variety of tools that can be used to tune the properties of ASO molecules. There are agents to improve target affinity (e.g. LNA) and to provide extreme enzymatic stability with good safety profiles (e.g. PMO). However, uptake into cells and productive intracellular trafficking remain

problematic and these limitations are inhibiting the development of oligonucleotide therapeutics.

1.4. Additional Chemical Modifications to ASOs

It has been established that the primary method of cell entry for ASOs is endocytosis and a number of different endocytotic pathways can be taken.[92] Once engulfed in the endosome, ASOs are internalised. Endosomes fuse with lysosomes which trap ASOs meaning even though they are internalised most are not able to act as intended.[37] Different strategies have been developed for more productive cellular uptake including attachment of Cell Penetrating Peptide (CPPs) to ASOs, attachment of lipids, and conjugation of ASOs to receptor-targeting molecules.

CPPs are readily attached to ASOs and provide systemic longevity to charge-neutral oligonucleotide analogues such as PMOs. A major problem with many CPP-ASOs remains however, is endosomal entrapment. When attached to negatively charged ASOs, cationic lipids disrupt the phospholipid bilayer by interactions with endogenous negatively charged lipids, thus facilitating ASO passage.[93] Receptor targeting conjugates of ASOs are also gaining popularity. The most successful is a trimer of N-acetylgalactosamine $(GalNAc)_3$ which targets the asialoglycoprotein receptor (ASGR) on hepatocytes, and is used as a delivery agent for multiple FDA approved double stranded siRNAs such as Inclisiiran.[94] Receptor targeting is an attractive strategy as it allows systemically delivered ASOs to preferentially target a desired cell type. However the ASGR receptors on hepatocytes are unique; they quickly internalise and release their cargo inside the cell. Moreover, they are highly abundant on the surface of cells that express them ($>10^5$ molecules per cell).[95] Only a small percentage (<1%) of ASO escapes the endosomes[96] but slow release of the siRNA inclisiran from endosomes means that treatment by injection is only necessary every few months. This specific receptor is present only in hepatic cells; similarly acting receptors in other cell types have proved elusive, and indeed may be non-existent.

One route that holds promise to address some of these issues as well as to improve the overall profile of ASO drugs is to replace some of phosphorothioate linkages with charge-neutral analogues while leaving some in place. Judicious use of charge-neutral backbones has been shown to increase ASO performance especially when used in unaided (gymnotic) delivery compared to ASOs with wholly phosphorothioate motifs, suggesting an increase in productive uptake might be achieved by a reduction in PS content.[97] These charge-neutral modifications can also vastly improve the safety profile of toxic ASO sequences.[36] This is explained by modulation in protein-ASO interactions; some level of serum binding still occurs so many of the benefits of the PS backbone are maintained by selective use of charge-neutral backbones. Many different types of charge-neutral linkages have been synthesised, however of interest here are triazoles and phosphonates.

1.4.1 Triazole Backbone Linkages in ASOs

Since the discovery of 'biorthogonal' click chemistry using Copper Catalysed Azide Alkyne Cycloaddition (CuAAC) or Strain-promoted Azide Alkyne Cycloaddition (SPAAC) as pioneered by Sharpless[98]/Meldal[99] and Bertozzi[100] respectively, the use of triazoles has become common especially for ligation and conjugation of oligonucleotide sequences.[101-113] Further work has been done to incorporate triazole linkages into the backbone of oligonucleotides starting with the first synthesis of triazole linked T-T dimers (pre-CuAAC) in 1997.[114, 115] Since then, a number of different analogues have been synthesized, most employing a 'dimer' strategy where nucleosides are furnished with an azide and alkyne functions and coupled together by solution phase chemistry.[116-120] The dimer is then converted to a phosphoramidite and incorporated into an oligonucleotide strand using standard solid phase oligonucleotide synthesis. An alternate approach was taken by Isobe et al. in 2008 when ligation was done on solid support with modified T

monomers where an azide replaces the 3´-hydroxyl and a protected alkyne replaces the 5´-hydroxyl.[121, 122]

However, in every case previously described, the triazole strongly destabilises the duplex, often reducing the melting temperature by over 5°C. Importantly, it has been shown that this can be reversed when LNA sugars are used to flank the triazole linkage.[123] Triazoles have been incorporated into ASOs and are active in both an exon skipping[119] (incorporated between bases 6 and 7 from the 3´-side of a 13mer) and RNase H knockdown[122] (incorporated as either the terminal 3´ or terminal 5´ linkagemodalities. This makes the triazole a promising modification as CuAAC 'click ligation' is compatible with solid phase chemistry. Different triazole linkages are shown in Figure 1.8.

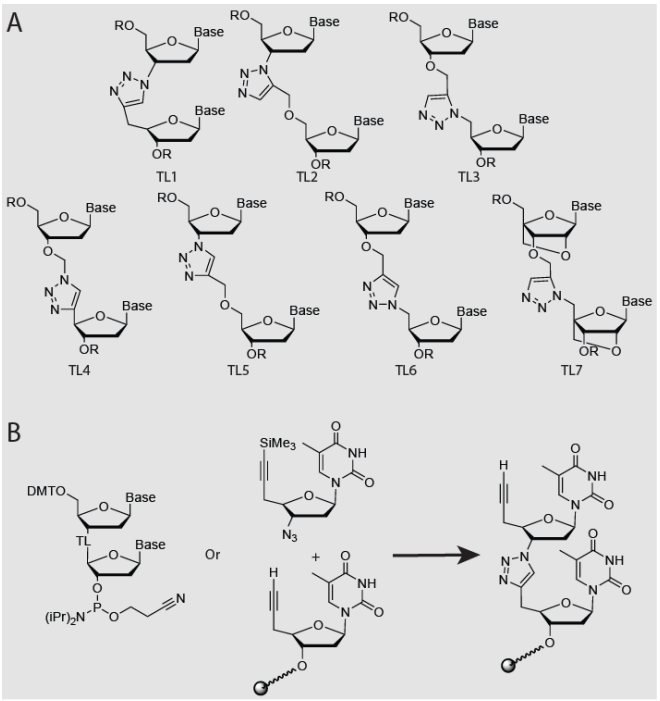


Figure 1.8: A. Previously synthesised triazoles linkages (TLs) in oligonucleotides. Triazoles 1-6 and Triazole 7[123] were taken from literature. **B.** The different methods of incorporation, left is a phosphoramidite dimer, right is the Isobe et al. on-column synthesis.[121] Of the listed triazoles TL-2 was used in an RNaseH dependent knockdown ASO (+0.6°C in duplex stability when used in the pattern LNA-TL-LNA compared to phosphorothioate) and TL-6 was used in an exon skipping ASO (-7.4°C in duplex stability compared to phosphorothioate)

1.4.2 Alkyl Phosphonates

Another family of charge-neutral oligonucleotide backbones is the alkyl phosphonates. Phosphonates are an obvious choice for ASO modification as like a phosphorothioates they maintain the core motif of an oxygen-phosphorus-oxygen bridge but have the advantage of a huge increases in nuclease stability compared to the natural phosphodiester. Methyl phosphonates were first reported in 1979 by Miller et al[124] who synthesised combinations of A and T dimers by condensing one unmodified monomer with a 3´-methyl phosphonate monomer. Subsequently a methyl phosphonate phosphoramidite precursor was developed[125, 126] in which the cyanoethyl group of a standard phosphoramidite building block is replaced with a methyl group. Other methods to create more sterically hindered phopshonates are also being investigated.[127]

Despite their relatively long history, phosphonates have yet to make an appearance in FDA-approved therapeutic ASOs. A major reason for this is their chemical instability which makes their synthesis and deprotection challenging. Phosphonates are generally base-labile meaning that they are easily hydrolysed during standard ammonia oligonucleotide deprotection.[128] Alternative deprotection methods are available, but usually employ nucleophilic amines that are not compatible with benzoyl protected cytosine due to transamination leading to addition of the deprotecting agent to the base.[129] These are inconveniences that can pose major issues when scaling up in a process development environment.

Alkyl phosphonates have shown promising effects in ASOs where they have strong nuclease resistance[125, 130-133] and can achieve a potent reduction in gene expression[134-136] though they can also show reduction in cellular internalisation, likely due to disruption of interactions with trafficking proteins compared to the PS modification.[16, 137, 138] Recently, renewed interest has been paid to phosphonate linkages due to their ability to improve the therapeutic index of toxic gapmer ASOs. It was shown

that a potential cause of toxicity in ASOs is the binding of paraspeckle RNA-binding proteins. Modifications such as LNA, cEt and phosphorothioates can form extremely tight complexes that mis-localise these proteins and adversely affect cellular health.[139]

It was recently shown that placing a MOP (methoxypropyl) or methylphosphonate modification in the ASO, particularly into the gap of the gapmer region, significantly disrupts this undesirable protein binding, making a much safer ASO while maintaining a high level of activity.[140] Further work expanded this concept to other phosphonate linkages as well as triesters, amides and formacetal backbones[141] showing that any non-canonical link that will disrupt this interaction will work, though a phosphonate remains arguably the easiest to implement. Importantly, while there has been much work done with RNase H mediated knockdown ASOs, this is not the case for splice switching ASOs which remain heavily focused on the PMO modality, meaning explorations of phosphonate backbones in this space holds promise.

1.5. Research Aims

The overall aim of this work is 1) develop modification strategies for the synthesis of oligonucleotides with charge-neutral backbones, 2) assess the activity of these modifications in an exon skipping or RNase H dependent knockdown context and 3) gain an understanding of causes behind observed differences in activity between ASO modifications.

The chapters

Chapter 2 focuses on the assessment of a solid-phase 'on-column' method to introduce an azide modification to the 5´-end of an oligonucleotide. Though methods currently exist, their scope is limited and it is unknown how they will respond to commonly used chemical modifcations. This chapter will test the compatibility with phosphorothioates and various different sugar modifications. Additionally using an on-column method allows for more flexible incorporation of the triazole backbone described as described in below the section on Chapter 3.

Chapter 3 follows on from the modification strategy in Chapter 2 by assessing the functionality of an on-column copper catalysed click reaction to create a charge-neutral triazole linkage between nucleosides. The on-column method requires synthesis only of an alkyne monomer. Previously, triazoles have been incorporated into a biologically active oligonucleotide by making a dimer of two riboses joined by a triazole, phosphitylation of the dimer and adding using standard a standard oligonucleotide synthesis cycle. Using the on-column method for both azide conversion and CuAAC means that only alkyne monomers need to be specially synthesized, allowing for greater flexibility in the position of incorporation. This process will be optimised for phosphorothioate oligonucleotides and assessed with phosphodiester oligonucleotides combined with common sugar modifications. The effect of the triazole on duplex stability will then be examined for each sugar modification tested.

Chapter 4 expands on the previous two chapters and employs the solid-phase click method to create splice switching ASOs with various different sugars at the 5´-side of the linkage. Those ASOs are assessed in a Luciferase-based splice switching assay.

Chapter 5 continues with an evaluation of different ribose sugars to find optimal modification patterns. These patterns are then combined with the MOP phosphonate linkage to assess its effect on the efficiency of exon skipping.

Chapter 6 starts assay development was then done to gain more insight into the reasons behind the observed patterns. First an attempt was made to create a nested-multiplex-PCR based assay where exact exon skipping percentages could be evaluated in a mouse based dystrophic cell line. Due to difficulties with the low mRNA transcript count it was determined that this assay is not well suited to screening of modifications.

A different approach was then taken with developing a more universal method for quantifying cellular localisation and internalisation of ASOs. In this method cells are treated with 5′-azide-modified ASOs then fixed, after which a cyclooctyne derivative of a fluorescent dye is added to create a fluorescently labelled ASO *in situ*. This avoids artefacts which can affect ASO activity and distribution when cells are directly treated with Dye-ASO conjugates.[142-145]

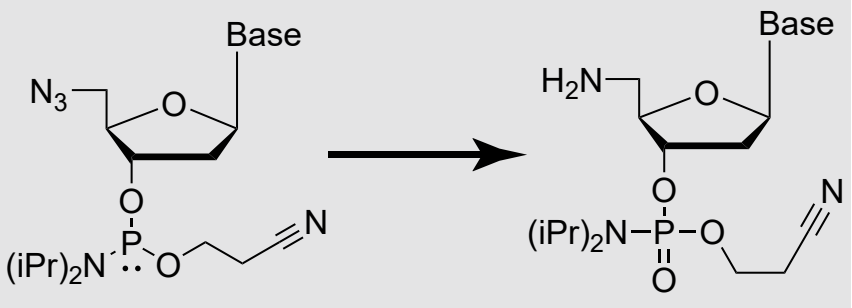
Chapter 2: On-Resin Conversion of Oligonucleotide 5´-OH to Azide During Solid-Phase Synthesis

2.1 Introduction

Solid-phase phosphoramidite chemical synthesis of oligonucleotides conventionally progresses in the 3′-5′ direction; upon completion of each cycle of monomer addition, as well as the overall oligonucleotide assembly, the terminal 5'-OH is left unprotected. This presents an opportunity for functionalisation of the oligonucleotide and many different special monomers are available to modify the 5′-end, including the addition of phosphoramidites of fluorescent dyes,[146-150] or amines which can be subsequently labelled with NHS esters of various reporter groups.[14, 142, 151, 152] Another functionality on the 5′-end of oligonucleotides is azide. Azides are used in click chemistry reactions (CuAAC and SPAAC) and such reactions have been widely exploited in the oligonucleotide field. Click reactions can be used to add peptides[153, 154], fluorescent dyes[155-159], or other moieties [160-162] to allow visualisation, facilitate cellular uptake or confer other benefits. Many commercially available reagents including azide, alkyne and cycloalkyne derivatives of fluorescent dyes are available.[163]

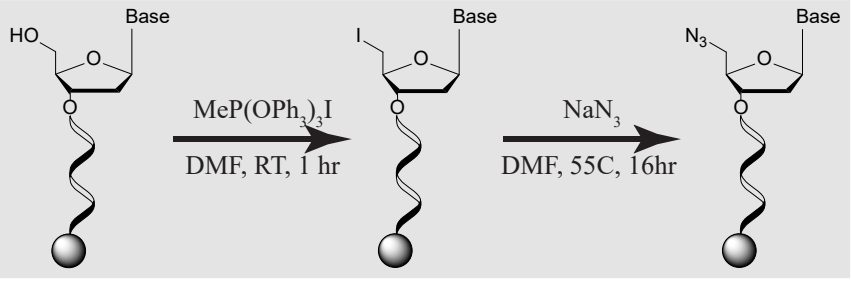
Several methods exist for the introduction of an azide to an oligonucleotide. Azides are not compatible with phosphoramidites as they undergo a Staudinger Reduction (Scheme 2.1) so standard oligonucleotide solid-phase synthesis is not an option. It is, however, possible to attach azido-alkyl groups to solid supports[164, 165] in order to add the N_3 functional group to the 3′-end of oligonucleotides, but this functionalises the linker rather than the free 5′-hydroxyl. It is also possible to use a mesyl-functionalised phosphoramidite monomer[166] which can be subsequently converted to azide. This is a useful strategy for introducing N_3 at any point in a given oligonucleotide sequence. However, it requires special amidites to be synthesised and also puts the azide at the terminus of an alkyl chain. Azides can also be added to the 5´ of a sequence after synthesis is complete using a combination of commercially available alkyl amino linker phosphoramidites[167] and NHS-ester-azides[168]. This strategy is effective for use as a

conjugation handle[169] but introduces spacers that make it unsuitable for the creation of triazole-backbone mimics such as those described in section 1.4.1.



Scheme 2.1: Intermolecular Staudinger Reduction of phosphoramidites.

To create these triazole-linkages an azide must be introduced without incorporating extra atoms that would create a disruption in the duplex formed from a strand containing the modification. As stated in section 1.4.1 this is mostly done using solution phase chemistry to perform the CuAAC reaction before phosphitylation, preventing the azide from coming into contact with a phosphine. This necessitates the synthesis of dimers[116-120, 123] with a distinct building block being made for every combination of nucleobase and ribose modification. A method that can use solid phase chemistry to install an azide to standard building blocks on a resin-bound oligo is to use the 5´-hydroxyl to create an azide through S_N2 reaction with an iodo intermediate[170] as seen in Scheme 2.2.



Scheme 2.2: Overview of the solid-phase OH to azide conversion process. The OH is first converted to iodo by treatment with methyltriphenoxyphosphonium iodide, then to azide by reaction with sodium azide.

This process was originally carried out on four DNA trimers: 5´-ATT-3´, 5´-CTT-3´,5´-GTT-3´, 5´-TTT-3´ where the iodo group was transformed into a variety of

functional groups including azides, thiols and sulfamides. The iodination step was found to be fast and efficient, complete within 15 minutes, and showing little dependence on the terminal nucleotide with efficiencies ranging from 92-94%.[170] The azide conversion step was found to be less efficient with a significant base dependency on the terminal nucleotide, with efficiencies of 77%, 77%, 85% and 94% for the 5′-terminal A, C, G and T respectively.[170]

One of the ways this method can be used is in oligonucleotide ligation. This allows for either creation of circular oligonucleotides by clicking the 5′- and 3′-ends of a single strand together[171] or for linear ligation of multiple sequences. [172] In order to utilise this transformation more widely, detailed studies are needed on the hydroxyl to azide conversion process, including the effect of different terminal sugars and phosphodiester analogues. With biological and therapeutic applications in mind it is also important to determine if the conversion is compatible with oligonucleotides that contain phosphorothioate backbones.

Described here is a systematic evaluation of alcohol to azide conversion with many commonly used sugars with both a phosphodiester and phosphorothioate backbone. The objective was to gain insight into the scope of this method and to evaluate potential its potential to create the azide handle necessary for the creation of triazole analogues of the phosphate backbone..

2.2 Methodology for Determination of Alcohol to Azide Conversion

Although the on-resin conversion of alcohol to azide has been studied with terminal deoxyribose (DNA) sugars in trinucleotides, it can have much broader applicability, especially as it can be used to functionalize any modified oligonucleotides that are compatible with solid phase synthesis without any additional modifications of the phosphoramidite synthesis cycle. In order to find if this method is indeed broadly applicable a number of sequences with various 5- terminal nucleotides were synthesized. The nucleobase, sugar and their respective chemical modifications were varied. All of these sequences consisted of 10 standard DNA thymidine nucleotides and one of the six modified sugars depicted in Figure 2.1.

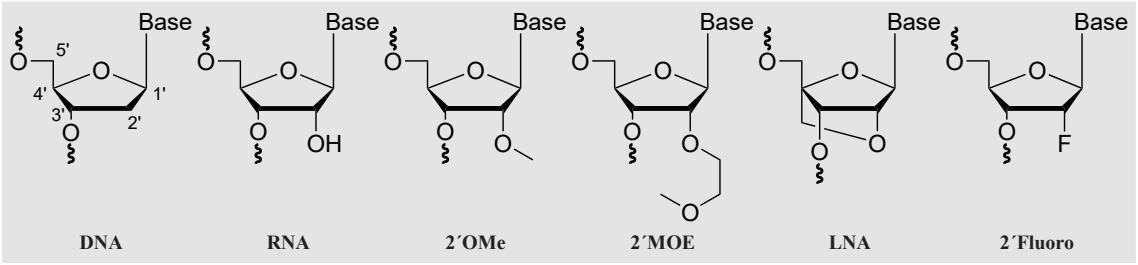


Figure 2.1: The six sugars used in the terminal 5´- position in this study. The sugars are deoxyribose (DNA), Ribose (RNA), 2´-O-Methyl (2´-OMe), 2´-O-Methoxyethyl (2´MOE), Locked Nucleic Acid (LNA), and 2´-Fluoro.

Combining the six sugars depicted in Figure 2.1 with four nucleobases and two phosphates (phosphodiester and phosphorothioate) gives a set 48 oligonucleotides in total. These modifications were selected as they are the most common in therapeutic oligonucleotides and all apart from LNA are used in FDA approved drugs.[173] Therefore they will provide useful insights into the scope and potential applications of the method. After synthesis (assembly) of these sequences the columns bearing the protected oligonucleotides with a free 5´-OH were removed from the synthesizer and dried under argon. No further treatment was necessary.

To fully utilize the advantages of solid phase organic chemistry, the hydroxyl to azide conversion was carried out with the oligonucleotide still bound to the CPG. This enables facile treatment and removal of excess reagents which can be added via syringe and the column washed multiple times to ensure no residual reactants remain in the column.

The procedure adopted involves adding reagents to the synthesis column manually via a syringe. A second syringe is attached to the other end of the column and the reagents in solution are passed back and forth through the column several times. This setup is depicted in Figure 2.2. It is important to ensure thorough and uniform contact of the reagents with the resin in the column. Once the mixing of reagents with resin is done the column is set aside for the desired time and temperature.

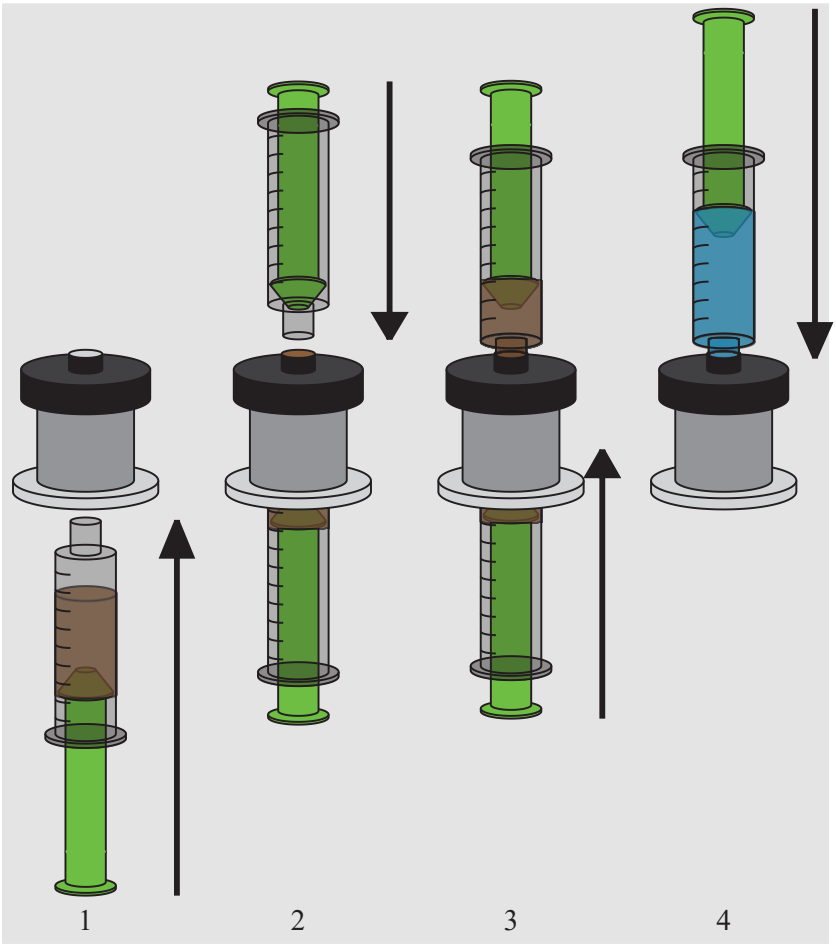


Figure 2.2: On-column reaction procedure 1) A syringe containing the reaction mixture is inserted then 2) pushed to the top of the column where a second syringe is placed. Next 3) the solution is passed through the column 4-5 times and allowed to sit for a set time.

Finally 4) the column is thoroughly washed with fresh solvent to ensure all excess reactants are removed.

This general procedure was followed in order to convert the 5´-OH to azide in the two-step process. The installation of the iodo group was achieved using a solution of 0.5 M methyltriphenoxyphosphonium iodide in DMF for 1 hour at room temperature. DMF is a good solvent in this case because of its high polarity and low volatility. This process was initially reported by Kool *et al.* with a reaction time of 15 minutes. In our case the reaction was allowed to proceed for 1 hour to ensure completion with different chemical modifications that could slow the reaction with steric or other effects. Finally, the column was washed with 5 x 1 mL of DMF, then 5 x 1mL of acetonitrile before being dried under a stream of argon for 5 minutes. The oligonucleotides were then taken directly into the azide conversion step without checking conversion to the iodo intermediate as deprotection conditions can revert the iodine back to a hydroxyl group.

Installation of the azide then proceeded using a solution of 0.5 M sodium azide in DMF. Sodium azide has limited solubility in DMF so 0.5 M represents a saturated solution. To maximise the solubility of sodium azide in DMF it was heated to 70°C for 15 minutes then cooled to room temperature. After this the column was treated with the sodium azide/DMF overnight at 55°C. After the overnight reaction the column was washed with 5 x 1 mL of DMF, 5 x 1 mL of water and then 5 x 1 mL of acetonitrile before being dried under an argon stream for 5 minutes. The aqueous wash is to ensure that all excess sodium azide is removed as it is readily soluble in water. The oligonucleotide is now ready for deprotection and evaluation of the efficiency of the azide conversion.

In order to analyse and quantify the azide conversion the oligonucleotide must first be cleaved from the resin and deprotected. For all except the RNA-containing oligonucleotides, the resin was immersed in aqueous ammonium hydroxide (~35%) for five hours at 55°C. After this time the ammonia was removed under vacuum. The

oligonucleotide was reconstituted in water and passed through a syringe filter to remove spent resin. For those sequences containing thiocarbamate protected RNA, the column was treated with a solution of 20% diethylamine in acetonitrile at room temperature for 15 minutes before being washed with acetonitrile and treated with 1:1 ethylenediamine:toluene for 6 hours at room temperature[174].

The oligonucleotide was then eluted from the column with water. In all cases the oligonucleotide was analysed by LC-MS to evaluate the conversion. Identity of peaks was determined using mass spectrometry. The trace of UV absorbance at 260 nm was integrated to determine percent composition of each peak with the peak corresponding to the target mass used to determine purity. Azide conversion percentage was determined as azide-purity/alcohol-purity x 100. A detailed description of parameters used can be found in section **6.1.4. Analysis of Oligonucleotides.** A visualisation of this process is depicted in Figure 2.3.

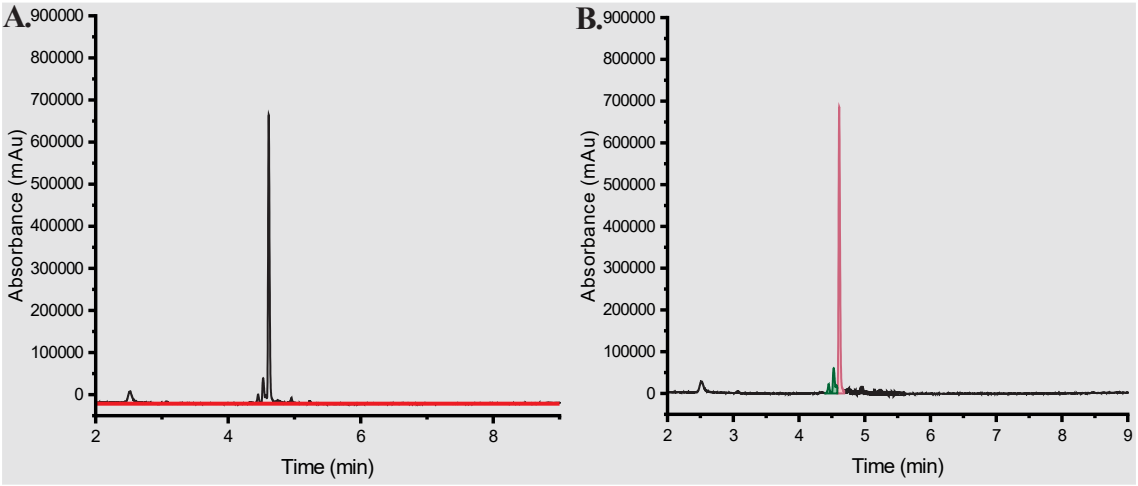


Figure 2.3. The integration process using ON-2.2 as seen in Figure 2.4 as an example using reversed-phase HPLC analysis on the Waters Xevo G2 QTof electrospray mass spectrometer. **A** shows baseline correction with the red line indicating the mean of all Y values. **B** indicates the integrated peaks. The pink shows the area contributing to the azide integral. The green indicates the area contributing to the integral of impurities (a mixture of unconverted 5´-OH and failed sequences).

Using this methodology the efficiency of conversion of 5´-OH to azide was determined for all of the sequences previously described. This allowed us to determine

any patterns, side-reactions and trends which might be related to the different sugar-phosphate chemistries.

2.3 OH to Azide Conversion for Phosphodiester Oligonucleotides

2.3.1 Oligonucleotides Used and Chromatograms of Azide Conversions of Phosphodiesters

To begin evaluation of the hydroxyl to azide conversion, 24 sequences were synthesized with phosphodiester backbones. The sequences consisted of 10 DNA thymidines with variation the 5´-nucleotide modification and nucleobase (Figure 2.4).

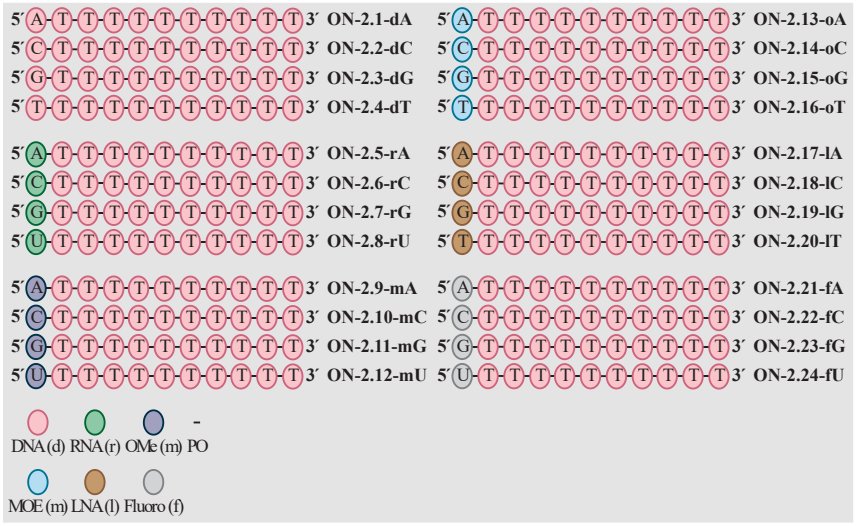


Figure 2.4: Phosphodiester oligonucleotides synthesized for the on-resin alcohol to azide conversion study.

In the selected 5´-nucleotides in this study there is a variety of 2´- modifications including 2´-O-methyl, 2´- methoxyethyl, 2´-fluoro and 2´-hydroxyl. These influence the conformation of the sugar in different ways. Chromatograms of azide conversions can be seen in Figure 2.5. LCMS analysis as described above and in the experimental chapter gave azide conversion percentages for each sequence, these are displayed in Table 2.1

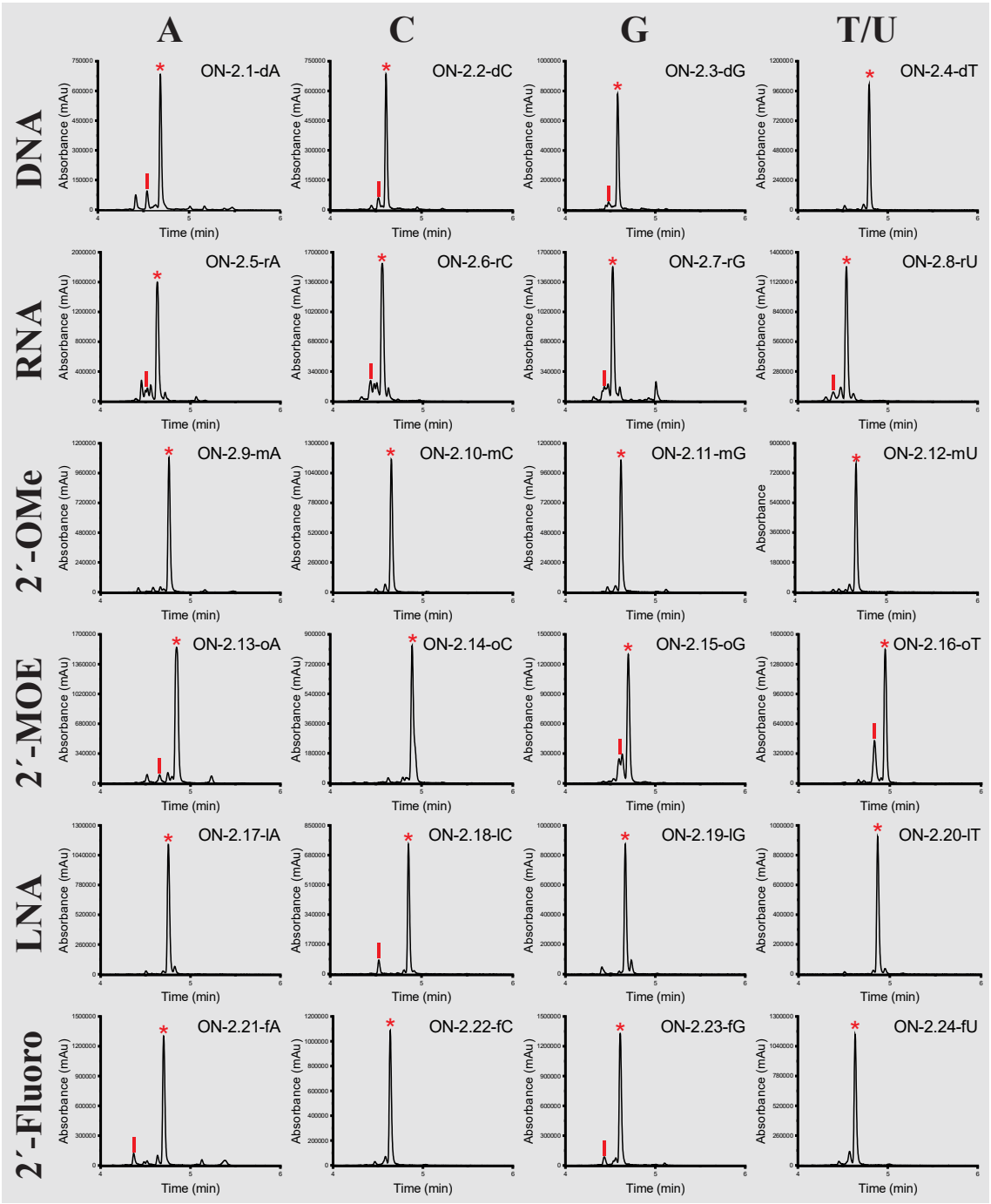


Figure 2.5: LCMS UV at A_{260} LC traces of ON-2.1 to ON-2.24 after on-resin alcohol to azide conversion procedure. Column headings of A, C, G and T/U indicate the 5´-terminal nucleobase while row headings of DNA, RNA, 2´-OMe, 2´-MOE, LNA and 2´-Fluoro indicate the 5´-terminal ribose sugar. * indicates peaks corresponding to the target mass of a 5´-terminal azide as listed in the Found Mass N_3 column of Table 2.1. I indicates peaks corresponding to the mass of the starting material, a 5´-terminal OH as indicated in the Found Mass OH column of Table 2.1.

Oligo	Calc. Mass OH	Found Mass OH	Calc. Mass N_3 (Da)	Found Mass N_3 (Da)	N_3 Conversion (%)
ON-2.1-dA	3293.2	3293.3	3318.2	3318.5	81
ON-2.2-dC	3269.2	3269.4	3294.2	3294.4	86
ON-2.3-dG	3309.2	3309.6	3334.2	3334.5	89
ON-2.4-dT	3284.2	3284.5	3309.2	3309.4	100
ON-2.5-rA	3309.2	3309.3	3334.2	3334.3	84
ON-2.6-rC	3285.2	3285.3	3310.2	3310	72
ON-2.7-rG	3325.2	3325.5	3350.2	3350.7	75
ON-2.8-rU	3286.2	3286.8	3311.2	3311.5	99
ON-2.9-mA	3323.2	3348.2	3323.8	3348.3	93
ON-2.10-mC	3299.2	3324.2	3299.4	3324.1	89
ON-2.11-mG	3339.2	3364.2	3339.2	3364.4	83
ON-2.12-mU	3300.2	3325.2	3300.3	3325.3	100
ON-2.13-oA	3367.3	3392.3	3367.2	3391.8	78
ON-2.14-oC	3357.3	3382.3	3356.8	3382.2	72
ON-2.15-oG	3383.3	3408.3	3382.8	3408.6	67
ON-2.16-oT	3358.2	3383.2	3357.6	3382.8	69
ON-2.17-lA	3321.2	3346.2	3321.3	3346.1	100
ON-2.18-lC	3311.2	3336.2	3311.5	3336.7	92
ON-2.19-lG	3337.2	3362.2	3337.3	3362.1	100
ON-2.20-lT	3312.2	3337.2	3312.3	3337.4	89
ON-2.21-fA	3311.2	3311.1	3336.2	3335.9	80
ON-2.22-fC	3287.2	3287.3	3312.2	3312.1	88
ON-2.23-fG	3327.2	3327.0	3352.2	3352	86
ON-2.24-fU	3288.1	3288.1	3313.1	3313.3	84

Table 2.1: Calculated mass, found mass and azide conversion percentage for oligonucleotides ON-2.1 to ON-2.24. N_3 conversion was calculated as (Azide Purity)/(Alcohol Purity)*100.

2.3.2. Analysis of Azide Conversions of Phosphodiester Oligonucleotides

After quantification of azide conversions, it was found that the mean conversion is 85.63% and that the nature of the sugar modification as well as the nucleobase identity has significant effect on the efficiency of the conversion. Averaging the four bases tested for each sugar gives values of 72%, 82%, 85%, 89%, 91% and 95% for 2´-MOE, RNA, 2´-Fluoro, DNA, LNA and 2´-OMe respectively. Averaging the six sugars for each base gives values of 83%, 84%, 86% and 90% for C, G, A and T/U respectively with a range of 7%. This indicates that in the case of phosphodiester there is an effect from the terminal base similar to that observed by Kool *et al.* The structural modification of the sugar contributes more significantly to the reaction efficiency, with a range of 24%. Plots of these ranges can be seen in Figure 2.6

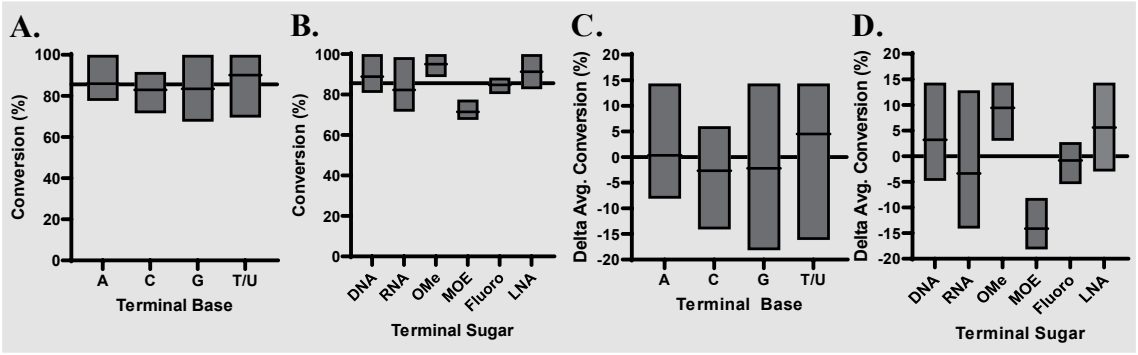


Figure 2.6: Graphical representations of 5′-alcohol to azide conversion for oligonucleotides ON-2.1 to ON-2.24. In each case the box represents the range of conversion percentage for a given group with the line across the box representing the mean. **A.** groups by terminal nucleobase with the six different sugars bucketed into A, C, G or T/U. **B.** groups by terminal sugar where the four nucleobases are bucketed into DNA, RNA, 2′-OMe, 2′-MOE, 2′-Fluoro and LNA. For both **A.** and **B.** a line across the plot is at 85.63%, the average of all conversion percentages. **C.** and **D.** are grouped the same as **A.** and **B.** respectively. For each condition of **C.** and **D.**, the total average of 85.63% was subtracted to give the delta to the average conversion. Lines across the plots of **C.** and **D.** are at 0%.

As shown in Figure 2.6, the influence of the sugar is larger than that of the base, however both have an some effect in shaping the total conversion percentage. For the averaged bases, the order is C≈G < A < T. Thymidine/uridine is the best performer on aggregate, though interestingly it is only the best in three out of the six sugar modifications (DNA, RNA and LNA). This is due to the fact that in the cases where it does not have the best conversion (2′-OMe, 2′-MOE and 2′-Fluoro) the range between the four bases is lower. The ranges from highest to lowest nucleobase in a given sugar for DNA, RNA and LNA are 19%, 27% and 17% respectively while for 2′-OMe, 2′-MOE and 2′-Fluoro they are 11%, 10% and 8% respectively. When all six examples per base examined as a group, the difference between the four averages is only 7%. If the only factor was the nucleobases, it would be expected to see the same difference in each sugar group and across the grand average meaning that the terminal base only has a minor effect on reaction efficiency.

When all bases in a group are averaged, the order of ribose sugars is 2′-MOE << RNA < 2′-Fluoro < DNA < LNA < 2′-OMe. It should be noted that 2′-MOE is a

significantly worse performer than the rest, with the average of 2´-MOE being 11% lower than RNA, the next lowest conversion average and the mean difference between sugars only being 4%. The same analysis as with nucleobase effect was conducted for ribose modification with the difference between all six sugars averaged in a given base being 20%, 22%, 31% and 33% for C, A, T/U and G respectively and the difference between the four bases averaged within a sugar being 24%. Although these differences are not exactly uniform they are significantly closer than with nucleobases, meaning the ribose sugar exerts a larger effect on the reaction.

2.3.2.1 Effects of the Nucleobase on Azide Conversion of Phosphodiester Oligonucleotides

The most obvious division between nucleobases is between purines and pyrimidines, where it might be expected that the added bulk of the purines could introduce steric hindrance, lowering the efficiency of the reaction. However, that does not seem to be the case as C and G are the worst performers. Nucleobases can occupy one of two positions, the *syn* or *anti* conformation[175] with free rotation about the glycosidic bond allowing transition between the two. Although the *syn* conformation can be found, especially on purine bases with tertiary interactions, *anti* is far more common.[176] In the *anti* conformation the extra purine ring is rotated away from the 5´, terminus of the sugar, perhaps explaining why there is no obvious difference in relation to pyrimidines.

It is not entirely clear what is the cause of the observed differences. Cytidine and thymidine both have oxygens substituents on the C2 position but are exhibit the worst and best conversions respectively so does not appear to have influence. Adenine, cytosine and guanosine all contain a primary amine, however this should not have much effect as no reagents used contain hydrogen bonding groups. In total the difference between bases

is small and so it is likely that no one feature of a nucleobase exerts a significant influence on the conversion process.

2.3.2.2 Effects of the Ribose Sugar on Azide Conversion of Phosphodiester Oligonucleotides

In the case of the sugars, it seems that the most important quality of 2´-modifications on the ribose sugar is size followed by being an electron donor. By far the worst performer is the 2´-MOE modification. This modification has a carbon chain with a high degree of rotational freedom that could be contributing to steric hinderance at the 5´-position. The next two are the most electron withdrawing modifications of the thiomorpholine-4-carbothioate (TC) protected 2´-hydroxyl and 2´-fluoro groups. Then follow the neutral DNA sugar with LNA coming next followed by 2´-OMe with the highest conversion efficiency. Among these modifications there does not appear to be a clear reason for the ranking. The two most electronegative modifications (TC-RNA and 2´-Fluoro) perform slightly worse than the DNA sugar, however the LNA and 2´-OMe modifications are also weakly electron withdrawing compared to the 2´-hydrogen of the DNA and these perform better. In addition these modifications are five bonds removed from the reactions site and so the electronics of the 2´-substituent should not have a large effect.

Another factor to consider is the ribose sugar conformation, though with the 24 oligonucleotides examined in this section this does not appear to be influential. Of the six sugars, DNA sugars are considered to be mostly in the C2´-*endo* in nature, 2´-OMe, 2´-MOE and RNA sugars are weakly C3´-*endo* promoting, and LNA and 2´-Fluoro sugars are strongly C3´-*endo* promoting.[177, 178] When compared with the ordering of performance there appears to be no correlation to this categorization.

For oligonucleotides with a phosphodiester backbone, robust conversion of the 5´-alcohol to an azide can be achieved however it is not equal for all nucleobases and ribose sugar modifications. For best results the terminal base should be a thymidine or uracil with a small electron donating group such as an O-methyl group at the 2´-position of the sugar.

2.4 OH to Azide Conversion of Phosphorothioate Oligonucleotides

2.4.1. Oligonucleotides Used and Chromatograms of Phosphorothioate Azide Conversions

As before with the phosphodiester sequences, a set of 24 oligonucleotides were synthesized with 10 DNA sugars and variations at the terminal base and sugar, all linked with phosphorothioate backbones. This can be seen in Figure 2.7.

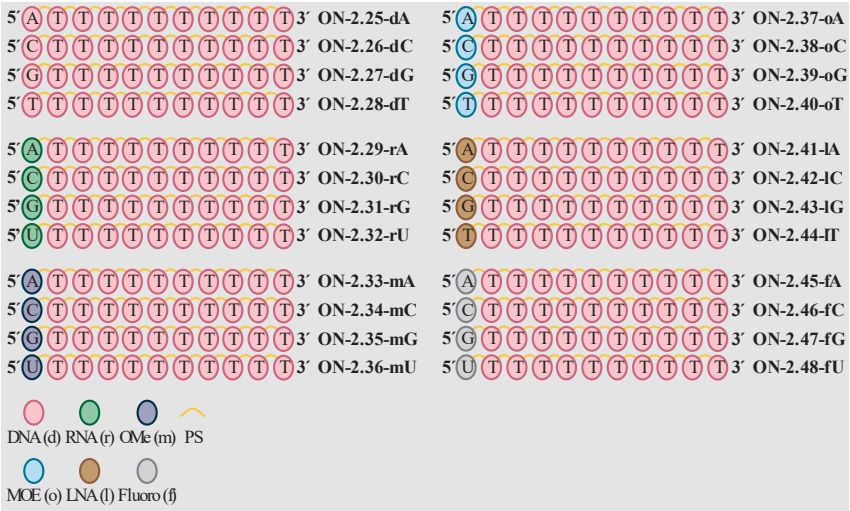


Figure 2.7: Phosphorothioate oligonucleotides synthesized for the on-resin alcohol to azide conversion study

Like with the phosphorothioate (PO) backbone oligonucleotides, a systematic study was conducted to assess the effect of the nucleobase and the sugar. As the phosphorothioate modification is ubiquitous for therapeutic antisense oligonucleotides addressing the compatibility could potentially open many new applications. Chromatograms of conversions can be seen in Figure 2.8 and conversion percentages can be seen in Table 2.2.

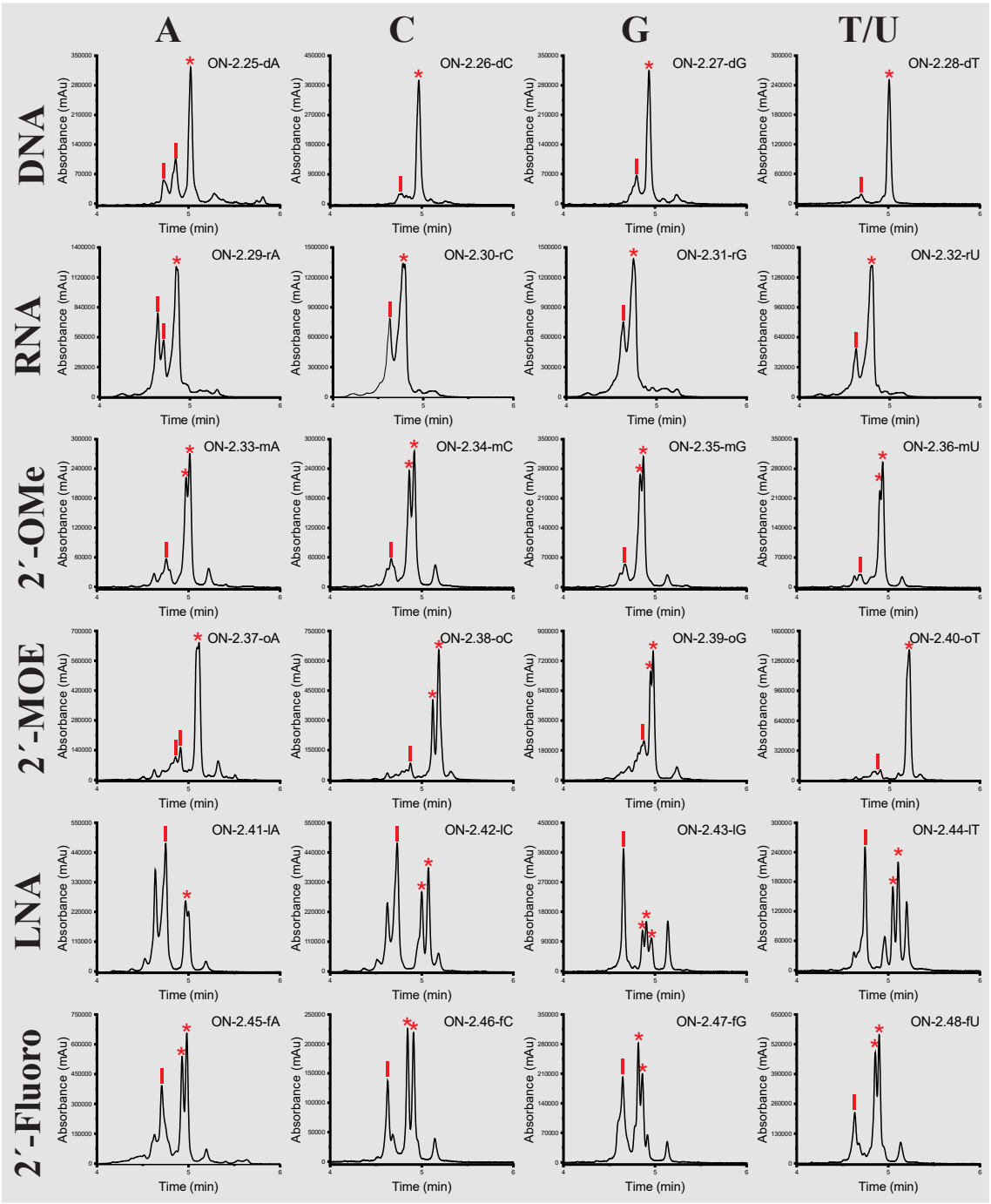


Figure 2.8: LCMS UV at A_{260} LC traces of ON-2.25 to ON-2.48 after on-resin alcohol to azide conversion procedure. Column headings of A, C, G and T/U indicate the 5´-terminal nucleobase while row headings of DNA, RNA, 2´-OMe, 2´-MOE, LNA and 2´-Fluoro indicate the 5´-terminal ribose sugar. * indicates peaks corresponding to the target mass of a 5´-terminal azide as listed in the Found Mass N_3 column of Table 2.2. | indicates peaks corresponding to the mass of the starting material, a 5´-terminal OH as indicated in the Found Mass OH column of Table 2.2.

Oligo	Calc. Mass OH (Da)	Found Mass OH (Da)	Calc. Mass N_3 (Da)	Found Mass N_3 (Da)	N_3 Conversion (%)
ON-2.25-dA	3453.8	3453.5	3478.8	3479.1	54.91
ON-2.26-dC	3429.8	3430.1	3454.8	3454.9	83.40
ON-2.27-dG	3469.8	3469.4	3494.8	3494.4	69.31
ON-2.28-dT	3444.8	3444.6	3469.8	3469.7	85.43
ON-2.29-rA	3469.8	3470.0	3494.8	3494.8	69.67
ON-2.30-rC	3445.8	3445.8	3470.8	3470.8	70.73
ON-2.31-rG	3485.8	3485.7	3510.8	3511.8	61.83
ON-2.32-rU	3446.8	3446.6	3471.8	3471.6	78.58
ON-2.33-mA	3483.8	3483.0	3508.8	3509.7	69.40
ON-2.34-mC	3459.8	3459.0	3484.8	3484.0	73.53
ON-2.35-mG	3499.8	3500.5	3524.8	3523.7	76.19
ON-2.36-mU	3460.8	3461.3	3485.8	3487.3	91.63
ON-2.37-oA	3527.9	3528.1	3552.9	3553.0	63.90
ON-2.38-oC	3517.9	3518.1	3542.9	3542.8	75.63
ON-2.39-oG	3543.9	3543.9	3568.9	3569.6	62.41
ON-2.40-oT	3518.9	3518.7	3543.9	3544.0	78.07
ON-2.41-lA	3481.8	3481.2	3506.8	3507.2	32.27
ON-2.42-lC	3471.8	3472.3	3496.8	3496.1	43.82
ON-2.43-lG	3497.8	3496.6	3522.8	3524.1	25.00
ON-2.44-lT	3472.8	3471.8	3497.8	3498.5	38.85
ON-2.45-fA	3471.8	3470.6	3496.8	3495.9	44.24
ON-2.46-fC	3447.8	3447.0	3472.8	3474.1	60.55
ON-2.47-fG	3487.8	3487.4	3512.8	3512.7	47.21
ON-2.48-fU	3448.8	3447.5	3473.8	3473.9	64.00

Table 2.2: Calculated mass, found mass and azide conversion percentage for oligonucleotides ON-2.25 to ON-2.48. N_3 conversion was calculated as (Azide Purity)/(Alcohol Purity)*100. Full Chromatograms of alcohols and azides can be seen in

2.4.2 Analysis of Azide Conversion Results with Phosphorothioate Oligonucleotides

Quantification of conversions reveals the mean conversion to be 63% with a large discrepancy between different nucleobases and sugar modifications. Averaging the four bases tested for each sugar gives values of 35%, 54%, 70%, 70%, 73% and 78% for the sugars LNA, 2´-Fluoro, 2´-MOE, RNA, DNA and 2´-OMe respectively. Averaging the six sugars for each base gives values of 56%, 57%, 68% and 73% for A, G, C and T/U respectively. In this case, conversion efficiency of phosphorothioate oligonucleotides is heavily influenced by the terminal sugar with a smaller but still very impactful impact coming from the terminal nucleobase. The range for the highest and lowest values of average azide conversion of the four bases within a sugar is 43% while the range for the average azide conversion of the six sugars within a given nucleobase is 17% supporting the above observation. Plots of average conversions across bases and sugars for phosphorothioate oligonucleotides can be seen in Figure 2.9.

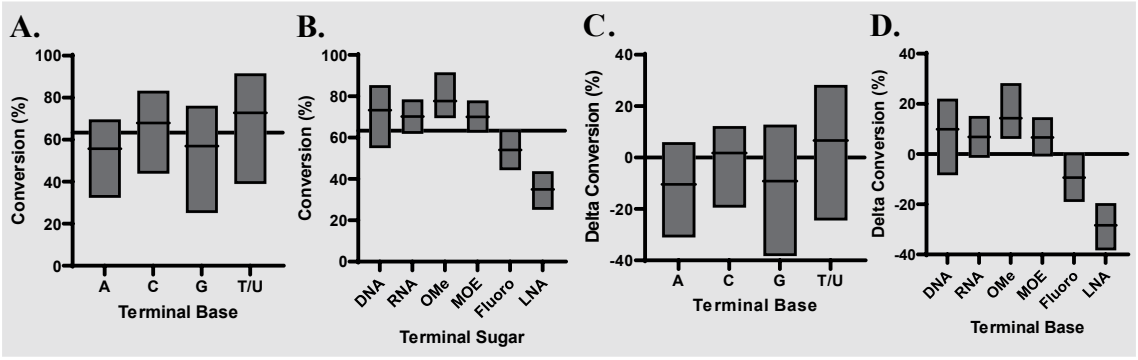


Figure 2.9: Graphical representations of 5´-alcohol to azide conversion for oligonucleotides ON-2.24 to ON-2.48. In each case the box represents the range of conversion percentage for a given group with a the line across the box representing the mean. **A.** groups by terminal nucleobase with the six different sugars bucketed into A, C, G or T/U. **B.** groups by terminal sugar where the four nucleobases are bucketed into DNA, RNA, 2´-OMe, 2´-MOE, 2´-Fluoro and LNA. For both **A.** and **B.** a line across the plot is at 63%, the average of all conversion percentages. **C.** and **D.** are grouped the same as **A.** and **B.** respectively. For each condition of **C.** and **D.**, the total average of 63% was subtracted to give the delta to the average conversion. Lines across the plots of **C.** and **D.** are at 0%.

A split in the nucleobases can be seen along the lines of purines and pyrimidines. Again thymidine/uridine is the best performer on average and is the best performer for all individual sugar groups except for that of LNA where cytidine performs 5% better than thymidine. Overall the difference of these two bases is small, with a 5% difference from the averages of the six sugars in each group. Additionally, the difference is only above 10% in the case of the 2´-OMe sugar where it is 18%. It is similar between adenosine and guanosine with a difference of only 1% between the averaged six sugars of the two and the only difference in any individual sugar group larger than 10% being that of DNA at 14%. If purines and pyrimidines across all sequences are averaged a difference of 14% emerges suggesting that the steric bulk of the larger pyrimidines is having an influence on the azide conversion for the phosphorothioate sequences.

What is also clear from these plots is the strong effect of the sugar modifications. In particular 2´-Fluoro and LNA sugars performed very poorly across all bases. This is indicative that unlike with the phosphodiester backbone there is a powerful influence

coming from the conformation of the ribose sugar, likely due to side reactions promoted by the combination of sugar conformation and phosphorothioate.

2.4.3. Unintended Reactions Stemming from Phosphorothioate Backbones

It can be observed that when subjected to the azide conversion conditions some product is observed, however a majority of the remaining sequence has a mass corresponding to the unreacted starting material. An example chromatogram of this phenomenon is shown with ON-2.42-fC in Figure 2.16.

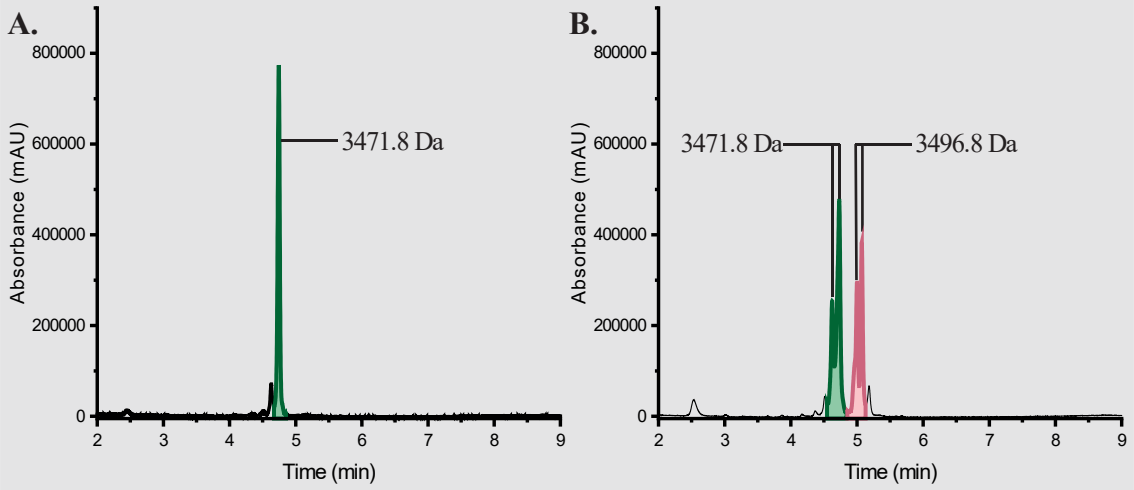


Figure 2.16: Chromatograms of ON-2.42-fC, a phosphorothioate oligonucleotide with LNA-C at the 5´-terminal position. **A.** shows 5´-alcohol before azide conversion. **B.** is the mixture of products after conversion. Peaks filled in with colour are labelled with the observed mass. 3471.8 Da corresponds to the 5´-alcohol oligonucleotide, 3496.8 Da corresponds to the 5´-azide oligonucleotide.

As the only difference to the phosphodiester oligonucleotides is the oxygen to sulfur switch this is likely to be the source of interference in the conversion process. A potential cause of this interference could stem from the interaction of the sulfur of the phosphorothioate backbone with intermediary iodo transformation step. The C3´-*endo* or 'north' conformation promoted most strongly by LNA but also by the 2´-Fluoro modification results in a puckered sugar that brings the sulfur much closer in proximity to the 5´-position than with a neutral 'central' conformation.[179] This shift in conformation

can introduce more steric strain on the reaction when combined with athe larger sulfur atom, preventing good efficiency of conversion This is depicted with DNA and LNA examples in Figure 2.17.

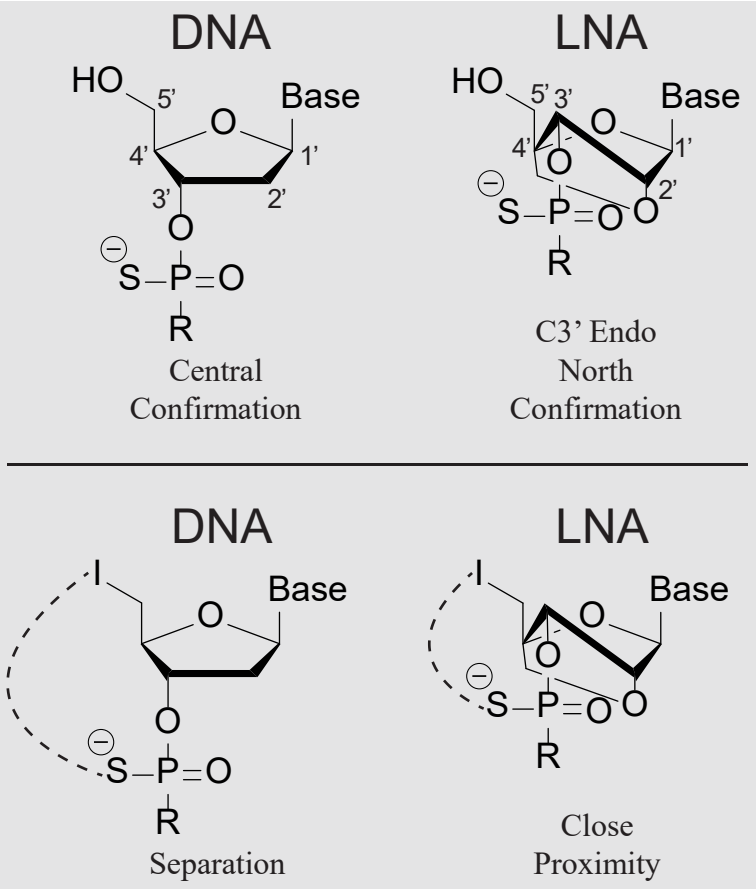


Figure 2.17: Sugar conformations with the 'central' DNA and the C3´-*endo* 'north' conformation of LNA. Dashed lines indicate spacing between sulfur and 5´-iodo intermediate.

Overall, it can be observed that this method can be used with phosphorothioate oligonucleotides, however terminal base and sugar selection is far more important than with its phosphodiester counterpart. Conditions do exist where over 90% conversion is possible but there is a strong effect from the conformation of the ribose sugar as well as slight bias towards pyrimidines over purines. These are factors that must be kept in mind when designing phosphorothioate sequences for azide conversion but do not preclude combination of the two.

2.5 Conclusion

Chapter 2 describes an exploration of using solid phase chemistry to install an azide modification to the 5´-end of chemically synthesized oligonucleotides. Azide groups are not compatible with the phosphorus(III) species found in phosphoramidtes used in standard oligonucleotide solid phase synthesis meaning that alternative N_3-functionalisation methods are required. Most current techniques use linkers or spacers to add azide which is unsuitable to the introduction of a triazole as a replacement for the phosphodiester backbone. This issue can be avoided by converting the 5´-terminal alcohol of a resin bound oligonucleotide to an azide. A method has been described in literature via an iodo intermediate, but its scope has not yet been explored with many of the common chemical modifications employed, especially for use in therapeutic antisense oligonucleotides. In order to assess compatibility a systematic study was conducted.

This study involved synthesis of various sequences containing 10 DNA T sugars with variation at the 5´-terminal base and sugar to assess how each affects conversion. Six of the most common ribose sugars were assessed: DNA, RNA, 2´-OMe, 2´-MOE, 2´-Fluoro and LNA. In addition to being widely used, these sugars also cover a spectrum of steric and conformational factors. For each sugar all four canonical nucleobases were tested: adenosine, cytosine, guanosine and either thymidine or uracil depending on the sugar. For each permutation azide conversion was assessed via LCMS , starting with the naturally occurring phosphodiester backbone.

Conversion across the 24 oligonucleotides studied with phosphodiester backbones proceeded generally well for most sugars and bases with a total average of 86%. While there was some influence of the terminal nucleobase it was fairly minimal. More variation was encountered when looking at differences between sugar modifications. In particular the chain of the 2´-MOE sugar hampered conversion resulting in the poorest efficiency across the six. The best performer was the 2´-OMe sugar groups with an average

conversion of 95% across the four bases. After this the process was repeated with the same sugar and base combinations paired with a phosphorothioate backbone.

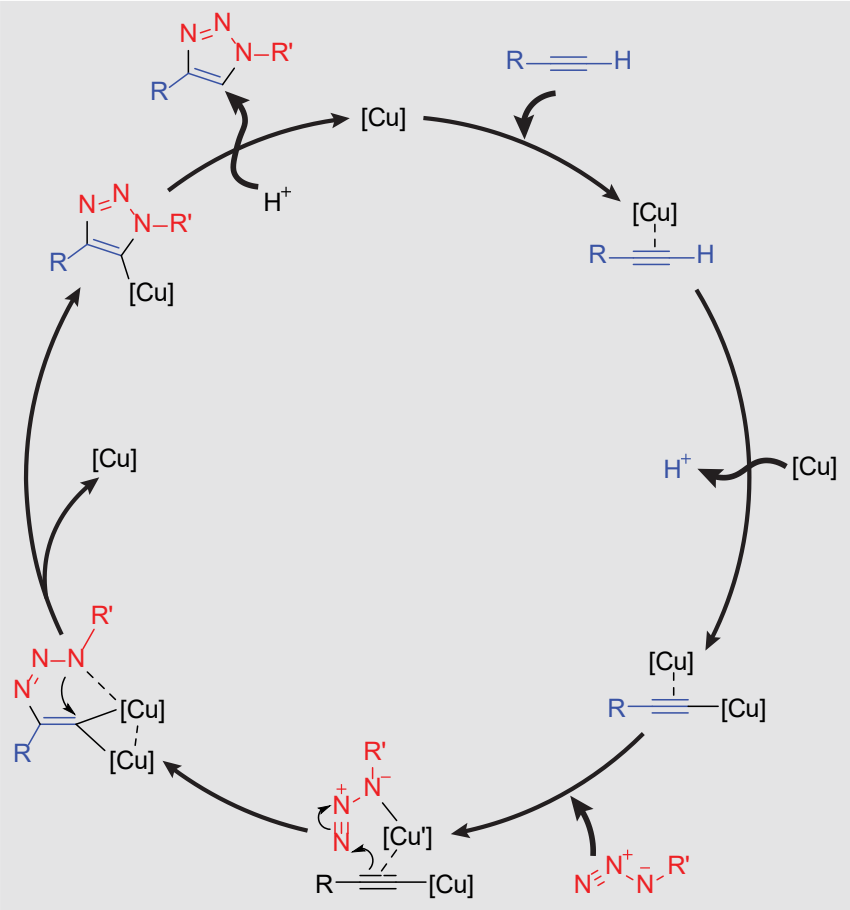
Conversion efficiency of phosphorothioate containing oligonucleotides contained far more variation than with the phosphodiesters with an average of 63%. A stronger bias in the nucleobases was observed along the pyrimidine/purine split, with preference shown for the smaller, less bulky pyrimidines. There was also a much larger influence from the terminal sugar. When combined with a strongly C3´ *endo* promoting sugar, phosphorothioate give very little alcohol to azide conversion. This is hypothesized to be due steric clashes of the larger sulfur atom when it is brought closer to the 5´-position by these C3´-*endo* conformed riboses. If these puckered sugars are avoided good conversion can be achieved, especially with thymidine bases, the best of which is 2´-OMe-thymidine which gave 92% desired product.

This method of converting the terminal 5´-alcohol to an azide while the oligonucleotide is fixed to resin can be used for a much broader set of chemistries than tested in the original description, however not all will give equal conversion. If it is being used with a phosphodiester oligonucleotide robust conversion is possible in most cases, as long as there are no large modifications near the terminal C5´. Phosphorothioate containing oligonucleotides can also be used in conjunction with this method provided strongly C3´ *endo* promoting ribose sugars are avoided in the terminal position. These studies expand the scope of the method and show it can be used for a much broader set of applications than previously explored.

Chapter 3: On-Resin Copper Click Reactions to Give Internucleoside Triazole Linkages

3.1 Introduction

Reported in 2002 by Professor Medal in Denmark[99] and Professor Sharpless in the USA[98], Copper-catalysed Azide-Alkyne Cycloaddition (CuAAC) quickly took off as a fast, efficient and easily accessible form of Professor Sharpless's concept of click chemistry. The process uses copper (I) to promote the formation of 1,4-1,2,3-triazoles between terminal azides and alkynes with a wide variety of substituents and reaction conditions with a catalytic cycle described in Scheme 3.1.



Scheme 3.1: The CuAAC catalytic cycle adopted from literature.[180]

This technique is useful in nucleic acid chemistry with applications developed around the introduction of click-compatible groups within a nucleic acid chain. Most often this takes the form of alkyne modifications due to the unwanted Staudinger reaction described last chapter. Options include placing the alkyne on the C5 position of uridine[181] or the 7 position of deaza guanosine or adenosine.[182] In these cases alkynes can be added

by Sonogashira Coupling. In particular this approach was used by Carrell et al to produce a method using different alkyne protection groups in conjunction with a resin-bound oligonucleotide to label a single oligonucleotide strand with three distinct conjugates.[183] Alkynes on carbon linkers have also been used to add groups like peptides and dyes to oligonucleotides.[184-186] All of these, however, are predicated on having an alkyne, not an azide in the strand and are not amenable to incorporation of a clickable group in the backbone of the oligonucleotide.

This is of particular importance for the use of click chemistry to introduce triazole linkages into an oligonucleotide which maintains polymerase compatibility but improves nuclease stability.[171, 187] Triazole linkages have been introduced into oligonucleotide backbones before using different methods. One option described by Isobe Et Al is to create monomers with azides at the 3´-position and alkynes at the 5´ which can then be clicked together to give a fully triazole-linked oligonucleotide.[121] This however precludes the triazole backbone to be combined with phosphodiesters or other backbones. Another option is to synthesize a dimer using a 5´-azide monomer and a 3´ alkyne monomer.[122, 188] These can be joined in solution phase and phosphitylated to give a phosphoramidite that can be incorporated with standard solid phase oligonucleotide synthesis.

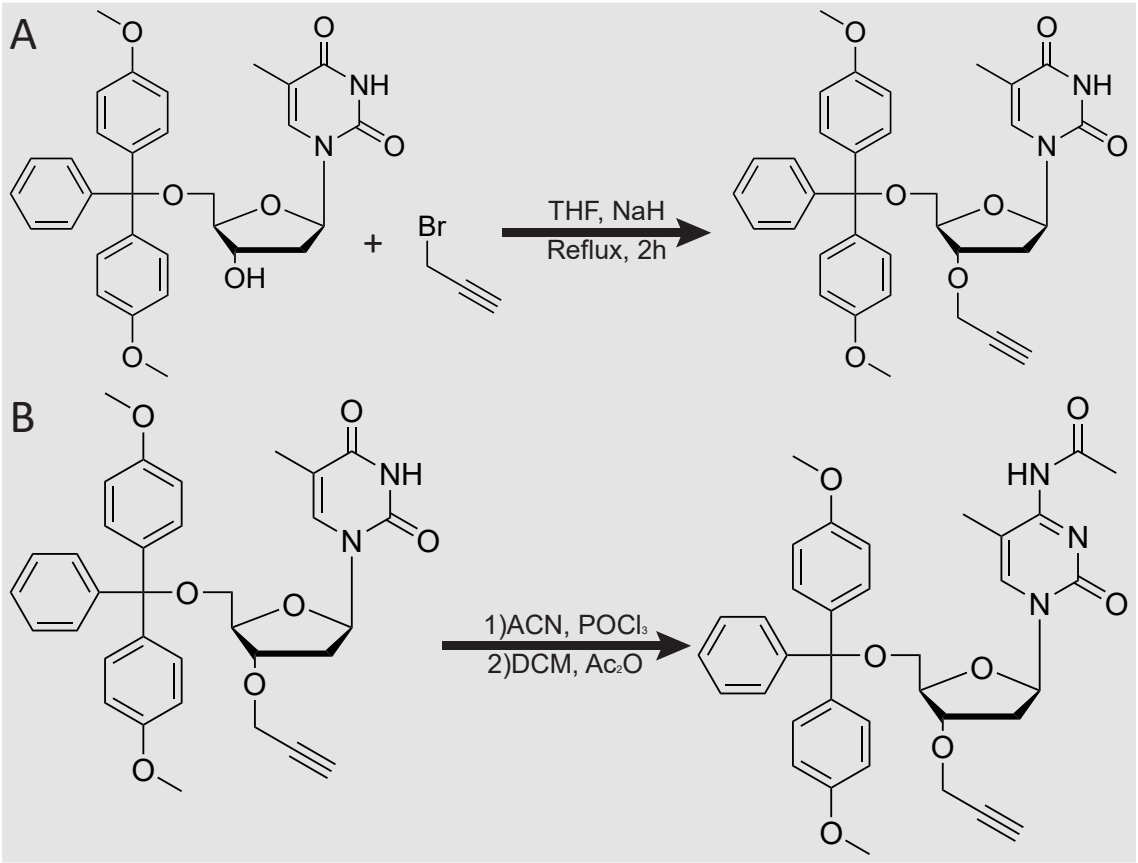
This method is advantageous as it allows triazoles to be incorporated with other linkages but the 5´-azide moiety developed in the last chapter gives the opportunity to create a triazole linkage in a more convenient way. Instead of synthesizing a dimer, the terminal azide can be clicked with an alkyne monomer while the sequence is attached to the resin. As before this allows for easy introduction and removal of a large excess of reagents. It also allows for greater flexibility as it does not necessitate the synthesis of a new dimer for every combination of chemistry or nucleobases desired in a given sequence.

Additionally, previous work has shown that while introducing a triazole linkage does lower the thermal stability of duplexes formed by the sequence, modifications of the 3´-side of the backbone can rescue the melting temperature, while those on the 5´ side have little to no effect.[123] This is a further benefit to this method as the modified sugars can be incorporated by standard solid phase synthesis and then converted to an azide as opposed to as a phosphitylated dimer. These can be combined with a single alkyne monomer to create a triazole with improved duplex thermal stability, an important measurement in determining performance in applications for PCR and for Antisense Oligonucleotide Therapeutics.

In this chapter, sequences containing terminal azides from the previous chapter were used in combination with click chemistry to assess its viability across various terminal bases and sugars. Then a series of oligonucleotides were synthesized with a triazole linkage in the middle to assess the effect of the 3´ sugar on the thermal stability of the duplex.

3.2 Initial On-Resin Copper Click Reactions with Phopshorothioate Oligonucleotides

To begin the assessment of click conversions the alkyne monomer building blocks were synthesized as previously described.[189] Two were used in this study, thymidine and 5-methyl-cytidine with an alkyne on the 3´ alcohol as seen in Scheme 3.2

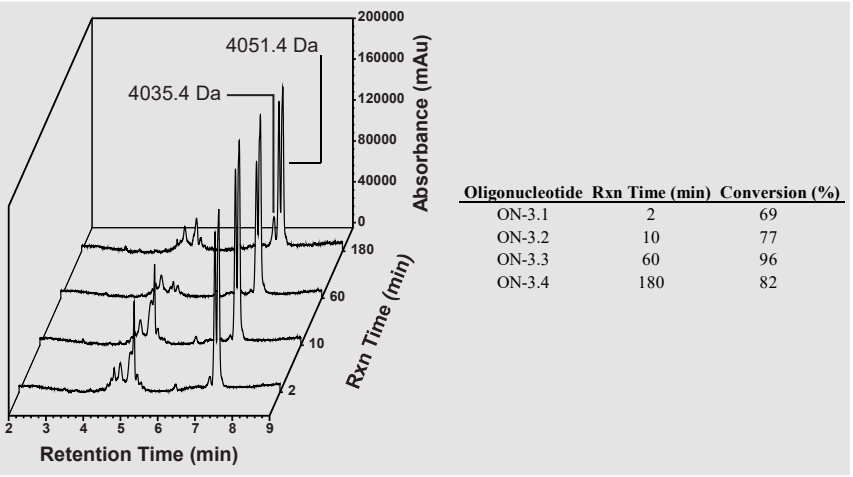


Scheme 3.2: A. Synthesis of the Alkyne T monomer with propargyl bromide and 5´-DMT protected T. B. Conversion of thymidine to 5-methyl-cytidine with phosphorus oxychloride followed by protection of the amine with acetic anhydride.

Once the monomers were obtained the on-resin reactions were conducted and analysed by the same methods described in the last chapter. In this instance the clicks were performed by combining a solution of 25 mM alkyne and 12.5 mM copper catalyst, copper(I)bromide dimethyl sulfide in 0.5 mL of DMSO per reaction. After the reaction was complete each oligonucleotide was washed with 5 X 1 mL of DMSO, 5 X 1 mL of 10mM Na_2EDTA in H_2O, 5 X 1 mL of H_2O, and 5 X 1 mL of ACN before being dried with an argon stream.

Phosphorothioate oligonucleotides can present a challenge for copper related chemistry as the introduction of copper can lead to loss of sulfur on the backbone.[190] This can be avoided with selection of the right copper ligands and dimethyl sulphide was found to have the best results in literature.[191] It is important to ensure compatibility with phosphorothioate to broaden the applicability to include therapeutics dependent on this motif.

In a similar fashion, it was shown that the amount of copper is not critical, with anything between 2.5 and 10 equivalents giving good results[191] and so a concentration of 12.5 mM or 6.25 equivalents was chosen as solubility limitations in DMSO prevent a full 10 equivalents from being achieved. The concentration of alkyne was doubled relatively to ensure that it would not limit the rate of reaction with a large 12.5 fold excess relative to the azide bound resin. Reaction time is important as despite the dimethyl sulfide ligand, loss of sulfur with phosphorothioate oligonucleotides will occur if left too long. Different reaction times were tested by splitting CPG from the same oligonucleotide synthesis run into different synthesis columns and conducting reactions with the same conditions of 12.5 mM copper(I)bromide dimethyl sulfide and 25 mM DNA-thymidine alkyne as described above. At timepoints 2 minutes, 10 minutes, 60 minutes and 180 minutes the reaction was halted by washing the column with the above protocol of DMSO, Na_2EDTA, H_2O and ACN. Results can be seen in Figure 3.1.



Oligonucleotide	Rxn Time (min)	Conversion (%)
ON-3.1	2	69
ON-3.2	10	77
ON-3.3	60	96
ON-3.4	180	82

Figure 3.1: Reaction times and conversion corresponding conversion percentages (click purity/azide purity multiplied by 100) for oligonucleotides ON-3.1 to ON-3.4. Chromatograms show the A_{260} UV trace, with 4051.4 Da corresponding to the desired mass and 4035.4 Da (-16 Da) corresponding to the desired mass with the one sulfur-oxygen conversion.

Reaction optimization was carried out on the oligonucleotide ON-2.28-dT obtained in the previous chapter. After 60 minutes starting material is nearly consumed and it is only after 180 minutes that a significant amount of sulfur-oxygen conversion takes place. As the oligonucleotides were analyzed with the 5´-DMT group attached which gives isomers that lead to the peak splitting observed.

The on-resin click reaction was then tested across the different terminal nucleobases and ribose sugars sugars of phosphodiester oligonucleotides as was done with the azide conversion in Chapter 2. Unlike the azide conversions in Chapter 2 the click reaction was not tested with these 5-variations in phosphorothioate oligonucleotides as many exhibited poor azide conversion. As the usefulness of phosphorothioate oligonucleotides most lies in therapeutic applications, the triazole modification was brought directly into antisense oligonucleotides that will be described in Chapter 4.

3.3 On-Resin CuAAC Reactions with Phosphodiester Oligonucleotides

To begin the process all 24 phosphodiester azide oligonucleotides were taken without further treatment and reacted with 25 mM of the thymidine alkyne and 12.5 mM of the copper bromide dimethyl sulphide catalyst for 1 hour as previously described. Sequences are shown in Figure 3.2.

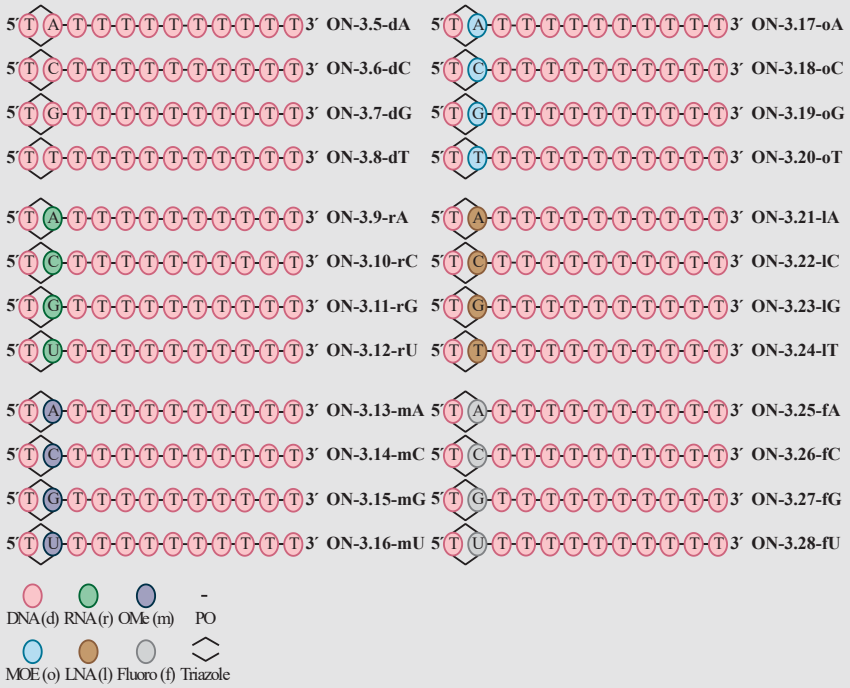


Figure 3.2: Phosphodiester sequences used in the study of CuAAC addition of thymidine in this chapter.

After the reactions were finished and evaluated via LC-MS as described in the previous chapter and section **6.1.4. Analysis of Oligonucleotides.** Chromatograms of the click reactions can be found in Figure 3.3. Calculated mass, found mass and CuAAC conversion percentage can be found in Table 3.1.

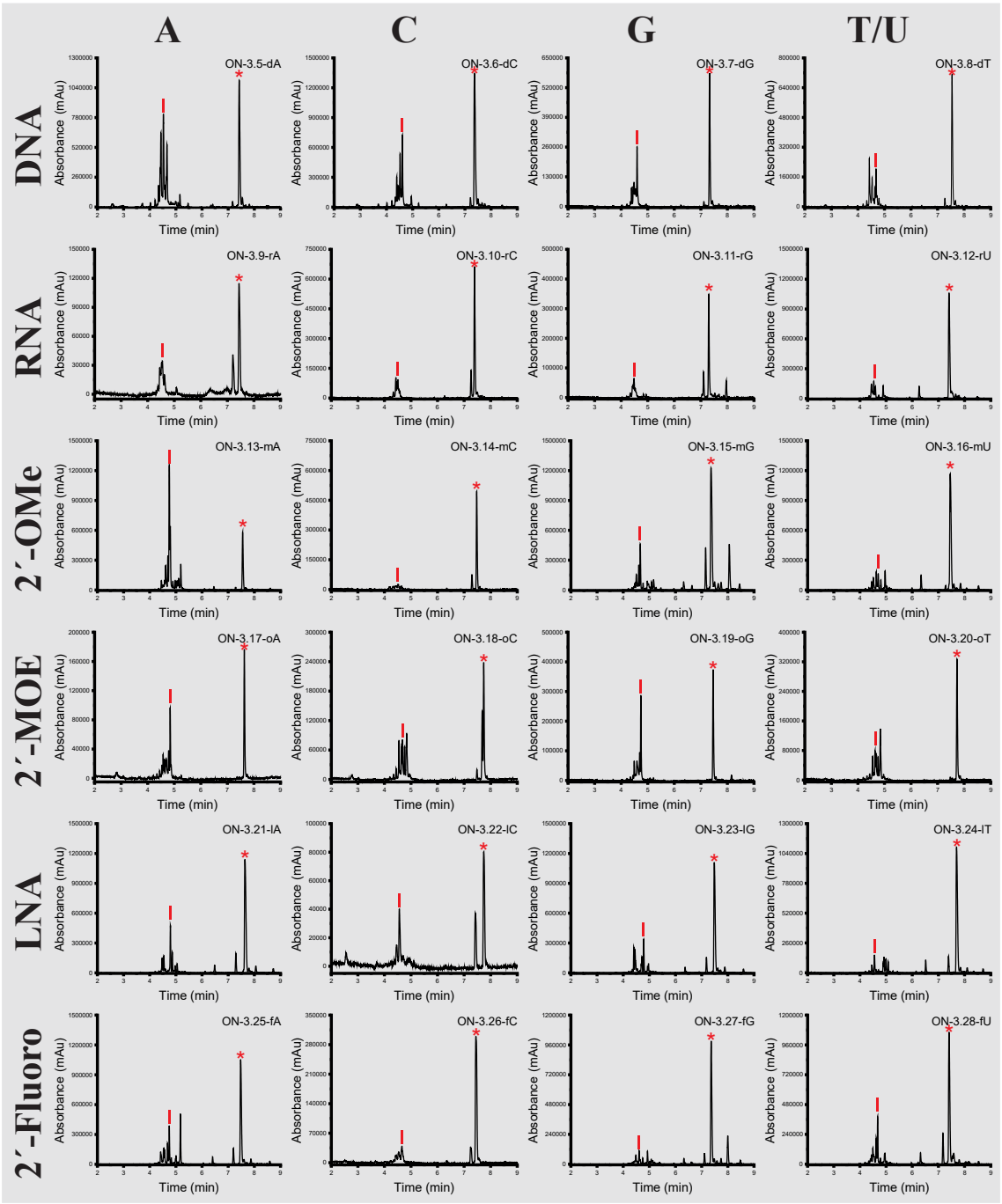


Figure 3.3: UV at A_{260} LC traces of ON-3.5 to ON-3.28 after on-resin CuAAC addition of a thymidine base. Column headings of A, C, G and T/U indicate the 5´-terminal nucleobase while row headings of DNA, RNA, 2´-OMe, 2´-MOE, LNA and 2´-Fluoro indicate the 5´-terminal ribose sugar. * indicates peaks corresponding to the target mass of the addition of a DNA thymidine with a triazole linkage at the 5´-end of the sequence as show in the Found Mass Click column of Table 3.1.**I** indicates peaks corresponding to the mass of the starting material, a 5 azide as shown in the Found Mass N_3 column of Table 3.1. Additional peaks likely stem from a mixture of failed sequences as either a 5´-alcohol, 5´-azide or with the thymidine added by CuAAC

Oligo	Calc. Mass Click	Found Mass Click	Click Conversion (%)
ON-3.5-dA	3900.8	3901.0	40
ON-3.6-dC	3876.8	3876.9	55
ON-3.7-dG	3916.8	3917.0	59
ON-3.8-dT	3891.8	3892.0	50
ON-3.9-rA	3916.8	3917.3	62
ON-3.10-rC	3892.8	3893.1	98
ON-3.11-rG	3932.8	3933.1	87
ON-3.12-rU	3893.8	3893.9	71
ON-3.13-mA	3930.9	3931.1	55
ON-3.14-mC	3906.8	3907.2	43
ON-3.15-mG	3946.8	3947.2	63
ON-3.16-mU	3907.8	3908.0	63
ON-3.17-oA	3974.9	3975.3	61
ON-3.18-oC	3964.9	3965.8	64
ON-3.19-oG	3990.9	3991.3	68
ON-3.20-oT	3965.9	3966.4	67
ON-3.21-lA	3928.8	3929.2	19
ON-3.22-lC	3918.8	3919.2	76
ON-3.23-lG	3944.8	3945.2	43
ON-3.24-lT	3919.8	3920.1	70
ON-3.25-fA	3918.8	3919.2	58
ON-3.26-fC	3894.8	3894.9	78
ON-3.27-fG	3934.8	3935.2	68
ON-3.28-fU	3895.8	3896.0	56

Table 3.1: Calculated mass, found mass and CuAAC conversion percentage for oligonucleotides ON-3.5 to ON-3.28. Click Conversion was calculated as (Click Purity)/(Azide Purity)*100. Chromatograms of the click reactions can be seen in Figure 6.9.

3.3.1. Analysis of On-Resin CuAAC Reactions

After analysing click conversion percentage across all of the sequences tested it can be found that the mean conversion for phosphodiester sequences is 61% with significant differences between the bases and sugars. When all four bases within a sugar are averaged they give conversions of 51%, 52%, 56%, 65%, 65% and 80% for DNA, 2´-OMe, 2´-MOE, 2´-Fluoro, LNA and RNA respectively. Averaging the six sugars within a given nucleobase gives 49%, 63%, 65% and 69% for A, T/U, G and C respectively. It can be seen that there is a large effect coming from the terminal sugar and that the nucleobase adenosine gives significantly lower conversions than the other three.

Additionally the averages across the six sugars in a base and the four bases within a sugar were plotted and can be seen in Figure 3.4.

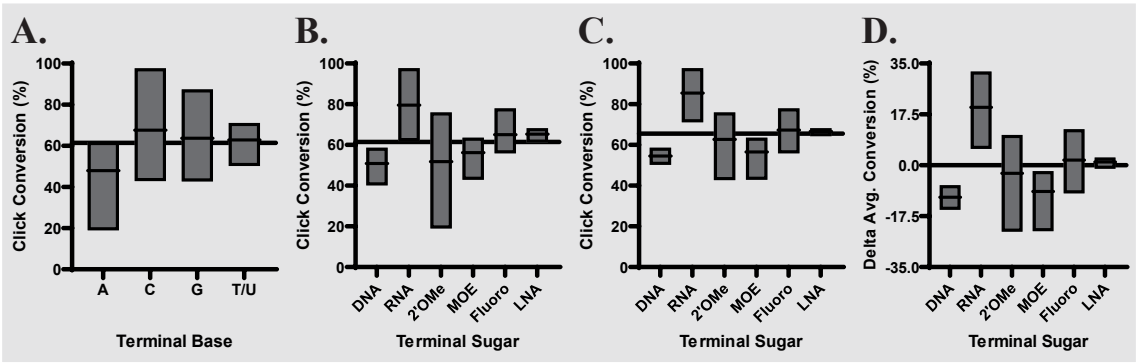


Figure 3.4: Graphical representations of on-resin CuAAC addition of thymidine for oligonucleotides ON-3.5 to ON-3.28. In each case the box represents the range of conversion percentage for a given group with the line across the box representing the mean. **A.** groups by terminal nucleobase with the six different sugars bucketed into A, C, G or T/U. **B.** groups by terminal sugar where the four nucleobases are bucketed into DNA, RNA, 2´-OMe, 2´-MOE, 2´-Fluoro and LNA. For both **A.** and **B.** a line across the plot is at 61.46%, the average of all conversion percentages. **C.** is grouped in the same fasion as **B.** where the data for adenosine has been removed from each group. The horizontal line is at the new total average of 65.53%. **D.**is the same plot as **C.** where the average of 65.53 has been subtracted from each data point and a horizontal line is placed at 0%.

As mentioned before when plotted it becomes clear that among nucleobases there is a discrepancy between adenosines and the other three across all riboses tested. It is between 14% and 20% worse than the other bases on average and is the base with the lowest conversion in 4 out of the 6 sugars, the exceptions being 2´-MOE and 2´-Fluoro. A likely explanation of this could be it is the bulkiest of the nucleobases when the click reaction is being performed. While the actual nucleobases of adenine and guanine are similar, this reaction is performed prior to the deprotection step while the oligonucleotide is still attached to the resin. In this state the primary amine of the adenosine is protected by a benzoyl group while the guanosine is protected with either an isobutyryl or dimethylformamidyl group, both of which are smaller.

Additionally, the N-6 position of the adenosine is closer to the 5´-end when the nucleobase is in the more common *anti* conformation. Combined with the fact that the first step in the CuAAC cycle is the complexing of the alkyne to the copper, the large benzoyl protecting group therefore could be interfering with the ability of the bulky copper/3´-alkyne-thymidine complex to reach the terminal azide. Once this is taken into

account, there is actually very little difference between the other nucleobases, with only 6% separating cytidine, guanosine and thymidine/uracil, meaning as with the azide conversion, the ribose sugars play a large role.

3.3.2. Effects of the 5´ ribose sugar on CuAAC Reaction Efficiency

In addition to the average conversion of each sugar being plotted in Figure 3.7, the average conversion for each sugar omitting adenosine as well as the average of each sugar with no adenosine with the total average of all conversions besides adenosine subtracted was also plotted. This was done as adenosine performed significantly worse than the other bases for many of the sugars and so created a large range within each sugar and the average conversion across the other three bases is very similar. This means that by omitting adenosine, the variation seen is almost entirely from the sugar and not clouded by the increased conversion range caused from the worst performing nucleobase.

The range within the sugars four all four bases is 19%, 36%, 57%, 21%, 22% and 7% for DNA, RNA, 2´-OMe, 2´-MOE, 2´-Fluoro and LNA respectively. Removing the adenosine gives ranges of 8%, 27%, 33%, 21%, 22% and 4% for sugars in the same order. In terms of performance the total average is increased to 66% (+4%) and the average of each base is increased to 55% (+4%), 57% (+/-0%), 63% (+11%), 67% (+1%), 67% (+2%) and 85% (+6%) for DNA, 2´-MOE, 2´-OMe, LNA, 2´-Fluoro and RNA respectively.

It can be seen that the removal of adenosine increases average conversion in all cases but 2´-OMe and RNA are increased significantly more than the others. It can also be seen that although the range of means between the sugars is 31%, over half of this,18%, is from the difference of RNA to 2´-Fluoro, the next best performer. Additionally, there seems to be a split into three categories, DNA and 2´-MOE which are below average, 2´-

OMe, LNA and 2´-Fluoro which are around the average and RNA which is above average. Figure 3.5 depicts these terminal ribose sugars as they would participate in the CuAAC reaction before deprotection from the CPG resin.

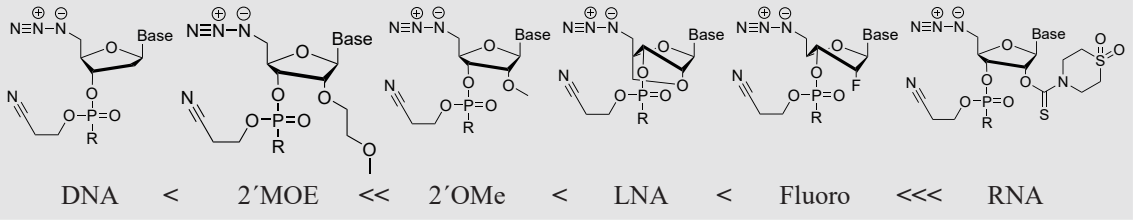


Figure 3.5: Terminal sugars ordered with relative conversion rates increasing left to right. The phosphate is group protected by a cyanoethyl group and the 2´-OH of the RNA protected by the 2´-thiomorpholine-4-carbothioate (TC) group.

There does not appear to be an obvious correlation between any one feature of the terminal ribose sugar and the reaction efficiency. DNA is the only example that exists in a C2´-*endo* conformation so it is possible that this can bring the nucleobase in closer proximity to the 5-azide, increasing steric hindrance. All other ribose sugars present are C3´-*endo* promoting, however not all to the same degree. LNA is the strongest promoter followed by 2´-Fluoro, with the other three being much weaker promoters. This does not appear to have undue influence as these two are in between weaker promoters in terms of efficiency. It is also possible that electronegativity is important. With reference to DNA all other substituents are more electronegative, with the fluorine and the carbothioate protected oxygen being the most. As these groups are five bonds removed from the reaction site the effect on the azide would be weak and it is unclear how this would aid the CuAAC reaction.

3.4 Duplex Melting Temperature of Triazole Containing Oligonucleotides

After assessing conversion efficiency, the effect on duplex thermal stability was investigated. This is an important metric as for virtually any application, an oligonucleotide must have a strong affinity for its compliment, either a DNA compliment for use in PCR or an RNA compliment for use in therapeutic applications where gene expression is altered at the mRNA level. 1,4-Triazole backbones are known to destabilise the resulting duplex.[188] However, it has been shown that introduction of LNA to the 3´-side of the linkage can rescue the binding affinity while the 5´ has little to no effect. It was hypothesised that this is because the LNA induces a rigid alpha form conformation by inducing a 3´-*endo* sugar conformation which has a strong effect at the 3´-side where the LNA is adjacent to a phosphate linkage. When adjacent to the triazole linkage this effect is lost as the unnatural ring cannot form an alpha type helix.[123]

All six of the previously tested sugars were used to determine their effect on the duplex melting temperature of a triazole-containing sequence as can be seen in Figure 3.6 with depictions of the linkages formed in Figure 3.7.

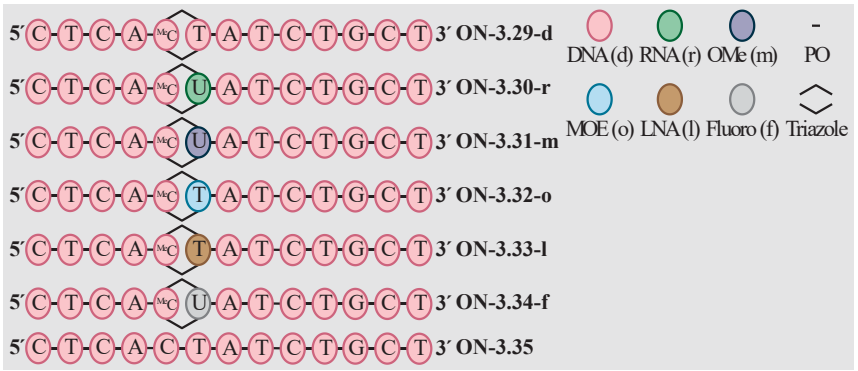


Figure 3.6: Triazole-containing oligonucleotides ON-3.29 ON-3.34 as well as the phosphate control oligonucleotide ON-3.35 used in this chapter. ^{Me}C indicates a Cytosine with a methyl on the C5 position of the nucleobase.

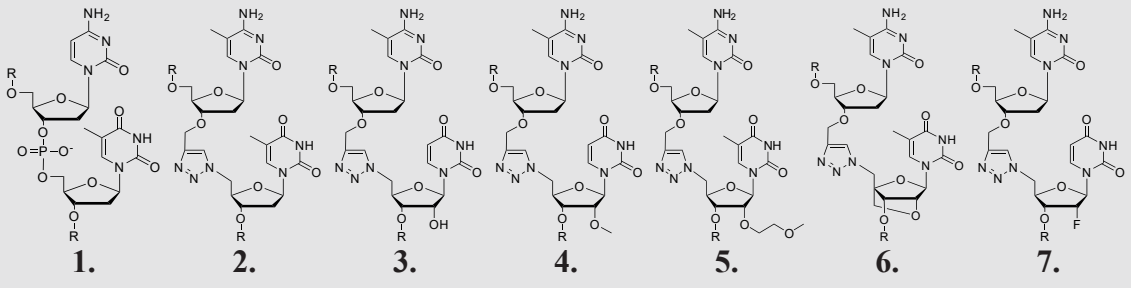


Figure 3.7: Natural phosphate and triazole linkages formed in each of the sequences. Linkages are referred to as follows **1.** Phosphodiester (ON-3.35), **2.** DNA triazole (ON-3.29-d), **3.** RNA triazole (ON-3.30-r), **4.** 2´-OMe triazole (ON-3.31-m), **5.** 2´-MOE triazole (ON-3.32-o), **6.** LNA triazole (ON-3.33-l) and **7.** 2´-Fluoro triazole (ON-3.34-f).

After HPLC purification, the duplex melting temperature was measured by ramping temperature from 20°C to 85°C and monitoring UV absorption at 260 nm. Conditions used can be found in as **6.3 UV Melting Studies**, the results were plotted and this data is displayed in Figure 3.8. And shown in Table 3.2.

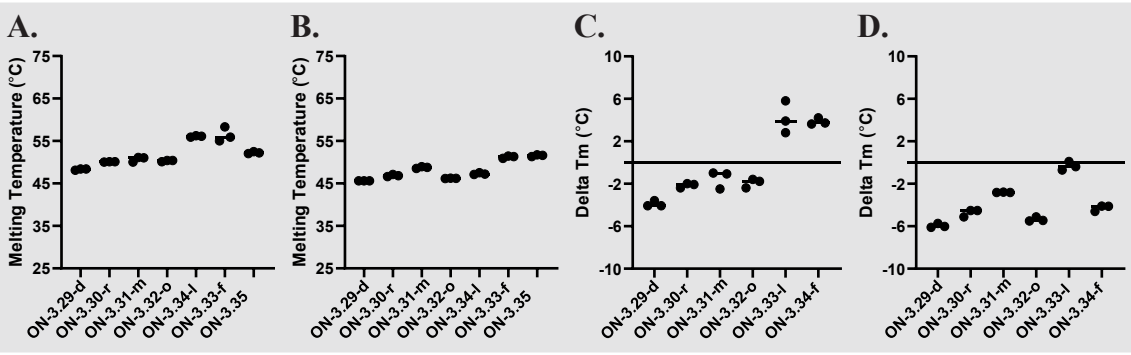


Figure 3.8: The measured melting temperatures of oligonucleotides ON-3.29 to ON-3.35. **A.** shows melting temperatures of a given oligonucleotide with an RNA reverse compliment, **B.** a DNA reverse compliment, **C.** the difference in melting temperature to a phosphate control (ON-3.35) with an RNA reverse compliment and **D.** the difference in melting temperature to a phosphate control (ON-3.35) with a DNA reverse compliment. In all cases data of three temperature ramps is shown with a line indicating the average value.

		Oligonucleotide						
Compliment	**Melting Temperature**	**ON-3.29-d**	**ON-3.30-r**	**ON-3.31-m**	**ON-3.32-o**	**ON-3.33-l**	**ON-3.34-f**	**ON-3.35**
RNA	Melting Temperature (°C)	48.31	50.08	50.71	50.31	56.40	56.08	52.23
	Delta Phosphate (°C)	-3.92	-2.15	-1.52	-1.92	4.17	3.85	-
DNA	Melting Temperature (°C)	45.60	46.83	48.74	46.19	51.22	47.27	51.56
	Delta Phosphate (°C)	-5.96	-4.72	-2.82	-5.37	-0.34	-4.28	-

Table 3.2: Numerical values for melting temperatures and delta melting temperatures plotted in Figure 3.2

3.4.1 Analysis of Duplex Melting Temperature for Triazole-Containing Oligonucleotides with an RNA Compliment

The pattern of melting temperatures found follows the trend that was expected. When paired with an RNA compliment, the triazole flanked by a DNA sugar on the 3´-side destabilises the duplex by about 4°C. The introduction of a weaker C3´-*endo* promoter such as a hydroxyl, methoxy or methoxy-O-ethyl group on the C2´ position (ON-3.30-r, ON-3.31-m and 3.32-o respectively) limits the destabilisation to around 1.5-2°C. Putting a stronger promoter of the C3´ *endo* conformation such as an LNA or 2´-Fluoro sugar actually increases the duplex stability over the unmodified phosphate control. This makes sense as the stricter the conformational locking of the sugar the more an A-form helix is promoted which increases duplex stability.

DNA sugars favour a C2´ *endo* conformation[192] (ON-3.29-d) and so will have the lowest duplex stability even with no triazole present. Additionally, there is no group to prevent disruptions in the duplex from the unnatural ribose linkage. With the RNA, 2´-OMe and 2´-MOE sugars at the 3´-end, a more stable conformation is already preferred and so work to make the structure more rigid[193] and therefore change less when the phosphate is replaced. LNA and Fluoro sugars are even more restrictive of the sugar conformation and so they enforce the A-form duplex the most, meaning they can tolerate the most change without disruption to the overall duplex shape. This is borne out in the measurements where they are still able to confer duplex stabilisation despite the addition of the triazole linkage.

3.4.2 Analysis of Duplex Melting Temperature for Triazole-Containing Oligonucleotides with a DNA Compliment

With a DNA compliment similar patterns to the RNA compliment are observed, though not exactly the same. It can be noticed that the destabilisation compared to the

phosphate control is greater in all cases than the RNA compliment. This is expected as DNA-DNA hybrids form the classic B-form helix that is less stable without any additional modifications. It is also a less rigid and compact structure meaning that the duplex will change shape more if linkages are changed, causing greater disruption.

This difference has also caused some changes in the trends seen regarding stabilisation afforded by modifications. As with the RNA compliment the natural DNA sugar displays the lowest thermal stability as it lacks any group to enforce rigidity and prevent duplex disruption. The RNA sugar is mildly stabilising as it weakly promotes an A-form helix, giving some resilience to the changes induced. Interestingly while both the 2´-OMe and 2´-MOE have as stabilising effect as with the RNA compliment, the 2´-OMe has a significantly stronger (delta Tm +2.55°C) influence. This is likely due to the overall difference in helix shape. With a DNA-RNA duplex where an A-form is dominant, the diameter of the helix is wider[194] and thus better able to tolerate the longer chain of the MOE group where in the narrower internal channel of a B-form helix the smaller 2´-OMe modification is more favourable causing a gap to open between the melting temperature of the two.

Differences to the RNA compliment can also be observed in the relative melting temperatures of LNA and 2´-Fluoro riboses. LNA is still the most stabilising modification, however, the small gap (delta Tm +0.32°C) has opened up to be much larger one (delta Tm +3.94°C). This is possibly due to differences in the mechanism by which these sugars increase the melting temperature of a duplex. The most common explanation as to why 2´-Fluoro groups increase duplex stability is what was stated previously where the sugar is forced into a C3´ *endo* conformation by the electronic interactions of the fluorine and the phosphate backbone.[178, 195] While this does contribute to the stabilisation, there is evidence to suggest that this is not the only or even main effect of the fluorinated sugar. Forcing a certain sugar or helical shape is an entropic explanation, however

measurements conducted show that the entropy difference between a 2´-fluoro and 2´-OH sugar is very small and instead differences in enthalpy are at work. It was therefore posited that electronegativity of the fluorine can affect the nucleobases electron density, increasing the strength of Watson-Crick base pairing interactions leading to an increase in enthalpy.[196, 197]

LNA sugars use a purely entropic mechanism as they force an extremely rigid sugar conformation, and this provides an explanation to the differences observed between the melting temperatures of the DNA-RNA and DNA-DNA duplexes. In the case of the more rigid A-form DNA-RNA duplex, the fluorine has a chance to exert this enthalpic effect as the base pairing is already stronger in this shape and the C3´ RNA sugars on the compliment are better able to hold the duplex in position. With a DNA-DNA duplex there is no such sugar to hold the conformation and therefore the Watson-Crick interactions are weakened thus the effect of the fluorine is dampened. LNA, which works by enforcing a strict C3´ *endo* conformation will be highly effective in both cases, as is observed.

Overall, the measured duplex stability values agree with those measured for triazole linkages with DNA and LNA sugars at the 3´-side. In addition, they expand the knowledge base on the effect of commonly used ribose modifications and shed light on factors that influence the melting temperature of triazole-containing sequences.

3.5 Conclusion

Using the work from Chapter 2, this chapter focused on taking oligonucleotides with azide groups at the 5´ end and employing Copper Catalysed Azide-Alkyne Cycloaddition to add an additional nucleobase with a charge-neutral triazole linkage connecting the two. Click chemistry and solid phase chemistry pair very well together, with the joining of the two coming during the development of CuAAC itself. The ability to use large excesses of reagents and quickly remove them is especially important when dealing with oligonucleotides which can be degraded by prolonged presence of metal catalysts making quick reaction times and complete removal of copper ions imperative. This is feasible here where the reaction column can easily be flooded with reagents to increase reaction rate then washed with a chelating agent such as EDTA to quickly and effectively render the oligonucleotide free from any potential harmful agents.

This method is also useful as it allows a charge-neutral triazole linkage to be inserted into a sequence with no special phosphoramidites needed. Triazole linkages have many benefits as they are PCR compatible and they confer much greater nuclease stability than a natural phosphodiester linkage. In addition the neutrality reduces the net negative charge of the oligonucleotide which has potential benefits with increasing permeability to cellular membranes. The lack of specialty phosphoramidites means the method is extremely flexible as only one alkyne monomer is required so it can be placed anywhere where that nucleobase is present in a desired sequence.

To begin, the coupling process was conducted with a phosphorothioate oligonucleotide to optimise the conditions. This was done to find the best reaction time as copper catalysts are destructive to such sequences, causing loss of sulfur from the backbone. The reaction was found to be completed after one hour with a conversion rate of 97%, with desulfurisation happening after three hours. After this the reaction efficiency was tested in the 24 phosphodiester sequences with terminal azides from the first chapter.

These sequences are grouped into six terminal ribose sugars with all four nucleobases for each. The same was not done for the phosphorothioate oligonucleotides as azide conversion was found to be far less efficient for many of the sequences meaning the method is not practical for every phosphorothioate sequence. It is however compatible, and this will be discussed in the next chapter.

Overall, the click reaction proceeds with an average efficiency of 61%, however the range between different permutations is very large. It was found that on average adenosine is detrimental to the reaction as it is on average 15% worse than the next nucleobase with only a 6% range between the averages of the other three. This is likely due to the bulk of the benzoyl protecting group causing steric interference with the large copper-alkyne complex. Additionally, it was found that having a TC-protected-RNA sugar at the 5´-terminus gave the most efficient conversion, though the cause is not entirely clear.

After this the effect of the triazole on the thermal duplex stability was assessed. It has been found that placing an LNA sugar at the 3´-side of the linkage is beneficial and so all six terminal sugars, including LNA were evaluated. It was found that sugars that promote a C3´ *endo* conformation such as RNA, 2´-OMe and 2´-MOE help stabilise the duplex with both DNA and RNA compliments by 1-3°C compared to a triazole with just a DNA sugar at the 3´-side. Both fluoro and LNA sugars were found to massively increase duplex stability with an RNA compliment, even increasing the melting temperature compared to a phosphate control. With a DNA compliment, the large effect from the LNA sugar was retained but was lost for the 2´-fluoro sugar. This is likely due to the differences by which the stabilisation is conferred, with LNA being exclusively from sugar conformational changes and 2´-fluoro possibly from a mix of sugar conformation changes and modulation of Watson-Crick interactions.

This chapter describes an easy, practical method for inserting a charge-neutral triazole linkage into an oligonucleotide on solid support. Triazole linkages in oligonucleotides have shown benefits in terms of nuclease stability and testing here and previously shows that when combined with the right sugar modifications at the 3´-side of the linkage duplex stability can also be retained. Adding a charge-neutral linkage to an oligonucleotide also has many potential benefits with phosphorothioate modified, therapeutic antisense oligonucleotides as will be explored in the next chapter.

Chapter 4: Synthesis and Assessment of Splice Switching ASOs Containing Triazole-Linkages

4.1 Introduction

Charge-neutral backbone replacements for the phosphodiester oligonucleotide linkage have long been used as a means of improving the performance of therapeutic antisense oligonucleotides. Phosphonates were among the first to be adopted[133] however others such as sulfamates[198], amides[97] and triazoles[119] have been used in literature. Arguably the most successful example of a charge-neutral backbone is the phosphorodiamidate linkage used in morpholino oligonucleotides such as the clinically approved molecules Eteplirsen, Golodirsen, Casimersen and Vitolarsen.[199] These four clinically approved oligonucleotides are all targeting the disease Duchenne's Muscular Dystrophy (DMD), an X-linked rare genetic disease caused by a mutation that disrupts the reading frame of the protein dystrophin.

Dystrophin is the longest gene in humans, singlehandedly accounting for 0.1% of total DNA, and perhaps due to its large size, mutations are a relatively common occurrence.[200] Accordingly DMD affects approximately 1 in 5,000 males[201] with a hotspot for deletions seen in exons 43 to 55, the top five being exons 51, 53, 45, 42 and 44.[202] Dystrophin is a membrane-associated protein that links cytoskeletal actin in muscle to the extracellular matrix, providing strength to myofiber structure. Mutations causing the loss of this protein therefore weakens muscle, leading to degeneration over time.[203] This degeneration presents itself in DMD causing complete loss of ambulation at a mean of 9.5 years old followed by death in late teens to early twenties most commonly caused by respiratory deficiencies.[204] Treatment options are limited, the only traditional small molecule option being corticosteroid therapy which has shown efficacy in extending ambulation and delaying death by a few years.[205, 206] Another option is splice switching Antisense Oligonucleotides (ssASOs) such as the four mentioned which can exclude problematic exons from the final mRNA and restore the reading frame as depicted in Figure 4.1.

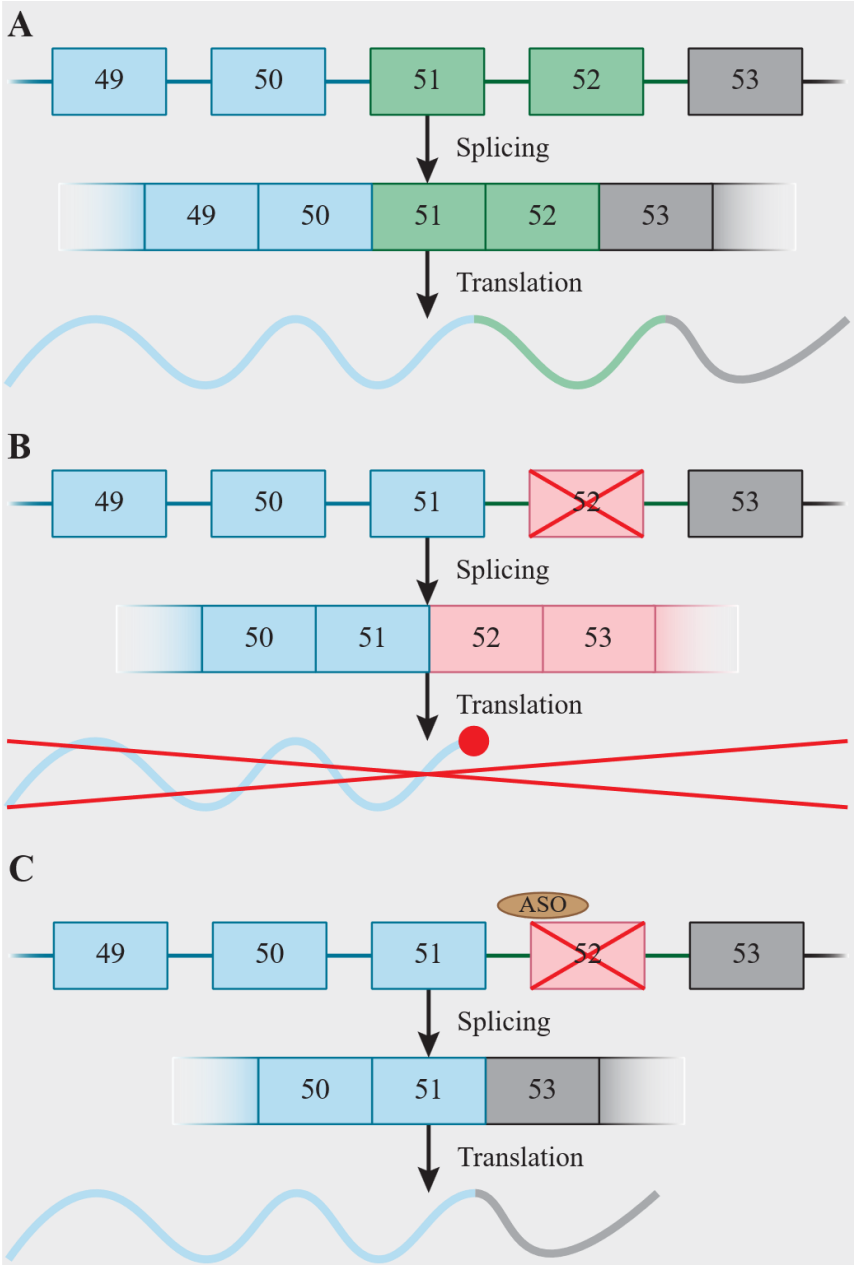


Figure 4.1: A depiction of DMD and exon skipping adapted from literature[207]. **A.** Healthy dystrophin transcript with full-length dystrophin. **B.** Dystrophic transcripts with a deletion in exon 52, causing frame shift leading to a premature stop codon. The incomplete mRNA which is immediately degraded producing no functional dystrophin. **C.** Dystrophic transcript treated with an ASO where the splicing of exon 51 is prevented, restoring the reading frame and leading to a shortened but mostly functional dystrophin protein.

Despite treatment with these phosphorodiamidate morpholino oligocleotides, dystrophin production in DMD patients remains modest, with only 0.9% (Eteplirsen), 1% (Golodirsen), 4.25% (Casimersen) and 5.9% (Vitolarsen) restored compared to healthy levels. These levels are not sufficient to provide significant clinical improvement, and as such although these drugs are approved by the Food and Drug Administration they are

not approved by the European Medicine Agency when presented with the same efficacy data.[208]

Given this, there is still a strong need to develop better exon skipping oligonucleotides for DMD and innovations in chemistry is a promising pathway to do this. It is known that the phosphorothioate modification is important for protein interaction and cellular trafficking and so a series of oligonucleotides were synthesized with a mixture of different charge-neutral backbones and phosphorothioate linkages then assessed for their exon skipping performance. These charge-neutral linkages were triazoles formed using the on-column method developed in the previous chapters as well as phosphonates that are more similar to the naturally occurring phosphodiester backbone. Performance was assessed both with and without the aid of a transfection agent to gain insight how the charge-neutral backbones are modulating the effect of exon skipping and general trends were attempted to be established into the ideal characteristics of a charge-neutral backbone.

4.2 Luciferase-Based Assay used to Determine Splice-Switching activity of ASOs

To assess the splice switching capacity of various oligonucleotides, a reporter system based on firefly luciferase was employed. In this system, the sequence of a thalassaemic human beta globin intron-2 was inserted into a plasmid containing a luciferase gene.[209] The intron contains a T to G point mutation at base pair 705 which causes aberrant splicing as seen in Figure 4.2.

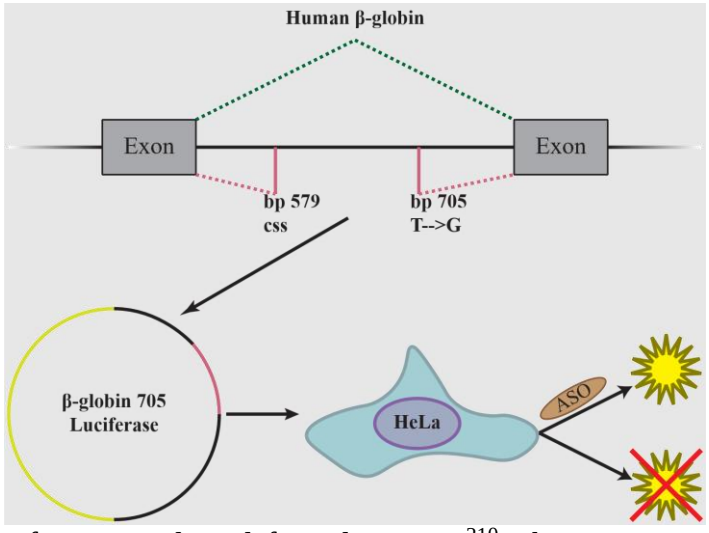


Figure 4.2: This figure is adapted from literature.[210] The mutation at base pair 705 disrupts the normal splicing depicted by the green dotted line. This creates an aberrant splice site at position 705 and activates a cryptic splice site (css) at base pair 579, including the piece of the intron between the two in the mRNA. This was inserted into a luciferase plasmid and inserted into HeLa cells. Treatment of the stably expressive HeLa cells with an ASO targeting base pair 705 leads to functional luciferase protein while untreated cells will produce no functional protein.

To perform the assay, the HeLa 705pLuc cells were dosed with either an ASO-Lipofectamine3000 complex (referred to as transfection) or with the ASO alone (referred to as gymnosis). Lipofectamine3000 is a mixture cationic and zwitterionic lipids such as DOPSA and DOPE with additional neutral lipids.[211] These form lipoplexes with the ASOs and can improve cellular uptake efficiency by over two orders of magnitude.[212] Additionally, the lipoplex stabilises the ASOs to nucleases, meaning they can be dosed in the normal serum supplemented cell growth media whereas gymnotic delivery occurs in reduced serum medium.

Luminescence measurements of treated cells were normalised to untreated wells as described in section **8.4.2 HeLa pLuc 705 Assays**. Additionally, on every plate the same 2´-O-methyl phosphorothioate control oligo was measured to provide not only the fold change over untreated wells but also the fold change over a positive control. Normalisation to untreated wells is sufficient when comparing ASOs that were measured on the same plate, however it is better to compare to a positive control when multiple plates are involved for several reasons.

The measure of untreated wells is essentially a measure of the background luminescence and will change from plate to plate based on the number of cells in the well, health of the cell population and other such factors. Since it is the background and therefore a relatively small luminescence value, relatively minor swings in the absolute magnitude could have a large impact on the output value for each ASO normalised to it.

Additionally, cells do not grow at the same rate on every plate even if seeded at the same density. A plate with more cells in each well will produce more luciferase when dosed with an ASO and therefore will have a higher change relative to the untreated wells. An attempt to mitigate this effect is made by normalising each well to the total amount of protein, however this is only a proxy for cell count and so is not a perfect solution. Placing the same ASO as a positive control and calculating statistical significance relative to that control eliminates some of this plate-to-plate variability as all of the factors mentioned will also affect its fold change over untreated value. This gives more confidence when comparing oligonucleotide performance on different plates and allows for more better evaluation of ASO performance.

4.3 Triazole Linkages in Splice-Switching ASOs

4.3.1 Oligonucleotides used to Evaluate Triazole Linkages in ssASOs

To begin testing triazoles in exon skipping ASOs in the assay described above, four alkyne monomers were used. This includes the DNA alkyne from the previous chapter, a 2´-methoxy-O-ethyl (MOE) alkyne, a 2´O-methyl (OMe) alkyne and a locked nucleic acid (LNA) alkyne. All were made with a thymidine nucleobase and the alkyne was added with sodium hydride and propargyl bromide in the same fashion as the previous chapter. The alkynes were added to a 2´-Omethyl phosphorothioate oligonucleotide, and the alkyne sugars as well as the linkages formed are shown in Figure 4.3.

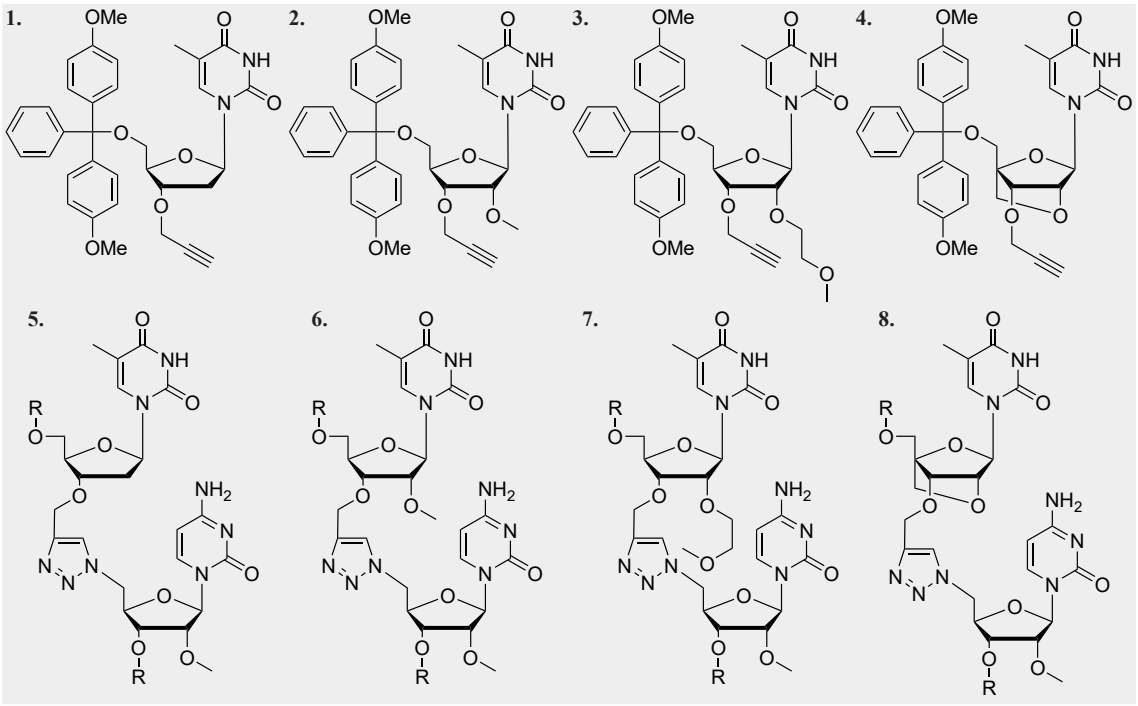


Figure 4.3: Alkyne monomers and triazole linkages formed in this study, referred to as follows, **1.** DNA alkyne, **2.** 2´-OMe alkyne, **3.** 2´-MOE alkyne, **4.** LNA alkyne, **5.** DNA triazole, **6.** 2´-OMe triazole, **7.** 2´-MOE triazole and **8.** LNA triazole.

The triazoles were formed with the on-column azide formation and copper click described in the previous chapters. The previous chapters also showed a terminal 2´-O-methyl sugar at the terminal position of a sequence is compatible with azide formation when coupled with phosphorothioate backbones. The control oligonucleotide used in this

study consists of 2´-OMe sugars linked by phosphorothioates and so this ribose was placed at the 3´-side of each of the triazoles. The 5´-side of the linkage was varied with different alkynes. As previously discussed, this side of the linkage is not expected to change the duplex melting temperature (Tm) significantly but minor changes can be observed. As the on-resin method uses monomers, it is relatively easy to vary the alkyne on the 5´ which takes advantage of the flexibility of the approach described in Chapters 2 and 3 while avoiding the problems associated with phosphorothioates and certain ribose modifications. These triazole linkages were placed in the middle of the splice switching ASO as shown in Figure 4.4.

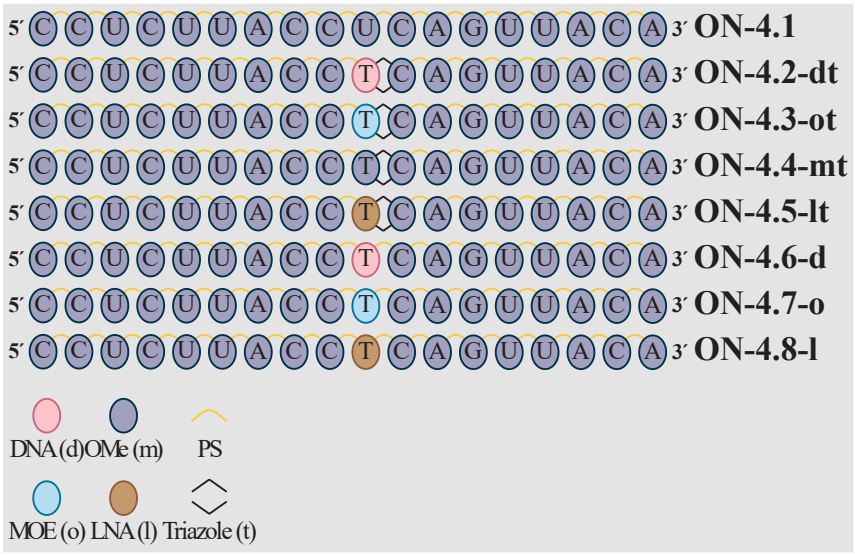


Figure 4.4: Oligonucleotides numbered ON-4.1 to ON-4.8: triazole-containing oligonucleotides as well as 2´-OMe-phosphorothioate sugar matching controls.

In addition to the triazole containing oligos, control oligos containing all phosphorothioate backbones with the same changes to sugar composition were synthesized. This was done in addition to the all 2´-OMe phosphorothioate to isolate the effect of changing the backbone from changing the sugar. In addition, the melting temperature for each sequence was measured compared to ON-4.1 the triazoles were measured at -5.48°C, -3.05°C, -3.47°C and -5.02°C for ONs 4.2-dt, 4.3-ot, 4.4-mt and 4.5-lt respectively. The control oligos compared to ON-4.1 were found to be -0.02°C, +9.82°C and +4.72°C for ONs 4.6-d, 4.7-o and 4.8-l respectively.

While the difference in melting temperature for the DNA and LNA controls is in line with expected values that for the MOE control is abnormally high, with literature values more in a 1-3°C range per addition.[213, 214] These sources also mention that there are sequence dependent effects so it is possible that some sort of base stacking is occurring within the sequence to cause the melting temperature to seem abnormally high. The values measured for the triazoles are as expected since as previously discussed it is the 3´-side of the linkage that is the dominant contributor to the duplex stability with only a minor role being played by the sugar on the 5´-side. After synthesis and purification, the oligonucleotides in Figure 4.4 were taken to the luciferase splice-switching assay.

4.3.2 Results of Triazole-Containing ASOs in a Splice-Switching Assay

Oligonucleotides ON-4.1-ON-4.8 were dosed with Lipofectamine3000 and gymnotically. Results of transfected oligonucleotides can be seen in Figure 4.5. Results of gymnotic oligonucleotides can be seen in Figure 4.6.

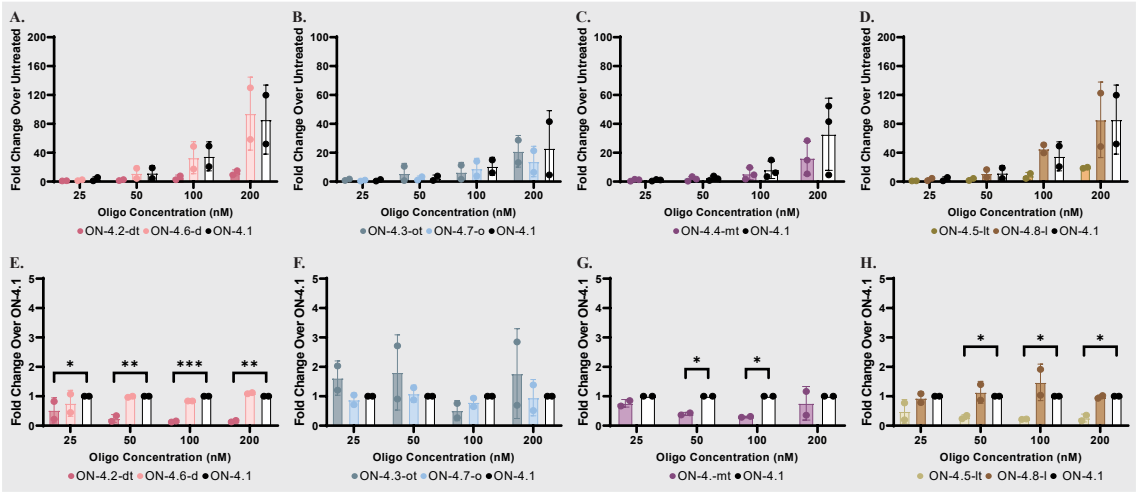


Figure 4.5: Exon skipping activity of triazole-containing and control oligonucleotides ON-4.1 to ON-4.8 when transfected with Lipofectamine 3000. Sections **A.** to **D.** show the fold change over untreated cells, sections **E.** to **H.** show the fold change over the control oligonucleotide ON-4.1. **A.** and **E.** show data for DNA triazole (ON-4.2-dT) and DNA control (ON-4.6-d) oligonucleotides, **B.** and **F.** 2´-MOE triazole (ON-4.3-ot) and 2´-MOE control (ON-4.7-o), **C.** and **G.** 2´-OMe triazole (ON-4.4-mt) and 2´-OMe control (ON-4.1) and **D.** and **H.** LNA triazole (ON-4.5-lt) and LNA control (ON-4.8-l).

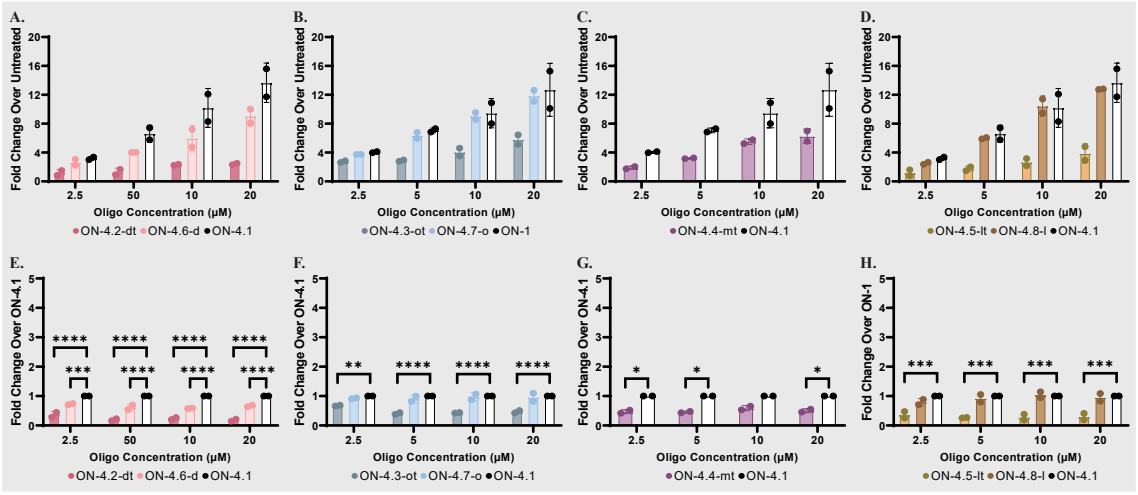


Figure 4.6: Exon skipping activity of triazole-containing and control oligonucleotides ON-4.1 to ON-4.8 when dosed gymnotically. Sections **A.** to **D.** show the fold change over untreated cells, sections **E.** to **H.** show the fold change over the control oligonucleotide ON-4.1. **A.** and **E.** show data for DNA triazole (ON-4.2-dt) and DNA control (ON-4.6-d) oligonucleotides, **B.** and **F.** 2´-MOE triazole (ON-4.3-ot) and 2´-MOE control (ON-4.7-o), **C.** and **G.** 2´-OMe triazole (ON-4.4-mt) and 2´-OMe control (ON-4.1) and **D.** and **H.** LNA triazole (ON-4.5-lt) and LNA control (ON-4.8-l).

As each ASO is normalised to the O-Methyl control at the same dose, the values of the fold change over ON-4.1 across the dose response range can be pooled and plotted together. Doing this consolidates the data sets to give an overall value of the performance of each ASO relative to the established control. This was done for each triazole containing ASO and each sugar control and is shown in Figure 4.7.

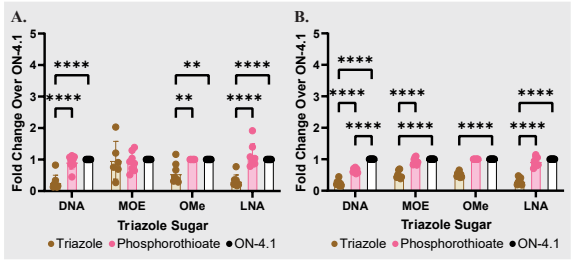


Figure 4.7: Plots of fold change over ON-4.1 across all doses tested for ASOs 4.2-4.8. **A.** shows data for oligonucleotides transfected with Lipofectamine 3000, **B.** shows data for oligonucleotides dosed gymnotically. For both **A.** and **B.** DNA triazole oligonucleotide is ON-4.2-dt, phosphorothioate oligonucleotide is ON-4.6-d. MOE triazole oligonucleotide is ON-4.3-ot, phosphorothioate is ON-4.7-o. OMe triazole oligonucleotide is ON-4.4-mt, phosphorothioate is ON-4.1. LNA triazole is ON-4.5-lt, phosphorothioate is ON-4.8-l. Statistical significance was calculated against both ON-4.1 and the matched sugar control

Examining Figure 4.7 A it can be seen that normalising to the phosphorothioate control (setting ON-4.1 as 100% activity), triazole-containing oligonucleotides

transfected with Lipofectamine3000 have mean activities across all four doses of 27%, 98%, 56% or 32% for ON-4.2-dt, ON-4.3-ot, ON-4.4-mt and ON-4.5-lt respectively. The DNA, MOE, and LNA phosphorothioate oligonucleotides ON-4.6-d, ON-4.7o and ON-4.8-l all were within 10% activity of ON-4.1. None of the phosphorothioate control oligonucleotides show statistical significance to ON-4.1. Three out of four triazole-containing oligos (ON-4.2-dt, ON-4.4-mt and ON-4.5-lt) have activities that are statistically lower than ON-4.1 while ON-4.3-ot has no difference.

Examining Figure 4.7 B it can be seen that normalising to the phosphorothioate control (setting ON-4.1as 100% activity), triazole-containing oligonucleotides dosed gymnotically have mean activities across all four doses of 24%, 50%, 51% and 30% for ON-4.2-dt, ON-4.3-ot, ON-4.4-mt and ON-4.5-lt respectively. While ON-4.7o and ON-4.8-l have activities of 94% and 93% respectively, ON-4.6-d has an activity of 65% and is the only phosphorothioate control with a statistically significant difference to ON-4.1. All four of the triazole containing ASOs show significant difference to ON-4.1.

4.4 Conclusions

This chapter describes the use of a luciferase-based splice switching assay to assess the efficacy of ASOs containing triazoles as a charge-neutral replacement for phosphodiester or phosphorothioate linkages. These triazole containing ASOs were synthesized using methods developed in Chapters 2 and 3 with four different ribose sugars (DNA, 2´OMe, 2´MOE and LNA) on the 5-side of the triazole-linkage. These oligonucleotides along with all-phosphorothioate containing oligonucleotides with the same ribose pattern as the triazole-ASOs were tested with both transfection agents and gymnotically.

Results from transfection assays show a wide range of activity depending on the sugar at the 5-side of triazole-linkage. DNA and LNA variants are roughly one-third as active as the 2´OMe-phosphorothioate control while the 2´OMe variant is half as active and the 2´MOE is nearly the same. When dosed gymnotically the DNA variant shows roughly one-quarter activity and the LNA variant shows roughly one-third activity while the 2´OMe and 2´MOE show roughly half activity compared to the 2OMe-phosphorothioate control.

One explanation could be thermal stability of the ASO-mRNA duplex. Duplex thermal stability as measured by the melting temperature is a proxy for target affinity and so lowering this value means that the oligonucleotide will have weaker interactions with the splice switching site and therefore be unable to correct the aberrant intron as effectively. ON-4.2-dt and ON-4.5-lt have duplex melting temperatures of -5.48°C and -5.02°C respectively, about 2°C lower than ON-4.3-ot and ON-4.4-mt which have duplex melting temperatures of -3.05°C and -3.47°C respectively. In both transfected and gymnotic dosing the two triazole-ASOs with the higher melting temperature performed better which seems to support this idea. It can also provide an explanation for the difference observed in ON-4.3-ot when transfected and ON-4.3-ot when dosed

gymnotically. Use of a transfection agent such as Lipofectamine3000 delivers more copies of an ASO into a cell as opposed to gymnotic dosing, meaning even if target affinity is lowered, the number of ASO-mRNA interactions is enough to compensate for this difference. In gymnotic dosing when there are fewer of these interactions any impairment to ASO efficiency such as a lowered affinity to the splice site will be more important. While these observations point to the importance of duplex thermal stability, others can be made that show it is certainly not the only factor.

One of these is the difference in transfected activity between ON-4.3-ot and ON-4.4-mt. These oligonucleotides show a 42% difference in splice-switching activity when transfected yet show less than 0.5°C difference in melting temperature. When considered with the observation that ON-4.3-ot showed no difference in activity compared to the 2´OMe-phosphorothioate control with a 3°C difference in melting temperature it can be seen that clearly other factors are at work as well.

A second of these observations is the gymnotic activity of ON-4.6-d which showed only 65% of the activity of the control oligonucleotide ON-4.1 with essentially no difference in melting temperature. As this reduction in activity was not observed when ON-4.6-d was transfected it could be that the DNA sugar is reducing nuclease resistance of the ASO which becomes more apparent in the four-day gymnotic study as opposed to the one-day transfection study. Considering that the oligonucleotide is otherwise completely modified with 2´OMe riboses and phosphorothioate linkages this would not necessarily be expected but it is possible.

Despite these two examples it is reasonable to think that in gymnotic dosing, thermal stability of the duplex is the most important factor to explain the discrepancy between the triazole-containing ASOs and the 2OMe control. As discussed gymnotic dosing leads to fewer copies of ASO in the cell, meaning lower target affinity that makes each splice-switching event less efficient will have a more pronounced effect on activity.

ASOs with 2´MOE or 2´OMe at the 5´-side of the triazole-linkage have a duplex melting temperature that is ~3°C lower than a 2´OMe-phosphorothioate control and a ~50% reduction in activity against the same. ASOs with DNA or LNA at the 5´-side of the triazole-linkage have a duplex melting temperature that is ~5°C lower than a 2´OMe-phosphorothioate control and a ~75% reduction in activity against the same. Charge-neutral backbones can theoretically improve gymnotic uptake by decreasing overall negative charge and increasing lipophilicity, thereby aiding in diffusion through the phospholipid bilayer. It seems however, in this case any advantage conferred is unable to overcome the deficiencies imposed by the lower melting temperature.

Overall, it can be surmised that changing the ribose sugar on the 5´-side of the triazole linkage has a significant impact on its splice switching activity in both transfected and gymnotic dosing, with a wide range of activity displayed between DNA, 2´MOE, 2´OMe and LNA varieties. Using 2´MOE ribose with a triazole-linkage in transfected testing shows no difference in activity from a 2´OMe-phosphorothioate positive control. In gymnotic testing using a 2´MOE or 2´OMe ribose with a triazole-linkage shows roughly 50% activity compared to a 2´OMe-phosphorothioate positive control.

These results show that triazole-linkages are active in splice-switching ASOs. However, the gymnotic performance of these ASOs never matched the 2OMe-phosphorothioate benchmark, likely due to the reduced duplex thermal stability. To improve this parameter, an LNA or 2´fluoro ribose could be placed at the 3´-side of the triazole-linkage. However, given that these are not compatible with the solid-phase synthesis method used to introduce the triazole, an alternative linkage was sought.

The next chapter starts by exploring substitutions of 2´OMe riboses with DNA, 2´MOE and LNA sugars to find the best platform to incorporate neutral linkages into. Then a methoxy-propyl phosphonate was introduced to this platform. Unlike the triazole, this backbone does not impose a significant penalty to duplex thermal stability. As this is

thought to be the major issue with the triazole linkage and the current method of introducing the triazole limits options to address this problem, the methoxy-propyl phosphonate is a good choice to confer the benefits of a charge-neutral linkage while omitting this undesirable property.

Chapter 5: Synthesis and Assessment of Splice Switching ASOs With alternate Ribose Patterns and Methoxypropyl Phosphonate-Linkages

5.2 Introduction

Building on the previous chapter, this section first investigates the effect of switching ribose sugars away from the 2´-OMe building block used in the positive control. This is done to create a platform that can then be further modified with charge-neutral linkages to attempt to address the issues of the duplex-destabilising triazole investigated in the last chapter. One class of modifications that fits into this role is the alkyl phosphonate, of which the methoxypropyl phosphonate (MOP) has shown promise in recent years.

Investigation of the mechanisms of toxicity of RNAse-H dependent gene-silencing ASOs revealed that tight binding interactions between locked sugars such as LNA and cET are a possible cause and that introduction of a 2OMe sugar either in the wings or in the DNA gap can reduce toxicity.[139] It was also noted that placing one MOP-linkage in the gap of the ASO has a similar effect, improving therapeutic properties of these oligonucleotides *in vivo* while only reducing duplex melting temperature by <1°C in most cases.[140] Although the pathway is different to the splice switching mechanism being explored here, a charge-neutral backbone that causes minimal disruption to duplex thermal stability also has potential benefit.

MOP-linkages are introduced by synthesis of modified phosphoramidites where the cyanoethyl group is replaced by the methoxypropyl group. Unlike in the case of the triazole-linkages, MOP phosphoramidites are made as monomers, meaning flexibility is not limited by the number of special building blocks necessitated by a dimer-phosphoramidite. Also of note is that phosphonates are not stable to standard deprotection conditions[128] and so the nucleophilic ethylene diamine was used as a faster and softer deprotection agent. Although helpful for phosphonates, nucleophilic amines such as ethylene diamine are not compatible with benzoyl-protected cytosine groups as they lead to transamination and so care must be taken with amidite selection and preparation to

avoid their use. Preparation of MOP-phosphoramidites and issues with deprotection conditions are depicted in Figure 5.1.

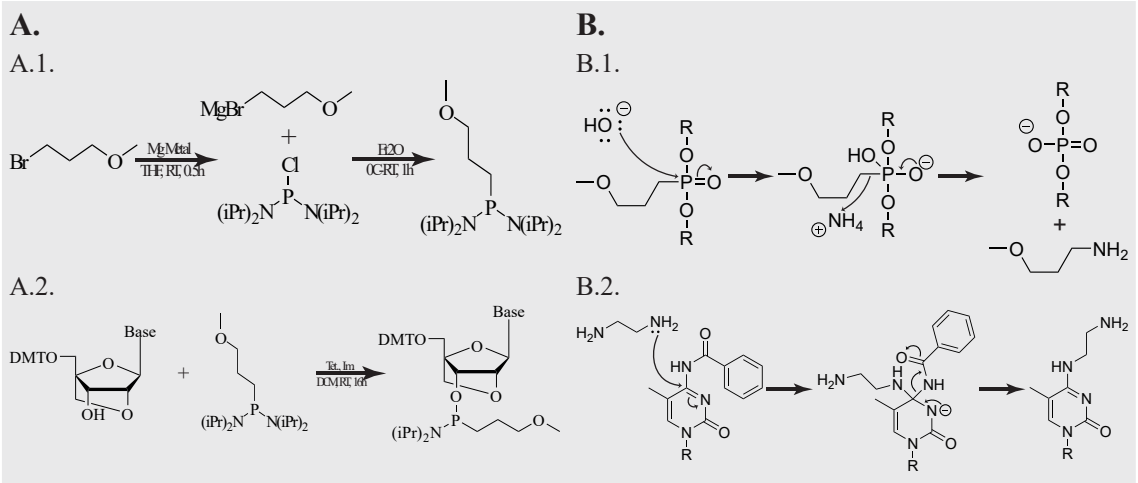


Figure 5.1: A. Synthesis of methoxypropyl phosphine and phosphoramidites A.1. The alkyl-bromide is made into a Grignard reagent and added to the chlorophosphine. A.2. Phosphitylation of T and DMF-Me-C. **B.** Incompatibility of MOP benzoyl cytosine with deprotection conditions B.1. With standard ammonium hydroxide the hydroxide ion can attack, leaving the alkyl chain susceptible to leaving. B.2. Using ethylene diamine for softer deprotection means the primary amine can attack the amine-carbon, eliminating the benzoyl amide and adding the extra CH_2-CH_2-NH_2 to the final molecule.

Work was then started to find a platform in which to incorporate this MOP-linkage. Changes were made to the 2´-OMe-phosphorothioate control to assess the effect of DNA, 2-MOE or LNA sugars, breaking the homogeneity of the molecule. These ASOs were then tested in the same luciferase-based exon-skipping assay as described in Chapter 4. Results were then used to inform the design of MOP-containing ASOs which were also evaluated for exon-skipping efficacy.

5.2 Ribsoe Substitutions in Splice-Switching ASOs

5.2.1 Oligonucleotides used to Evaluate Ribose Sugar Substitutions in ssASOs

To evaluate the relationship of sugar changes to ASO activity a series of oligonucleotides containing one to three substitutions were synthesized as shown in Figure 4.8.

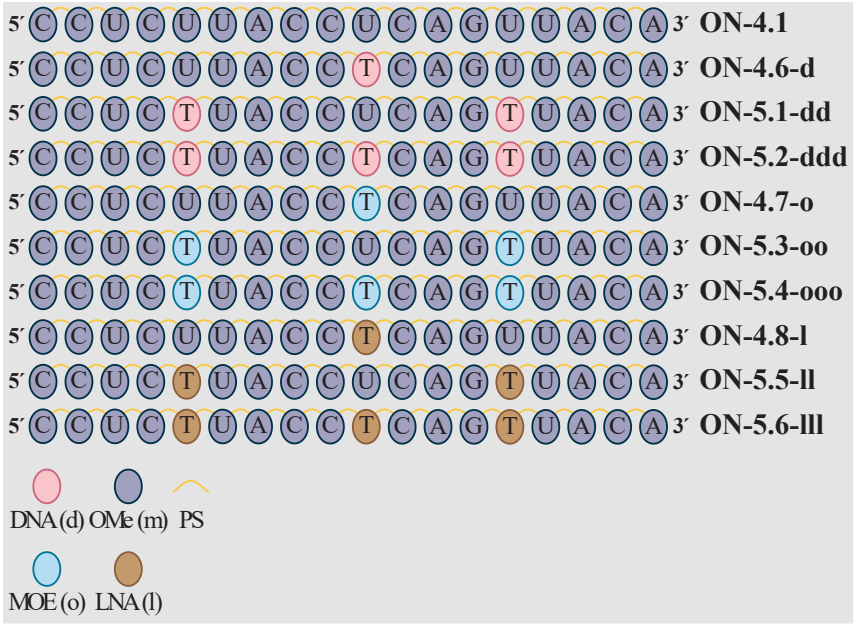


Figure 5.2: ASOs synthesized to evaluate the effect of sugar substitutions on the control oligonucleotide ON-4.1. 2´-OMe ribose sugars were swapped in one, two or three locations with DNA (ON-4.6-d, ON-5.1-dd, ON-5.2-ddd respectively), 2´-MOE (ON-4.7-o, ON-5.3-oo, ON-5.4-ooo respectively), and LNA (ON-4.8-l, ON-5.5-ll, ON-5.6-lll respectively).

Each of the three alternate sugars tested with the triazole linkages were placed in the sequence with an even dispersion throughout. This was done to break up any local effects or interference caused from clustering. For example, three DNA sugars in proximity could increase recognition of the sequence by nucleases. This should not be the case as a phosphorothioate backbone is maintained throughout, however, it is possible. Additionally, spacing out the LNA sugars should lead to a greater increase in duplex stability as the conformational shift imposed by the locked sugar will hold more of the duplex in a sharp A-form helix shape.

Duplex melting temperatures were measured for each sequence and compared to ON-4.1 were found to be -0.02°C, -2.27°C, -2.77°C for ON-4.6-d, ON-5.1-dd and ON-5.2-ddd, +9.82°C, +10.74°C and +11.73°C for ON-4.7-o, ON-5.3-oo, and ON-5.4-ooo and +4.72°C, +9.26°C and +>20°C for ON-4.8-l, ON-5.5-ll and ON-5.5-lll respectively. Again, it should be noted that the temperature increase from the MOE modification is much higher for one addition but interestingly does not seem to possess and additive effect. This is in contrast to the LNA modifications which add up to give a final melting temperature that was over 75°C, the limit to quantification of the system.

Reduced salt buffer was used obtaining these melting temperature measurements. Higher salt concentrations are associated with higher duplex stability as the cations can screen the negatively charged backbone as well interact with bind in the grooves.[215] In an attempt to lower the melting temperatures to within the measurable range, all ASO duplexes were measured with a 25 mM solution of sodium chloride in phosphate buffer, approximately one-fifth of physiological conditions.[216] Despite this the LNA modification still pushed the melting temperature outside of the measurable range.

5.2.2 Results of Ribose-Substituted ASOs in Splice-Switching Assays

The splice switching activity of oligonucleotides ON-4.6-d, ON-5.1-dd, ON-5.2-ddd, ON-4.7-o, ON-5.3-oo and ON-5.4-ooo were measured. Results of oligonucleotides dosed with Lipofectamine3000 are shown in Figure 5.3. Results of oligonucleotides dosed gymnotically are shown in Figure 5.4

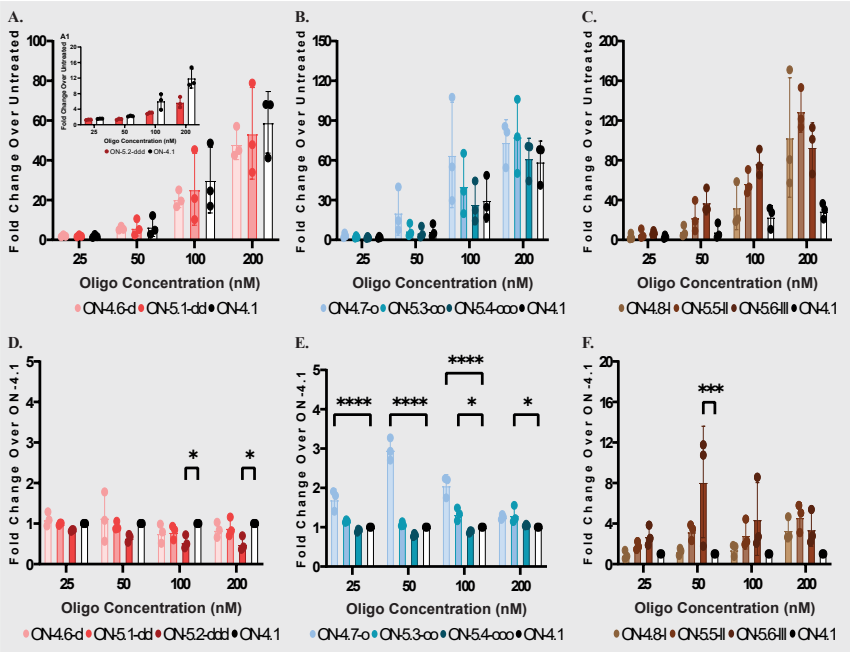


Figure 5.3: Exon skipping activity of sugar-substituted ON-4.6-d, ON-5.1-dd, ON-5.2-ddd, ON-4.7-o, ON-5.3-oo and ON-5.4-ooo as well as the 2´-OMe control oligonucleotide ON-4.1 when transfected with Lipofectamine 3000. Sections **A.** to **C.** show the fold change over untreated cells, sections **D.** to **F.** show the fold change over the control oligonucleotide ON-4.1. Sections **A.** and **D.** show data for oligonucleotides with one, two, or three deoxy ribose sugars (ON-4.6-d, ON-5.1-dd and ON-5.2-ddd respectively), **B.** and **E.** oligonucleotides with one, two, or three 2´-MOE ribose substitutions (ON-4.7-o, ON-5.3-oo and ON-5.4-ooo respectively), and **C.** and **F.** oligonucleotides with one, two or three LNA ribose substitutions (ON-4.8-l, ON-5.5-ll and ON-5.6-lll respectively). A note is that the experimentation of ON-5.1-dd was carried out in a separate instance from ON-5.1-d and ON-5.2-ddd and so is displayed in a separate window (**A1**.)

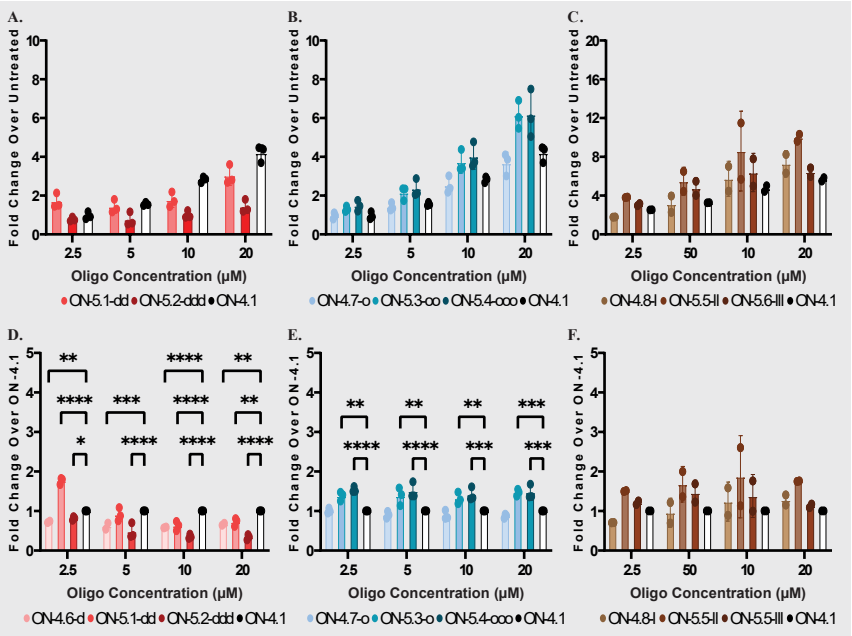


Figure 5.4: Exon skipping activity of sugar-substituted ON-4.6-d, ON-5.1-dd, ON-5.2-ddd, ON-4.7-o, ON-5.3-oo and ON-5.4-ooo as well as the 2´-OMe control oligonucleotide ON-4.1 when dosed gymnotically. Sections **A.** to **C.** show the fold change over untreated cells, sections **D.** to **F.** show the fold change over the control oligonucleotide ON-4.1. Sections **A.** and **D.** show data for oligonucleotides with one, two, or three deoxy ribose sugars (ON-4.6-d, ON-5.1-dd and ON-5.2-ddd respectively), **B.** and **E.** oligonucleotides with one, two, or three 2´-MOE ribose substitutions (ON-4.7-o, ON-5.3-oo and ON-5.4-ooo respectively), and **C.** and **F.** oligonucleotides with one, two or three LNA ribose substitutions (ON-4.8-l, ON-5.5-ll and ON-5.6-lll respectively).

As before since the ASOs were all normalised to the 2´-OMe control at each concentration, the fold change over ON-4.1 values for each dose can be consolidated and plotted together to give an aggregated effect of the different permutations. This allows comparisons to not only be made between a sugar and the 2´-OMe control but also between the number of substitutions made and between the different sugars. This is all shown in Figure 5.5.

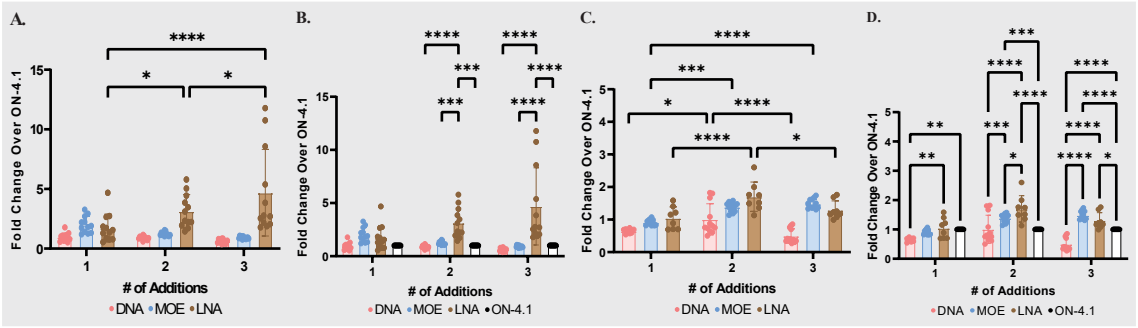


Figure 5.5: Plots of fold change over ON-4.1 across all doses tested for oligonucleotides with one, two or three additions of DNA (ON-4.6-d, ON-5.1-dd and ON-5.2-ddd respectively), MOE (ON-4.7-o, ON-5.3-oo and ON-5.4-ooo respectively) and LNA (ON-4.8-l, ON-5.5-ll and ON-5.6-lll respectively). **A.** and **B.** show data for oligonucleotides transfected with Lipofectamine 3000. **A.** makes comparisons between different numbers of additions of the same substitute ribose sugar and **B.** makes comparisons between the same number of substitutions of different substitute ribose sugars and to the ON-4.1 control. **C.** and **D.** are the same as **A.** and **B.** respectively except with data from gymnotically dosed oligonucleotides.

It can be seen that when transfected, LNA substitutions perform the best and their performance increases with an increase in the number of additions. In fact, it is the only ribose form that saw a statistically significant difference between the number of sugar substitutions in the ASO, going from 1.73 fold increase over ON-4.1 with one LNA, to 3.13 fold increase with two LNAs to 4.69 fold increase with three LNAs. LNA performs statistically better than all ribose substitutions with two and three additions.

More statistically significant comparisons emerge with gymnotic dosing. When comparing the number of substitutions within a sugar there is a difference between every combination except when going from two to three MOE sugars. Substituting in DNA sugars seems to confer no benefit as at best it performs at the same level as ON-4.1 Three additions reduced the activity to half that of ON-4.1. Adding MOE sugars seems to have a modest effect rising from on par with ON-4.1 to about 1.5 times the activity of ON-4.1. However, there is no statistical significance between two and three additions, meaning that the small effect seen cannot necessarily be improved by adding more. There is significance between ASOs with one, two and three LNAs but it is not strictly cumulative.

One LNA gives a mean of 1.05 fold over ON-4.1, two LNAs 1.70 fold and three LNAs 1.29 fold.

Comparing the sugars to each other and ON-4.1 also yields many statistically significant differences. For one addition, there is no difference between DNA and MOE, however DNA is statistically worse than LNA and ON-4.1. For two additions, LNA is the best performer with significance to everything. Additionally, MOE is statistically better than ON-4.1 and DNA. For three additions, DNA is by far the worst, with significance to everything. DNA and MOE are both statistically better than ON-4.1 but not to each other.

5.2.3 Analysis of Results from Ribose Substituted ssASO Activity

The results are interesting as they show differences between the relative performance of an ASO to the control when transfected with an agent and without. When transfected with Lipofectamine3000, the LNA modified sugar confers great improvement over the 2´-OMe control and more additions are better. Additionally, there is no difference between the 2´-OMe ASO, the MOE and the DNA containing ASOs. This is not the same as when transfected. LNA is still the best performing modification, however the peak efficiency goes from 4.69 fold increase over the 2´-OMe ASO to 1.70 fold increase. This peak is also seen with two additions in the gymnotic dosing, with efficiency decreasing when three LNA sugars are added. Apart from this it can be seen that adding DNA sugars decreases efficiency, especially when three are added and modest gains can be had from the addition of MOE sugars.

These results are likely due to a combination of melting temperature and protein-ASO interactions. When transfected with Lipofectamine, the oligonucleotides with extremely high duplex melting temperatures perform well because a comparatively large

amount enters cells, binding very tightly to many target pre-mRNAs, producing high amounts of functional luciferase. This means that adding more LNAs is beneficial as it provides this huge duplex stability.

It is not the case when dosed gymnotically and smaller amounts are penetrating cells. The high duplex affinity caused with multiple LNA additions means the ASO is slower to release from a given pre-mRNA intron, potentially even after splicing has occurred. This means that it functions less in a ‘catalytic’ fashion where one ASO can bind and release from multiple pre-mRNA strands giving many copies of functional luciferase from each molecule. Duplex stability is still important, and increasing it to a point as seen from two additions of LNA provides improvement, but there is a balance to be struck. This also can explain why MOE sugars give a benefit as multiple additions provides a modest amount of duplex stabilisation.

The other aspect is protein-ASO interactions. It could be that over the course of 96 hours the DNA sugars reduce the ASO’s resilience to nucleases and are degraded more, contributing to why three additions in particular is not statistically different from ON-4.1 when transfected, however showing half the activity when gymnotically dosed.

LNA on the other hand is stable to nucleases compared to DNA, but also has a high affinity for RNA- binding proteins such as the paraspeckle protein p54nrb. In the gymnotic environment, where each copy of oligonucleotide is precious, some are bound to these proteins rendering them unable to form a duplex with the pre-mRNA. Additionally, when transfected with Lipofectamine, the ASOs are encapsulated in a lipoplex that can shield them from proteins, preventing interaction with nucleases or RNA-binding proteins and shuttling them to the nucleus directly where they can be effective.

These results raise the question as to how an ASO with an charge-neutral backbone would perform with these ribose-modified platforms. As DNA sugars had a detrimental effect on gymnotic activity, the choice of platform is between a 2´MOE and LNA substituted ASO. Between these two, there was no instance where 2´MOE provided a statistically significant benefit over an LNA-substituted ASO. LNA showed statistical benefit over 2´MOE with two and three additions of both sugars when transfected and with two additions of both sugars when dosed gymnotically. Additionally, a combination of a MOP-linkage and LNA could maintain the benefits of high thermal stability while preventing detrimental ASO-protein interactions. This could have a synergistic effect that would not be seen with the 2´MOE modification does not provide as much duplex thermal stability or have these negative interactions with RNA-binding proteins. For these reasons, LNA substituted ASOs were selected to test the efficacy of the MOP-linkage. To that end a series of oligonucleotides with an LNA-methoxypropyl phosphonate backbone were synthesized.

5.3 Methoxypropyl Phosphonate (MOP) Backbone in Splice-Switching ASOs

5.3.1 Oligonucleotides used to Study LNA-PS and LNA-MOP Linkgaes in ssASOs

To begin the study, MOP-phosphoramidites were synthesised as shown in Figure 5.1. Amidites were created using LNA-thymidine. The phosphoramidites are then added using standard phosphoramidite synthesis with a sulfurisation cycle. As the methoxy propyl phosphine was placed on an LNA sugar the MOP-phosphorothioate linkage was incorporated to be at the 3-side of the LNA sugar to give the linkages shown in Figure 5.6.

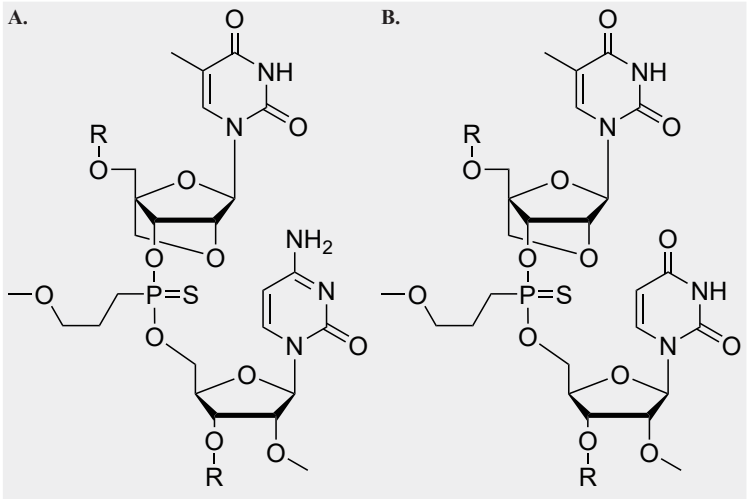


Figure 5.6: MOP-phosphorothioate linkages. between **A.** LNA-thymidine and 2´-OMe cytidine and **B.** LNA-thymidine and 2´-OMe-uracil.

ASOs were then synthesized with these linkages, deprotected with ethylene diamine. The oligonucleotides made are shown in Figure 5.7.

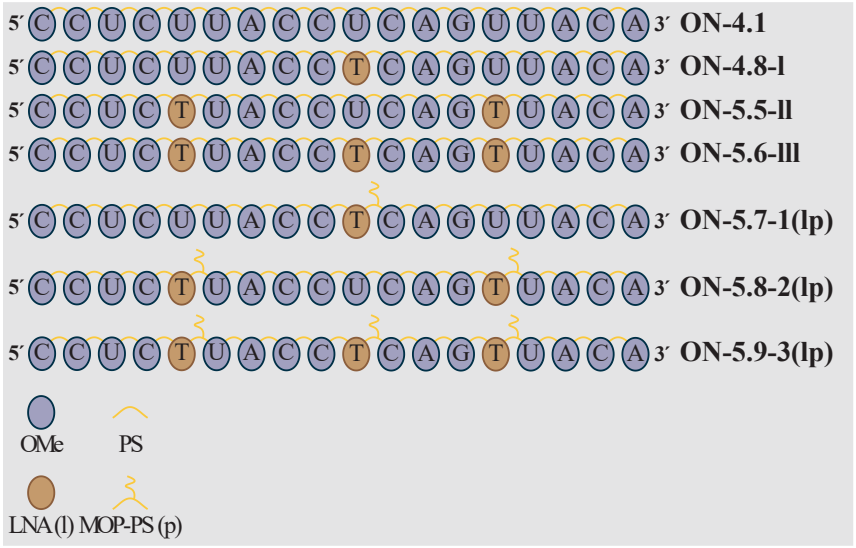


Figure 5.7: Oligonucleotides synthesised with one two and three additions of LNA (ON-4.8-l, ON-5.5-ll and ON-5.6-lll respectively) and one, two or three additions of LNA-methoxypropyl phosphorothioate linkages (ON-5.7-1(lp), ON-5.8-2(lp) and ON-5.9-3(lp) respectively). These along with the 2′-OMe control ON-4.1 were used to evaluate the effect of a phosphonate linkage on exon skipping activity.

The melting temperature for the MOP-phosphorothioate oligonucleotides was measured and found to be +11.26°C, +14.17°C, and +16.73°C compared to ON-4.1. As with the MOE modifications, there appears to be a very large effect from one addition which does not add when more are inserted into the sequence. It could again be the alkyl chain that is providing stabilisation to the duplex if it is in the interior of the duplex. It is one carbon longer than the MOE linkage but also positioned on the phosphate backbone, slightly further away. This linkage also is a stereo-centre and the alkyl chain would only be able to provide this effect in one conformation meaning separating the isomers and testing each individually could provide insights in the future. Overall, the melting temperatures are similar to that found in the LNA ASOs with only a few degrees either way across the number of additions.

5.3.2 Results of ssASOs with LNA-PS and LNA-MOP linkages

Oligonucleotides ON-5.7 to ON-5.9 were dosed with lipofectamine and gymnotically. Results are shown in Figure 4.16.

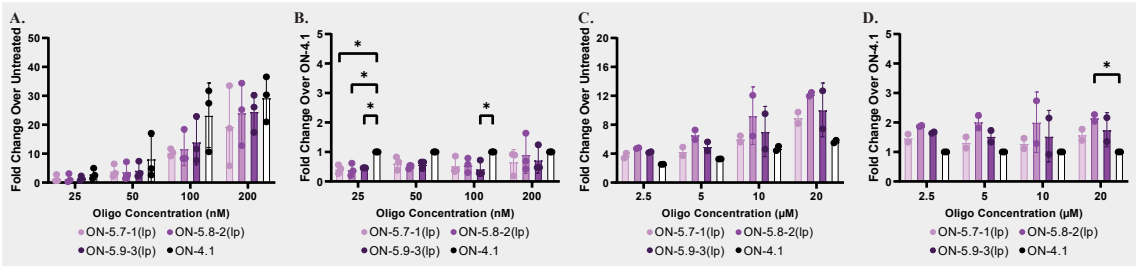


Figure 5.8: Exon skipping activity of MOP containing oligonucleotides ON-5.7 to ON-5.9. **A.** and **B.** show data for oligonucleotides transfected with Lipofectamine 3000, **C.** and **D.** for oligonucleotides dosed gymnotically. **A.** and **C.** show data with respect to untreated cells, **B.** and **D.** with respect to the control oligonucleotide ON-4.1.

As before the fold change over the 2´-OMe control was pooled across all concentrations for an ASO to give an aggregate effect. This was also compared to the oligonucleotides containing LNA sugars and phosphorothioate linkages (ON-4.8-l, ON-5.5-ll, ON-5.6-lll) and is shown in Figure 5.9

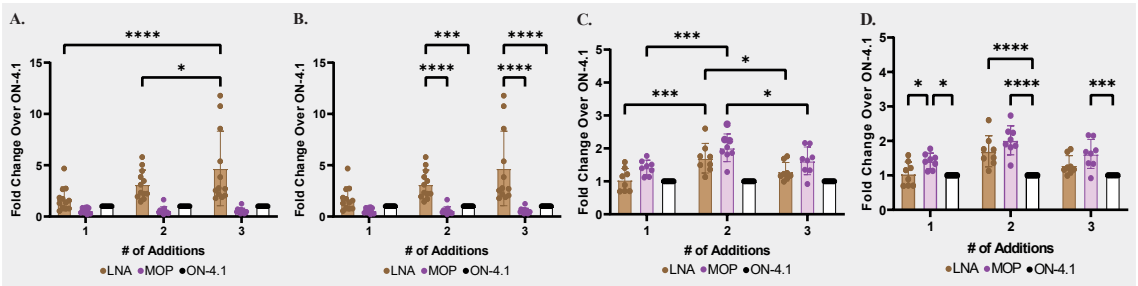


Figure 5.9: Plots of fold change over ON-4.1 across all doses tested for oligonucleotides with one, two or three additions of LNA (ON-4.8-l, ON-5.5-ll and ON-5.6-lll respectively), and LNA-MOP (ON-5.7-1(lp), ON-5.8-2(lp) and ON-5.9-3(lp) respectively. **A.** and **B.** show data for oligonucleotides transfected with Lipofectamine 3000. **A.** makes comparisons between different numbers of additions of the same substitute ribose sugar and **B.** makes comparisons between the same number of substitutions of different substitute ribose sugars and to the ON-4.1 control. **C.** and **D.** are the same as **A.** and **B.** respectively except with data from gymnotically dosed oligonucleotides.

Interestingly, there is a difference between the relative activities of ASOs when dosed with a transfection agent compared to when dosed without. When transfected with Lipofectamine, there is no statistical difference between the MOP containing ASOs with

one, two and three additions or between MOP ASOs and the 2´-OMe control. This means that LNA-phosphorothioate remains the most effective modification. By contrast, when dosed gymnotically the gap between the MOP and LNA ASOs is very narrow. The only statistical difference between the LNA-MOP and LNA-PS modifications comes with ON-4.8-l and ON-5.7-1(lp), where the MOP containing ASO is better. The difference is relatively minor, with ON-5.7-1(lp) performing 1.42 fold better than ON-4.1 and ON-4.8-l performing 1.04 fold better. In both cases the best results come from two additions where ON-5.8-2(lp) is 2.01 fold over ON-4.1 and ON-5.5-ll is 1.70 fold. The MOP ASO is also statistically better than ON-4.1 with three additions where the LNA ASO has no significant difference.

5.3.3 Analysis of Results of ssASOs Containing LNA-PS and LNA-MOP Linkages

The difference in performance between transfected and gymnotically dosed ASOs likely comes from several factors. As previously discussed, the lipoplex can shield the LNA containing ASO from detrimental ASO-protein interactions, allowing the high target affinity to give benefit. While the MOP-ASOs also have significantly higher melting temperatures than the 2´-OMe control, they also have charge-neutral linkages that could be disrupting lipoplex formation. The positively charged lipids must complex to the backbone of the ASO and having alkyl chains could potentially be problematic for this, meaning that although each molecule of ASO is more effective, transfection efficiency is lower. This is not a problem with the gymnotic dosing, however, and the activity of the MOP ASOs is higher than ON-4.1. It also seems that two additions are ideal for both the MOP and LNA containing ASOs with gymnotic dosing, however some more questions are raised. As such further investigations using LNA and LNA-MOP containing ASOs were performed.

5.4 Additional Investigations of Splice Switching ASOs with LNA-PS and LNA-MOP Modifications

5.4.1 Oligonucleotides Used to Study the Effects of Additional LNA Sugars

While it would appear from the previous investigation that two additions of either LNA or LNA-MOP modifications is ideal for gymnotic dosing, questions remain open. It is possible that the addition of multiple LNA sites across the ASO is responsible for stronger interactions to RNA-binding proteins which are detrimental to efficacy. However, this is a separate issue from duplex stability where more LNA sugars could be beneficial. Oligonucleotides were designed with more than one LNA in the same area. LNA sugars in neighbouring positions will still provide additional duplex stabilisation compared to one by itself, however the protein binding characteristics will be altered. In particular, one MOP linkage flanked by LNA on either side could prevent unwanted interactions for both at the same time. Additionally, an oligonucleotide was made where the sulfurisation step of coupling the LNA-MOP phosphoramidite was replaced with oxidation.This gives one oligonucleotide with a LNA-MOP-phosphodiester (LNA-MOP-PO) motif in addition to the LNA-MOP-PS motif and the LNA-PS motif. Oligonucleotides used are shown in Figure 5.10.

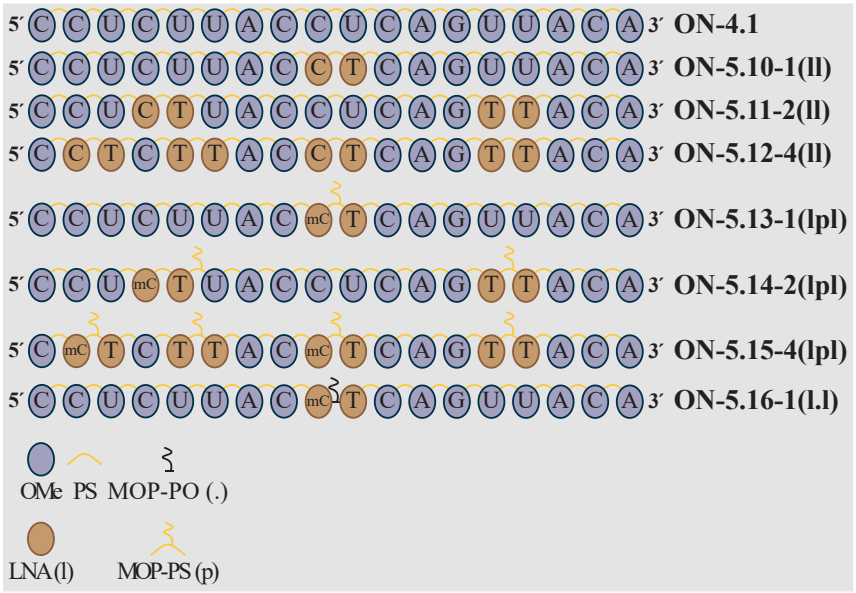


Figure 5.10: ASOs synthesised with one, two or four additions of two clustered LNA modifications (ON-5.10-1(ll), ON-5.11-2(ll) and ON-5.12-4(ll) respectively) and two clustered LNA sugars with a phosphorothioate-MOP linkage (ON-5.13-1(lpl), ON-5.14-2(lpl) and ON-5.15-4(lpl) respectively). Additionally ON-5.16-1(l.l) was synthesised with one cluster of two LNA sugars joined by a phosphodiester-MOP linkage.

Melting temperatures were measured for these ASOs as +15.74°C, +>20°C, +>20°C, +13.78°C, +19.46°C, +>20°C and +4.19°C for ON-5.10-1(ll), ON-5.11-2(ll), ON-5.12-4(ll), ON-5.13-1(lpl), ON-5.14-2(lpl), ON-5.15-4(lpl) and ON-5.16-1(l.l) respectively. As expected the LNA-PS-LNA and LNA-MOP-LNA modifications provide significant thermal stabilisation to the duplex, with the LNA-PS-LNA providing slightly more stabilisation. Curiously, the PO-MOP variant provided less stabilisation than the PS-MOP, however in both cases, the thermal stability is significantly higher than the 2´OMe-control. These oligonucleotides were then measured for exon-skipping efficacy.

5.4.2 Results of ssASOs Containing clustered LNA riboses with PS, MOP-PS and MOP-PO linkages

Oligonucleotides ON-5.10 to ON-5.16 were dosed with Lipofectamine3000. Results are shown in Figure 5.11.

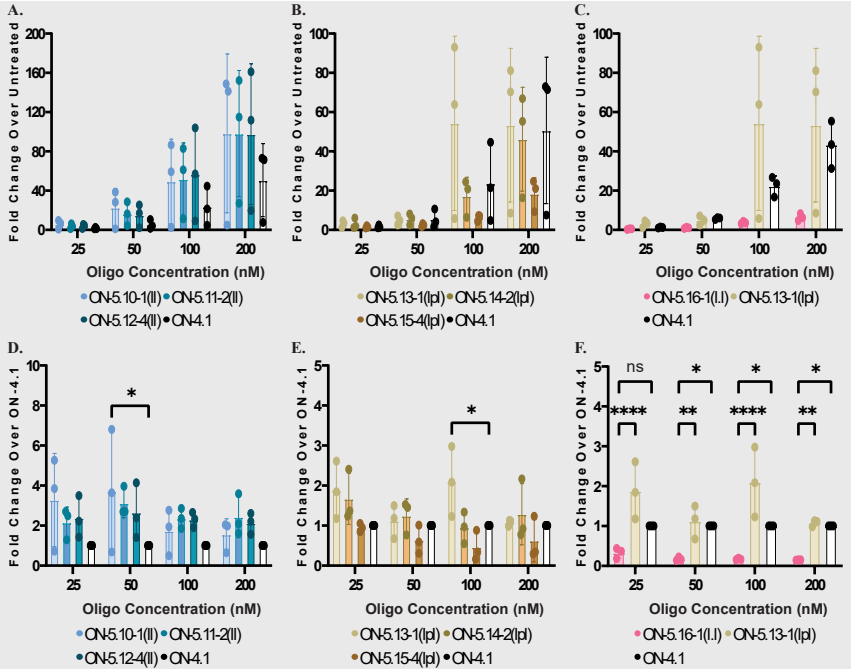


Figure 5.11: Exon skipping activity of oligonucleotides ON-5.10 to ON-5.16 transfected with Lipofectamine 3000. Sections A., B. and C. show activity with respect to untreated cells. Sections D., E. and F. show activity with respect to the control ASO ON-4.1. A. and D. show oligos with one, two or four additions of two clustered LNA sugars (ON-5.10-1(ll), ON-5.11-2(ll) and ON-5.12-4(ll) respectively). B and E. show oligos with one, two or four additions of two LNA sugars joined by a PS-MOP linkage (ON-5.13-1(lpl), ON-5.14-2(lpl) and ON-5.15-4(lpl) respectively). C. and F. show oligonucleotides wit one addition of two LNA sugars joined by either a PS-MOP linkage (ON-5.13-1(lpl)) or PO-MOP linkage (ON-5.16-1(l.l)).

After delivery with Lipofectamine3000, oligonucleotides ON-5.10 to ON-5.15. were dosed gymnotically. Results are shown in Figure 5.12.

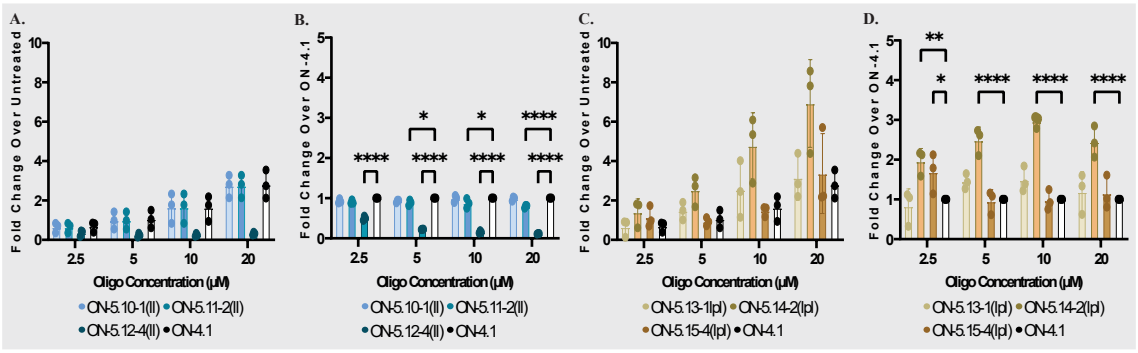


Figure 5.12: Exon skipping activity of oligonucleotides ON-5.10 to ON-5.15. Sections A. and C. show activity with respect to untreated cells. Sections B. and D. show activity with respect to the control ASO ON-4.1. Sections A. and B. show data for oligonucleotides with one, two, or four additions of two clustered LNA sugars (ON-5.10-1(ll), ON-5.11-2(ll) and ON-5.12-4(ll) respectively). Sections C. and D. show data for oligonucleotides with one, two, or four additions of two clustered LNA sugars joined by a PS-MOP linkage (ON-5.13-1(lpl), ON-5.14-2(lpl) and ON-5.15-4(lpl) respectively).

As before the fold change over ON-4.1 values for double-LNA and double-LNA-MOP phosphorothioates were pooled across all doses of an ASO to give an aggregated view as shown in Figure 5.13.

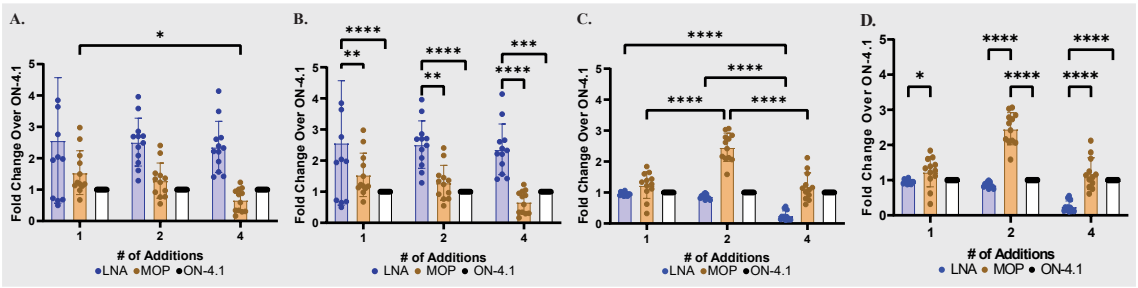


Figure 5.13: Plots of fold change over ON-4.1 across all doses tested for oligonucleotides with one, two or three additions of two clustered LNA sugars (5.10-1(ll), ON-5.11-2(ll) and ON-5.12-4(ll) respectively), and two LNA sugars joined by a PS-MOP linkage (ON-5.13-1(lpl), ON-5.14-2(lpl) and ON-5.15-4(lpl) respectively. **A.** and **B.** show data for oligonucleotides transfected with Lipofectamine 3000. **A.** makes comparisons between different numbers of additions of the same substitute ribose sugar and **B.** makes comparisons between the same number of substitutions of different substitute ribose sugars and to the ON-4.1 control. **C.** and **D.** are the same as **A.** and **B.** respectively except with data from gymnotically dosed oligonucleotides.

5.4.3 Analysis of Results of ssASOs with LNA-PS and LNA-MOP-PS Linkages

Oligonucleotide ON-5.16-1(l.l) performed significantly worse than the control oligonucleotide ON-4.1 and MOP-PS counterpart ON-5.13-1(lpl). Reasons are not entirely clear as the phosphonate linkage provides resistance to nucleases so the difference between ON-5.13-1(lpl) and ON-5.16-1(l.l) should be fairly subtle. Due to this poor activity it was not taken into gymnosis or plotted in Figure 5.13.

When dosed with Lipofectamine3000, oligonucleotides with LNA-PS motifs (ON-5.10 to ON-5.12) show no difference to each other. For those with LNA-MOP-PS motifs (ON-5.13 to ON-5.15), there is only difference between ON-5.13 and ON-5.15 and it is slight. Each oligonucleotide with a LNA-PS motif outperform their LNA-MOP-PS counterparts and ON-4.1. This is could be due to the extremely high melting temperate of 70°C (+15°C compared to ON-4.1) and higher for this group for reasons previously mentioned. There is no difference with the MOP ASOs as again, the melting temperature is high, but perhaps transfection efficiency is lower and modulation of ASO-protein interactions is less impactful because of the shielding effect coming from the lipoplex.

When dosed gymnotically the LNA-MOP-PS containing ASOs are statistically better than the LNA-PS-ASOs in every case. Improvement is also observed in ON-5.14-2(lpl) compared to ON-4.1. In fact, this oligonucleotide with four LNA sugars and two MOP-phosphorothioate linkages is the best gymnotic ASO, at a 2.46 fold increase over ON-4.1. Additionally ASOs ON-5.10-1(ll), ON-5.11-2(ll), ON-5.13-1(lpl) and ON-5.15-4(lpl) maintained the same level of activity as ON-4.1 while ON-5.12-4(ll) exhibited a decrease in activity, falling to 25% as activ9lpl)e as ON-4.1.

MOP linkages seem to increase the number of LNA sugars that can be tolerated in an ASO. This allows for oligonucleotides to have a significantly increased duplex melting temperature compared to an all-2´-OMe ASO while not suffering from adverse

oligo-protein interactions. There also appears to be a limit to how high the duplex melting temperature can become without having an adverse effect on activity as seen in the difference between ON-5.14-2(lpl) and ON-5.15-4(lpl). In both cases the phosphonate linkage should reduce the protein binding affinity however ON-5.15-4(lpl) which has a higher melting temperature is less effective.

5.5 Generalisations on ASOs modified with LNA-PS and LNA-MOP-PS Linkages

As the LNA proved to be the most successful substitute sugar, it is important to determine the optimal composition of the ASO, starting with the number of LNAs in the sequence as displayed in Figure 5.14.

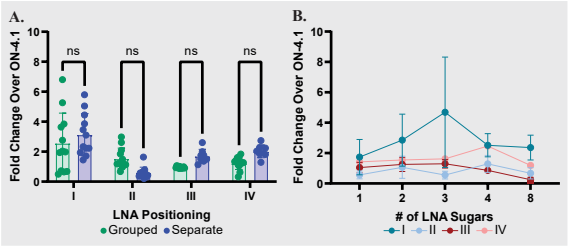


Figure 5.14: A. Shows a comparison of Exon skipping activity of ASOs with two additions of LNA and one addition of two clustered LNA sugars with respect to the control oligo ON-4.1 across all doses tested. **I** refers to LNA substituted ASOs (ON-5.5-ll and ON-5.10-1(ll)) transfected with Lipofectamine 3000. **II** refers to LNA-PS-MOP substituted ASOs (ON-5.7-2(lp) and ON-5.13-1(lpl)) transfected with Lipofectamine 3000. **III** and **IV** refer to the same conditions as **I** and **II** respectively except with the oligonucleotides dosed gymnotically. **B.** shows a comparison of exon skipping activity of ASOs with respect to the control oligo ON-4.1 plotted against the number of LNA sugars in the ASO. **I** refers to LNA modified ASOs (ON-4.8-d, ON-5.5-dd, ON-5.6-ddd, ON-5.10-1(ll), ON-5.11-2(ll), ON-5.12-4(ll)) transfected with Lipofectamine3000. **II** refers to LNA-PS-MOP modified ASOs (ON-5.7-1(lp), ON-5.8-2(lp), ON-5.9-3(lp), ON-5.13-1(lpl), ON-5.14-2(lpl), and ON-5.15-4(lpl)) transfected with Lipofectamine3000. **III** and **IV** refer to the same conditions as **I** and **II** except with the oligonucleotides dosed gymnotically.

As seen in **A.** first a comparison was made between ASOs containing two LNA sugars. The two LNAs can either be spaced apart in the sequence or added in the same location at the centre of the strand. Comparison shows that there is no significance between these sets under any of the conditions tested. Perhaps this indicates there is not much impact of LNA position, only from total LNA count.

In **B.** it can be seen that the addition of LNA has a marked effect when transfected with Lipofectamine3000 and three additions gave the best results. Two to three additions of LNA also seems to be the best when dosed gymnotically, however the effect is smaller. The effect is reversed when a MOP linkage is introduced, with a larger improvement

coming with gymnotic dosing as opposed t when transfected with Lipofectamine3000. Also of note is that the optimal number of LNAs goes from three to four (ON-5.14-2(lpl)). Next it is important to consider the correlation of melting temperature to activity as seen in Figure 4.23.

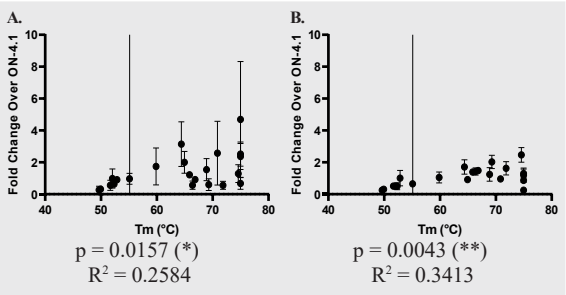


Figure 5.15: Duplex melting temperature of ON-4.1 to ON-4.8 and ON-5.1 to ON-5.16 plotted against the exon skipping activity of an ASO with respect to the control the oligo ON-4.1. Statistical significance and correlation coefficient of linear correlation are shown along with a vertical line indicating the melting temperature of ON-4.1. **A.** refers to ASOs transfected with Lipofectamine 3000, **B.** refers to ASOs dosed gymnotically.

A severe limitation is imposed by the upper limit of detection. All oligos with more than three LNAs are not within the limit of detection, and are plotted at 75°C though the value is higher than this. It is possible to extrapolate based on the difference in melting temperature from a lower number of additions, however as seen several modifications in this chapter, melting temperature does not necessarily correlate linearly with modification additions. There is a correlation between the two variables given the low p values, however the correlation is fairly week from the Pearson's R squared value (for a linear fit). This indicates that while melting temperature is important, it is not the only factor.

This can be seen with the charge-neutral MOP-linkage where an advantage is seen in only in gymnotic dosing. It is possible that they can help push the balance that must be struck between duplex stabilising effects from the LNA sugars and the detrimental ASO-RNA-binding protein interactions caused LNA in a more favourable direction. The addition of the MOP allows for more LNAs to be placed in a sequence which can allow for ASOs with higher duplex thermal stability without getting bogged down and

inactivated with these unwanted binding interactions. This is only true to a certain point as too many additions of the LNA-MOP also reduced activity. It therefore seems that there is perhaps an optimal melting temperature that is far higher than that of an mRNA/2´-OMeASO duplex and that adding these charge-neutral LNA modifications allows a duplex to get closer to this temperature. This is on top of reducing the overall negative charge which can also aide in passive diffusion through the cell membrane.

These results have important implications for the use of this style of ASO modification in splice switching therapeutics. Currently, none of the exon skipping ASOs approved for DMD use any kind of lipoplex for delivery.[17] To move forward, more ASO modifications must be tested, however the luciferase assay used thus far has some limitations, especially with precision of results and the use of a non-dystrophic sequence. As such different assays were explored for future testing.

5.6 Conclusions

This chapter started with the investigation of ribose changes to a 2´OMe-phosphorothiate oligonucleotide and the effect thereof on splice-switching activity. Three different riboses were used, DNA, 2´MOE and LNA. Of these three it was found that LNA sugars provide a large benefit when transfected with Lipofectamine3000 while no difference was observed between DNA, 2´MOE and the 2´OMe control. When dosed gymnotically it was observed that DNA sugars are detrimental to activity compared to the all-2´OMe ASO while both 2´MOE and LNA can confer some benefit. With two additions, both show statistically significant improvement to the 2´OMe ASO and LNA has a statistically significant advantage over 2´MOE. At three additions 2´MOE showed the best activity, however, both 2´MOE and LNA show statistically significant improvement over the 2´OMe control, there is no significance between the two of them and 2 additions of LNA gave the best activity of any of the ASOs tested.

Given the observations of the first section, LNA was selected to be the platform for the charge-neutral MOP backbone and the next section describes the splice-switching activity of LNA-MOP ASOs in comparison to the LNA-PS. Results show that when transfected there is no change in activity compared to the 2´OMe-phosphorothioate control, thereby making the activity lower than the ASOs with the LNA-PS. This is different from gymnotic dosing where LNA-MOP ASOs showed statistically significant improvement over the 2´OMe-control with one, two and three additions as well as statistically significant improvement over the LNA-ASO with two additions of each modification. Two additions was the best of the series for both the LNA and LNA-MOP with the LNA-MOP having the highest overall activity, though again, not statistically significant to the LNA alone.

Based on these results, where adding additional sites of LNA or LNA-MOP did not seem to be beneficial, a different approach was taken where additional LNA sugars

were added by clustering them together to give either an LNA-PS-LNA motif or an LNA-MOP-LNA motif. Results from splice-switching assays with these ASOs continue the trend observed with the LNA-PS and LNA-MOP. The LNA-PS-LNA ASOs were more active than the 2´OMe control and the LNA-MOP-LNA ASOs which showed no difference to each other. In gymnotic dosing the LNA-PS-LNA provided no benefit with one and two additions and had a deleterious effect compared to the 2´OMe control with four additions. The LNA-MOP-LNA ASOs show statistical benefit over the 2´OMe control with two and four additions and benefit over the LNA-PS-LNA with one two and four additions. Of all the oligonucleotides tested in Chapter 4 or 5, ON-5.14-2(lpl) with two additions of the LNA-MOP-LNA motif showed the highest activity when dosed gymnotically with a 2.46-fold improvement over the 2´OMe control.

The difference in trends and activity between the same oligonucleotides that are transfected or dosed gymnotically can provide explanations for the results observed. It can be seen across all six variants of LNA-PS ASOs tested that adding LNA to a splice-switching oligonucleotide can bring large increases to activity, with anything from one LNA sugar to 8 LNA sugars consistently giving 2 to 3-fold improvement over the 2´OMe control. Gymnotic dosing shows that one two three LNA sugars make no difference or at best show modest improvement compared to the 2´OMe control and anything more starts to be detrimental, possibly due to interactions between LNA-ASOs and things other than the target mRNA.

LNA leads to strong interactions between and ASO and entities in a cell. The interaction to the target mRNA will be strengthened which is the intended and helpful effect of adding LNA. LNA will also lead to stronger interactions with sequences of mRNA that are not fully complementary, meaning it can interact with off-target genes.[66] *In vivo* this is a toxicity concern, however in this context it could be that transcripts of the LNA-ASO are tied up interacting with some gene unrelated to luciferin. This is not as

much of an issue with transfection as the number of copies of ASO in a cell is high, meaning that if some copies are not functioning as intended the effect is not significant overall, and the benefit of stronger ASO-target interactions gives higher activity. This the opposite with gymnotic dosing where a low ASO copy-count in each cell means that if any of these copies are unable to be removed from an off-target mRNA a large effect will be seen. The same logic applies to the target mRNA. To function efficiently an ASO should bind to the splice site, alter the splicing then detach to find another transcript of mRNA to alter. The same interactions that can tie an ASO to an off-target mRNA can hinder the detachment from the target mRNA, lowering the overall efficiency.

Interactions between LNA-ASOs and proteins are analogous to those of LNA-ASOs to mRNA. It has been found that LNA promotes strong binding to various proteins[65, 139-141] which can have a similar effect of sequestering some copies of LNA-ASOs inside cells, preventing them from carrying out their desired function. As with the off-target mRNA this effect might be negligible with the relative abundance of copies provided by transfection but far more consequential with gymnotic dosing. The effects of off-target mRNA interactions and protein interactions could be additive with each other and the number of LNAs in an ASO, with both taking away more copies of functional ASO the more LNA is in that ASO.

The fact that the transfected-gymnotic trend is reversed with LNA-MOP ASOs is likely due to these same factors, or rather, how the MOP addresses them. The reason the MOP was first synthesized was to address the issue of LNA-ASOs binding to proteins and it was found to effectively prevent this from occurring.[140] If there is a significant reduction in these ASO-protein interactions this will free more of those ASO copies in a cell to perform their intended function, boosting gymnotic activity while having a small or no effect on transfected activity as described above.

As the MOP is slightly destabilizing to an ASO-RNA duplex, it can also address the issues described above with mRNA. Although the overall duplex stability of the LNA-MOP ASOs tested is significantly higher than the 2´OMe control, perhaps the placement of the MOP adjacent to the LNA is what Is giving the benefit, especially with regards to off target-mRNA. Any increase in off-target mRNA interactions that stem from an LNA-ASO will occur at the region where the LNA is present and increasing the duplex stability. Since the MOP is also in the same region, it cold be lowering this local duplex stability which leads to less of these unwanted interactions and more ASO available to alter splicing. The same could be true of the target mRNA where even slight reductions of duplex stability in the area of the LNAs could make offloading of the ASO after the splice-event is completed easier.

Even with the LNA-MOP ASOs there is a limit to how many additions is beneficial. As more LNAs are added it is possible that the MOP does not weaken the undesired interactions of the LNA enough meaning as with just the LNA, they begin to outweigh the benefit of a stronger ASO-target interaction. This can also be supported by the observation that there can be benefit from clustering two LNAs around the MOP where it can function for the LNA-protein and LNA-mRNA of both at the same time while the target affinity is raised by more than with one LNA by itself.

The above observations can provide insight into the reasons behind the increased activity of LNA-MOP ASOs, however many questions remain unanswered. In particular it remains uncertain how these translate from a luciferase reporter assay to a more clinically relevant model. Additionally, a good way to provide further evidence for the mRNA and protein interactions as causes for changes in activity is to image oligonucleotides in cells. Solutions to these issues were explored in the next chapter.

Chapter 6: Alternative Splice Switching Assays and Methods for Imaging Oligonucleotides in Cells

6.1 Introduction

The first section of this chapter describes evaluation of exon-skipping with the H2K cell line. These are myotubes derived from the dystrophic mouse that is commonly used as an animal model for testing splice switching ASOs targeting DMD.[217] This is done because the issue stemming from frame shifting mutations is akin to that in humans, however the genes are not exactly the same, with the mutation occurring in Exon 23[218], not a common pattern in humans. After dosing with an ASO the total RNA of the cells can be extracted, followed by RT-qPCR to amplify and quantify the levels of mRNA both with and without Exon 23, giving a skipping percentage.

This assay has several benefits. Firstly, although not exactly the same as the dystrophin sequence found in humans, it is a much closer model than the hybrid luciferase/β-globin system. Secondly, the use of qPCR quantifies the actual exon skipping percentage and does not rely on the proxy of luminescence. This measurement will also have no dependence on the number of cells as it is a measurement of the ratio of the two mRNA sequences, meaning it also does rely on protein quantity as a proxy for cell count. This means that data from this assay should be both more representative of the true disease state than the luciferase reporter assay as well as more precise. This chapter attempts to use qPCR to establish such a precise assay.

Parallel to the alternate exon-assay described above, investigations were carried out to develop a method for imaging ASOs inside of cells independent of mode of action (splice-switching or gene silencing) or target. An ideal method would have the ability to establish the relative quantity of ASO present in a cell as well as its intracellular location. It would also allow for co-localisation with proteins of interest, such as the RNA-binding proteins associated with LNA-related toxicity. Such a method could be used with HeLa pLuc705 assay used in Chapters 4 and 5 to give a more detailed picture as to how modifications affect the behaviour of the ASO.

Additionally, co-localisation with important organelles such as endosomes and nuclear accumulation can establish the effect of modifications on productive ASO uptake. It is known that therapeutic oligonucleotides are often unable to escape endosomes[219-224], meaning although they are inside a cell, they are not active. Overall, imaging allows more insight into what makes an ASO effective and can lead to more rational design of effective gene-regulating oligonucleotides in future.

To that end this section uses ASOs that cause RNAse mediated knockdown of the long non-coding RNA MALAT-1 to test different dyes and procedures to develop this method. MALAT-1 overexpression is associated with different types of cancer[225-229] and so is a good target for gene silencing using ASOs. In addition, it is one of the most common targets for ASOs in literature.[230-239] To start, the ASOs were conjugated to dyes before dosing, however it was found that dyes can influence ASO activity. After this development began on a method to attach a dye to an ASO *in situ* to allow imaging without this possible interference.

6.2: H2K Exon-skipping Assay

6.2.1: Methods for and Results from a Splice-Switching Assay in H2K Cells

Literature that employs this assay usually follows the general procedure of a RT-PCR followed by quantification of skipped and un-skipped sequences on agarose gel.[240-242] This method is sound, however, it is not as accurate or precise as quantification using qPCR and so a slightly different approach was taken. After harvesting the total mRNA of the H2K cells, RT-PCR is done with an outer set of primers ranging from exons 20-26 of the mouse dystrophin mRNA. It was found that the quantity of RNA is insufficient to quantify from one round of PCR so a second amplification step was added to give a so-called nested-PCR.[243] The second round of amplification was done between Exons 22-24, the region of interest. As these primers will amplify both the skipped and unskipped sequences, two TaqMan probes are used with different dyes for transcript quantification. This is summarised in Figure 6.1.

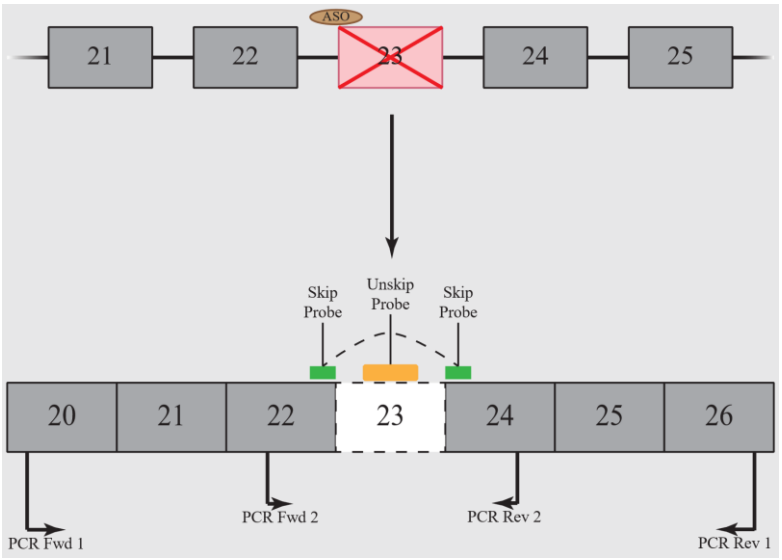


Figure 6.1: Nested PCR approach. mRNA harvested is subject to one round of RT-PCR from Exons 20-26 then a round of qPCR from Exons 22-24. Two probes are employed, one located on Exon 23 complementary only to un-skipped mRNA, one that is at the junction of Exons 22-24 complementary only to skipped mRNA.

Using this approach, it is possible to quantify the amount of skipped and un-skipped mRNA in a given sample using standard curves, as custom sequences of these lengths (approximately 1000 nucleotides at longest) are commercially available from

companies such as Integrated DNA Technologies (IDT). This approach also has the advantage of amplifying both sequences in the same PCR well, eliminating as many extraneous variables as possible. Results are displayed in Figure 6.2.

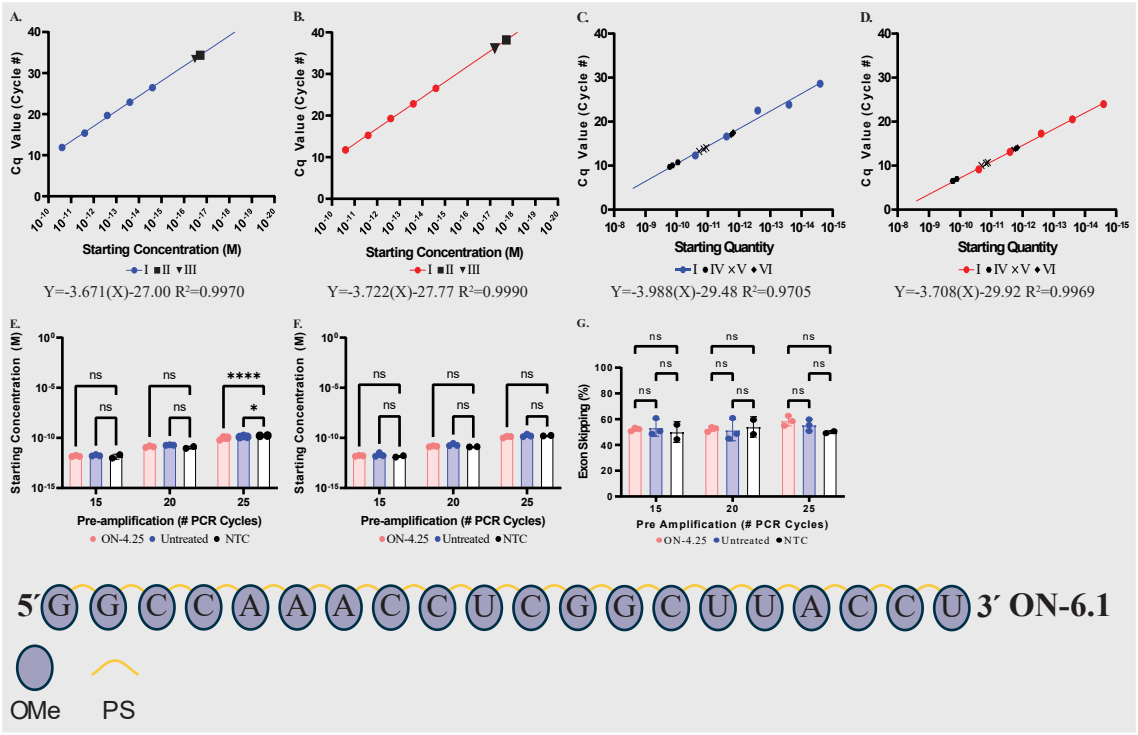


Figure 6.2: Results from H2K PCR exon skipping quantification. **A.** shows one step RT-qPCR results targeting unskipped mRNA **I** refers to known concentration standards, **II** refers to mRNA concentration calculated from the standard curve for untreated cells, **III** refers to concentration of mRNA calculated from the standard curve for cells treated with the ASO ON-4.25. **B.** is the same as **A.** except where the RT-qPCR is targeting skipped mRNA. Note that **A.** and **B.** show data from two different probes added to the same PCR reaction. **C.** shows nested RT-PCR-qPCR targeting unskipped RNA. **I** refers to known concentration standards. **IV** is a group of mRNA concentrations calculated from the standard curve for untreated cells, cells treated with 25 cycles of amplification in the RT-PCR phase, **V** with 20 cycles of amplification and **VI** with 15 cycles. **D.** is the same as C. except where RT-PCR-qPCR is targeting skipped mRNA. For **A.**, **B.**, **C.** and **D.** the equation and correlation coefficient of the standard curve is displayed under the graph. **E.** shows a plot of unskipped mRNA concentrations calculated using the standard curve method for cells treated with ON-4.25, untreated cells, and a Non-Targeting Control (NTC) where no mRNA was added to the RT-PCR reaction. Pre-amplification refers to the number of PCR cycles in the RT-PCR step. **F.** is the same as **E.** except with data for skipped mRNA. **G.** shows exon skipping percentages for cells treated with ON-4.25, untreated cells and NTC PCR samples with 15, 20 and 25 PCR cycles in the RT-PCR step.

Sections **A.** and **B.** show the Cq values for some conditions are above 35 for a single amplification step, the usual limit of quantification for qPCR. Nesting PCRs brings the Cq values into the limit of quantification if the right number of cycles in the RT-PCR

step is used, however does not give reliable quantification information. There is no difference between the number of skipped copies for cells that have been treated with an ASO, those that are untreated and a negative control that had no mRNA loaded. Additionally, there is no difference in skipping percentages between these three conditions.

6.2.2: Analysis of Results from a splice-switching assay in H2K Cells

These results show no difference between PCR reactions loaded with mRNA from H2K cells treated with ASO, mRNA from untreated H2K cells and water and so establish that this method is not viable in this form. This is likely due to extremely low abundance of the mRNA as dystrophin protein only accounts for 0.002% of all muscle protein[244] and 0.01% to 0.001% of total muscle RNA[245] (or about 5-10 molecules per nucleus in human adult skeletal muscle[246]). Combined with the fact that almost all dystrophin mRNA exists as a nascent, not complete state[247] which might not contain the sequence targeted by PCR, it seems likely that there are just not enough copies of the transcript to be accurately quantified by qPCR when cells are cultured on the small surface area of multi-well (24 well) plate. This makes it not ideal for high throughput screening of ASO modifications.

While it would be possible to culture the cells in larger wells to yield more RNA, this is not optimal for high throughput screening as it requires large volumes and amounts of each ASO. In addition, this assay leaves questions unanswered such as transfection efficiency of each ASO and intracellular location of each ASO. As such a efforts were moved to establishing a universal method for imaging oligonucleotides in cells without altering their activity with pre-conjugated dyes as a way to supplement pre-existing assays such as the one used in Chapters 4 and 5.

6.3 Imaging of RNaseH-Dependent Knockdown ASOs in HeLa Cells

6.3.1 Effects of Dyes on Pre-Labelled ASOs

The most common way to visualise oligonucleotides is via conjugation to a fluorescent dye as shown in Figure 6.3.[142-145] This method is convenient as it allows for easy population level quantification of oligonucleotide in cells via techniques such as flow cytometry and more precise localisation with confocal microscopy, however it assumes that the activity and localisation are not affected by the attached dye.

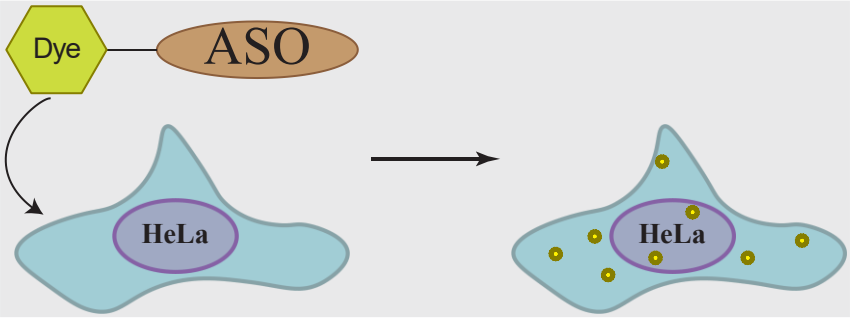


Figure 6.3: ASOs pre-conjugated to fluorescent dyes are transfected into cells and then visualised.

To test this assumption a series of ASOs silencing MALAT-1 were synthesized. The ‘gapmer’ ASOs were made with a series of dyes covering different wavelengths of fluorescence. These ASOs are shown in Figure 6.4.

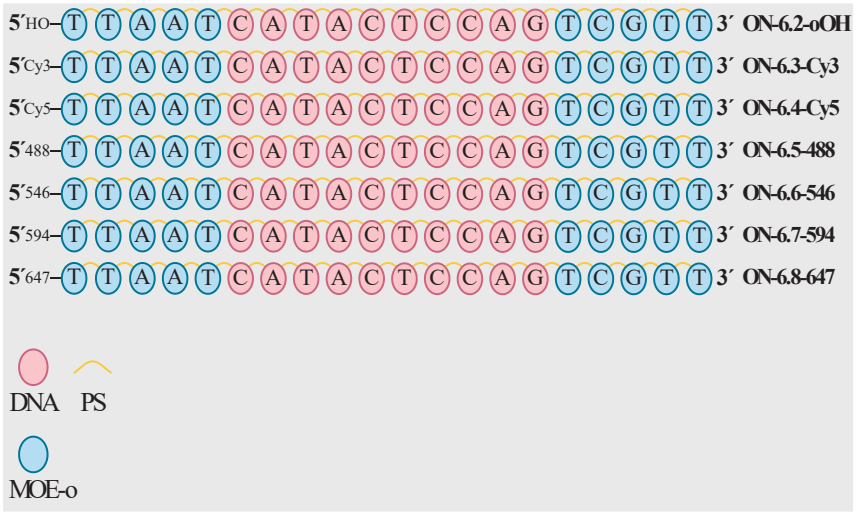


Figure 6.4: MALAT-1 targeting ASOs ON-6.2 to ON-6.8. All are follow a 5-10-5 2′MOE-DNA-2′MOE, fully phosphorothioate 'gapmer' pattern. ON-6.2 has a terminal 5′-alcohol. ON-4.27 to ON-4.32 are conjugated to dyes with abbreviations as follows, Cyanine3 (Cy3), Cyanine5 (Cy5), AlexaFluorophore488 (488), AlexaFluorophore546 (546), AlexaFluorophore594 (594) and AlexaFluorophore647 (647).

Dyes were conjugated to the ASO using Strain Promoted Azide-Alkyne Cycloaddition (SpAAC). First the 5′-terminal alcohol was converted to an azide while on the solid support as described in Chapter 2. The ASO was deprotected, purified, then incubated with dyes containing either bicylcononyne (BCN) for Cy3 or Dibenzocyclooctyne (DBCO) for all others. These ASOs were then dosed into standard HeLa cells using the transfection agent Lipofectamine3000, the results are shown in Figure 6.5. The mRNA knockdown was then assessed with qPCR using the delta delta Cq method.[248]

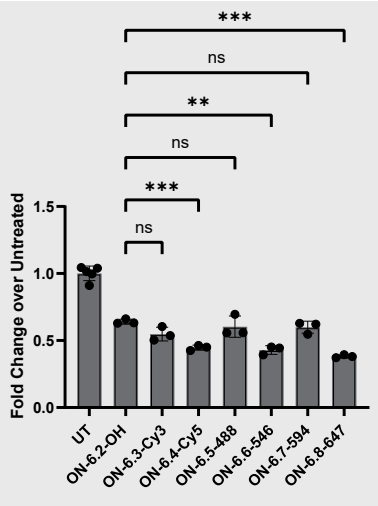


Figure 6.5: MALAT-1 knockdown plotted as fold change over untreated oligonucleotides ON-6.2 to ON-6.8 dosed at 200 nM concentration. The activity of dye-conjugated ASOs ON-6.3 to ON-ON-6.8 are compared for statistical significance to the 5´-alcohol ASO ON-6.2.

It can be seen it is not safe to assume that a dye will have no effect on the activity of an ASO. Of the six tested, three (Cy3 AF488, and AF594) showed no statistical difference to the alcohol, however the other three (Sulfo Cy5, AF546 and AF647) perform statistically better. Perhaps this is not surprising given the large size and hydrophobic nature of some dyes, especially those with higher wavelength emissions such as Cy5 and AF647. Structures of each dye tested can be found in Figure 6.6.

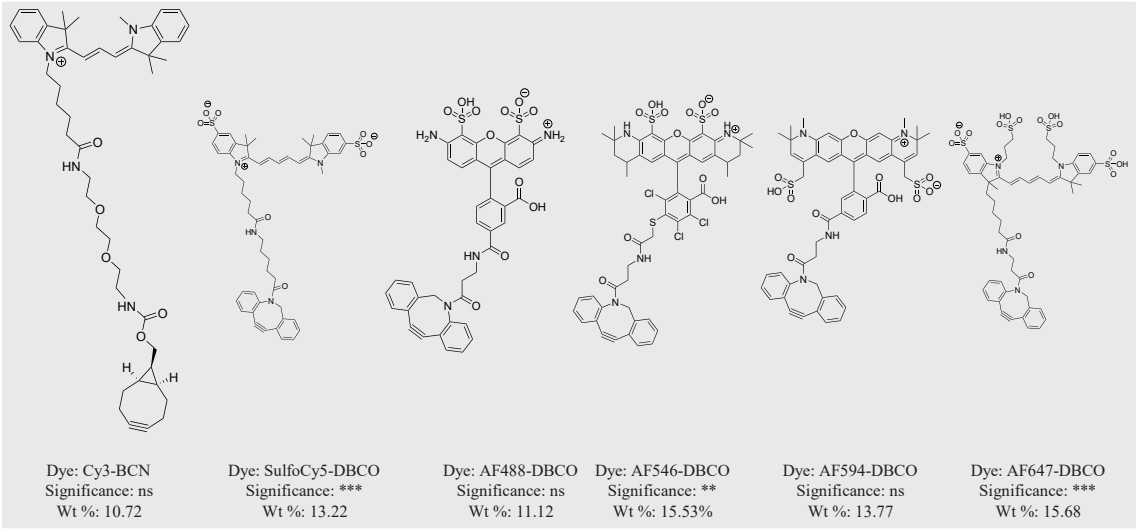


Figure 6.6: Chemical structure of the strained alkyne dyes used. Each structure is show along with its statistical significance compared to the 5´-alcohol ASO ONas well as the dye's percent by molecular weight of the ASO.

As can be seen from the two figures, the dyes constitute 10-15% of the weight of the ASO and contain hydrophobic motifs that can impact an oligonucleotide's ability to undergo both passive diffusion through the phospholipid bilayer and endocytosis.[212, 249, 250] This seems to be especially pronounced with the Cy5 and AF647 dyes which contain a five-carbon chain with conjugated alkenes. Even for those dyes that do not impact the activity of the ASO it cannot be known how the intracellular distribution is affected. It is possible that little or no changes are made, however without a method of visualising unconjugated ASOs the question will remain unanswered. As such an alternate, less disruptive method was sought.

6.3.2 Fixed Cell, In-Situ Labelling of ASOs using Click Chemistry

An alternative approach is to use the method developed here to transfect an oligonucleotide with a terminal 5´-azide. The azide moiety is a very small (25 Da) change to the terminal alcohol and thus should have a much smaller impact on the activity and distribution of an ASO than a dye. After transfection the cells can be fixed then stained with either an alkyne dye and copper catalyst or a strained alkyne dye as seen in Figure 6.7.

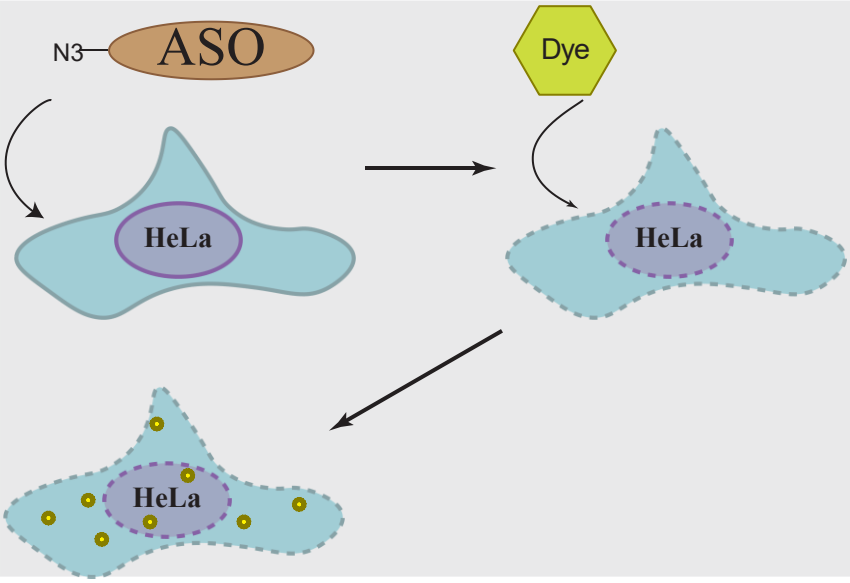


Figure 6.7: Alternative approach to ASO monitoring where the terminal alcohol is changed to an azide, the cells are fixed, stained with alkyne dyes then visualised.

To test the feasibility of this method a 5´N_3 version of the 2´MOE-DNA-2´MOE gapmer ON-6.2-oOH was synthesized as seen in Figure 6.8.

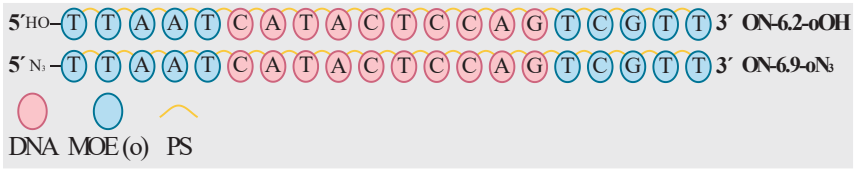


Figure 6.8: ASOs ON-6.2-oOH and ON-6.9-oN_3, synthesised to test differences in efficacy between 5´-alcohol and 5´-azide groups.

After synthesis these ASOs were dosed in HeLa cells at 200 nM concentration with Lipofectamine 3000. The knockdown activity was then assessed, as plotted in Figure 6.9.

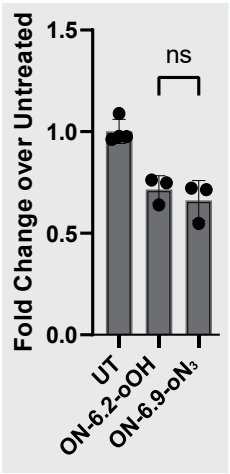


Figure 6.9: Knockdown activity of terminal alcohol and azide ASOs ON-6.2-oOH and ON-6.9-oN_3 transfected at 200 nM concentration with Lipofectamine3000. The comparison for statistical significance was done between ON-6.2-oOH and ON-6.9-oN_3.

Comparing the pair of oligonucleotides shows that there is no statistically significant difference, indicating that the azide modification does not influence the properties of a 2´MOE gapmer ASO as much as some conjugated dyes.

6.3.3 Optimisation of Blocking Conditions for Fixed Cell Clicks

While click chemistry in fixed cells is done[251-255], conditions for the staining must be optimised. This is especially true in the case of DBCO dyes which are known to have unspecific reactivity with groups such as thiols, a problem in fixed cells rich in proteins that contain cysteines.[256, 257] This leads to high background fluorescence, leading to faint

ASO signals being lost and limiting the usefulness the method. As such proper blocking conditions and staining concentrations must be established.

A screening panel was done with the use of automated microscopy. HeLa cells were seeded then fixed. Different wells were then blocked with different reagents then stained with a range of dye concentrations using AF488 DBCO and AF488 alkyne with a copper catalyst then with CellTracker DeepRed. CellProfiler software[258], was used to process the images. Details can be found in section **6.7.3.3 Click Background Data Collection Parameters.**

This method was used to test the two common blocking reagents casein (0.5% in PBS) and BSA (3% in PBS). For AF488 DBCO another step of was added, first blocking with iodoacetamine (100 mM in PBS) before the primary blocking agent. This was done to block any cysteine amino acids present in the cells. In each case, staining with AF488 was done in a concentration range of 50 µM to 0.024 µM. Results are displayed in Figure 6.10.

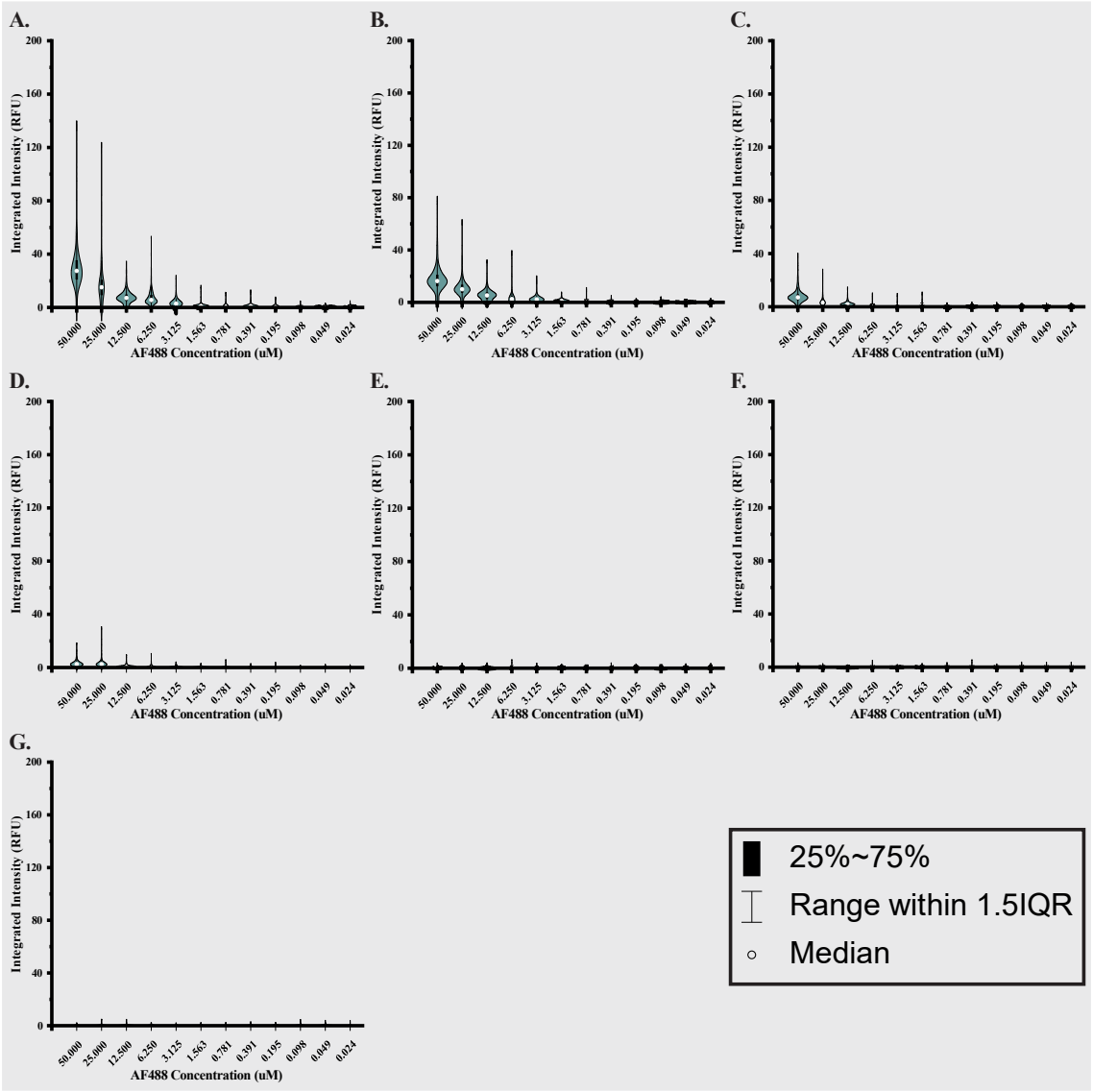


Figure 6.10: Background fluorescence measurements used to screen blocking and staining conditions of fixed HeLa cells. Plots show the integrated fluorescence intensity as measured by confocal microscopy after staining with concentrations of AF488 ranging from 50 µM to 24 nM . Two replicates of each condition were performed and the data pooled to give the results shown. Sections **A.** to **D.** show results of staining with AF488 DBCO dye, **E.** to **G.** staining with AF488 alkyne dye with a copper catalyst. Blocking conditions used are as follows, **A.** no blocking, **B.** 0.5% casein, **C.** 3% BSA, **D.** 100 mM iodoacetamide followed by 3% BSA, **E.** no blocking, **F.** 0.5% casein and **G.** 3% BSA.

The plot indicates that there is very little background in cells stained with the AF488 alkyne dye while the background can be significant with the AF488 DBCO dye. This is expected as a DBCO is a much more reactive group than a standard alkyne and as stated, is known to have some unspecific reactions. Using proper blocking conditions and the right concentration of dye, this background can be brought back to baseline levels. BSA gave better results than casein in this case and that using a pre-blocking step of

iodoacetamide can reduce background even further. With the iodoacetamide-BSA combination, up to 6.25 µM can be used without noticeable increase in background fluorescence. This is in line with reagents such as CellTracker Deep Red recommend staining concentrations of 250 nM-1 µM.[259]

The next step is to assess ASO staining efficiency. This will be done by transfecting an ASO with a dye on the 3´-side and a 5´-terminal azide then staining with a range of AF488 dye using the iodoacetamine-BSA blocking condions. Plotting the ratio of 5´/3´ dyes should give a sigmoidal curve as the concentration of AF488 is increased, allowing the relative staining efficiency to be calculated and establishing the optimal dye concentration. However, as this project is ongoing, this experiment has yet to be performed.

6.3 Conclusions

This chapter attempted to create methods that enable further investigation of charge-neutral backbones in ASOs. The first way of doing this was to find a find an assay that more closely mimics the disease state of DMD; a nested qPCR approach using the H2K dystrophic mouse cell line. While this is a more disease relevant model, issues were had with the qPCR where the treated, untreated and negative controls were indistinguishable from each other both in terms of exon skipping percentage and total number of mRNA copies. This is likely due to the extreme scarcity of dystrophin mRNA, even in healthy muscle cells, meaning it falls below the reliable quantification limit of qPCR in a high throughput screening context.

Next was an attempt to establish a method of imaging ASOs in cells without relying on a pre-attached dye that can influence the properties of the oligo of interest. This approach was tested in a MALAT-1 knockdown context as the goal is to create a more universal method with application in gene knockdown or splice switching modalities. First, an ASO with various commonly used dyes conjugated was transfected where it was observed that these dyes can have an impact on ASO activity This is not surprising given the large and hydrophobic nature of some dyes which can aid is passing through the phospholipid bilayer or change intracellular distribution. To address this, an ASO was made with a terminal azide that can then be clicked to a dye in a fixed cell. This *in-situ* conjugation allows quantification and localisation without affecting the observation with a dye. It was found that an azide group has no effect on activity in three of the most commonly used chemistries and then a method was established and used to find optimal blocking and staining conditions for both a DBCO and an alkyne dye

Further work is in progress to determine labelling efficiency which will provide a technique for quantifying ASO in a cell, determining subcellular-localisation of an oligonucleotide and co-localisation of an ASO with key markers or proteins. This can be

used in conjunction with an assay such as the luciferase assay used in Chapters 4 and 5 or a gene silencing assay to provide insights as to what a chemical modification does to change the activity of an ASO overall.

Chapter 7: Conclusions and Future Directions

The aim of this work was to create new methods for the modification of oligonucleotides and assess their impact when applied to different ASO modalities. This was done in three main sections, the first of which is an investigation of azide functionality while the oligonucleotide was bound to solid support. Second was a study of a copper click of these azide conversions while still on the resin to add a charge-neutral triazole linkage. This triazole-backbone was then evaluated in a luciferase-based exon skipping assay as well as investigations into alternate methods of testing.

7.1 Results and Conclusions

Chapter 2 tested the efficiency of an on-resin azide reaction across different oligonucleotides. These oligonucleotides consisted of a string of ten thymidine DNA sugars and then a variation in nucleobase and ribose chemistry at the eleventh position. These variations included the four main nucleobases as well as one of six ribose sugars, DNA, RNA, 2´-OMe, 2´-MOE, 2´-Fluoro or LNA. Efficiency of reaction was measured via LCMS for all combinations thereof with both a phosphodiester and a phosphorothioate backbone.

It was found that with phosphodiester oligonucleotides the conversion proceeds well with some differences observed between the base and sugar groups. A very small difference could be seen between the nucleobases A and T/U were marginally better performing than C and G. A larger difference was observed between the groups of terminal sugars where 2´-MOE was significantly worse than the rest and 2´-OMe performed the best. Due to the similarities in electronic properties between the two, it seems likely that the conversion will proceed well as long as the 2´-substituent is not too long which can hinder the reaction. With the phosphorothioate oligonucleotides it was found that there was a purine/pyrimidine split where the bulk of the purines seemed to give slightly worse conversion. A large difference was observed between the sugars where 3´-*endo* promoting modifications such as 2´-Fluoro and LNA performed very

poorly. This could be due to the proximity of the sulfur to the iodo intermediate in this conformation which leads to a ring formation which is then disrupted upon addition of sodium azide or deprotection in aqueous ammonia.

Chapter 3 involved testing an on-resin CuAAC reaction to introduce a charge-neutral triazole linkage into an oligonucleotide. The process was first optimised with a phosphorothioate oligonucleotide before being tested for efficiency in the phosphodiester oligonucleotides from Chapter 2. It was found that adenosine in particular is detrimental to the click reaction with only a small discrepancy between the other three nucleobases, likely due the bulky purine base with a large benzoyl protecting group. Across the six sugars it was found that RNA sugars showed the most conversion. Then the triazole was placed in a heterogeneous sequence to test the effect of a triazole-ribose combination on the duplex stability with both a DNA compliment and an RNA compliment. It was found that overall the destabilising effect of the triazole was less pronounced with an RNA target and that the strongly 3´-*endo* promoting modifications of 2´-Fluoro and LNA more than compensate for the triazole effect. With a DNA target only LNA managed to bring the melting temperature back to level with a naturally occurring phosphate linkage.

Chapter 4 revolved around testing different ASOs and investigating the effects of chemical modifications on activity. First the triazole linkage from Chapter 3 was tested for splice-switching activity in a luciferase-based assay while changing sugars on the 5´-side of the linkage, either DNA, 2´OMe, 2´MOE or LNA. When transfected, the triazole with 2´MOE performed the same as an all 2´OMe-PS control, the triazole with 2´OMe performed half as well, and triazoles with DNA or LNA had one-third the activity of the 2´OMe-PS control. In gymnotic delivery triazoles with 2OMe or 2MOE performed half as well as the 2´OMe-PS control while triazoles with DNA or LNA had one-quarter of the activity. These results show that the triazole-linkage does lead to active splice-switching ASOs and that changing sugars accompanying the triazole will change

performance. The activity is likely hindered by the reduction in duplex thermal stability, measured as a duplex melting temperature 3°C to 5°C lower than that of the 2´OMe-PS control. This led to investigations of the impact of different ribose patterns as well as other charge-neutral linkages.

Chapter 5 continued from Chapter 4 as different patterns of sugar substitutions were evaluated in the same luciferase-based splice-switching assay. This was done to find a platform to which a charge-neutral methoxypropyl phosphonate could be added. In total one, two or three of the 2´OMe riboses in the control were changed to either DNA, LNA or 2´MOE. It was found that when transfected, LNA provided the most while DNA and 2´MOE showed no difference to the all-2´OMe control. In gymnotic dosing it was found that DNA additions reduced activity compared to the 2´OMe control while both 2´MOE and LNA gave improvement with two or three additions. With two additions the 2´MOE had activity that was statistically significantly higher than the 2´OMe control and LNA had activity statistically higher than both. At three additions both the LNA and 2´MOE were statistically better than the 2´OMe control but not significant to each other.

Based on these results, LNA was then combined with a methoxypropyl phosphonate linkage and tested in the same fashion. The charge-neutral linkage gave no benefit with transfection but did gymnosis. This was then carried further where sequences with more additions of LNA were added and a similar pattern was observed. Again, when used with a transfection agent no benefit was seen but the overall best performing gymnotic ASO was found to have four LNAs and two methoxypropyl phosphonate linkages. Adding more LNA-MOP linkages reduced the activity of the ASO.

These results are likely due to a combination of effects on the duplex melting temperature and protein-ASO interactions. A higher duplex melting temperature from the LNA will give better affinity to the target, however it will also raises affinity to partially complementary strands that can reduce the number of ASOs able to interact with the

target. Similarly, if affinity to the target is too high, the ASO might not be released from the mRNA, even after splicing has occurred, preventing it from releasing the spliced mRNA to find another copy of pre-mRNA, reducing efficiency. LNA also increases affinity of an ASO to certain proteins which act analogously, binding to the ASO and making it unavailable to interact with the desired splice-site. MOP-linkages will decrease affinity for both off-target mRNA, by lowering the duplex thermal stability in the region of the LNA, and to proteins that bind to LNA-containing ASOs. This can be an explanation as to why the MOP only provides benefit when dosed gymnotically. In transfection, a relatively high amount of ASO enters the cell meaning the effect of some copies of ASO not being able to function as intended is negligible. In gymnosis, far less ASO penetrates the cell meaning each indisposed copy has a more meaningful impact. This led to the desire to develop different assays to provide more insight in to these factors.

Chapter 6 describes work done to develop these new methods of testing ASO modifications. First a qPCR-based exon skipping assay using dystrophic mouse cells was used, however due to a low mRNA transcript count no meaningful data was able to be extracted on this small scale. Development on a method to localise ASOs using click chemistry inside fixed cells was then started. It was first determined that pre-conjugation of ASOs to dyes can in some cases influence the activity and so alternate strategies are required. Next an ASO was functionalised with a 5´-azide were synthesised in the manner developed in Chapter 2 and the azide was found to have no effect on ASO performance with a 2´MOE-DNA-2´MOE gapmer. Blocking and staining conditions were tested using high throughput confocal microscopy for both SPAAC and CuAAC pathways. This method has potential to provide information on the amount of ASO inside a cell, the subcellular-localisation of the ASO, and co-localisation data with key proteins or markers. Using these points together with assays such as the luciferase-based splice-

switching one used here will enable a deeper explanation of the results such as those found in Chapters 4 and 5.

7.2 Future Directions

Short term directions for the triazole and methoxy propyl modifications should include using the luciferase-based splice-switching assay employed in this thesis to test different positions in the sequence of the ASO and different ribose patterns. To start, walking a triazole or MOP from one end of the sequence to another will provide further optimisation on the design of the splice-switching ASO and give insight into any positions that are not tolerated or show a boost in efficacy. This is of particular importance with the triazole as it will likely thermally destabilise a duplex to a greater or lesser extent depending on its position in a sequence.

Both modifications should also be tested with ribose substitutions made in different places of the ASO. In the cases tested here, changes from the 2´OMe riboses of the control ASO were made adjacent to the charge-neutral linkage. Separating substitutions of 2´OMe to 2´MOE, LNA or even 2´fluoro from the charge-neutral linkage to different positions in the sequence will provide address points left open both the triazole and the MOP. For the triazole it will investigate if the decrease in activity observed was due to reduction in duplex stability or some other factor. It will also address if it is enough to increase the overall duplex thermal stability or if the problem is the acute local destabilisation of the triazole-linkage. In the case of the MOP it can provide insight into if it is in fact the dampening of the unwanted interactions of LNA with off-target mRNA or various proteins that is the source of the LNA-MOP's increased activity or if it some other factor.

Also in the short term, the method for imaging ASOs in fixed cells using the 5-azide handle should be further developed. Conditions tested here show blocking and staining conditions that can be used, however the labelling efficiency of the ASO in fixed

cells must be investigated. This can be done by pre-conjugating the ASO with a dye and using a click to label with a fluorophore with a different emission wavelength. Co-localising the two signals will give insight into how well the click labelling works. This method must also be compared to antibodies that target phosphorothioate or 2-modifications of an ASO. Additionally, conditions for co-localising the ASO to endosomes, key-proteins, nuclei and cytosol must be optimised and the results compared with other methods such as anti-phosphorothioate or anti-2´OMe antibody staining.

The last set of experiments for short term completion is the use of a technique such as Dynamic Light Scattering (DLS) to monitor the formation of lipoplexes with Lipofectamine3000 and the ASOs containing charge-neutral linkages. This technique can monitor the size of particles in a solution and thereby give insights into any effects on lipoplex size and tightness of size-distribution that stem from these neutral linkages. These points can in turn provide information on if the performance of the transfection agent is altered by charge-neutral chemical modifications.

Medium term plans for the triazole and MOP should build on the results found in the short term. ASOs made with optimised ribose patterns and charge-neutral linkage placement should be used in conjunction with the fixed-click method. This will give insights into why some permutations are more active than others. Some important questions that can be addressed with this combination are if more ASO is entering the cell in total with these charge-neutral linkages, if more ASO is escaping endosomes and if these charge-neutral linkages do prevent association with off-target mRNA or proteins.

Long term activities with the triazole and MOP should be about testing the translatability of these modifications to other targets and modes of action. In particular it should be seen if the ribose patterns and positions for these charge-neutral linkages will remain the same from one splice-switching sequence to another. In parallel, the imaging techniques used with the splice-switching assay used here should provide a workflow that

will influence the design of new chemical modifications to be brought up to make more desirable ASO molecules.

The work of this thesis shows that charge-neutral chemical modifications in ASOs can lead to increases in activity compared control sequences. It also shows that there are differences in the relative performance of ASOs depending on the method of delivery leading to questions about the mechanism by which these increases come to be. To answer these and design modifications that confer even more benefit assays such as the ones being developed in Chapter 4 need to be employed. Optimisation of fixed-cell labelling efficiency will allow for ASO activity to be correlated with accumulation and localisation inside cells. This enables better evaluation of incredibly important ASO characteristics such as propensity for cellular internalisation and endosomal escape. The effect of modifications such as the methoxypropyl and triazole on these characteristics can then also be evaluated leading to the development of more potent ASOs in future.

Chapter 8: Experimental

8.1 Oligonucleotides

8.8.1 Synthesis

Synthesis reagents, phosphoramidites and CPG supports were purchased from either Link Technologies, Glen Research or Sigma Aldrich. Synthesis was performed on an Automated Biosystems 394 machine using standard steps of detritylation, coupling, capping and oxidation on a 1.0 µmole scale. Standard DNA phosphoramidites were used in all DNA-containing sequences (note C was always acetal protected). TC-protected RNA was used in all instances of RNA incorporation. 2´-OMe, 2´-MOE, 2´-Fluoro and LNA phosphoramidites were purchased from Link Technologies and the EDITH reagent was used for all sulfurisations with an exposure time of 5 minutes. Phosphoramidites dissolved in anhydrous ACN (except for LNA-C CE and MOP which were dissolved in 1:1 DCM:ACN v/v) to a concentration of 0.1M. Coupling times for DNA phosphoramidites were 40 seconds, 10 minutes for RNA phosphoramidites and 6 minutes for 2´-OMe, 2´-MOE, 2´-Fluoro and LNA.

8.1.2 Deprotection

Deprotection for DNA, 2´-OMe, 2´-MOE, 2´-Fluoro and LNA oligonucleotides was done by exposing resin to concentrated aqueous ammonia for 5 hours at 55°C. Deprotection of TC-RNA containing oligonucleotides was done with slow addition of 1 mL of 1:1 ethylene diamine: toluene (v/v) to the synthesis column for 6 hours at room temperature. Following this the column was washed with 2 X 1 mL of dry toluene drying with argon then removal of the RNA with 2 X 1 mL of water. Deprotection of MOP containing oligonucleotides was done in a similar manner but with 1:1 ethylene diamine: THF (v/v) and an exposure of 15 minutes at 55°C

8.1.3 Purification and Desalting

Oligonucleotide HPLC Purification and Desalting. Automated high-performance liquid chromatography separations were carried out on an Agilent 1260 Infinity instrument equipped with an autosampler, a column oven, a diode array detector and a fraction collector. For instrument control, data acquisition and data processing, OpenLab CDS 2.7 (Agilent Technologies) software was used. Ion-pairing reversed-phase separations of oligonucleotides were carried out on Phenomenex Kinetex® EVO C18, 5 µm, 100 Å, 250 x 10.0 mm column (mobile phase A: 100 mM triethylammonium acetate, pH 7.0 in water, mobile phase B: 100 mM triethylammonium acetate, pH 7.0 in water/acetonitrile 2:3 (v/v). For phosphodiester oligonucleotides purifications were done with the last DMT group removed on the synthesiser. For these sequences conditions of linear gradient: 0-10% B over 1 min, 10-40% B over 23 min, then 100% B for 4 min, temperature 55 °C, flow rate 5 mL/min, detection at 260 nm were used. For phosphorothioate oligonucleotides purification used in cellular studies purification was carried out with the 5´- DMT group left on with the same conditions except that the 10-40% gradient is replaced with a 30-70% gradient. Purified fractions of these oligonucleotides were incubated with an equal volume of 50% acetic acid in water for 30 minutes to remove the terminal DMT. For all oligonucleotides desalting was done using Amicon® Ultra-4 3 kDa MWCO centrifugal filters following the manufacturer's recommendations. After the first round of centrifugation (concentration of samples), samples washed with water, 100 mM sodium chloride to exchange the backbone counterion then washed three more times with water.

8.1.4. Analysis of Oligonucleotides

Oligonucleotides were injected onto a Waters Xevo G2 QTof electrospray mass spectrometer and analysed by MassLynx software. Identity of peaks was determined using mass spectrometry to confirm calculated masses of major peaks. Purity was

determined via integration of the UV trace at 260 nm. For the determination of purity, the baseline of the chromatogram was corrected using the mean Y value of all data points collected. Then integration was carried out using a threshold local maxima approach. First the threshold was set at 5% by height of the largest Y value. Then peaks were found by looking for a local maxima, meaning a change from a positive to negative slope of the first derivative of the chromatogram. This was only counted as a peak if true within a given set of 15 data points to minimize any false peaks being detected. Once a peak is identified the area under the curve is calculated the closest intersection of Y=0 on both sides of the local maxima. All of the peak areas are then added up to calculate the percentage of each component.

8.2 Organic Synthesis

General Organic Synthesis. Anhydrous solvents were obtained using an mBraun SPS-800 bench top solvent purification system running anhydrous alumina columns, and where possible, dried on 3Å molecular sieves overnight. The starting material DMT-thymidine was purchased from Sigma Aldrich and all other chemicals were purchased from commercial sources (usually Sigma Aldrich) and used without further purification. Notably other nucleosides (2´-OMe, 2´-MOE, LNA) were purchased from Hongene Biotech. All glassware was oven-dried at 110°C and reactions were conducted under an inert argon atmosphere.

Reaction progress was monitored on thin layer chromatography (TLC) using Merck pre-coated 0.23 mm plates covered in Kieselgel 60 F254 and visualized using UV (= 254 nm) or heating until cleavage of DMT group, creating an orange spot. Column chromatography was done using various sizes of Biotage Duo cartridges on a Biotage Isolera Four or manually on Geduran Silica Gel 60 (Merck).

NMR data for 1H and 13C was recorded on either a Brucker AVIIHD 400 or a Brucker AVII 500 spectrometer, operating at 400 and 500 MHz respectively for 1H and 101 MHz for 13C. Both use an internal deuterium lock at ambient probe temperatures and all carbon and hydrogen shifts are referenced with respect to a residual solvent peak. 1H NMR shifts (δ) are reported to the nearest 0.01 ppm, 13C shifts (δ) to the nearest 0.1 ppm. Hydrogen coupling constants (J) are given to the nearest 0.1 Hz. Peak multiplicity is written with standard abbreviations, s (singlet), d (doublet), t (triplet), q (quartet), p (pentet), dd (doublet of doublets), m (multiplet). NMR shifts are written in the following order shift (multiplicity, coupling constant, integration, assignment).

Small molecule high resolution mass-spectrometry (HRMS) was done as follows: flow injection analysis was performed on an ACQUITY I-Class PLUS UPLC System (Waters) coupled to an ACQUITY RDa mass spectrometer (Waters) equipped with an ESI probe, in positive ion mode. The flow rate was set to 0.300 mL/min using a 50% methanol(aq) + 0.1% formic acid eluent. Scan parameters were set as follows: analyser mode, full scan; scan range, 50 2000 m/z; scan rate, 2 Hz; cone voltage, 30 V; capillary voltage, 1.5 kV; desolvation temperature, 550°C; and intelligent data capture, on.

8.3 UV Melting Studies

UV melting measurements were done on a Varian Cary 4000 UV-Vis spectrophotometer with Cary temperature controller and Cary Win UV Thermal software. Samples were prepared in 1 mL cuvettes (1 cm pathlength) at 1 µM duplex concentration in phosphate buffer (10 mM NaH2PO4, 200 mM NaCl for Chapter 3, 40 mM NaCl for Chapter 4). UV

Ramp	Data Collection Interval (°C)	Rate (°C/min)	End Temperature (°C)	Hold Time (min)
1	1	10	85	2
2	0.1	1	20	2
3	0.1	1	85	2
4	0.1	1	20	2
5	0.1	1	85	2
6	0.1	1	20	2
7	0.1	1	85	2
8	1	10	20	2

absorption at 260 nM was measured as successive ramps of denaturing (heating to 85°C) and annealing (cooling to 20°C) were performed as summarized below. Melting temperature was obtained by recording the maxima of the derivative of absorption vs temperature. Data from ramps 3,5 and 7 were averaged to give the melting temperature of each duplex.

8.4 Cell Culture and Assays

8.4.1 Culture Conditions

HeLa 705pLuc and HeLa cells were cultured in Dulbecco's Modified Eagle Medium (DMEM) GlutaMAX Supplement, pyruvate with 10% Fetal Bovine Serum (FBS) at 37°C in 5% CO2. For transfection aided delivery, seeding was done at 20,000 cells/well in a 96 well plate After 24 hours and 70-80% confluency oligonucleotides were transfected according to manufacturer's instructions with Lipofectamine 3000. After a further 24 hours the cells were harvested. For gymnotic delivery cells were seeded at 8,000 cells/well. After 24 hours the media was replaced with Minimum Essential Medium (MEM) containing oligonucleotide and left for 96 hours before harvest.

H2K Cell culture was done in DMEM with 20% FBS, 1% chicken embryo extract and Interferon Gamma according to manufacturer's instructions at 33°C with 10% CO_2. Flasks and plates were coated in Matrigel according to manufacturer's procedures before culture. Experiments were performed in 24 well plates where seeding was done at 20,000 cells/well. When 70% confluency was reached (24-48 hours) the media and incubation was changed to differentiation conditions (DMEM, 5% horse serum, 37°C, 5% CO_2). After an additional 24 hours the media was switched to fresh differentiation media containing oligonucleotide for gymnotic delivery. This was left for 96 hours before harvest.

8.4.2 HeLa pLuc 705 Assays

Dosing was done with 200 nM, 100 nM, 50 nM and 25 nM for ASOs transfected with Lipofectamine 3000 and 20 µM, 10 µM, 5 µM and 2.5 µM for gymnotically dosed ASOs. Dosing was done in triplicate on each plate for each condition.

The cells were lysed after either 24 hours (transfection) or 96 hours (gymnosis) with 100 µL of GloLysis Buffer. 50 µL the lysate was mixed with luciferin and the luminescence measured. Another 25 µL of lysate was used in a Pierce BCA Protein Assay Kit according to the manufacturer's instructions for protein quantification.. The luminescence is then normalised to the protein concentration. This value was further normalised to the luminescence/protein value of untreated wells on the plate to give a fold change over untreated value.

Statistical significance was calculated with a two way anova test (for groups of three or more ASOs) or multiple unpaired t-tests (groups of two ASOs). Statistical significance is represented by asterisks (not displayed =$p > 0.05$ * = $p \leq 0.05$, ** = $p \leq 0.01$, *** = $p \leq 0.001$, **** = $p \leq 0.0001$).

8.4.3 qPCR Based Assays

In all cases, the total RNA was extracted according to the manufacturer's guidelines (including optional gDNA digestion) using the Monarch Total RNA Miniprep Kit.

Exon Skipping: RT-PCR was done according to the manufacturer's instructions using the Luna Universal Probe One-Step RT-qPCR kit for single PCR amplification with probes and with no probes for nested PCR, in both cases with 25 ng of RNA loaded. The second PCR in the nest was done using the Luna Universal Probe qPCR Kit. Primers and probes were ordered from Integrated DNA Technologies.Two sets of primers were ordered, one set for Exons 20-26 (Forward CCCAGTCTACCACCCTATCAGAGC, Reverse CCTGCCTTTAAGGCTTCCTT) and one for Exons 22-24 (Forward

CGTGGATCCAGCAGTCAGAAAGC, Reverse GGCAGGCCATTCCTCTTTCAGG). Probes were for made for both skipped (GGAAATTACAGGAATCACAT, FAM dye) and unskipped (AGGAGATGGCCAAGAAAGCACCTTC, JOE Dye) transcripts. Standard curves were made using gBlocks DNA purchased from Integrated DNA Technologies for Skipped (Exons 22 joined to Exon 24) and Unskipped (Exons 22, 23 and 24) using the known sequence of mouse dystrophin (NCBI Reference Sequence: NM_007868.6).

Statistical significance was calculated with a two way anova test. Statistical significance is represented by asterisks (not displayed =$p > 0.05$ * = $p \leq 0.05$, ** = $p \leq 0.01$, *** = $p \leq 0.001$, **** = $p \leq 0.0001$).

MALAT1: RT-qPCR was done according to the manufacturer's instructions using the Luna Universal One-Step RT-qPCR kit with 25 ng of RNA loaded. Primers were order from Integrated DNA Technologies, one set for MALAT1 (Forward TCCATGACGCAGGGAGAATTGC, Reverse GCCTTCCCGTACTTCTGTCTTCC) and one for GAPDH (Forward TCAAGGCTGAGAACGGGAAG, Reverse CGCCCCACTTGATTTTGGAG). Knockdown was determined by the delta delta Cq method, 2-((Sample CqMALAT1-Sample CqGAPDH)-(Untreated CqMALAT1-UntreatedCq GAPDH)).

Statistical significance was calculated with a Brown-Forsyth and Welch anova test. Statistical significance is represented by asterisks (not displayed =$p > 0.05$ * = $p \leq 0.05$, ** = $p \leq 0.01$, *** = $p \leq 0.001$, **** = $p \leq 0.0001$).

8.5 Data for Chapter 2

8.5.1 LC-MS Data for Oligonucleotides ON-2.1 to ON-2.24

Oligo	Sequence (5'-3')	Calc. Mass OH	Calc. Mass N_3 (Da)	Found Mass OH	Found Mass N_3 (Da)	OH Purity (%)	N3 Purity (%)	N3 Conversion (%)
ON-2.1-dA	ATTTTTTTTTT	3293.2	3318.2	3293.3	3318.5	100	81	81
ON-2.2-dC	CTTTTTTTTTT	3269.2	3294.2	3269.4	3294.4	100	86	86
ON-2.3-dG	GTTTTTTTTTT	3309.2	3334.2	3309.6	3334.5	100	89	89
ON-2.4-dT	TTTTTTTTTT	3284.2	3309.2	3284.5	3309.4	100	100	100
ON-2.5-rA	**A**TTTTTTTTTT	3309.2	3334.2	3309.3	3334.3	76	64	84
ON-2.6-rC	**C**TTTTTTTTTT	3285.2	3310.2	3285.3	3310.0	90	64	72
ON-2.7-rG	**G**TTTTTTTTTT	3325.2	3350.2	3325.5	3350.7	81	61	75
ON-2.8-rU	**U**TTTTTTTTTT	3286.2	3311.2	3286.8	3311.5	80	79	99
ON-2.9-mA	*A* TTTTTTTTTT	3323.2	3348.2	3323.8	3348.3	100	100	100
ON-2.10-mC	*C* TTTTTTTTTT	3299.2	3324.2	3299.4	3324.1	100	92	92
ON-2.11-mG	*G* TTTTTTTTTT	3339.2	3364.2	3339.2	3364.4	100	100	100
ON-2.12-mU	*U* TTTTTTTTTT	3300.2	3325.2	3300.3	3325.3	100	89	89
ON-2.13-oA	***A*** TTTTTTTTTT	3367.3	3392.3	3367.2	3391.8	100	78	78
ON-2.14-oC	***C*** TTTTTTTTTT	3357.3	3382.3	3356.8	3382.2	100	72	72
ON-2.15-oG	***G*** TTTTTTTTTT	3383.3	3408.3	3382.8	3408.6	100	67	67
ON-2.16-oT	***T*** TTTTTTTTTT	3358.2	3383.2	3357.6	3382.8	100	69	69
ON-2.17-lA	**A**TTTTTTTTTT	3321.2	3346.2	3321.3	3346.1	100	93	93
ON-2.18-lC	**C**TTTTTTTTTT	3311.2	3336.2	3311.5	3336.7	100	89	89
ON-2.19-lG	**G**TTTTTTTTTT	3337.2	3362.2	3337.3	3362.1	100	83	83
ON-2.20-lT	**T**TTTTTTTTTT	3312.2	3337.2	3312.3	3337.4	100	100	100
ON-2.21-fA	~~A~~TTTTTTTTTT	3311.2	3336.2	3311.1	3335.9	100	80	80
ON-2.22-fC	~~C~~TTTTTTTTTT	3287.2	3312.2	3287.3	3312.1	100	88	88
ON-2.23-fG	~~G~~TTTTTTTTTT	3327.2	3352.2	3327.0	3352.0	100	86	86
ON-2.24-fU	~~U~~TTTTTTTTTT	3288.1	3313.1	3288.1	3313.3	100	84	84

Table 8.1: Table containing sequences along with calculated and observed masses and azide conversion data for ON-2.1 to ON-2.24. Chemistries are indicated as follows: DNA, **RNA**, *2´-OMe*, ***2´-MOE***, **LNA**, ~~2´-Fluoro~~. Capitalised letters indicate phosphodiester linkages.

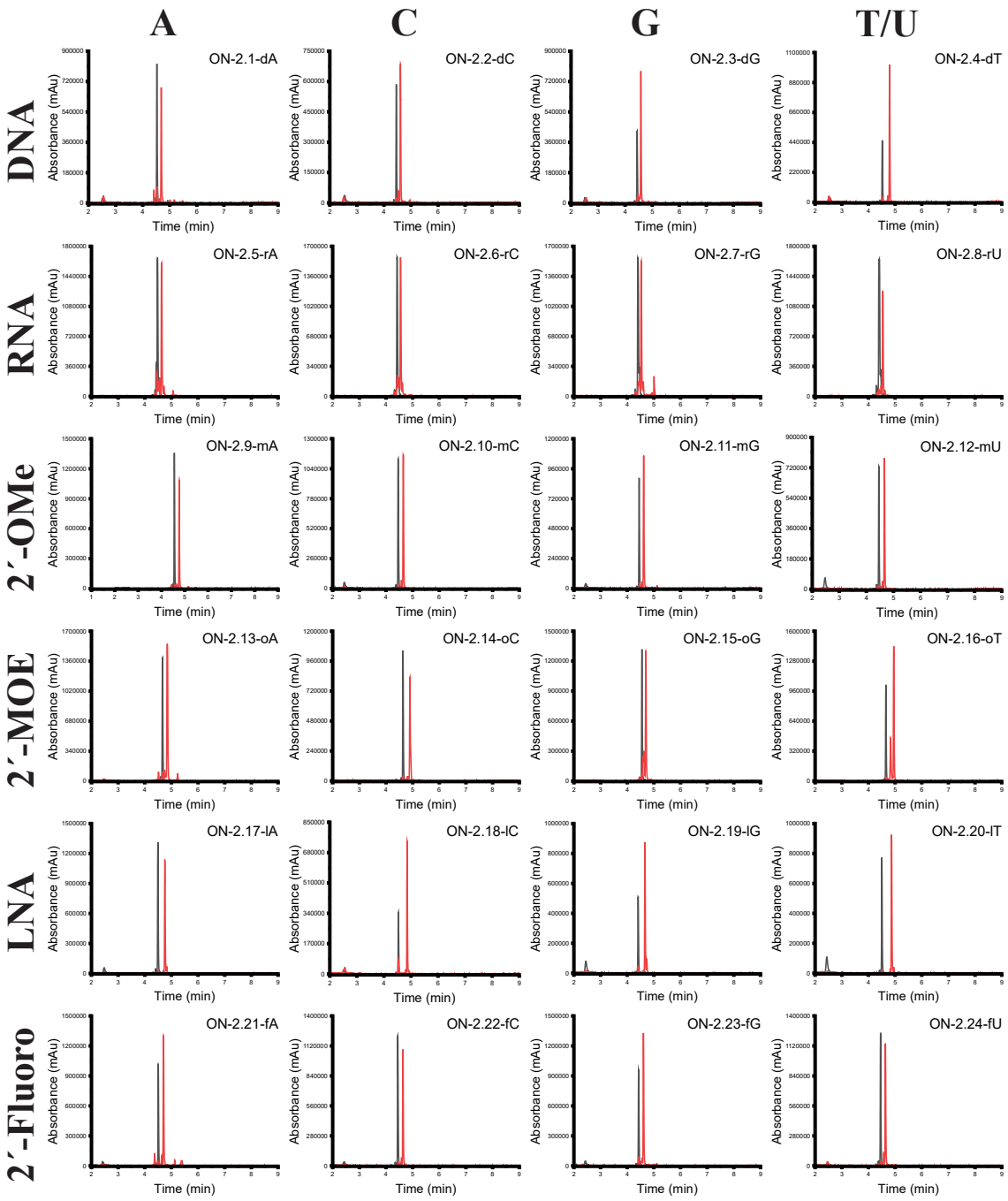


Figure 8.1: A_{260} LC traces used for the determination of azide conversion for ON-2.1 to ON-2.24. Traces in black correspond to the starting material sequences, traces in red correspond to the sequences after the azide conversion process. Purity as determined by integration is listed in Table 6.1 Columns of A, C, G and T/U refer to the terminal 5´ nucleobase before azide conversion. Rows of DNA, RNA, 2´OMe, 2´MOE, LNA, and 2´Fluoro refer to the modification of the terminal 5´ ribose before azide conversion.

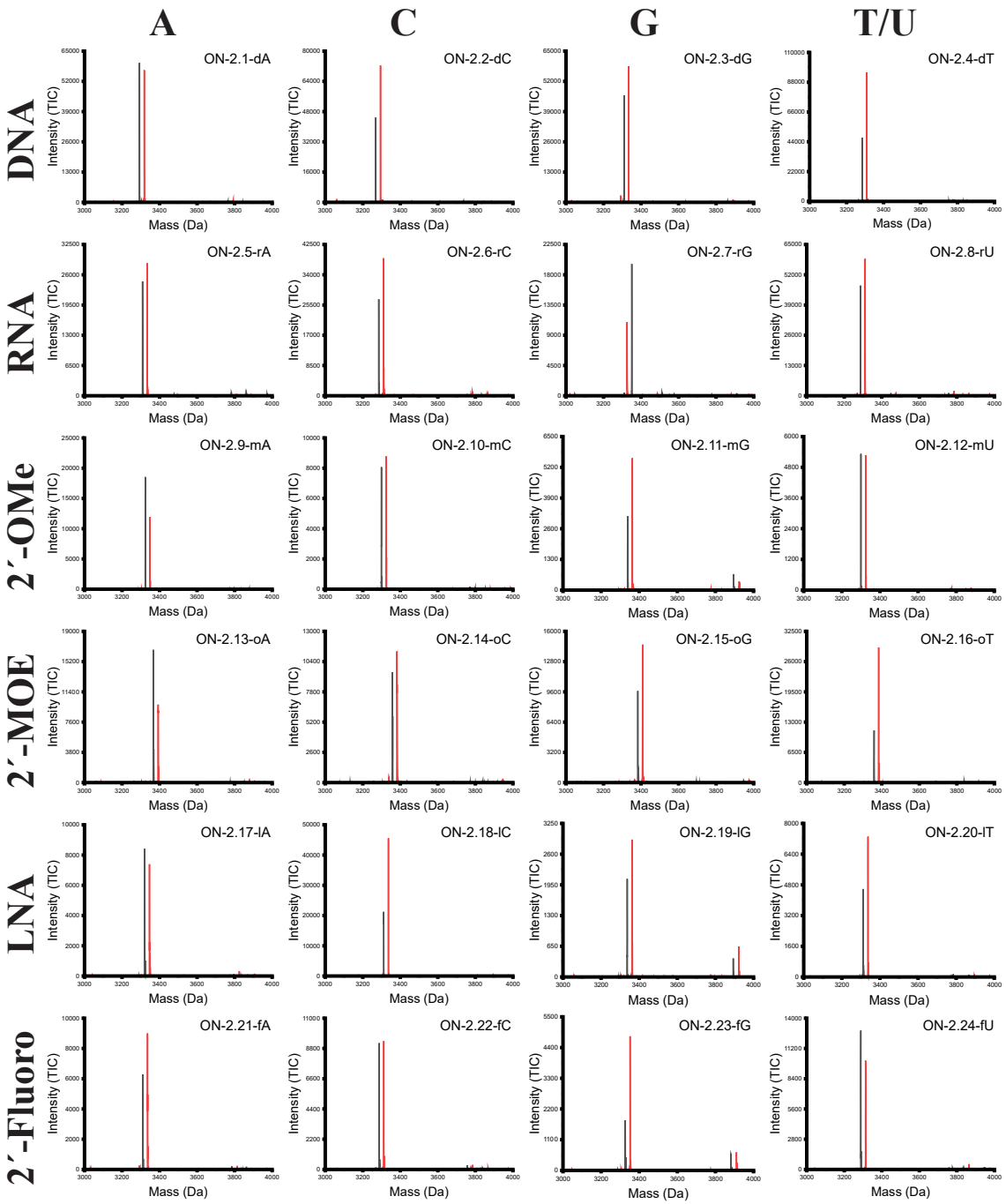
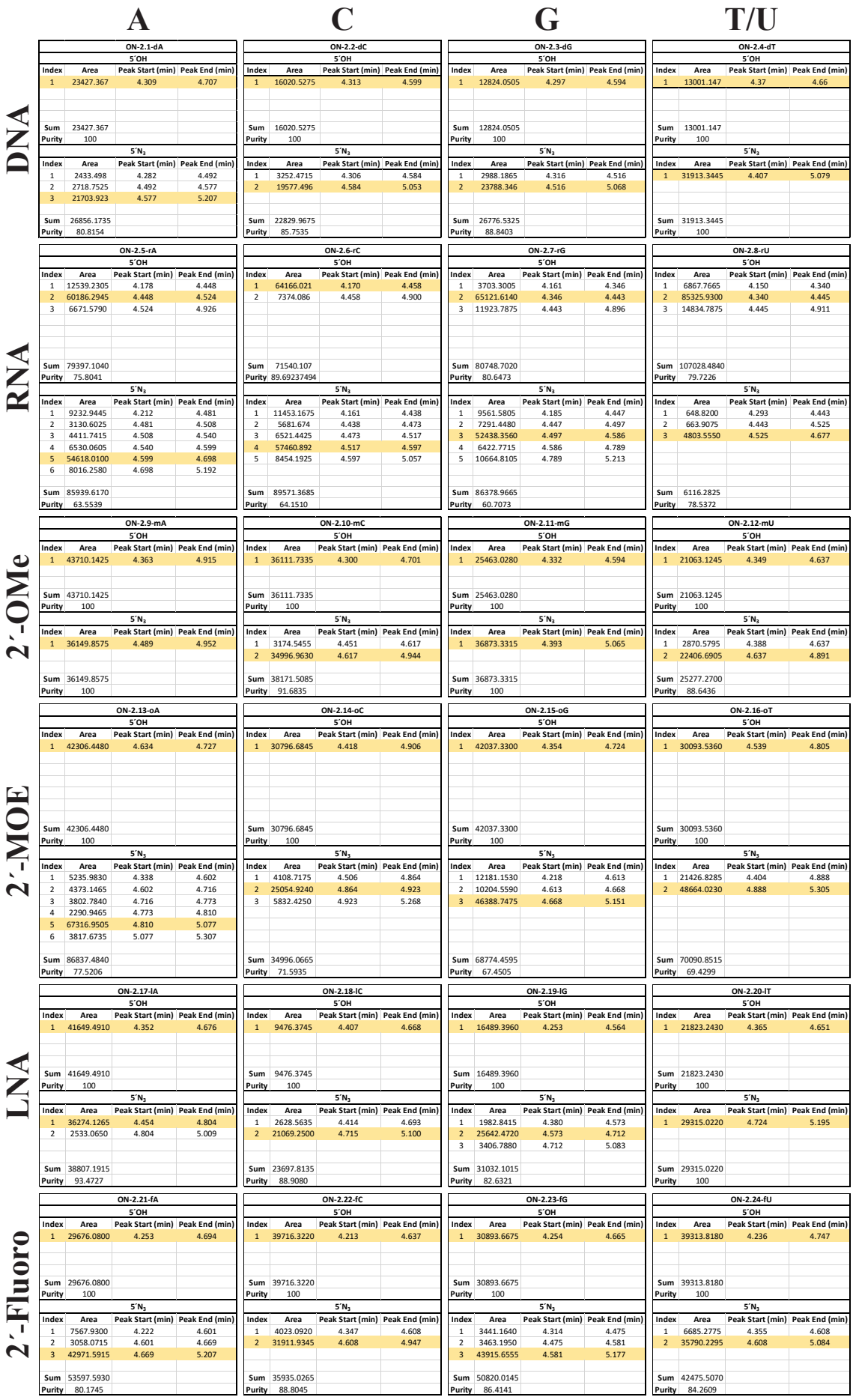


Figure 8.2: MS TIC traces for the peaks taken as desired product in Figure 6.1 for ON-2.1 to ON-2.24. Traces in black correspond to the starting material sequences, traces in red correspond to the sequences after the azide conversion process. Calculated and observed masses can be found in Table 8.1. Columns of A, C, G and T/U refer to the terminal 5´ nucleobase before azide conversion. Rows of DNA, RNA, 2´OMe, 2´MOE, LNA, and 2´Fluoro refer to the modification of the terminal 5´ ribose before azide conversion.



ON-2.1-dA			
5´OH			
Index	Area	Peak Start (min)	Peak End (min)
1	23427.367	4.309	4.707
Sum	23427.367		
Purity	100		
5´N_3			
Index	Area	Peak Start (min)	Peak End (min)
1	2433.498	4.282	4.492
2	2718.7525	4.492	4.577
3	21703.923	4.577	5.207
Sum	26856.1735		
Purity	80.8154		

ON-2.2-dC			
5´OH			
Index	Area	Peak Start (min)	Peak End (min)
1	16020.5275	4.313	4.599
Sum	16020.5275		
Purity	100		
5´N_3			
Index	Area	Peak Start (min)	Peak End (min)
1	3252.4715	4.306	4.584
2	19577.496	4.584	5.053
Sum	22829.9675		
Purity	85.7535		

ON-2.3-dG			
5´OH			
Index	Area	Peak Start (min)	Peak End (min)
1	12824.0505	4.297	4.594
Sum	12824.0505		
Purity	100		
5´N_3			
Index	Area	Peak Start (min)	Peak End (min)
1	2988.1865	4.316	4.516
2	23788.346	4.516	5.068
Sum	26776.5325		
Purity	88.8403		

ON-2.4-dT			
5´OH			
Index	Area	Peak Start (min)	Peak End (min)
1	13001.147	4.37	4.66
Sum	13001.147		
Purity	100		
5´N_3			
Index	Area	Peak Start (min)	Peak End (min)
1	31913.3445	4.407	5.079
Sum	31913.3445		
Purity	100		

ON-2.5-rA			
5´OH			
Index	Area	Peak Start (min)	Peak End (min)
1	12539.2305	4.178	4.448
2	60186.2945	4.448	4.524
3	6671.5790	4.524	4.926
Sum	79397.1040		
Purity	75.8041		
5´N_3			
Index	Area	Peak Start (min)	Peak End (min)
1	9232.9445	4.212	4.481
2	3130.6025	4.481	4.508
3	4411.7415	4.508	4.540
4	6530.0605	4.540	4.599
5	54618.0100	4.599	4.698
6	8016.2580	4.698	5.192
Sum	85939.6170		
Purity	63.5539		

ON-2.6-rC			
5´OH			
Index	Area	Peak Start (min)	Peak End (min)
1	64166.021	4.170	4.458
2	7374.086	4.458	4.900
Sum	71540.107		
Purity	89.69237494		
5´N_3			
Index	Area	Peak Start (min)	Peak End (min)
1	11453.1675	4.161	4.438
2	5681.674	4.438	4.473
3	6521.4425	4.473	4.517
4	57460.892	4.517	4.597
5	8454.1925	4.597	5.057
Sum	89571.3685		
Purity	64.1510		

ON-2.7-rG			
5´OH			
Index	Area	Peak Start (min)	Peak End (min)
1	3703.3005	4.161	4.346
2	65121.6140	4.346	4.443
3	11923.7875	4.443	4.896
Sum	80748.7020		
Purity	80.6473		
5´N_3			
Index	Area	Peak Start (min)	Peak End (min)
1	9561.5805	4.185	4.447
2	7291.4480	4.447	4.497
3	52438.3560	4.497	4.586
4	6422.7715	4.586	4.789
5	10664.8105	4.789	5.213
Sum	86378.9665		
Purity	60.7073		

ON-2.8-rU			
5´OH			
Index	Area	Peak Start (min)	Peak End (min)
1	6867.7665	4.150	4.340
2	85325.9300	4.340	4.445
3	14834.7875	4.445	4.911
Sum	107028.4840		
Purity	79.7226		
5´N_3			
Index	Area	Peak Start (min)	Peak End (min)
1	648.8200	4.293	4.443
2	663.9075	4.443	4.525
3	4803.5550	4.525	4.677
Sum	6116.2825		
Purity	78.5372		

ON-2.9-mA			
5´OH			
Index	Area	Peak Start (min)	Peak End (min)
1	43710.1425	4.363	4.915
Sum	43710.1425		
Purity	100		
5´N_3			
Index	Area	Peak Start (min)	Peak End (min)
1	36149.8575	4.489	4.952
Sum	36149.8575		
Purity	100		

ON-2.10-mC			
5´OH			
Index	Area	Peak Start (min)	Peak End (min)
1	36111.7335	4.300	4.701
Sum	36111.7335		
Purity	100		
5´N_3			
Index	Area	Peak Start (min)	Peak End (min)
1	3174.5455	4.451	4.617
2	34996.9630	4.617	4.944
Sum	38171.5085		
Purity	91.6835		

ON-2.11-mG			
5´OH			
Index	Area	Peak Start (min)	Peak End (min)
1	25463.0280	4.332	4.594
Sum	25463.0280		
Purity	100		
5´N_3			
Index	Area	Peak Start (min)	Peak End (min)
1	36873.3315	4.393	5.065
Sum	36873.3315		
Purity	100		

ON-2.12-mU			
5´OH			
Index	Area	Peak Start (min)	Peak End (min)
1	21063.1245	4.349	4.637
Sum	21063.1245		
Purity	100		
5´N_3			
Index	Area	Peak Start (min)	Peak End (min)
1	2870.5795	4.388	4.637
2	22406.6905	4.637	4.891
Sum	25277.2700		
Purity	88.6436		

ON-2.13-oA			
5´OH			
Index	Area	Peak Start (min)	Peak End (min)
1	42306.4480	4.634	4.727
Sum	42306.4480		
Purity	100		
5´N_3			
Index	Area	Peak Start (min)	Peak End (min)
1	5235.9830	4.338	4.602
2	4373.1465	4.602	4.716
3	3802.7840	4.716	4.773
4	2290.9465	4.773	4.810
5	67316.9505	4.810	5.077
6	3817.6735	5.077	5.307
Sum	86837.4840		
Purity	77.5206		

ON-2.14-oC			
5´OH			
Index	Area	Peak Start (min)	Peak End (min)
1	30796.6845	4.418	4.906
Sum	30796.6845		
Purity	100		
5´N_3			
Index	Area	Peak Start (min)	Peak End (min)
1	4108.7175	4.506	4.864
2	25054.9240	4.864	4.923
3	5832.4250	4.923	5.268
Sum	34996.0665		
Purity	71.5935		

ON-2.15-oG			
5´OH			
Index	Area	Peak Start (min)	Peak End (min)
1	42037.3300	4.354	4.724
Sum	42037.3300		
Purity	100		
5´N_3			
Index	Area	Peak Start (min)	Peak End (min)
1	12181.1530	4.218	4.613
2	10204.5590	4.613	4.668
3	46388.7475	4.668	5.151
Sum	68774.4595		
Purity	67.4505		

ON-2.16-oT			
5´OH			
Index	Area	Peak Start (min)	Peak End (min)
1	30093.5360	4.539	4.805
Sum	30093.5360		
Purity	100		
5´N_3			
Index	Area	Peak Start (min)	Peak End (min)
1	21426.8285	4.404	4.888
2	48664.0230	4.888	5.305
Sum	70090.8515		
Purity	69.4299		

ON-2.17-lA			
5´OH			
Index	Area	Peak Start (min)	Peak End (min)
1	41649.4910	4.352	4.676
Sum	41649.4910		
Purity	100		
5´N_3			
Index	Area	Peak Start (min)	Peak End (min)
1	36274.1265	4.454	4.804
2	2533.0650	4.804	5.009
Sum	38807.1915		
Purity	93.4727		

ON-2.18-lC			
5´OH			
Index	Area	Peak Start (min)	Peak End (min)
1	9476.3745	4.407	4.668
Sum	9476.3745		
Purity	100		
5´N_3			
Index	Area	Peak Start (min)	Peak End (min)
1	2628.5635	4.414	4.693
2	21069.2500	4.715	5.100
Sum	23697.8135		
Purity	88.9080		

ON-2.19-lG			
5´OH			
Index	Area	Peak Start (min)	Peak End (min)
1	16489.3960	4.253	4.564
Sum	16489.3960		
Purity	100		
5´N_3			
Index	Area	Peak Start (min)	Peak End (min)
1	1982.8415	4.380	4.573
2	25642.4720	4.573	4.712
3	3406.7880	4.712	5.083
Sum	31032.1015		
Purity	82.6321		

ON-2.20-lT			
5´OH			
Index	Area	Peak Start (min)	Peak End (min)
1	21823.2430	4.365	4.651
Sum	21823.2430		
Purity	100		
5´N_3			
Index	Area	Peak Start (min)	Peak End (min)
1	29315.0220	4.724	5.195
Sum	29315.0220		
Purity	100		

ON-2.21-fA			
5´OH			
Index	Area	Peak Start (min)	Peak End (min)
1	29676.0800	4.253	4.694
Sum	29676.0800		
Purity	100		
5´N_3			
Index	Area	Peak Start (min)	Peak End (min)
1	7567.9300	4.222	4.601
2	3058.0715	4.601	4.669
3	42971.5915	4.669	5.207
Sum	53597.5930		
Purity	80.1745		

ON-2.22-fC			
5´OH			
Index	Area	Peak Start (min)	Peak End (min)
1	39716.3220	4.213	4.637
Sum	39716.3220		
Purity	100		
5´N_3			
Index	Area	Peak Start (min)	Peak End (min)
1	4023.0920	4.347	4.608
2	31911.9345	4.608	4.947
Sum	35935.0265		
Purity	88.8045		

ON-2.23-fG			
5´OH			
Index	Area	Peak Start (min)	Peak End (min)
1	30893.6675	4.254	4.665
Sum	30893.6675		
Purity	100		
5´N_3			
Index	Area	Peak Start (min)	Peak End (min)
1	3441.1640	4.314	4.475
2	3463.1950	4.475	4.581
3	43915.6555	4.581	5.177
Sum	50820.0145		
Purity	86.4141		

ON-2.24-fU			
5´OH			
Index	Area	Peak Start (min)	Peak End (min)
1	39313.8180	4.236	4.747
Sum	39313.8180		
Purity	100		
5´N_3			
Index	Area	Peak Start (min)	Peak End (min)
1	6685.2775	4.355	4.608
2	35790.2295	4.608	5.084
Sum	42475.5070		
Purity	84.2609		

Figure 8.3: Peak data used for determination of azide conversion of ON-2.1 to ON-

2.24. All peaks found in chromatograms from Figure 8.1 are listed as with elution time (minutes) total area by integration (mAu^2). Peaks found to have the mass of the desired product as shown in Figure 8.2 are highlighted. Columns of A, C, G and T/U refer to the terminal 5´ nucleobase before azide conversion. Rows of DNA, RNA, 2´OMe, 2´MOE, LNA, and 2´Fluoro refer to the modification of the terminal 5´ ribose before azide conversion.

8.5.2 LC-MS Data for Oligonucleotides ON-2.25 to ON-2.48

Oligo	Sequence (5´-3´)	Calc. Mass OH (Da)	Calc. Mass N3 (Da)	Found Mass OH (Da)	Found Mass N_3 (Da)	OH Purity (%)	N3 Purity (%)	N3 Conversion (%)
ON-2.25-dA	atttttttttt	3453.8	3478.8	3453.5	3479.1	100	55	55
ON-2.26-dC	ctttttttttt	3429.8	3454.8	3430.1	3454.9	100	83	83
ON-2.27-dG	gtttttttttt	3469.8	3494.8	3469.4	3494.4	100	69	69
ON-2.28-dT	ttttttttttt	3444.8	3469.8	3444.6	3469.7	100	85	85
ON-2.29-rA	**a**ttttttttttt	3469.8	3494.8	3470.0	3494.8	83	58	70
ON-2.30-rC	**c**ttttttttttt	3445.8	3470.8	3445.8	3470.8	85	60	71
ON-2.31-rG	**g**ttttttttttt	3485.8	3510.8	3485.7	3511.8	86	53	62
ON-2.32-rU	**u**ttttttttttt	3446.8	3471.8	3446.6	3471.6	83	65	79
ON-2.33-mA	*a* ttttttttttt	3483.8	3508.8	3483.0	3509.7	100	69	69
ON-2.34-mC	*c* ttttttttttt	3459.8	3484.8	3459.0	3484.0	100	74	74
ON-2.35-mG	*g* ttttttttttt	3499.8	3524.8	3500.5	3523.7	100	76	76
ON-2.36-mU	*u* ttttttttttt	3460.8	3485.8	3461.3	3487.3	89	81	92
ON-2.37-oA	***a*** ttttttttttt	3527.9	3552.9	3528.1	3553.0	88	56	64
ON-2.38-oC	***c*** ttttttttttt	3517.9	3542.9	3518.1	3542.8	100	76	76
ON-2.39-oG	***g*** ttttttttttt	3543.9	3568.9	3543.9	3569.6	83	52	62
ON-2.40-oT	***t*** ttttttttttt	3518.9	3543.9	3518.7	3544.0	100	78	78
ON-2.41-lA	**a**ttttttttttt	3481.8	3506.8	3481.2	3507.2	80	26	32
ON-2.42-lC	**c**ttttttttttt	3471.8	3496.8	3472.3	3496.1	89	39	44
ON-2.43-lG	**g**ttttttttttt	3497.8	3522.8	3496.6	3524.1	100	25	25
ON-2.44-lT	**t**ttttttttttt	3472.8	3497.8	3471.8	3498.5	94	36	39
ON-2.45-fA	atttttttttt	3471.8	3496.8	3470.6	3495.9	100	44	44
ON-2.46-fC	ctttttttttt	3447.8	3472.8	3447.0	3474.1	100	61	61
ON-2.47-fG	gtttttttttt	3487.8	3512.8	3487.4	3512.7	100	47	47
ON-2.48-fU	~~u~~ttttttttttt	3448.8	3473.8	3447.5	3473.9	100	64	64

Table 8.2: Table containing sequences along with calculated and observed masses and azide conversion data for ON-2.25 to ON-2.48. Chemistries are indicated as follows: DNA, **RNA**, *2´-OMe*, ***2´-MOE***, **LNA**, ~~2´-Fluoro~~. Lower case letters indicate phosphorothioate linkages.

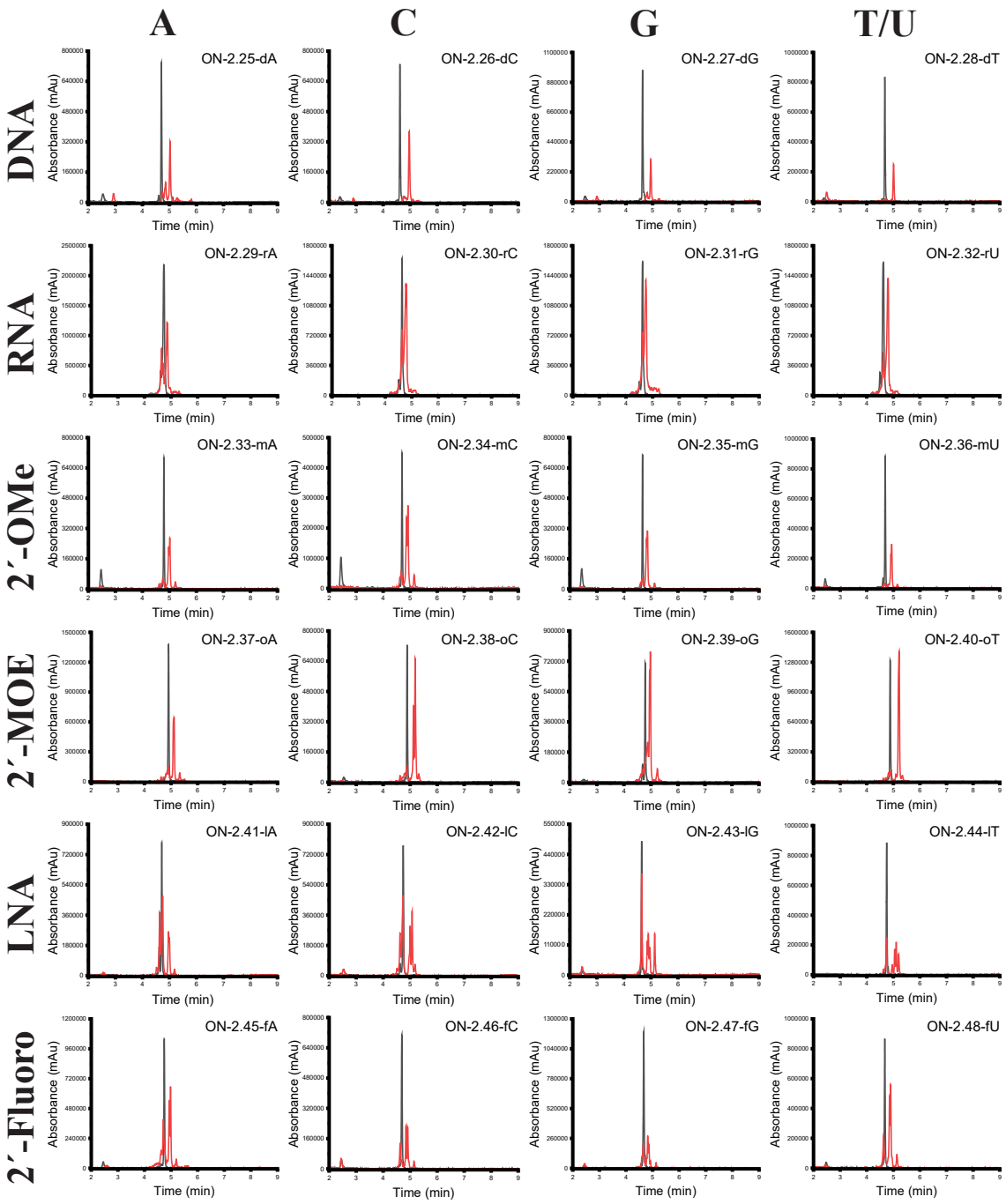


Figure 8.4: A_{260} LC traces used for the determination of azide conversion for ON-2.25 to ON-2.48. Traces in black correspond to the starting material sequences, traces in red correspond to the sequences after the azide conversion process. Purity as determined by integration is listed in Table 8.2. Columns of A, C, G and T/U refer to the terminal 5´ nucleobase before azide conversion. Rows of DNA, RNA, 2´OMe, 2´MOE, LNA, and 2´Fluoro refer to the modification of the terminal 5´ ribose before azide conversion.

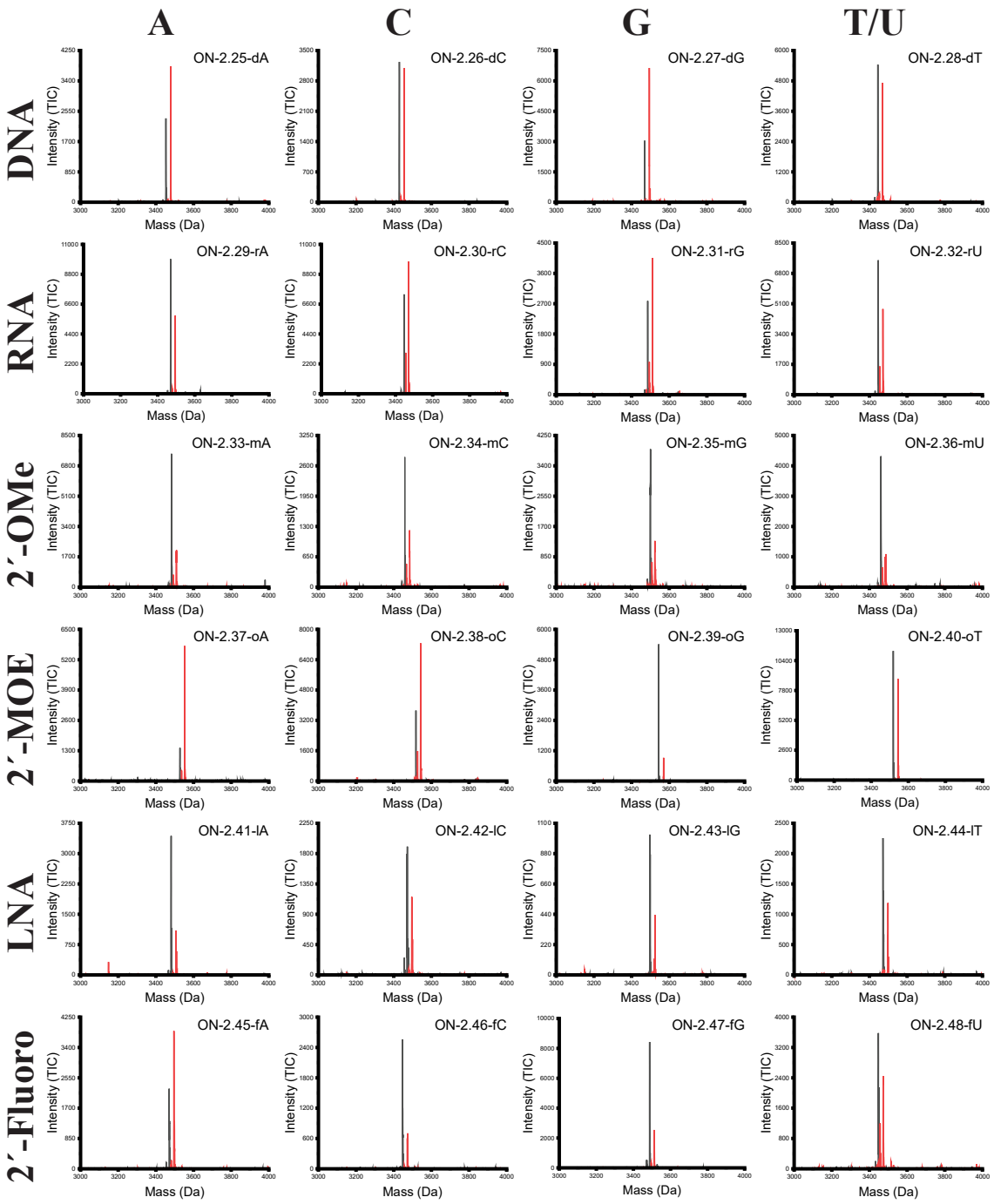


Figure 8.5: MS TIC traces for the peaks taken as desired product in Figure 8.4 for ON-2.25 to ON-2.48. Traces in black correspond to the starting material sequences, traces in red correspond to the sequences after the azide conversion process. Calculated and observed masses can be found in Table 8.2. Columns of A, C, G and T/U refer to the terminal 5´ nucleobase before azide conversion. Rows of DNA, RNA, 2´OMe, 2´MOE, LNA, and 2´Fluoro refer to the modification of the terminal 5´ ribose before azide conversion.

	A	C	G	T/U
DNA	ON-2.25-dA 5´OH Index / Area / Peak Start (min) / Peak End (min) 1 / 31140.6775 / 4.415 / 5.224 Sum 31140.6775 Purity 100 5´N3 1 / 4066.3285 / 4.626 / 4.794 2 / 7351.1370 / 4.794 / 4.931 3 / 17681.3080 / 4.931 / 5.182 4 / 3101.4790 / 5.182 / 5.565 Sum 32200.2525 Purity 54.9105	ON-2.26-dC 5´OH Index / Area / Peak Start (min) / Peak End (min) 1 / 28842.3030 / 4.378 / 4.952 Sum 28842.3030 Purity 100 5´N3 1 / 1173.2640 / 4.633 / 4.762 2 / 1359.2815 / 4.762 / 4.811 3 / 941.8480 / 4.811 / 4.852 4 / 832.6195 / 4.852 / 4.894 5 / 21638.0940 / 4.894 / 5.401 Sum 25945.1070 Purity 83.3995	ON-2.27-dG 5´OH Index / Area / Peak Start (min) / Peak End (min) 1 / 40365.6145 / 4.308 / 4.899 Sum 40365.6145 Purity 100 5´N3 1 / 5736.1200 / 4.601 / 4.854 2 / 17615.1145 / 4.854 / 5.142 3 / 2064.6065 / 5.142 / 5.452 Sum 25415.8410 Purity 69.3076	ON-2.28-dT 5´OH Index / Area / Peak Start (min) / Peak End (min) 1 / 31117.8145 / 4.392 / 4.930 Sum 31117.8145 Purity 100 5´N3 1 / 2068.3315 / 4.401 / 4.817 2 / 12129.9675 / 4.817 / 5.157 Sum 14198.2990 Purity 85.4325
RNA	ON-2.29-rA 5´OH Index / Area / Peak Start (min) / Peak End (min) 1 / 34716.8440 / 4.102 / 4.641 2 / 172870.2435 / 4.641 / 5.273 Sum 207587.0875 Purity 83.2760 5´N3 1 / 10093.9550 / 4.143 / 4.545 2 / 47168.1770 / 4.545 / 4.674 3 / 27310.1580 / 4.674 / 4.745 4 / 113371.1080 / 4.745 / 5.053 5 / 10306.0440 / 5.053 / 5.254 6 / 4932.4335 / 5.254 / 5.474 Sum 213181.8755 Purity 58.0149	ON-2.30-rC 5´OH Index / Area / Peak Start (min) / Peak End (min) 1 / 15225.4510 / 4.141 / 4.556 2 / 88675.6790 / 4.556 / 5.137 Sum 103901.1300 Purity 85.3462 5´N3 1 / 76575.9005 / 3.946 / 4.677 2 / 90873.7485 / 4.677 / 4.787 3 / 49350.7585 / 4.787 / 4.908 4 / 15495.6470 / 4.908 / 5.407 Sum 232296.0545 Purity 60.3646	ON-2.31-rG 5´OH Index / Area / Peak Start (min) / Peak End (min) 1 / 15584.3440 / 4.125 / 4.546 2 / 94673.6870 / 4.546 / 5.157 Sum 110258.0310 Purity 85.8656 5´N3 1 / 78621.7275 / 3.845 / 4.668 2 / 123941.4330 / 4.668 / 4.862 3 / 4734.2240 / 4.862 / 4.917 4 / 6781.0235 / 4.917 / 5.004 5 / 6282.1465 / 5.004 / 5.088 6 / 6328.6760 / 5.088 / 5.177 7 / 6744.4015 / 5.177 / 5.470 Sum 233433.6320 Purity 53.0949	ON-2.32-rU 5´OH Index / Area / Peak Start (min) / Peak End (min) 1 / 24268.2640 / 3.952 / 4.547 2 / 118530.4075 / 4.547 / 5.273 Sum 142798.6715 Purity 83.0053 5´N3 1 / 49139.1650 / 3.947 / 4.669 2 / 125533.5595 / 4.669 / 4.861 3 / 17794.3145 / 4.861 / 5.394 Sum 192467.0390 Purity 65.2234
2´-OMe	ON-2.33-mA 5´OH Index / Area / Peak Start (min) / Peak End (min) 1 / 26203.0080 / 4.355 / 5.046 Sum 26203.0080 Purity 100 5´N3 1 / 1629.9130 / 4.462 / 4.662 2 / 5160.3535 / 4.662 / 4.846 3 / 10348.8645 / 4.846 / 4.990 4 / 11554.0900 / 4.990 / 5.131 5 / 2867.4975 / 5.131 / 5.464 Sum 31560.7185 Purity 69.3994	ON-2.34-mC 5´OH Index / Area / Peak Start (min) / Peak End (min) 1 / 17596.3760 / 4.395 / 4.872 Sum 17596.3760 Purity 100 5´N3 1 / 1937.1975 / 4.419 / 4.633 2 / 3967.8750 / 4.633 / 4.742 3 / 11860.3890 / 4.742 / 4.887 4 / 13031.3080 / 4.887 / 5.059 5 / 3055.9755 / 5.059 / 5.407 Sum 33852.7450 Purity 73.5293	ON-2.35-mG 5´OH Index / Area / Peak Start (min) / Peak End (min) 1 / 25678.1340 / 4.347 / 4.870 Sum 25678.1340 Purity 100 5´N3 1 / 1901.4495 / 4.438 / 4.637 2 / 3472.4885 / 4.637 / 4.731 3 / 12932.4050 / 4.731 / 4.855 4 / 12136.5180 / 4.855 / 5.043 5 / 2462.0245 / 5.043 / 5.405 Sum 32904.8855 Purity 76.1860	ON-2.36-mU 5´OH Index / Area / Peak Start (min) / Peak End (min) 1 / 4017.7850 / 4.318 / 4.643 2 / 31493.1965 / 4.643 / 4.963 Sum 35510.9815 Purity 88.6858 5´N3 1 / 1388.9775 / 4.478 / 4.657 2 / 1982.5870 / 4.657 / 4.752 3 / 1166.5245 / 4.752 / 4.823 4 / 8613.4285 / 4.823 / 4.920 5 / 11065.1310 / 4.920 / 5.058 6 / 1805.6935 / 5.058 / 5.415 Sum 24216.6485 Purity 81.2605
2´-MOE	ON-2.37-oA 5´OH Index / Area / Peak Start (min) / Peak End (min) 1 / 8249.1015 / 4.359 / 4.852 2 / 58014.6325 / 4.852 / 5.382 Sum 66263.7340 Purity 87.5511 5´N3 1 / 3537.2795 / 4.305 / 4.671 2 / 2463.4460 / 4.671 / 4.746 3 / 9639.4095 / 4.746 / 4.881 4 / 6816.8625 / 4.881 / 4.954 5 / 1189.8895 / 4.954 / 4.983 6 / 1764.6220 / 4.983 / 5.023 7 / 23434.7705 / 5.023 / 5.104 8 / 19815.2250 / 5.104 / 5.188 9 / 8646.0955 / 5.188 / 5.622 Sum 77307.6000 Purity 55.9453	ON-2.38-oC 5´OH Index / Area / Peak Start (min) / Peak End (min) 1 / 28981.3295 / 5.448 / 6.113 Sum 28981.3295 Purity 100 5´N3 1 / 2095.0505 / 4.434 / 4.657 2 / 4056.0105 / 4.657 / 4.807 3 / 2104.7475 / 4.807 / 4.852 4 / 3452.7025 / 4.852 / 4.927 5 / 17466.6185 / 4.927 / 5.148 6 / 29607.9170 / 5.148 / 5.268 7 / 3462.0795 / 5.268 / 5.577 Sum 62245.1260 Purity 75.6277	ON-2.39-oG 5´OH Index / Area / Peak Start (min) / Peak End (min) 1 / 5411.5175 / 4.459 / 4.733 2 / 26324.7580 / 4.733 / 5.052 Sum 31736.2755 Purity 82.9485 5´N3 1 / 4765.0180 / 4.233 / 4.649 2 / 6062.3935 / 4.649 / 4.745 3 / 4472.9655 / 4.745 / 4.796 4 / 4845.8530 / 4.796 / 4.829 5 / 16277.1660 / 4.829 / 4.912 6 / 19773.3105 / 4.912 / 4.963 7 / 26957.8075 / 4.963 / 5.095 8 / 7110.3180 / 5.095 / 5.537 Sum 90264.8320 Purity 51.7711	ON-2.40-oT 5´OH Index / Area / Peak Start (min) / Peak End (min) 1 / 56914.5470 / 5.434 / 6.296 Sum 56914.5470 Purity 100 5´N3 1 / 13745.0200 / 4.266 / 4.863 2 / 7203.6660 / 4.863 / 5.029 3 / 3815.4175 / 5.029 / 5.121 4 / 88153.7520 / 5.121 / 5.785 Sum 112917.8555 Purity 78.0689
LNA	ON-2.41-lA 5´OH Index / Area / Peak Start (min) / Peak End (min) 1 / 7353.7175 / 4.409 / 4.658 2 / 29811.7230 / 4.658 / 5.201 Sum 37165.4405 Purity 80.2136 5´N3 1 / 3143.0195 / 4.339 / 4.561 2 / 17869.5005 / 4.561 / 4.674 3 / 31415.5790 / 4.674 / 4.866 4 / 11393.4770 / 4.866 / 4.988 5 / 7790.5810 / 4.988 / 5.091 6 / 2495.8525 / 5.091 / 5.374 Sum 74108.0095 Purity 25.8866	ON-2.42-lC 5´OH Index / Area / Peak Start (min) / Peak End (min) 1 / 4173.6300 / 4.435 / 4.672 2 / 32567.8040 / 4.672 / 5.204 Sum 36741.4340 Purity 88.6405 5´N3 1 / 3582.9485 / 4.312 / 4.558 2 / 12758.3330 / 4.558 / 4.660 3 / 29805.5055 / 4.660 / 4.841 4 / 16164.1685 / 4.841 / 5.033 5 / 15720.5495 / 5.033 / 5.135 6 / 4052.9010 / 5.135 / 5.416 Sum 82084.4060 Purity 38.8438	ON-2.43-lG 5´OH Index / Area / Peak Start (min) / Peak End (min) 1 / 16768.6650 / 4.476 / 4.918 Sum 16768.6650 Purity 100.0000 5´N3 1 / 17933.6335 / 4.414 / 4.809 2 / 4277.9725 / 4.809 / 4.883 3 / 5084.6455 / 4.883 / 4.931 4 / 4730.7820 / 4.931 / 5.041 5 / 7234.3940 / 5.041 / 5.409 Sum 39261.4275 Purity 25.0002	ON-2.44-lT 5´OH Index / Area / Peak Start (min) / Peak End (min) 1 / 30273.6175 / 4.459 / 4.791 2 / 1972.6450 / 4.791 / 5.009 Sum 32246.2625 Purity 93.8826 5´N3 1 / 1753.7290 / 4.474 / 4.645 2 / 12633.6240 / 4.645 / 4.845 3 / 3746.8980 / 4.845 / 5.009 4 / 5895.2125 / 5.009 / 5.078 5 / 8236.7255 / 5.078 / 5.155 6 / 6476.1095 / 5.155 / 5.472 Sum 38742.2985 Purity 36.4768
2´-Fluoro	ON-2.45-fA 5´OH Index / Area / Peak Start (min) / Peak End (min) 1 / 43401.6665 / 4.262 / 5.250 Sum 43401.6665 Purity 100.0000 5´N3 1 / 6209.9745 / 4.097 / 4.491 2 / 2088.4485 / 4.491 / 4.550 3 / 9445.1710 / 4.550 / 4.655 4 / 29494.2650 / 4.655 / 4.823 5 / 3137.9655 / 4.823 / 4.881 6 / 21257.3780 / 4.881 / 4.955 7 / 25587.6305 / 4.955 / 5.094 8 / 8668.7880 / 5.094 / 5.685 Sum 105889.6210 Purity 44.2395	ON-2.46-fC 5´OH Index / Area / Peak Start (min) / Peak End (min) 1 / 30963.0980 / 4.343 / 4.986 Sum 30963.0980 Purity 100.0000 5´N3 1 / 7052.6205 / 4.331 / 4.664 2 / 2559.1020 / 4.664 / 4.753 3 / 181.4455 / 4.753 / 4.766 4 / 8848.8375 / 4.766 / 4.877 5 / 9677.2655 / 4.877 / 5.070 6 / 2277.4060 / 5.070 / 5.342 Sum 30596.6770 Purity 60.5494	ON-2.47-fG 5´OH Index / Area / Peak Start (min) / Peak End (min) 1 / 57681.8975 / 4.240 / 5.203 Sum 57681.8975 Purity 100.0000 5´N3 1 / 17020.4915 / 4.322 / 4.742 2 / 12324.6595 / 4.742 / 4.841 3 / 7657.8790 / 4.841 / 4.898 4 / 2758.3855 / 4.898 / 5.049 5 / 2563.1710 / 5.049 / 5.388 Sum 42324.5865 Purity 47.2126	ON-2.48-fU 5´OH Index / Area / Peak Start (min) / Peak End (min) 1 / 37001.1085 / 4.348 / 5.176 Sum 37001.1085 Purity 100.0000 5´N3 1 / 13592.8630 / 4.133 / 4.667 2 / 3436.6535 / 4.667 / 4.718 3 / 1618.4030 / 4.718 / 4.760 4 / 21265.6680 / 4.760 / 4.879 5 / 22643.8560 / 4.879 / 5.057 6 / 6053.2085 / 5.057 / 5.431 Sum 68610.6520 Purity 63.9981

Figure 8.6: Peak data used for determination of azide conversion of ON-2.25 to ON-2.48. All peaks found in chromatograms from Figure 8.4 are listed as with elution time (minutes) total area by integration (mAu^2). Peaks found to have the mass of the desired product as shown in Figure 8.5 are highlighted. Columns of A, C, G and T/U refer to the terminal 5´ nucleobase before azide conversion. Rows of DNA, RNA, 2´OMe, 2´MOE, LNA, and 2´Fluoro refer to the modification of the terminal 5´ ribose before azide conversion.

8.6 Data for Chapter 3

8.6.1 LC-MS Data for Oligonucleotides ON-3.1 to ON-3.4

Oligo	Sequence (5´-3´)	Calc. Mass Click	Found Mass Click	N3 Purity (%)	Click Purity (%)	Click Conversion (%)
ON-3.1	T=ttttttttttt	4051.4	4052.6	85	59	69
ON-3.2	T=ttttttttttt	4051.4	4053.4	85	66	78
ON-3.3	T=ttttttttttt	4051.4	4051.4	85	83	97
ON-3.4	T=ttttttttttt	4051.4	4051.6	85	71	83

Table 8.3: Table containing sequences along with calculated and observed masses and CuAAC conversion data for ON-3.1 to ON-3.4. DNA is indicated by plain text. Lower case letters indicate phosphorothioate linkages, = indicates a 1,4-triazole linkage formed by CuAAC.

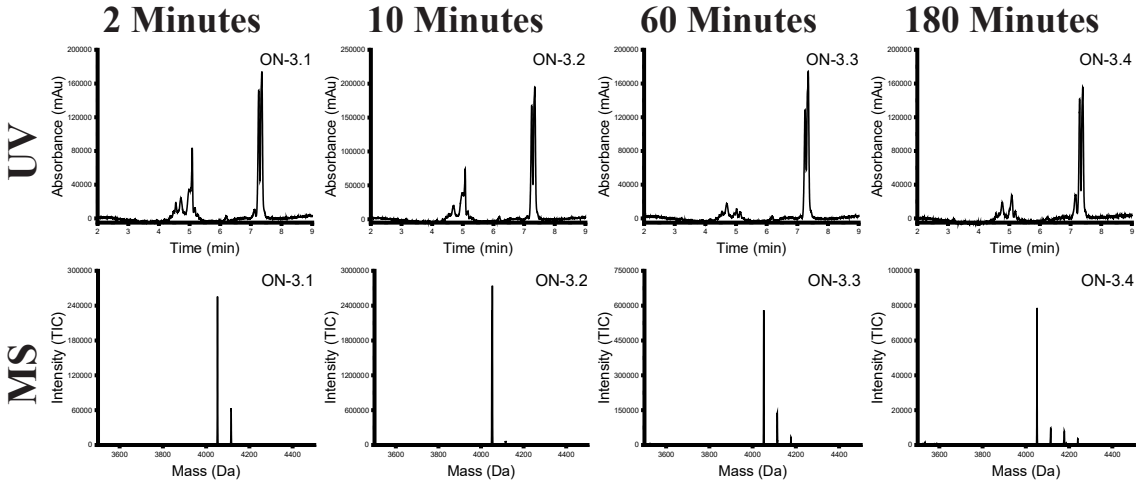


Figure 8.7: UV at A_{260} traces from LC and MS-TIC traces for ON-3.1 to ON-3.4. UV traces were used to determine purity as shown in Table 8.3. MS-TIC was used to confirm target identity, calculated and observed masses can be seen in Table 8.3.

2 Minutes

ON-3.1			
Index	Area	Peak Start (min)	Peak End (min)
1	1800.4090	4.345	4.604
2	3038.7015	4.604	4.853
3	2793.3065	4.853	5.003
4	1162.9565	5.003	5.038
5	3915.8240	5.038	5.130
6	1081.8095	5.130	5.307
7	881.2325	6.988	7.173
8	8625.2225	7.173	7.299
9	12518.9285	7.299	7.588
Sum	35818.3905		
Purity	59.0315		

10 Minutes

ON-3.2			
Index	Area	Peak Start (min)	Peak End (min)
1	3179.5360	4.421	4.832
2	4599.9425	4.832	5.029
3	3580.4070	5.029	5.120
4	939.5505	5.120	5.358
5	9962.3820	7.020	7.290
6	14203.2135	7.290	7.577
Sum	36465.0315		
Purity	66.2706		

60 Minutes

ON-3.3			
Index	Area	Peak Start (min)	Peak End (min)
1	781.2105	4.412	4.591
2	2095.8000	4.591	4.873
3	1605.7065	4.873	5.267
4	8194.4025	7.019	7.293
5	13198.5470	7.293	7.584
Sum	25875.6665		
Purity	82.6759		

180 Minutes

ON-3.4			
Index	Area	Peak Start (min)	Peak End (min)
1	2441.8395	4.532	4.943
2	2458.0295	4.943	5.139
3	499.9760	5.139	5.250
4	2521.7200	6.998	7.217
5	7749.0710	7.217	7.339
6	11204.6000	7.339	7.793
Sum	26875.2360		
Purity	70.5247		

Figure 8.8: Peak data used for determination of CuAAC conversion for ON-3.1 to ON-3.4. All peaks found in chromatograms from Figure 8.7 are listed as with elution time (minutes) total area by integration (mAu^2). Peaks found to have the mass of the desired product as shown in Figure 8.7 are highlighted

8.6.2 LC-MS Data for ON-3.5 to ON-3.28

Oligo	Sequence (5´-3´)	Calc. Mass Click	Found Mass Click	N3 Purity (%)	Click Purity (%)	Click Conversion (%)
ON-3.5-dA	T=ATTTTTTTTTTT	3900.8	3901.0	81	32	40
ON-3.6-dC	T=CTTTTTTTTTT	3876.8	3876.9	86	47	55
ON-3.7-dG	T=GTTTTTTTTTT	3916.8	3917.0	89	52	59
ON-3.8-dT	T=TTTTTTTTTTT	3891.8	3892.0	100	50	50
ON-3.9-rA	T=**A**TTTTTTTTTTT	3916.8	3917.3	64	39	62
ON-3.10-rC	T=**C**TTTTTTTTTT	3892.8	3893.1	64	63	98
ON-3.11-rG	T=**G**TTTTTTTTTT	3932.8	3933.1	61	53	87
ON-3.12-rU	T=**U**TTTTTTTTTT	3893.8	3893.9	79	56	71
ON-3.13-mA	T=*A* TTTTTTTTTT	3930.9	3931.1	100	43	55
ON-3.14-mC	T=*C* TTTTTTTTTT	3906.8	3907.2	92	31	43
ON-3.15-mG	T=*G* TTTTTTTTTT	3946.8	3947.2	100	43	63
ON-3.16-mU	T=*U* TTTTTTTTTT	3907.8	3908.0	89	44	63
ON-3.17-oA	T=***A*** TTTTTTTTTT	3974.9	3975.3	78	57	61
ON-3.18-oC	T=***C*** TTTTTTTTTT	3964.9	3965.8	72	57	64
ON-3.19-oG	T=***G*** TTTTTTTTTT	3990.9	3991.3	67	56	68
ON-3.20-oT	T=***T*** TTTTTTTTTT	3965.9	3966.4	69	67	67
ON-3.21-lA	T=**A**TTTTTTTTTT	3928.8	3929.2	93	19	19
ON-3.22-lC	T=**C**TTTTTTTTTT	3918.8	3919.2	89	70	76
ON-3.23-lG	T=**G**TTTTTTTTTT	3944.8	3945.2	83	43	43
ON-3.24-lT	T=**T**TTTTTTTTTT	3919.8	3920.1	100	62	70
ON-3.25-fA	T=~~A~~TTTTTTTTTT	3918.8	3919.2	80	47	58
ON-3.26-fC	T=~~C~~TTTTTTTTTT	3894.8	3894.9	88	69	78
ON-3.27-fG	T=~~G~~TTTTTTTTTT	3934.8	3935.2	86	59	68
ON-3.28-fU	T=~~U~~TTTTTTTTTT	3895.8	3896.0	84	47	56

Table 8.4: Table containing sequences along with calculated and observed masses and CuAAC conversion data for ON-3.5 to ON-3.28. Chemistries are indicated as follows: DNA, **RNA**, *2´-OMe*, ***2´-MOE***, **LNA**, ~~2´-Fluoro~~. Capitalised letters indicate phosphodiester linkages and = indicates a 1,4-triazole linkage formed by CuAAC.

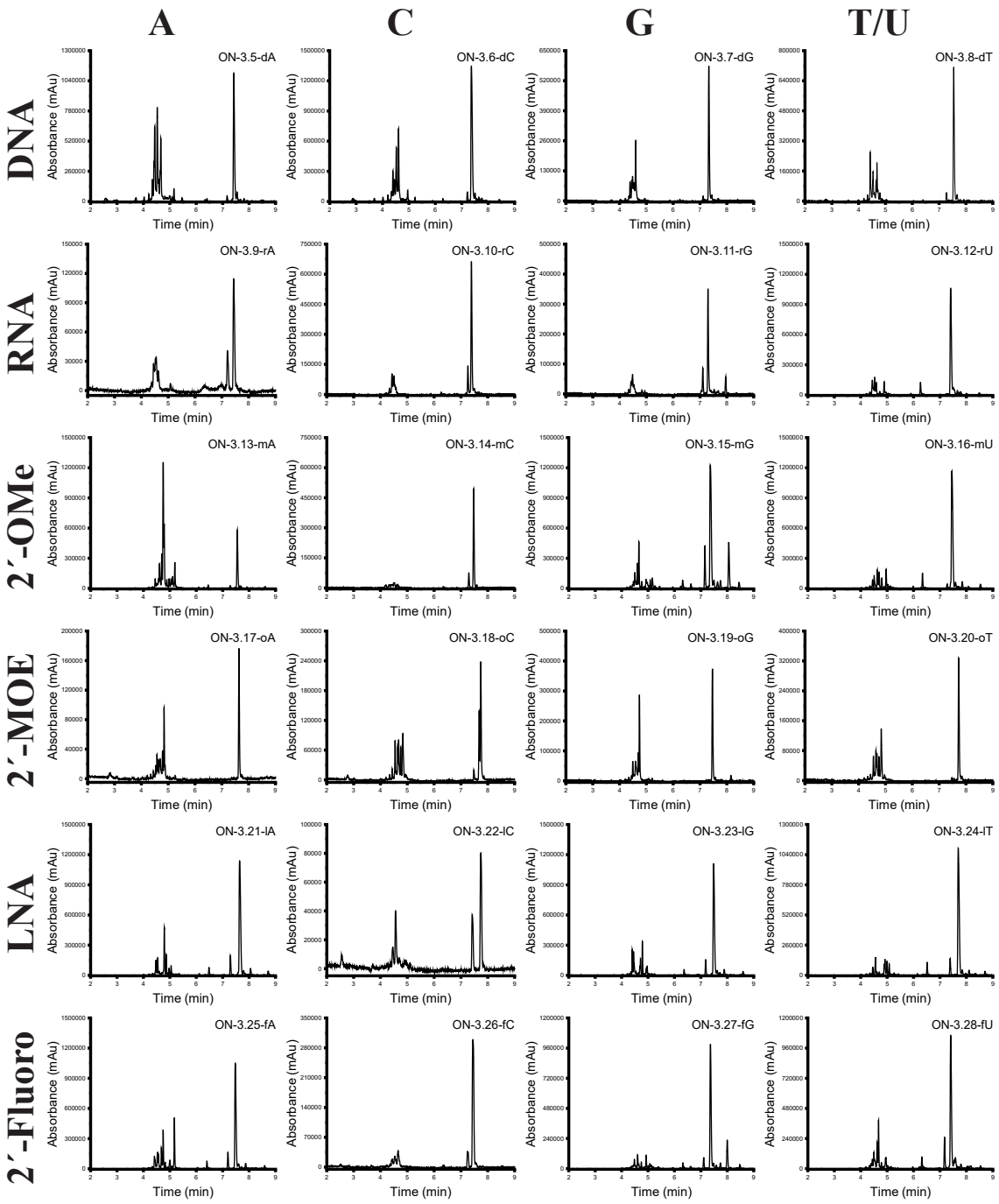


Figure 8.9: A_{260} LC traces used for the determination of CuAAC conversion for ON-3.5 to ON-3.28. Purity as determined by integration is listed in Table 8.4. Columns of A, C, G and T/U refer to the terminal 5´ nucleobase before CuAAC. Rows of DNA, RNA, 2´OMe, 2´MOE, LNA, and 2´fluoro refer to the modification of the terminal 5´ ribose before CuAAC.

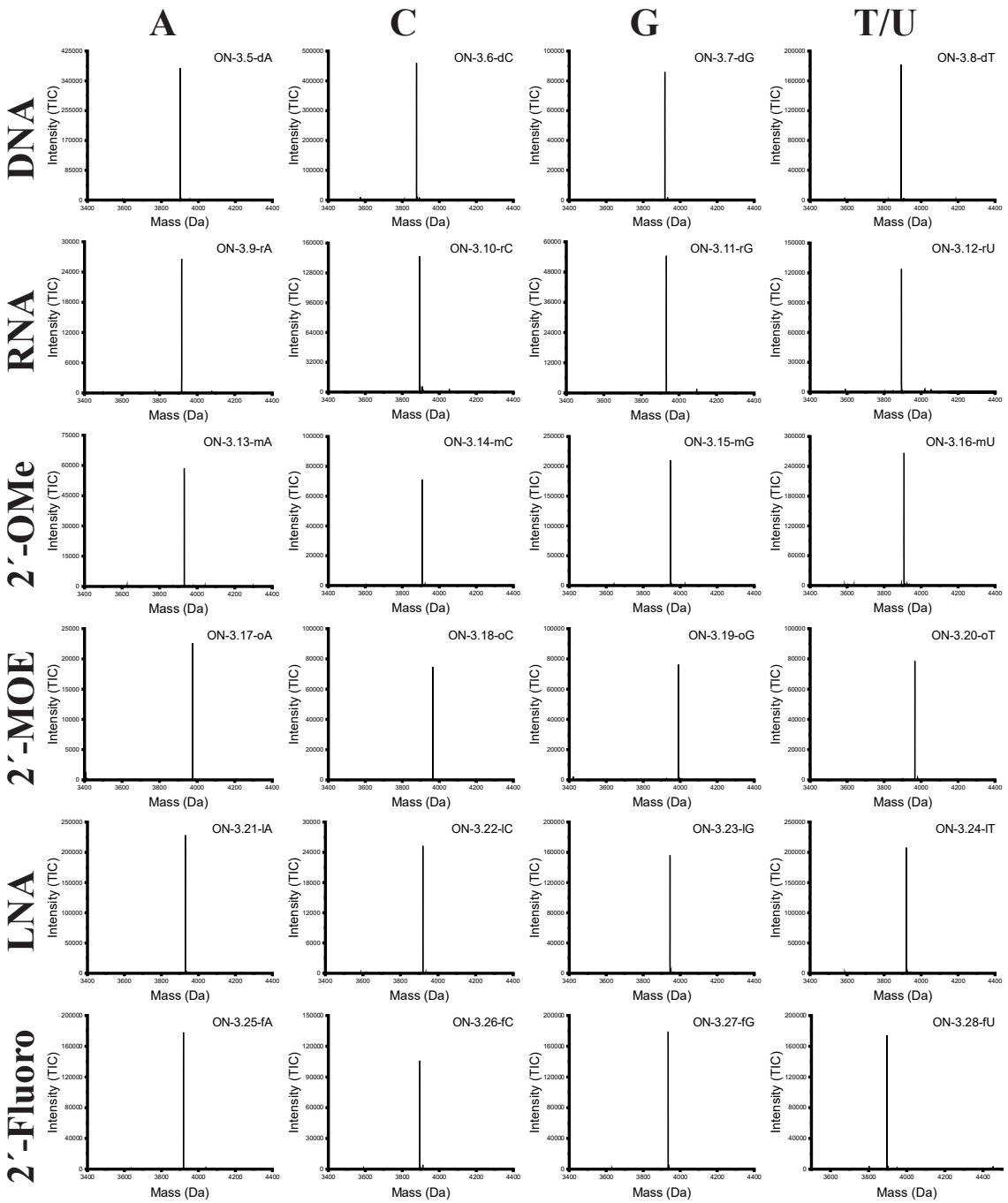
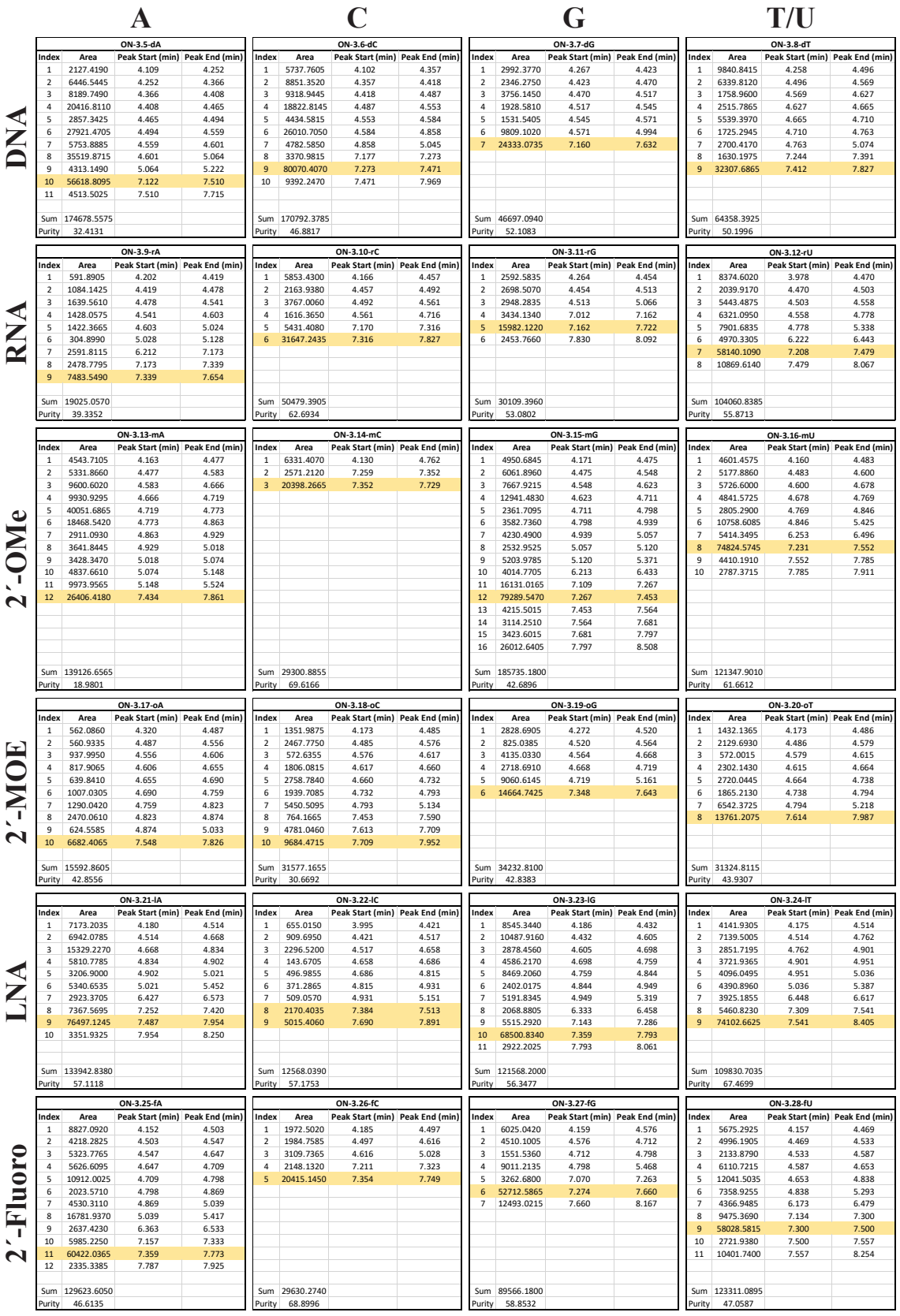


Figure 8.10: MS TIC traces for the peaks taken as desired product in Figure 8.8 for ON-3.5 to ON-3.28, calculated and observed masses can be found in Table 8.4. Columns of A, C, G and T/U refer to the terminal 5´ nucleobase before CuAAC. Rows of DNA, RNA, 2´OMe, 2´MOE, LNA, and 2´Fluoro refer to the modification of the terminal 5´ ribose before CuAAC.



ON-3.5-dA			
Index	Area	Peak Start (min)	Peak End (min)
1	2127.4190	4.109	4.252
2	6446.5445	4.252	4.366
3	8189.7490	4.366	4.408
4	20416.8110	4.408	4.465
5	2857.3425	4.465	4.494
6	27921.4705	4.494	4.559
7	5753.8885	4.559	4.601
8	35519.8715	4.601	5.064
9	4313.1490	5.064	5.222
10	56618.8095	7.122	7.510
11	4513.5025	7.510	7.715
Sum	174678.5575		
Purity	32.4131		

ON-3.6-dC			
Index	Area	Peak Start (min)	Peak End (min)
1	5737.7605	4.102	4.357
2	8851.3520	4.357	4.418
3	9318.9445	4.418	4.487
4	18822.8145	4.487	4.553
5	4434.5815	4.553	4.584
6	26010.7050	4.584	4.858
7	4782.5850	4.858	5.045
8	3370.9815	7.177	7.273
9	80070.4070	7.273	7.471
10	9392.2470	7.471	7.969
Sum	170792.3785		
Purity	46.8817		

ON-3.7-dG			
Index	Area	Peak Start (min)	Peak End (min)
1	2992.3770	4.267	4.423
2	2346.2750	4.423	4.470
3	3756.1450	4.470	4.517
4	1928.5810	4.517	4.545
5	1531.5405	4.545	4.571
6	9809.1020	4.571	4.994
7	24333.0735	7.160	7.632
Sum	46697.0940		
Purity	52.1083		

ON-3.8-dT			
Index	Area	Peak Start (min)	Peak End (min)
1	9840.8415	4.258	4.496
2	6339.8120	4.496	4.569
3	1758.9600	4.569	4.627
4	2515.7865	4.627	4.665
5	5539.3970	4.665	4.710
6	1725.2945	4.710	4.763
7	2700.4170	4.763	5.074
8	1630.1975	7.244	7.391
9	32307.6865	7.412	7.827
Sum	64358.3925		
Purity	50.1996		

ON-3.9-rA			
Index	Area	Peak Start (min)	Peak End (min)
1	591.8905	4.202	4.419
2	1084.1425	4.419	4.478
3	1639.5610	4.478	4.541
4	1428.0575	4.541	4.603
5	1422.3665	4.603	5.024
6	304.8990	5.028	5.128
7	2591.8115	6.212	7.173
8	2478.7795	7.173	7.339
9	7483.5490	7.339	7.654
Sum	19025.0570		
Purity	39.3352		

ON-3.10-rC			
Index	Area	Peak Start (min)	Peak End (min)
1	5853.4300	4.166	4.457
2	2163.9380	4.457	4.492
3	3767.0060	4.492	4.561
4	1616.3650	4.561	4.716
5	5431.4080	7.170	7.316
6	31647.2435	7.316	7.827
Sum	50479.3905		
Purity	62.6934		

ON-3.11-rG			
Index	Area	Peak Start (min)	Peak End (min)
1	2592.5835	4.264	4.454
2	2698.5070	4.454	4.513
3	2948.2835	4.513	5.066
4	3434.1340	7.012	7.162
5	15982.1220	7.162	7.722
6	2453.7660	7.830	8.092
Sum	30109.3960		
Purity	53.0802		

ON-3.12-rU			
Index	Area	Peak Start (min)	Peak End (min)
1	8374.6020	3.978	4.470
2	2039.9170	4.470	4.503
3	5443.4875	4.503	4.558
4	6321.0950	4.558	4.778
5	7901.6835	4.778	5.338
6	4970.3305	6.222	6.443
7	58140.1090	7.208	7.479
8	10869.6140	7.479	8.067
Sum	104060.8385		
Purity	55.8713		

ON-3.13-mA			
Index	Area	Peak Start (min)	Peak End (min)
1	4543.7105	4.163	4.477
2	5331.8660	4.477	4.583
3	9600.6020	4.583	4.666
4	9930.9295	4.666	4.719
5	40051.6865	4.719	4.773
6	18468.5420	4.773	4.863
7	2911.0930	4.863	4.929
8	3641.8445	4.929	5.018
9	3428.3470	5.018	5.074
10	4837.6610	5.074	5.148
11	9973.9565	5.148	5.524
12	26406.4180	7.434	7.861
Sum	139126.6565		
Purity	18.9801		

ON-3.14-mC			
Index	Area	Peak Start (min)	Peak End (min)
1	6331.4070	4.130	4.762
2	2571.2120	7.259	7.352
3	20398.2665	7.352	7.729
Sum	29300.8855		
Purity	69.6166		

ON-3.15-mG			
Index	Area	Peak Start (min)	Peak End (min)
1	4950.6845	4.171	4.475
2	6061.8960	4.475	4.548
3	7667.9215	4.548	4.623
4	12941.4830	4.623	4.711
5	2361.7095	4.711	4.798
6	3582.7360	4.798	4.939
7	4230.4900	4.939	5.057
8	2532.9525	5.057	5.120
9	5203.9785	5.120	5.371
10	4014.7705	6.213	6.433
11	16131.0165	7.109	7.267
12	79289.5470	7.267	7.453
13	4215.5015	7.453	7.564
14	3114.2510	7.564	7.681
15	3423.6015	7.681	7.797
16	26012.6405	7.797	8.508
Sum	185735.1800		
Purity	42.6896		

ON-3.16-mU			
Index	Area	Peak Start (min)	Peak End (min)
1	4601.4575	4.160	4.483
2	5177.8860	4.483	4.600
3	5726.6000	4.600	4.678
4	4841.5725	4.678	4.769
5	2805.2900	4.769	4.846
6	10758.6085	4.846	5.425
7	5414.3495	6.253	6.496
8	74824.5745	7.231	7.552
9	4410.1910	7.552	7.785
10	2787.3715	7.785	7.911
Sum	121347.9010		
Purity	61.6612		

ON-3.17-oA			
Index	Area	Peak Start (min)	Peak End (min)
1	562.0860	4.320	4.487
2	560.9335	4.487	4.556
3	937.9950	4.556	4.606
4	817.9065	4.606	4.655
5	639.8410	4.655	4.690
6	1007.0305	4.690	4.759
7	1290.0420	4.759	4.823
8	2470.0610	4.823	4.874
9	624.5585	4.874	5.033
10	6682.4065	7.548	7.826
Sum	15592.8605		
Purity	42.8556		

ON-3.18-oC			
Index	Area	Peak Start (min)	Peak End (min)
1	1351.9875	4.173	4.485
2	2467.7750	4.485	4.576
3	572.6355	4.576	4.617
4	1806.0815	4.617	4.660
5	2758.7840	4.660	4.732
6	1939.7085	4.732	4.793
7	5450.5095	4.793	5.134
8	764.1665	7.453	7.590
9	4781.0460	7.613	7.709
10	9684.4715	7.709	7.952
Sum	31577.1655		
Purity	30.6692		

ON-3.19-oG			
Index	Area	Peak Start (min)	Peak End (min)
1	2828.6905	4.272	4.520
2	825.0385	4.520	4.564
3	4135.0330	4.564	4.668
4	2718.6910	4.668	4.719
5	9060.6145	4.719	5.161
6	14664.7425	7.348	7.643
Sum	34232.8100		
Purity	42.8383		

ON-3.20-oT			
Index	Area	Peak Start (min)	Peak End (min)
1	1432.1365	4.173	4.486
2	2129.6930	4.486	4.579
3	572.0015	4.579	4.615
4	2302.1430	4.615	4.664
5	2720.0445	4.664	4.738
6	1865.2130	4.738	4.794
7	6542.3725	4.794	5.218
8	13761.2075	7.614	7.987
Sum	31324.8115		
Purity	43.9307		

ON-3.21-lA			
Index	Area	Peak Start (min)	Peak End (min)
1	7173.2035	4.180	4.514
2	6942.0785	4.514	4.668
3	15329.2270	4.668	4.834
4	5810.7785	4.834	4.902
5	3206.9000	4.902	5.021
6	5340.6535	5.021	5.452
7	2923.3705	6.427	6.573
8	7367.5695	7.252	7.420
9	76497.1245	7.487	7.954
10	3351.9325	7.954	8.250
Sum	133942.8380		
Purity	57.1118		

ON-3.22-lC			
Index	Area	Peak Start (min)	Peak End (min)
1	655.0150	3.995	4.421
2	909.6950	4.421	4.517
3	2296.5200	4.517	4.658
4	143.6705	4.658	4.686
5	496.9855	4.686	4.815
6	371.2865	4.815	4.931
7	509.0570	4.931	5.151
8	2170.4035	7.384	7.513
9	5015.4060	7.690	7.891
Sum	12568.0390		
Purity	57.1753		

ON-3.23-lG			
Index	Area	Peak Start (min)	Peak End (min)
1	8545.3440	4.186	4.432
2	10487.9160	4.432	4.605
3	2878.4560	4.605	4.698
4	4586.2170	4.698	4.759
5	8469.2060	4.759	4.844
6	2402.0175	4.844	4.949
7	5191.8345	4.949	5.319
8	2068.8805	6.333	6.458
9	5515.2920	7.143	7.286
10	68500.8340	7.359	7.793
11	2922.2025	7.793	8.061
Sum	121568.2000		
Purity	56.3477		

ON-3.24-lT			
Index	Area	Peak Start (min)	Peak End (min)
1	4141.9305	4.175	4.514
2	7139.5005	4.514	4.762
3	2851.7195	4.762	4.901
4	3721.9365	4.901	4.951
5	4096.0495	4.951	5.036
6	4390.8960	5.036	5.387
7	3925.1855	6.448	6.617
8	5460.8230	7.309	7.541
9	74102.6625	7.541	8.405
Sum	109830.7035		
Purity	67.4699		

ON-3.25-fA			
Index	Area	Peak Start (min)	Peak End (min)
1	8827.0920	4.152	4.503
2	4218.2825	4.503	4.547
3	5323.7765	4.547	4.647
4	5626.6095	4.647	4.709
5	10912.0025	4.709	4.798
6	2023.5710	4.798	4.869
7	4530.3110	4.869	5.039
8	16781.9370	5.039	5.417
9	2637.4230	6.363	6.533
10	5985.2250	7.157	7.333
11	60422.0365	7.359	7.773
12	2335.3385	7.787	7.925
Sum	129623.6050		
Purity	46.6135		

ON-3.26-fC			
Index	Area	Peak Start (min)	Peak End (min)
1	1972.5020	4.185	4.497
2	1984.7585	4.497	4.616
3	3109.7365	4.616	5.028
4	2148.1320	7.211	7.323
5	20415.1450	7.354	7.749
Sum	29630.2740		
Purity	68.8996		

ON-3.27-fG			
Index	Area	Peak Start (min)	Peak End (min)
1	6025.0420	4.159	4.576
2	4510.1005	4.576	4.712
3	1551.5360	4.712	4.798
4	9011.2135	4.798	5.468
5	3262.6800	7.070	7.263
6	52712.5865	7.274	7.660
7	12493.0215	7.660	8.167
Sum	89566.1800		
Purity	58.8532		

ON-3.28-fU			
Index	Area	Peak Start (min)	Peak End (min)
1	5675.2925	4.157	4.469
2	4996.1905	4.469	4.533
3	2133.8790	4.533	4.587
4	6110.7215	4.587	4.653
5	12041.5035	4.653	4.838
6	7358.9255	4.838	5.293
7	4366.9485	6.173	6.479
8	9475.3690	7.134	7.300
9	58028.5815	7.300	7.500
10	2721.9380	7.500	7.557
11	10401.7400	7.557	8.254
Sum	123311.0895		
Purity	47.0587		

Figure 8.11: Peak data used for determination of CuAAC conversion for ON-3.5 to ON-3.28. All peaks found in chromatograms from Figure 8.9 are listed as with elution time (minutes) total area by integration (mAu2). Peaks found to have the mass of the desired product as shown in Figure 8.10 are highlighted. Columns of A, C, G and T/U refer to the terminal 5´ nucleobase before CuAAC. Rows of DNA, RNA, 2´OMe, 2´MOE, LNA, and 2´Fluoro refer to the modification of the terminal 5´ ribose before CuAAC.

8.6.3 LC-MS Data for Oligonucleotides ON-3.29 to ON-3.33

Oligo	Sequence (5´-3´)	Calc. Mass	Found Mass
ON-3.29-d.1	N_3-TATCTGCT	2400.6	2400.5
ON-3.29-d.2	^{Me}C=TATCTGCT	2982.3	2982.6
ON-3.29-d.3	CTCA^{Me}C=TATCTGCT	23876.7	3876.1
ON-3.30-r.1	N_3-**U**ATCTGCT	2402.6	2402.6
ON-3.30-r.2	^{Me}C=**U**ATCTGCT	2984.2	2984.6
ON-3.30-r.3	CTCA^{Me}C=**U**ATCTGCT	3878.6	3878.4
ON-3.31-m.1	N_3-*U* ATCTGCT	2416.6	2416.7
ON-3.31-m.2	^{Me}C=*U* ATCTGCT	2998.3	2998.6
ON-3.31-m.3	CTCA^{Me}C=*U* ATCTGCT	3892.7	3878.4
ON-3.32-o.1	N_3-***T*** ATCTGCT	2474.7	2475.3
ON-3.32-o.2	^{Me}C=***T*** ATCTGCT	3056.3	3056.6
ON-3.32-o.3	CT^{Me}CAC=***T*** ATCTGCT	3951.8	3949.8
ON-3.33-l.1	N_3-**T**ATCTGCT	2428.6	2429.0
ON-3.33-l.2	^{Me}C=**T**ATCTGCT	3010.3	3010.4
ON-3.33-l.3	CTCA^{Me}C=**T**ATCTGCT	3905.7	3904.0
ON-3.34-f.1	N_3-~~U~~ATCTGCT	2406.6	2405.2
ON-3.34-f.2	^{Me}C=~~U~~ATCTGCT	2986.2	2986.2
ON-3.34-f.3	CTCA^{Me}C=~~U~~ATCTGCT	3880.6	3879.6
ON-3.35	CTCACTATCTGCT	3860.7	3860.9
ON-3.36	AGCAGATAGTGAG	4047.7	4048.1
ON-3.37	**AGCAGAUAGUGAG**	4227.6	4228.6

Table 8.5: Table containing sequences along with calculated and observed masses and CuAAC conversion data for ON-3.29 to ON-3.37. Chemistries are indicated as follows: DNA, **RNA**, *2´-OMe*, ***2´-MOE***, **LNA**, ~~2´-Fluoro~~. Capitalised letters indicate phosphodiester linkages, = indicates a 1,4-triazole linkage formed by CuAAC, and ^{Me}C indicates a C-5 methyl substituent on cytidine. Suffix of .1 .2 or .3 indicates one sequence monitored at different stages, .1 with a 5´-terminal azide, .2 after CuAAC addition of ^{Me}C and .3 the final sequence after strand extension.

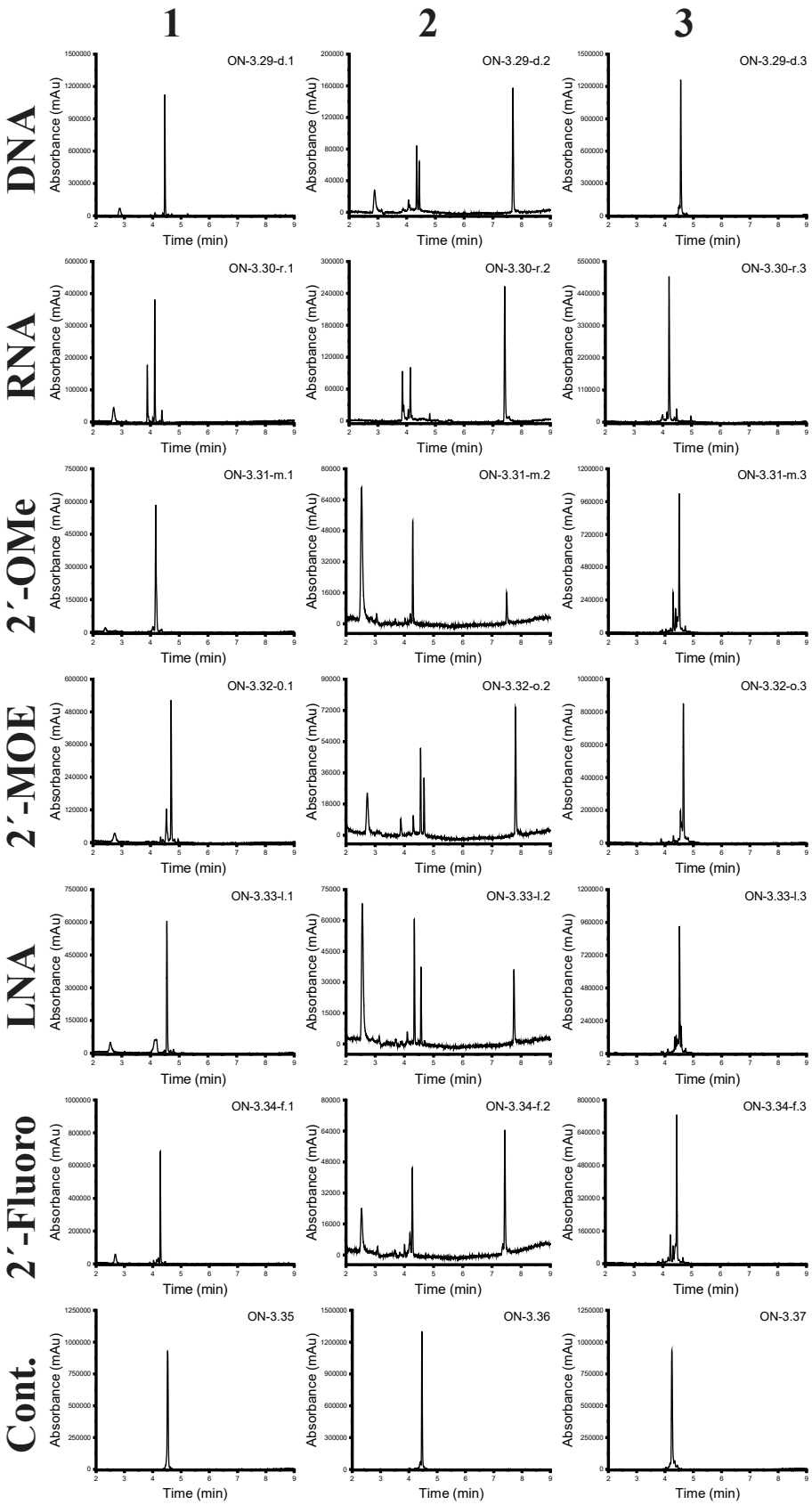


Figure 8.12: A_{260} LC traces corresponding to ON-3.29 to ON-3.37. Suffixes of .1, .2 and .3 indicate the intermediate 5´ azide, strand after CuAAC addition of ^{Me}C and the final sequence after extension respectively. Columns of 1, 2, and 3 correspond to these suffixes for ribose sugar indicated on the left of the chromatograms. Cont. indicates the control oligonucleotides of an all phosphate sequence (ON-3.35), RNA reverse compliment (ON-3.36) and DNA reverse compliment (ON-3.37).

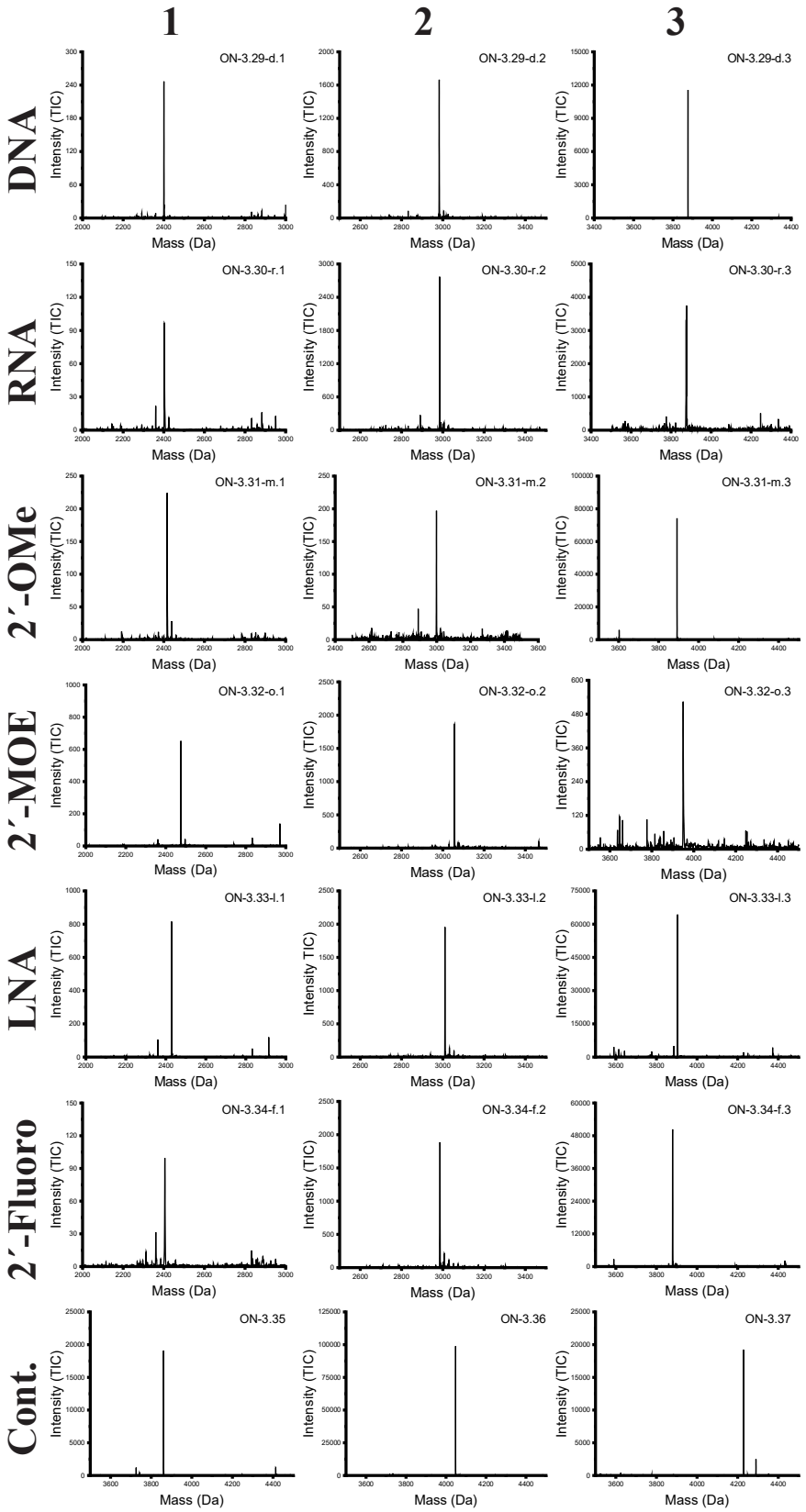
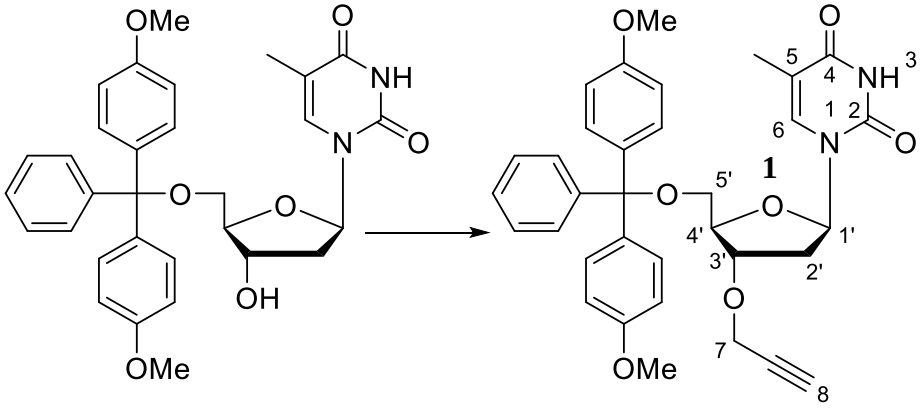


Figure 8.13: MS-TIC traces corresponding to ON-3.29 to ON-3.37. Suffixes of .1, .2 and .3 indicate the intermediate 5´ azide, strand after CuAAC addition of ^{Me}C and the final sequence after extension respectively. Columns of 1, 2, and 3 correspond to these suffixes for ribose sugar indicated on the left of the chromatograms. Cont. indicates the control oligonucleotides of an all-phosphate sequence (ON-3.35), RNA reverse compliment (ON-3.36) and DNA reverse compliment (ON-3.37).

8.6.4 Organic Chemistry for Compounds of Chapter 3
Propargylation of DMT-Thymidine (Compound 1)



5´-DMT-protected thymidine (3.58 g, 6.57 mmol, 1 eq) was coevaporated with dry THF three times then dissolved in more of the same (180 mL). The solution was cooled to 0°C and sodium hydride (60% dispersion in mineral oil, 657 mg, 16.43 mmol, 2.5 eq) was added slowly. The resulting mixture was stirred for 1 hour at RT then cooled back to 0°C before propargyl bromide (80% solution in toluene, 911 µL, 8.21 mmol, 1.25 eq) was added. The reaction was refluxed for 2 hours then quenched with water (110 mL). The THF was removed *in vacuo* and the aqueous layer extracted with DCM (4 x 40 mL). The combined organic layers were washed with brine (100 mL), dried over sodium sulfate and concentrated under reduced pressure. Silica gel column chromatography (0-3% methanol in dichloromethane with 0.1% TEA as an additive) gave compound **3**.

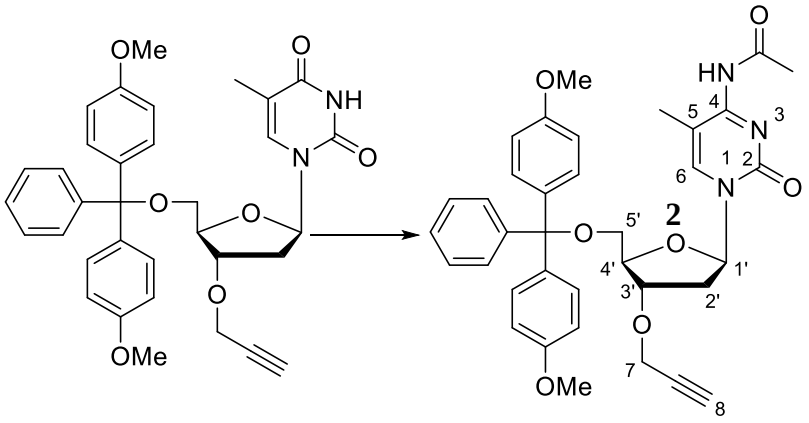
^{1}H NMR (400 MHz, $CDCl_3$) δ 9.05 (s, 1H, H-3), 7.48 (m, 3H H-Ar), 7.35 (m, 6H, H-Ar), 7.28 (m, 1H, H-Ar), 6.91 (m, 4H, H-Ar), 6.19 (t, *J* = 9.7 Hz, 1H, H-1´), 4.51 (p, *J* = 3.1 Hz, 1H, H-3´), 4.21 (t, *J* = 2.4 Hz, 2H, H-2´), 4.08 (q, *J* = 3.4 Hz, 1H, H-4´), 3.80 (s, 6H, DMT-OMe), 3.33 (m, 2H, H5´), 2.75 (t, *J* = 2.4 Hz, 1H, H-8), 2.40 (m, 1H, H-7), 2.31 (m, 1H, H-7), 1.52 (d, *J* = 1.1 Hz, 3H, Thymine CH_3)

^{13}C NMR (101 MHz, $CDCl_3$) δ 164.2 (C-Ar), 159.4 (C-Ar), 151.0 (C-Ar), 145.5 (C-Ar), 136.4 (C-Ar), 136.2 (C-6), 136.1 (C-Ar), 130.6 (C-Ar), 128.6(C-Ar), 128.5 (C-Ar), 127.6 (C-Ar), 113.8 (C-Ar), 110.9 (C-Ar)), 87.1 (C-Ar), 85.0 (C-1´), 83.9 (C-4´) 79.0 (C-3´), 75.7 (C-8), 64.1 (C-5´), 56.9 (H-7), 55.5 (DMT-OMe), 37.5 (C-2´), 11.9 (Thymidine CH_3)

HRMS: Found 583.2390 Da, Calculated 583.2439 Da

LR-LCMS: Found 605 Da, Calc. 605.23 (Na Adduct)

Conversion of Thymine to 5-Methyl-Cytidine (Compound 2)



A distillation apparatus was set up and 10 mL of phosphorus oxychloride was heated slowly, until reflux occurred around 75°C while under reduced pressure. Separately, Compound **3** (500 mg, 0.86 mmol, 1 eq) was coevaporated three times with dry pyridine before being dissolved in more of the same (5 mL). N-methylimidizole (890 µL, 11.2 mmol, 13 eq) was added and stirred at 0°C for 15 minutes. Distilled phosphorus oxychloride (304 µL, 3.227 mmol, 4 eq) was added at 0°C over the course of 30 minutes. The mixture was stirred for an additional 30 minutes on ice, then 30 minutes at room temperature. Concentrated aqueous ammonia (5 mL) was added at 0°C and the mixture was stirred for 16 hours at room temperature. Solvents were removed in vacuo, the residue taken up in dichloromethane, washed with water and saturated potassium chloride, dried over sodium sulfate and concentrated. The resultant solid was taken up in dimethylformadine (5 mL) and acetic anhydride (325 uL, 3.44 mmol, 4 eq) was added and stirred at room temperature for 20 hours. After concentration, the residue was dissolved in dichloromethane, washed with water and brine, dried on sodium sulfate. Purification on silica gel (0-3% methanol in dichloromethane with 0.1% TEA added) gave compound 4 (309 mg, 0.45 mmol, 52%).

^{1}H NMR (400 MHz, $CDCl_3$) δ 8.16 (d, *J* = 8 Hz, 2H, H-Ar), 7.62-7.24 (m, 13H, H-Ar), 6.92 (d, *J* = 12 Hz), 6.15 (t, *J* = 8.1 Hz, 1H, H-1´), 4.50 (p, *J* = 3.1 Hz, 1H, H-3´), 4.24 (t, *J* = 2.26 Hz, 2H, H-2´), 4.13 (q, *J* = 3.6 Hz, 1H, H-4´), 3.75 (s, 6H, DMT-OMe), 3.53 (t, *J* = 2.4 Hz, 1H, H-8), 3.30 (d, 4.0 Hz, 1H, H5´), 3.24 (dd, *J* = 10.7Hz, 3.2 Hz, 1H, H-5´), 2.49-2.36 (m, 2H, H-7), 1.68 (s, 3H, Cytosine CH_3)

^{13}C NMR (101 MHz, $CDCl_3$) δ 186.5 (Bz C=O), 158.7 (C-2), 145.1 (C-Ar), 135.8 (C-Ar), 135.6 (C-Ar), 133.1 (C-Ar), 130.2 (C-Ar), 129.8 (C-Ar), 128.8 (C-Ar), 128.5 (C-Ar), 128.2 (C-Ar), 127.4 (C-Ar), 120.9 (C-Ar), 113.8 (C-Ar), 110.5 (C-5), 86.6 (C-Ar), 85.6 (C-Ar), 83.6 (C-1´), 80.5 (C-4´), 78.3 (C-3´), 78.0 (C-8), 63.9 (C-5´), 56.6 (C-7), 55.6 (DMT-OMe), 37.3 (C-2´), 14.3 (Cytosine CH_3)

HR-MS: Found 624.2704 Da, Calculated 624.2709 Da

8.7 Data for Chapter 4

8.7.1 LC-MS Data for Oligonucleotides ON-4.1 to ON-4.8

Oligo	Sequence (5´-3´)	Calc. Mass (Da)	Found Mass (Da)	Tm R1 (°C)	Tm R2 (°C)	Tm R3 (°C)	Tm Avg. (°C)
ON-4.1	*ccucuuaccucaguuaca*	6098.8	6098.5	55.21	55.11	55.12	55.15
ON-4.2-dt	*ccucuuacc* t=*caguuaca*	6068.8	6067.5	49.70	49.70	49.59	49.66
ON-4.3-ot	*ccucuuacc* ***t****= caguuaca*	6142.9	6141.6	51.83	52.13	52.23	52.06
ON-4.4-mt	*ccucuuacct=caguuaca*	6096.8	6095.5	51.74	51.65	51.65	51.68
ON-4.5-lt	*ccucuuacc* **t**=*caguuaca*	6099.8	6097.8	49.90	49.92	50.01	49.94
ON-4.6-d	*ccucuuacc* t*caguuaca*	6082.8	6082.5	55.13	55.13	55.13	55.13
ON-4.7-o	*ccucuuacc* ***t*** *caguuaca*	6156.9	6156.6	64.73	65.04	65.14	64.97
ON-4.8-l	*ccucuuacc* **t***caguuaca*	6110.8	6110.5	59.87	59.87	59.87	59.87

Table 8.6: Table containing sequences along with calculated and observed masses and duplex melting temperature data for ON-4.1 to ON-4.8. Chemistries are indicated as follows: DNA, *2´-OMe*, ***2´-MOE***, **LNA**. Lower case letters indicate phosphodiester linkages and = indicates a 1,4-triazole linkage formed by CuAAC. Tm R1, Tm R2 and Tm R3 refer to the duplex melting temperature observed in three different temperature ramps along with the average as described in section 8.3.

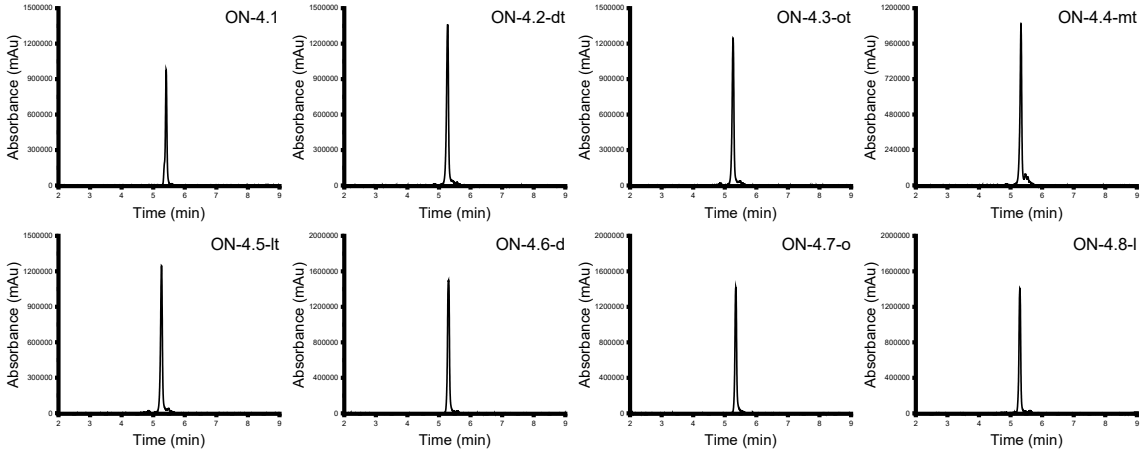


Figure 8.14: UV at A_{260} LC traces for HPLC purified olionucleotides ON-4.1 to ON-4.8.

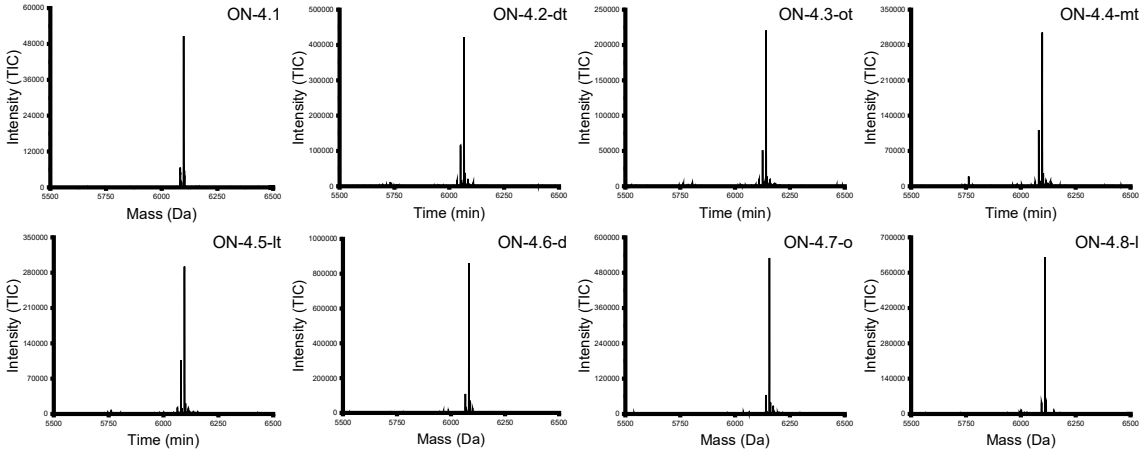


Figure 8.15: MS-TIC traces for the main peaks of ON-4.1 to ON-4.8 as shown in Figure 8.14. Calculated and observed masses can be seen in Table 8.6.

8.7.2 Data for Luciferase Intron-Skipping Assays in Chapter 4

Replicate 1 **Replicate 2**

A. Untreated

A.1.

		200 nM				100 nM				50 nM				25 nM			
		01	02	03	04	05	06	07	08	09	10	11	12				
ON-4.2-dt	A	15.008			7.966			2.793			1.267						
ON-4.3-ot	B	19.964			11.254			4.462			1.144						
ON-4.6-d	C	129.993			48.689			18.335			2.583						
ON-4.7-o	D	122.578			50.883			16.530			4.511						
ON-4.1	E	119.727			49.207			18.995			5.757						

A.2.

		200 nM				100 nM				50 nM				25 nM			
		01	02	03	04	05	06	07	08	09	10	11	12				
ON-4.2-dt	A	9.244			2.548			1.480			0.924						
ON-4.3-ot	B	18.486			4.421			1.519			0.868						
ON-4.6-d	C	58.474			17.396			4.378			1.205						
ON-4.7-o	D	48.555			39.711			6.103			1.221						
ON-4.1	E	52.153			20.762			4.364			1.123						

B. Untreated

B.1.

		200 nM				100 nM				50 nM				25 nM			
		01	02	03	04	05	06	07	08	09	10	11	12				
ON-4.4-mt	A	15.108			5.889			1.612			1.499						
ON-4.5-lt	B	28.376			9.824			3.492			1.634						
ON-4.8-l	C	49.586			30.322			8.861			4.081						
ON-4.1	D	52.280			3.465			1.995			1.114						

B.2.

		200 nM				100 nM				50 nM				25 nM			
		01	02	03	04	05	06	07	08	09	10	11	12				
ON-4.4-mt	A	13.219			1.645			0.733			0.809						
ON-4.5-lt	B	5.397			1.737			0.294			0.267						
ON-4.8-l	C	6.433			3.955			1.045			0.415						
ON-4.1	D	4.639			6.104			0.809			0.399						

A. OMe

A.1.

		200 nM				100 nM				50 nM				25 nM			
		01	02	03	04	05	06	07	08	09	10	11	12				
ON-4.2-dt	A	0.125			0.162			0.147			0.220						
ON-4.3-ot	B	0.167			0.229			0.235			0.199						
ON-4.6-d	C	1.086			0.989			0.965			0.449						
ON-4.7-o	D	1.024			1.034			0.870			0.784						
ON-4.1	E	1.000			1.000			1.000			1.000						

A.2.

		200 nM				100 nM				50 nM				25 nM			
		01	02	03	04	05	06	07	08	09	10	11	12				
ON-4.2-dt	A	0.177			0.123			0.339			0.823						
ON-4.3-ot	B	0.354			0.213			0.348			0.773						
ON-4.6-d	C	1.121			0.838			1.003			1.073						
ON-4.7-o	D	0.931			1.913			1.398			1.087						
ON-4.1	E	1.000			1.000			1.000			1.000						

B. OMe

B.1

		200 nM				100 nM				50 nM				25 nM			
		01	02	03	04	05	06	07	08	09	10	11	12				
ON-4.4-mt	A	0.289			1.699			0.808			1.346						
ON-4.5-lt	B	0.543			2.835			1.750			1.467						
ON-4.8-l	C	0.948			8.751			4.441			3.663						
ON-4.1	D	1.000			1.000			1.000			1.000						

B.2.

		200 nM				100 nM				50 nM				25 nM			
		01	02	03	04	05	06	07	08	09	10	11	12				
ON-4.4-mt	A	2.849			0.269			0.906			2.030						
ON-4.5-lt	B	1.163			0.285			0.363			0.670						
ON-4.8-l	C	1.387			0.648			1.292			1.041						
ON-4.1	D	1.000			1.000			1.000			1.000						

Figure 8.16: Data for oligonucleotides ON-4.1 to ON-4.8 transfected using Lipofectamine 3000. Rows of the table are arranged in Groups A and B with replicate plates displayed side by side. Plates were done in duplicate with replicates arranged into columns 1-2. Rows of each plate were treated with the same oligonucleotide as noted to the left of the values. Columns of each plate were treated with four different concentrations of a given oligonucleotide. Concentrations were dosed three times each. Values displayed are the total luminescence of a well divided by the total protein amount in that well relative to either untreated wells (indicated as row **A. Untreated** and **B. Untreated**) or to untreated wells and the activity over untreated of the 2´OMe-phosphorothioate control ON-4.1 at the same dose (indicated as row **A. OMe** and **B. OMe**). Each value is the average of the three replicate dosings of an oligonucleotide.

Replicate 1 **Replicate 2**

A. Untreated

A.1.		20 uM			10 uM			5 uM			2.5 uM		
		1	2	3	4	5	6	7	8	9	10	11	12
ON-4.2-dt	A	2.504			2.240			1.681			1.502		
ON-4.3-ot	B	4.807			3.163			2.033			1.601		
ON-4.6-d	C	8.099			4.763			4.023			3.052		
ON-4.7-o	D	12.744			9.479			5.889			2.383		
ON-4.1	E	11.733			8.286			7.428			3.372		

A.2		20 uM			10 uM			5 uM			2.5 uM		
		01	02	03	04	05	06	07	08	09	10	11	12
ON-4.2-dt	A	2.300			2.375			0.931			0.844		
ON-4.3-ot	B	2.950			2.179			1.492			0.752		
ON-4.6-d	C	9.987			7.186			4.005			2.230		
ON-4.7-o	D	12.822			11.416			6.081			2.659		
ON-4.1	E	15.593			12.091			5.777			3.000		

B. Untreated

B.1.		20 uM			10 uM			5 uM			2.5 uM		
		01	02	03	04	05	06	07	08	09	10	11	12
ON-4.4-mt	A	5.131			3.523			2.971			2.851		
ON-4.5-lt	B	5.559			5.244			3.258			1.738		
ON-4.8-l	C	11.098			8.569			6.795			3.739		
ON-4.1	D	10.105			8.017			6.842			4.131		

B.2.		20 uM			10 uM			5 uM			2.5 uM		
		01	02	03	04	05	06	07	08	09	10	11	12
ON-4.4-mt	A	6.441			4.605			2.788			2.628		
ON-4.5-lt	B	6.973			5.782			3.149			2.057		
ON-4.8-l	C	12.607			9.549			5.960			3.734		
ON-4.1	D	15.283			10.893			7.303			3.971		

A. OMe

A.1.		20 uM			10 uM			5 uM			2.5 uM		
		1	2	3	4	5	6	7	8	9	10	11	12
ON-4.2-dt	A	0.213			0.270			0.226			0.445		
ON-4.3-ot	B	0.410			0.382			0.274			0.475		
ON-4.6-d	C	0.690			0.575			0.542			0.905		
ON-4.7-o	D	1.086			1.144			0.793			0.707		
ON-4.1	E	1.000			1.000			1.000			1.000		

A.2.		20 uM			10 uM			5 uM			2.5 uM		
		01	02	03	04	05	06	07	08	09	10	11	12
ON-4.2-dt	A	0.148			0.196			0.161			0.281		
ON-4.3-ot	B	0.189			0.180			0.258			0.251		
ON-4.6-d	C	0.640			0.594			0.693			0.743		
ON-4.7-o	D	0.822			0.944			1.053			0.886		
ON-4.1	E	1.000			1.000			1.000			1.000		

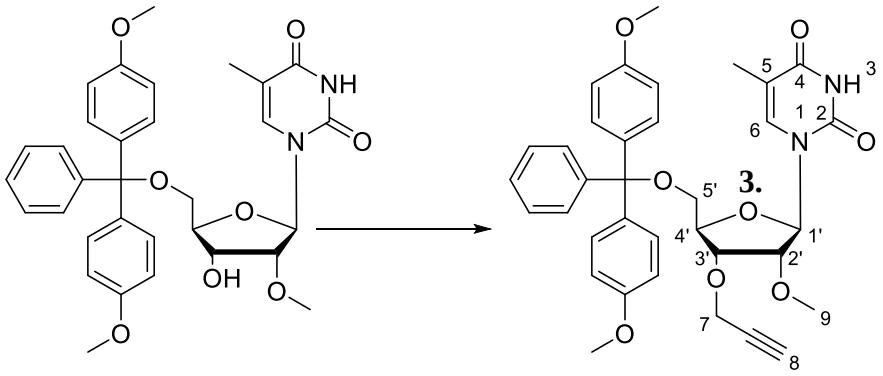
B. OMe

B.1.		20 uM			10 uM			5 uM			2.5 uM		
		01	02	03	04	05	06	07	08	09	10	11	12
ON-4.4-mt	A	0.508			0.439			0.434			0.690		
ON-4.5-lt	B	0.550			0.654			0.476			0.421		
ON-4.8-l	C	1.098			1.069			0.993			0.905		
ON-4.1	D	1.000			1.000			1.000			1.000		

B.2.		20 uM			10 uM			5 uM			2.5 uM		
		01	02	03	04	05	06	07	08	09	10	11	12
ON-4.4-mt	A	0.421			0.423			0.382			0.662		
ON-4.5-lt	B	0.456			0.531			0.431			0.518		
ON-4.8-l	C	0.825			0.877			0.816			0.940		
ON-4.1	D	1.000			1.000			1.000			1.000		

Figure 8.17: Data for oligonucleotides ON-4.1 to ON-4.8 dosed gymnotically. Rows of the table are arranged in Groups A and B with replicate plates displayed side by side. Plates were done in duplicate with replicates arranged into columns 1-2. Rows of each plate were treated with the same oligonucleotide as noted to the left of the values. Columns of each plate were treated with four different concentrations of a given oligonucleotide. Concentrations were dosed three times each. Values displayed are the total luminescence of a well divided by the total protein amount in that well relative to either untreated wells (indicated as row **A. Untreated** and **B. Untreated**) to untreated wells and the activity over untreated of the 2´OMe-phosphorothioate control ON-4.1 at the same dose (indicated as row **A. OMe** and **B. OMe**). Each value is the average of the three replicate dosings of an oligonucleotide.

8.7.3 Organic Chemistry Data for Compounds of Chapter 4
Propargylation of 5´-DMT-2´-OMe Thymidine (Compound 3)



5´-DMT-2´-OMe-T (500 mg, 0.87 mmol, 1 eq) dissolved in THF (25 mL). The solution was cooled to 0 °C, and sodium hydride (87 mg, 2.17 mmol, 60% suspension in mineral oil) was added slowly. The resulting mixture was stirred for 1 hour at room temperature and then cooled to 0 °C. Propargyl bromide (170 µL, 1.52 mmol, 80% solution in toluene, 1.75 eq) was added and the reaction was refluxed overnight. Water (30 mL) was added to quench the reaction, THF was evaporated in vacuo and the aqueous layer was extracted with DCM (7 x 40 mL). The combined organic layers were washed with brine (100 mL), dried over sodium sulfate and concentrated in vacuo. Column chromatography in 0-3% methanol in dichloromethane gave the compound as a white foam (349 mg, 66%).

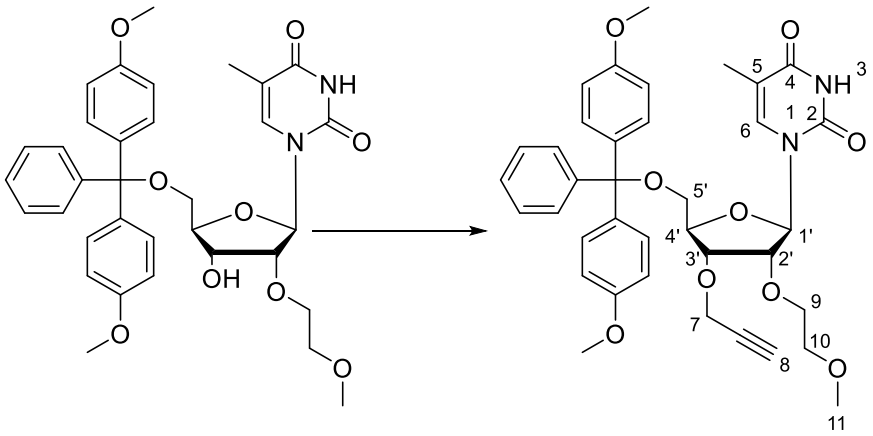
^{1}H NMR (400 MHz, $CDCl_3$) δ 7.64 (s, 1H, H-N), 7.36 (d, *J* = 8 Hz, 2H, H-Ar), 7.28-7.13 (m, 8H, H-Ar), 6.81-6.74 (m, 4H, H-Ar), 5.92 (d, *J* = 4 Hz, 1H, H-1´), 4.48 (t, *J* = 4 Hz, 1H, H-2´), 4.20 (dd, *J* = *8* Hz, 2 Hz, 2H, H-5´), 4.18-4.12 (m, 3H, H-3´, H-5´), 3.96 (q, *J* = 2 Hz, 1H, H-4´), 3.72 (s, 6H, DMT-OMe), 3.53 (s, 3H, H-9), 3.49 (dd, *J* = 8 Hz, 2 Hz, 1H, H-7), 3.34 (dd, *J* = 8 Hz, 2 Hz, 1H, H-7), 2.37 (t, *J* = 2 Hz, 1H, H8), 1.29 (s, 3H, Thymidine CH_3)

^{13}C NMR (101 MHz, CDCl3) δ 163.61 (C-Ar), 158.75 (C-Ar), 150.06 (C-Ar), 144.31 (C-Ar), 135.39 (C-Ar), 135.30 (C-Ar), 135.25 (C-Ar), 130.16 (C-Ar), 128.20 (C-Ar), 128.03 (C-Ar), 127.18 (C-Ar), 113.30 (C-Ar), 110.95 (C-Ar), 87.71 (C-1´), 82.24 (C5´), 81.20 (C4´), 73.99 (H-2´), 61.52 (H-7), 58.53 (C-9), 57.54 (C-3´), 55.27 DMT-OMe), 46.24 (H-8), 11.62. (Thymidine CH_3)

HR-MS: Found 613.2464, Calculated 613.2544

LR-LCMS : Found 635, Calculated 635.24 (Na adduct)

Propargylation of 5´-DMT-2´-MOE Thymidine (Compound 4)



5´-DMT-2´-OMe-T (500 mg, 0.81 mmol, 1 eq) dissolved in THF (25 mL). The solution was cooled to 0 °C, and sodium hydride (80 mg, 2.01 mmol, 60% suspension in mineral oil) was added slowly. The resulting mixture was stirred for 1 hour at room temperature and then cooled to 0 °C. Propargyl bromide (156 µL, 1.41 mmol, 80% solution in toluene) was added and the reaction was refluxed overnight. Water (30 mL) was added to quench the reaction, THF was evaporated in vacuo and the aqueous layer was extracted with DCM (7 x 40 mL). The combined organic layers were washed with brine (100 mL), dried over sodium sulphate and concentrated in vacuo. Column chromatography in 0-3% MeOH in DCM gave the product as a white foam (402 mg 74%).

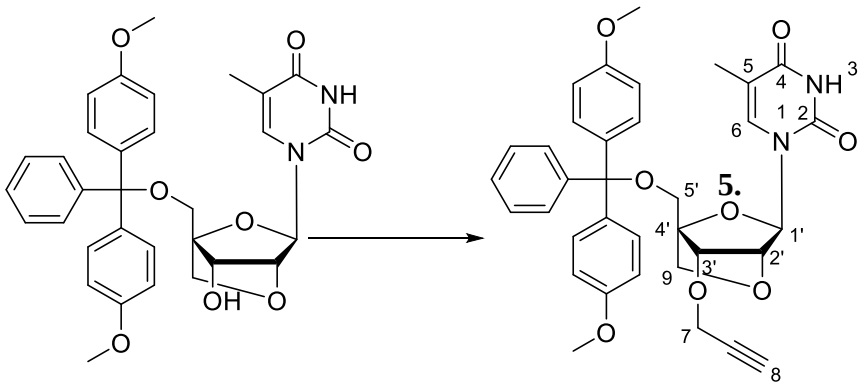
^{1}H NMR (400 MHz, $CDCl_3$) δ 7.64 (s, 1H, H-N), 7.37 (d, *J* = 8 Hz, 2H, H-Ar), 7.27-7.13 (m, 8H, H-Ar), 6.77 (d, *J* = 8 Hz, 4H, H-Ar), 5.91 (d, *J* = 4 Hz, 2H, H-1´), 4.49 (t, *J* = 4 Hz, 1H, H2´), 4.34-4.13 (m, 4H, H-3´ H-4´ H-5´), 3.96-3.76 (m, 2H, H-10), 3.72 (s, 6H, DMT-OMe), 3.56-3.49 (m, 2H, H-9), 3.48-3.49 (qd, *J* = 40 Hz, 8 Hz, 2 Hz, 2H, H-7), 2.35 (t, *J* = 2 Hz, 1H, H-8), 1.29 (s, 3H, Thymidine CH_3)

^{13}C NMR (101 MHz, CDCl3) δ 163.52 (C-Ar), 158.74 (C-Ar), 150.04 (C-Ar), 144.36 (C-Ar), 135.52 (C-Ar), 135.28 (C-Ar), 130.16 (C-Ar), 128.19 (C-Ar), 128.02 (C-Ar), 127.12 (C-Ar), 113.31 (C-Ar), 110.82 (C-Ar), 88.12 (C-1´), 81.49 (C-5´, C-4´), 81.40 (C-5´, C-4´), 79.23, 75.43, 73.99 (C-2´), 72.33 (C-9), 69.98 (C-10), 61.64 (C-7), 59.08 (C-11), 57.33 (C-3´), 55.27 (DMT-OMe), 46.24 (H-8), 11.56 (Thymidine CH_3)

HR-MS : Measured 679.2666, Calculated 679.2626 (Na Adduct)

LR-LCMS : Found 679, Calculated 679.26 (Na adduct)

Propargylation of 5´-DMT-LNA Thymidine (Compound 5)



5´-DMT-LNA-T (2 g, 3.36 mmol, 1 eq) dissolved in THF (50 mL). The solution was cooled to 0 °C, and sodium hydride (220 mg, 2.23 mmol, 60% suspension in mineral oil) was added slowly. The resulting mixture was stirred for 1 hour at room temperature and then cooled to 0 °C. Propargyl bromide (713 µL, 1.56 mmol, 80% solution in toluene) was added and the reaction was refluxed overnight. Water (30 mL) was added to quench the reaction, THF was evaporated in vacuo and the aqueous layer was extracted with DCM (7 x 40 mL). The combined organic layers were washed with brine (100 mL), dried over sodium sulfate and concentrated in vacuo. Column chromatography in 0-3% MeOH in DCM gave the product as an off white foam (261 mg 49%).

^{1}H NMR (400 MHz, $CDCl_3$) δ 7.69 (s, 1H, N-H), 7.39 (d, *J* = 8 Hz, 2H, H-Ar), 7.33-7.12 (m, 8H, H-Ar), 6.78 (dd, *J* = 8 Hz, 2Hz, 4H, H-Ar), 5.59 (s, 1H, H-1´), 4.58 (s, 1H, H-2´), 4.29 (s, 1H, H-4´), 4.24-4.03 (qd, *J* = 40 Hz, 16 Hz, 2.6 Hz, 2H, H-5´), 3.77 (d, *J* = 8 Hz, 1H, H-9), 3.73 (s, 6H, DMT-OMe), 3.68 (d, *J* = 8 Hz, 1H, H-9), 3.46 (d, *J* = 12 Hz, 1H, H-7), 3.31 (d, *J* = 12 Hz, 1H, H-7), 2.38 (t, *J* = 2 Hz, 1H, H-8), 1.60 (s, 3H, Thymidine CH_3)

^{13}C NMR (101 MHz, CDCl3) δ 163.70 (C-Ar), 158.75 (C-Ar), 149.72 (C-Ar), 144.38 (C-Ar), 135.26 (C-Ar), 134.51 (C-Ar), 130.10 (C-Ar), 130.06 (C-Ar), 128.05 (C-Ar), 127.15, (C-Ar) 113.36 (C-Ar), 113.33 (C-Ar), 110.53 (C-Ar), 87.36 (H-1´), 78.56 (C-2´), 75.89 (C-3´), 75.48 (C-4´), 72.22 (C-9), 58.01 (C-7), 57.58 (C-5´), 55.26 (DMT-OMe), 46.18 (C-8), 12.64 (Thymidine CH_3)

HR-MS : Measured 611.2401 , Calculated 611.2388

LR-LCMS : Found 633, Calculated 633.22 (Na adduct)

8.8 Data for Chapter 5

8.8.1 LC-MS Data for Oligonucleotides ON-5.1 to ON-5.16

Oligo	Sequence (5´-3´)	Calc. Mass (Da)	Found Mass (Da)	Tm R1 (°C)	Tm R2 (°C)	Tm R3 (°C)	Tm Avg. (°C)
ON-5.1-dd	*ccuc* t*uaccucag* t*uaca*	6066.8	6066.5	52.85	52.94	52.85	52.88
ON-5.2-ddd	*ccuc* t*uacc* t*cag* t*uaca*	6050.9	6050.5	52.08	52.48	52.56	52.37
ON-5.3-oo	*ccuc* ***t*** *uaccucag* ***t*** *uaca*	6215.0	6214.7	65.95	65.86	65.85	65.89
ON-5.4-oo	*ccuc* ***t*** *uacc* ***t*** *cag* ***t*** *uaca*	6273.0	6272.7	66.97	66.77	66.88	66.87
ON-5.5-ll	*ccuc* **t***uaccucag* **t***uaca*	6122.8	6122.6	64.29	64.43	64.49	64.40
ON-5.6-lll	*ccuc* **t***uacc* **t***cag* **t***uaca*	6134.8	6134.5	>75	>75	>75	>75
ON-5.7-1(lp)	*ccucuuacc* **t*** *caguuaca*	6169.3	6166.7	66.50	66.21	66.50	66.40
ON-5.8-2(lp)	*ccuc* **t*** *uaccucag* **t*** *uaca*	6239.4	6234.8	68.91	69.61	69.42	69.31
ON-5.9-3(lp)	*ccuc* **t*** *uacc* **t*** *cag* **t*** *uaca*	6309.6	6302.9	72.23	71.73	71.68	71.88
ON-5.10-1(ll)	*ccucuuac* **ct***caguuaca*	6107.8	6108.6	70.98	70.73	70.95	70.89
ON-5.11-2(ll)	*ccu* **ct***uaccucag* **tt***aca*	6132.8	6132.7	>75	>75	>75	>75
ON-5.12-4(ll)	*c* **cu***c* **tt***ac* **cu***cag* **tt***aca*	6166.8	6170.5	>75	>75	>75	>75
ON-5.13-1(lpl)	*ccucuuac* **^{Me}c*** **t***caguuaca*	6177.8	6180.5	68.59	69.19	69.00	68.93
ON-5.14-2(lpl)	*ccu* **^{Me}c*** **t***uaccucag* **t*** **t***aca*	6260.8	6259.6	74.68	74.47	74.68	74.61
ON-5.15-4(lpl)	*c* **^{Me}c*** **u***c* **t*** **t***ac* **^{Me}c*** **u***cag* **t*** **t***aca*	6418.8	6417.8	>75	>75	>75	>75
ON-5.16-1(l.l)	*ccucuuac* **^{Me}c^** **t***caguuaca*	6161.8	6161.0	59.31	59.52	59.20	59.34

Table 8.7: Table containing sequences along with calculated and observed masses and duplex melting temperature data for ON-5.1 to ON-5.16. Chemistries are indicated as follows: DNA, *2´-OMe*, ***2´-MOE***, **LNA**. Lower case letters indicate phosphodiester linkages, ^{Me}C indicates the 5-methyl-modified cytosine nucleobase, * indicates a methoxypropyl-phosphorothioate charge-neutral linkage and ^ indicates a methoxypropyl-phosphodiester charge-neutral linkage. Tm R1, Tm R2 and Tm R3 refer to the duplex melting temperature observed in three different temperature ramps along with the average as described in section 8.3.

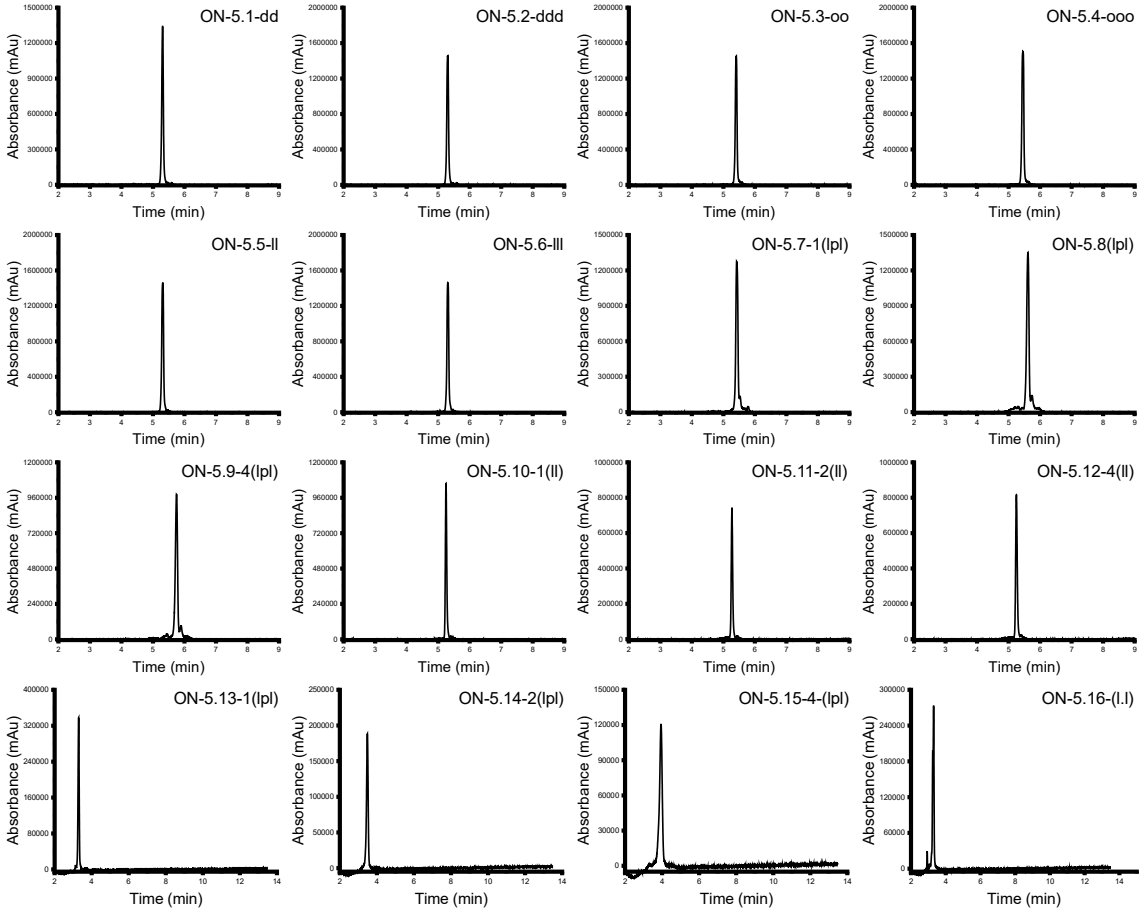


Figure 8.18: UV at A_{260} LC traces for HPLC purified olionucleotides ON-5.1 to ON-5.16.

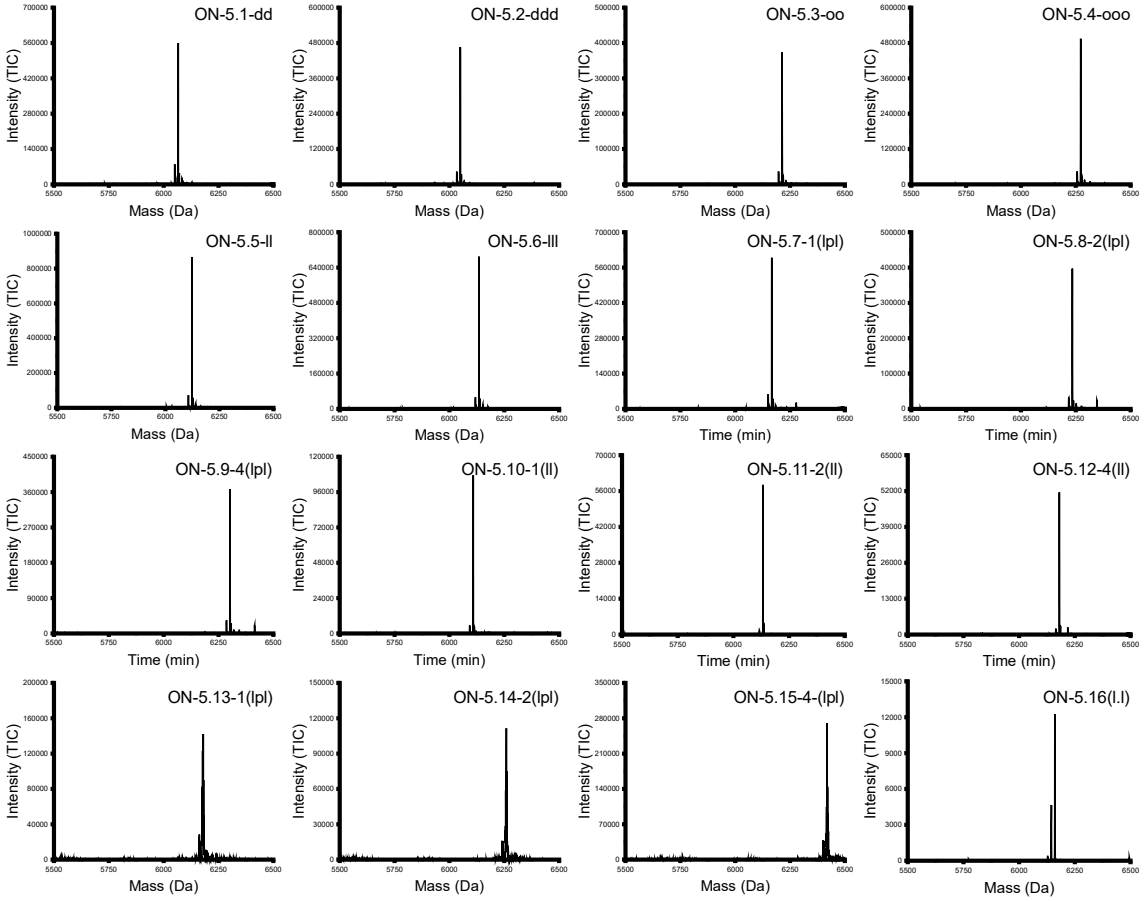


Figure 8.19: MS-TIC traces for the main peaks of ON-5.1 to ON-5.16 as shown in Figure 8.18. Calculated and observed masses can be seen in Table 8.7.

8.8.2 Data for Luciferase Intron-Skipping Assays in Chapter 5

A. Untreated

A.1.

		200 nM			100 nM			50 nM			25 nM		
		01	02	03	04	05	06	07	08	09	10	11	12
ON-4.6-d	A	57.113			25.140			6.873			2.558		
ON-5.1-dd	B	78.906			45.392			10.594			2.738		
ON-4.7-o	C	85.605			107.600			39.898			5.168		
ON-5.3-oo	D	106.004			65.309			12.616			3.228		
ON-5.4-ooo	E	70.144			44.438			10.310			2.524		
ON-4.1	F	68.120			48.725			12.192			2.713		

A.2.

		200 nM			100 nM			50 nM			25 nM		
		01	02	03	04	05	06	07	08	09	10	11	12
ON-4.6-d	A	42.510			16.748			4.991			1.512		
ON-5.1-dd	B	33.918			10.173			2.476			1.121		
ON-4.7-o	C	54.446			29.661			7.584			1.649		
ON-5.3-oo	D	50.144			19.762			3.194			1.344		
ON-5.4-ooo	E	44.396			14.399			2.135			1.114		
ON-4.1	F	41.206			16.960			2.802			1.171		

A.3.

		200 nM			100 nM			50 nM			25 nM		
		01	02	03	04	05	06	07	08	09	10	11	12
ON-4.6-d	A	44.962			19.520			5.302			1.808		
ON-5.1-dd	B	47.836			20.823			5.170			1.677		
ON-4.7-o	C	81.354			55.084			14.379			2.994		
ON-5.3-oo	D	77.781			36.657			5.124			1.864		
ON-5.4-ooo	E	70.607			22.310			3.882			1.452		
ON-4.1	F	67.956			24.642			4.903			1.660		

B. Untreated

B.1.

		200 nM			100 nM			50 nM			25 nM		
		01	02	03	04	05	06	07	08	09	10	11	12
ON-5.2-ddd	A	4.517			2.776			1.554			1.334		
ON-4.1	B	10.714			3.846			2.128			1.575		

B.2.

		200 nM			100 nM			50 nM			25 nM		
		01	02	03	04	05	06	07	08	09	10	11	12
ON-5.2-ddd	A	5.356			3.148			1.474			1.332		
ON-4.1	B	14.752			7.855			2.189			1.568		

B.3.

		200 nM			100 nM			50 nM			25 nM		
		01	02	03	04	05	06	07	08	09	10	11	12
ON-5.2-ddd	A	7.172			3.163			1.257			1.212		
ON-4.1	B	10.288			6.356			2.337			1.497		

C. Untreated

C.1.

		200 nM			100 nM			50 nM			25 nM		
		01	02	03	04	05	06	07	08	09	10	11	12
ON-5.7-1(lp)	A	18.769			11.673			6.481			2.813		
ON-5.8-2(lp)	B	34.382			18.450			7.204			3.084		
ON-5.9-2(lp)	C	26.103			22.907			7.405			2.311		
ON-4.8-I	D	57.260			58.648			14.784			6.774		
ON-5.5-II	E	121.592			70.753			39.764			11.099		
ON-5.6-III	F	112.984			65.179			30.358			9.371		
ON-4.1	G	20.986			31.744			17.063			4.985		

C.2.

		200 nM			100 nM			50 nM			25 nM		
		01	02	03	04	05	06	07	08	09	10	11	12
ON-5.7-1(lp)	A	33.524			10.406			3.209			0.672		
ON-5.8-2(lp)	B	25.230			8.304			2.606			0.900		
ON-5.9-2(lp)	C	17.366			7.667			3.182			1.157		
ON-4.8-I	D	171.105			21.006			6.297			1.357		
ON-5.5-II	E	113.375			53.215			18.748			3.628		
ON-5.6-III	F	101.171			74.426			52.225			6.369		
ON-4.1	G	36.564			27.442			4.856			2.503		

C.3.

		200 nM			100 nM			50 nM			25 nM		
		01	02	03	04	05	06	07	08	09	10	11	12
ON-5.7-1(lp)	A	5.816			9.183			2.168			0.607		
ON-5.8-2(lp)	B	12.782			8.415			1.413			0.282		
ON-5.9-2(lp)	C	30.185			11.606			2.216			0.791		
ON-4.8-I	D	80.785			18.465			4.062			1.092		
ON-5.5-II	E	153.250			47.377			9.048			2.395		
ON-5.6-III	F	66.220			91.332			30.771			5.384		
ON-4.1	G	30.361			10.651			2.613			1.400		

A. OMe

A.1.

		200 nM			100 nM			50 nM			25 nM		
		01	02	03	04	05	06	07	08	09	10	11	12
ON-4.6-d	A	0.838			0.516			0.564			0.943		
ON-5.1-dd	B	1.158			0.932			0.869			1.009		
ON-4.7-o	C	1.257			2.208			3.273			1.905		
ON-5.3-oo	D	1.556			1.340			1.035			1.190		
ON-5.4-ooo	E	1.030			0.912			0.846			0.930		
ON-4.1	F	1.000			1.000			1.000			1.000		

A.2.

		200 nM			100 nM			50 nM			25 nM		
		01	02	03	04	05	06	07	08	09	10	11	12
ON-4.6-d	A	1.032			0.987			1.781			1.291		
ON-5.1-dd	B	0.823			0.600			0.884			0.957		
ON-4.7-o	C	1.321			1.749			2.707			1.408		
ON-5.3-oo	D	1.217			1.165			1.140			1.148		
ON-5.4-ooo	E	1.077			0.849			0.762			0.952		
ON-4.1	F	1.000			1.000			1.000			1.000		

A.3.

		200 nM			100 nM			50 nM			25 nM		
		01	02	03	04	05	06	07	08	09	10	11	12
ON-4.6-d	A	0.662			0.792			1.081			1.089		
ON-5.1-dd	B	0.704			0.845			1.055			1.010		
ON-4.7-o	C	1.197			2.235			2.933			1.804		
ON-5.3-oo	D	1.145			1.488			1.045			1.123		
ON-5.4-ooo	E	1.039			0.905			0.792			0.875		
ON-4.1	F	1.000			1.000			1.000			1.000		

B. OMe

B.1.

		200 nM			100 nM			50 nM			25 nM		
		01	02	03	04	05	06	07	08	09	10	11	12
ON-5.2-ddd	A	0.422			0.722			0.730			0.847		
ON-4.1	B	1.000			1.000			1.000			1.000		

B.2.

		200 nM			100 nM			50 nM			25 nM		
		01	02	03	04	05	06	07	08	09	10	11	12
ON-5.2-ddd	A	0.363			0.401			0.673			0.850		
ON-4.1	B	1.000			1.000			1.000			1.000		

B.3.

		200 nM			100 nM			50 nM			25 nM		
		01	02	03	04	05	06	07	08	09	10	11	12
ON-5.2-ddd	A	0.697			0.498			0.538			0.810		
ON-4.1	B	1.000			1.000			1.000			1.000		

C. OMe

C.1.

		200 nM			100 nM			50 nM			25 nM		
		01	02	03	04	05	06	07	08	09	10	11	12
ON-5.7-1(lp)	A	0.894			0.368			0.380			0.564		
ON-5.8-2(lp)	B	1.638			0.581			0.422			0.619		
ON-5.9-2(lp)	C	1.244			0.722			0.434			0.464		
ON-4.8-I	D	2.729			1.848			0.866			1.359		
ON-5.5-II	E	5.794			2.229			2.330			2.227		
ON-5.6-III	F	5.384			2.053			1.779			1.880		
ON-4.1	G	1.000			1.000			1.000			1.000		

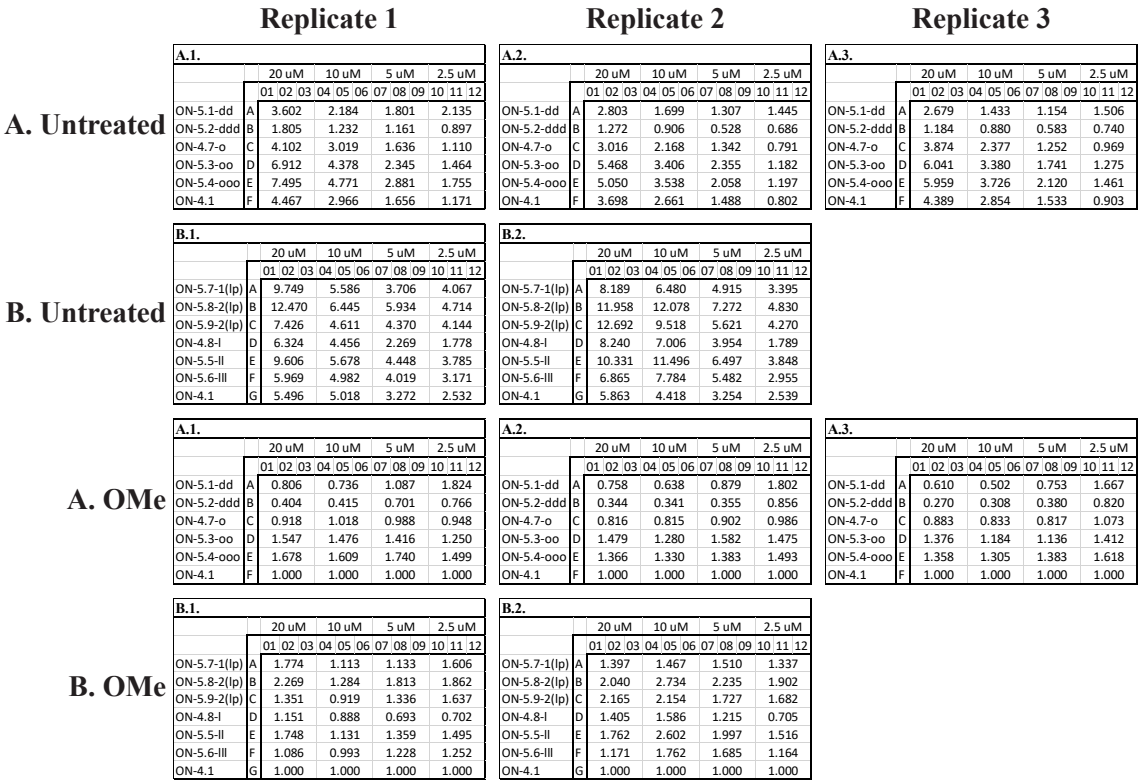
C.2.

		200 nM			100 nM			50 nM			25 nM		
		01	02	03	04	05	06	07	08	09	10	11	12
ON-5.7-1(lp)	A	0.917			0.379			0.661			0.269		
ON-5.8-2(lp)	B	0.690			0.303			0.537			0.360		
ON-5.9-2(lp)	C	0.475			0.279			0.655			0.462		
ON-4.8-I	D	4.680			0.765			1.297			0.542		
ON-5.5-II	E	3.101			1.939			3.861			1.450		
ON-5.6-III	F	2.767			2.712			10.756			2.545		
ON-4.1	G	1.000			1.000			1.000			1.000		

C.3.

		200 nM			100 nM			50 nM			25 nM		
		01	02	03	04	05	06	07	08	09	10	11	12
ON-5.7-1(lp)	A	0.192			0.862			0.830			0.433		
ON-5.8-2(lp)	B	0.421			0.790			0.541			0.201		
ON-5.9-2(lp)	C	0.994			1.090			0.848			0.565		
ON-4.8-I	D	2.661			1.734			1.554			0.780		
ON-5.5-II	E	5.048			4.448			3.463			1.711		
ON-5.6-III	F	2.181			8.575			11.777			3.845		
ON-4.1	G	1.000			1.000			1.000			1.000		

Figure 8.20: Data for oligonucleotides ON-4.1 and ON-5.1 to ON-5.9 transfected with Lipofectamine3000. Rows of the table are arranged in Groups A B and C with replicate plates displayed side by side. Plates were done in triplicate with replicates arranged into columns 1-3. Rows of each plate were treated with the same oligonucleotide as noted to the left of the values. Columns of each plate were treated with four different concentrations of a given oligonucleotide. Concentrations were dosed three times each. Values displayed are the total luminescence of a well divided by the total protein amount in that well relative to either untreated wells (indicated as row **A. Untreated, B. Untreated** and **C. Untreated**) or to untreated wells and the activity over untreated of the 2´OMe-phosphorothioate control ON-4.1 at the same dose (indicated as row **A. OMe, B. OMe** and **C. OMe**). Each value is the average of the three replicate dosings of an oligonucleotide.



A. Untreated

A.1.

		20 uM		10 uM		5 uM		2.5 uM	
		01	02	03	04	05	06	07	08	09	10	11	12
ON-5.1-dd	A	3.602		2.184		1.801		2.135	
ON-5.2-ddd	B	1.805		1.232		1.161		0.897	
ON-4.7-o	C	4.102		3.019		1.636		1.110	
ON-5.3-oo	D	6.912		4.378		2.345		1.464	
ON-5.4-ooo	E	7.495		4.771		2.881		1.755	
ON-4.1	F	4.467		2.966		1.656		1.171	

A.2.

		20 uM		10 uM		5 uM		2.5 uM	
		01	02	03	04	05	06	07	08	09	10	11	12
ON-5.1-dd	A	2.803		1.699		1.307		1.445	
ON-5.2-ddd	B	1.272		0.906		0.528		0.686	
ON-4.7-o	C	3.016		2.168		1.342		0.791	
ON-5.3-oo	D	5.468		3.406		2.355		1.182	
ON-5.4-ooo	E	5.050		3.538		2.058		1.197	
ON-4.1	F	3.698		2.661		1.488		0.802	

A.3.

		20 uM		10 uM		5 uM		2.5 uM	
		01	02	03	04	05	06	07	08	09	10	11	12
ON-5.1-dd	A	2.679		1.433		1.154		1.506	
ON-5.2-ddd	B	1.184		0.880		0.583		0.740	
ON-4.7-o	C	3.874		2.377		1.252		0.969	
ON-5.3-oo	D	6.041		3.380		1.741		1.275	
ON-5.4-ooo	E	5.959		3.726		2.120		1.461	
ON-4.1	F	4.389		2.854		1.533		0.903	

B. Untreated

B.1.

		20 uM		10 uM		5 uM		2.5 uM	
		01	02	03	04	05	06	07	08	09	10	11	12
ON-5.7-1(lp)	A	9.749		5.586		3.706		4.067	
ON-5.8-2(lp)	B	12.470		6.445		5.934		4.714	
ON-5.9-2(lp)	C	7.426		4.611		4.370		4.144	
ON-4.8-I	D	6.324		4.456		2.269		1.778	
ON-5.5-II	E	9.606		5.678		4.448		3.785	
ON-5.6-III	F	5.969		4.982		4.019		3.171	
ON-4.1	G	5.496		5.018		3.272		2.532	

B.2.

		20 uM		10 uM		5 uM		2.5 uM	
		01	02	03	04	05	06	07	08	09	10	11	12
ON-5.7-1(lp)	A	8.189		6.480		4.915		3.395	
ON-5.8-2(lp)	B	11.958		12.078		7.272		4.830	
ON-5.9-2(lp)	C	12.692		9.518		5.621		4.270	
ON-4.8-I	D	8.240		7.006		3.954		1.789	
ON-5.5-II	E	10.331		11.496		6.497		3.848	
ON-5.6-III	F	6.865		7.784		5.482		2.955	
ON-4.1	G	5.863		4.418		3.254		2.539	

A. OMe

A.1.

		20 uM		10 uM		5 uM		2.5 uM	
		01	02	03	04	05	06	07	08	09	10	11	12
ON-5.1-dd	A	0.806		0.736		1.087		1.824	
ON-5.2-ddd	B	0.404		0.415		0.701		0.766	
ON-4.7-o	C	0.918		1.018		0.988		0.948	
ON-5.3-oo	D	1.547		1.476		1.416		1.250	
ON-5.4-ooo	E	1.678		1.609		1.740		1.499	
ON-4.1	F	1.000		1.000		1.000		1.000	

A.2.

		20 uM		10 uM		5 uM		2.5 uM	
		01	02	03	04	05	06	07	08	09	10	11	12
ON-5.1-dd	A	0.758		0.638		0.879		1.802	
ON-5.2-ddd	B	0.344		0.341		0.355		0.856	
ON-4.7-o	C	0.816		0.815		0.902		0.986	
ON-5.3-oo	D	1.479		1.280		1.582		1.475	
ON-5.4-ooo	E	1.366		1.330		1.383		1.493	
ON-4.1	F	1.000		1.000		1.000		1.000	

A.3.

		20 uM		10 uM		5 uM		2.5 uM	
		01	02	03	04	05	06	07	08	09	10	11	12
ON-5.1-dd	A	0.610		0.502		0.753		1.667	
ON-5.2-ddd	B	0.270		0.308		0.380		0.820	
ON-4.7-o	C	0.883		0.833		0.817		1.073	
ON-5.3-oo	D	1.376		1.184		1.136		1.412	
ON-5.4-ooo	E	1.358		1.305		1.383		1.618	
ON-4.1	F	1.000		1.000		1.000		1.000	

B. OMe

B.1.

		20 uM		10 uM		5 uM		2.5 uM	
		01	02	03	04	05	06	07	08	09	10	11	12
ON-5.7-1(lp)	A	1.774		1.113		1.133		1.606	
ON-5.8-2(lp)	B	2.269		1.284		1.813		1.862	
ON-5.9-2(lp)	C	1.351		0.919		1.336		1.637	
ON-4.8-I	D	1.151		0.888		0.693		0.702	
ON-5.5-II	E	1.748		1.131		1.359		1.495	
ON-5.6-III	F	1.086		0.993		1.228		1.252	
ON-4.1	G	1.000		1.000		1.000		1.000	

B.2.

		20 uM		10 uM		5 uM		2.5 uM	
		01	02	03	04	05	06	07	08	09	10	11	12
ON-5.7-1(lp)	A	1.397		1.467		1.510		1.337	
ON-5.8-2(lp)	B	2.040		2.734		2.235		1.902	
ON-5.9-2(lp)	C	2.165		2.154		1.727		1.682	
ON-4.8-I	D	1.405		1.586		1.215		0.705	
ON-5.5-II	E	1.762		2.602		1.997		1.516	
ON-5.6-III	F	1.171		1.762		1.685		1.164	
ON-4.1	G	1.000		1.000		1.000		1.000	

Figure 8.21: Data for oligonucleotides ON-4.1 and ON-5.1 to ON-5.9 dosed gymnotically. Rows of the table are arranged in Groups A B and C with replicate plates displayed side by side. Plates were done in duplicate or triplicate with replicates arranged into columns 1-3. Rows of each plate were treated with the same oligonucleotide as noted to the left of the values. Columns of each plate were treated with four different concentrations of a given oligonucleotide. Concentrations were dosed three times each. Values displayed are the total luminescence of a well divided by the total protein amount in that well relative to either untreated wells (indicated as row **A. Untreated** and **B. Untreated**) or to untreated wells and the activity over untreated of the 2´OMe-phosphorothioate control ON-4.1 at the same dose (indicated as row **A. OMe,** and **B. OMe**). Each value is the average of the three replicate dosings of an oligonucleotide.

Replicate 1 **Replicate 2** **Replicate 3**

A. Untreated

A.1.		200 nM		100 nM		50 nM		25 nM	
		01	02	03	04	05	06	07	08	09	10	11	12
ON-5.13-1(lpl)	A	24.741		7.145		3.245		2.122	
ON-5.14-2(lpl)	B	66.876		24.437		8.115		6.040	
ON-5.15-4(lpl)	C	81.158		93.073		7.122		4.626	
ON-5.10-1(II)	D	148.751		86.613		38.623		9.654	
ON-5.11-2(II)	E	152.234		82.857		28.533		6.250	
ON-5.12-4(II)	F	161.033		103.920		25.377		5.569	
ON-4.1	G	72.947		44.660		10.614		2.509	

A.2.		200 nM		100 nM		50 nM		25 nM	
		01	02	03	04	05	06	07	08	09	10	11	12
ON-5.13-1(lpl)	A	21.064		7.259		2.452		1.381	
ON-5.14-2(lpl)	B	55.322		20.795		6.017		1.788	
ON-5.15-4(lpl)	C	70.279		63.857		4.901		3.421	
ON-5.10-1(II)	D	141.292		59.228		28.194		6.899	
ON-5.11-2(II)	E	114.996		61.263		16.413		3.536	
ON-5.12-4(II)	F	111.714		57.035		17.160		4.582	
ON-4.1	G	71.474		21.459		4.146		1.311	

A.3		200 nM		100 nM		50 nM		25 nM	
		01	02	03	04	05	06	07	08	09	10	11	12
ON-5.13-1(lpl)	A	9.314		4.194		1.642		0.958	
ON-5.14-2(lpl)	B	16.392		6.346		2.469		1.247	
ON-5.15-4(lpl)	C	8.567		5.830		2.434		1.188	
ON-5.10-1(II)	D	4.905		2.373		1.108		0.732	
ON-5.11-2(II)	E	27.164		11.197		4.393		1.296	
ON-5.12-4(II)	F	19.763		9.007		2.278		1.435	
ON-4.1	G	7.577		4.751		1.623		1.010	

B. Untreated

B.1.		200 nM		100 nM		50 nM		25 nM	
		01	02	03	04	05	06	07	08	09	10	11	12
ON-5.16-1(I.I)	A	8.320		4.384		1.336		0.520	
ON-4.1	B	55.350		26.697		6.002		1.200	

B.2.		200 nM		100 nM		50 nM		25 nM	
		01	02	03	04	05	06	07	08	09	10	11	12
ON-5.16-1(I.I)	A	6.177		3.249		1.009		0.536	
ON-4.1	B	43.460		16.704		6.250		1.460	

B.3.		200 nM		100 nM		50 nM		25 nM	
		01	02	03	04	05	06	07	08	09	10	11	12
ON-5.16-1(I.I)	A	4.817		3.666		0.729		0.176	
ON-4.1	B	31.315		23.540		5.282		0.974	

A. OMe

A.1.		200 nM		100 nM		50 nM		25 nM	
		01	02	03	04	05	06	07	08	09	10	11	12
ON-5.13-1(lpl)	A	0.339		0.160		0.306		0.846	
ON-5.14-2(lpl)	B	0.917		0.547		0.765		2.408	
ON-5.15-4(lpl)	C	1.113		2.084		0.671		1.844	
ON-5.10-1(II)	D	2.039		1.939		3.639		3.848	
ON-5.11-2(II)	E	2.087		1.855		2.688		2.491	
ON-5.12-4(II)	F	2.208		2.327		2.391		2.220	
ON-4.1	G	1.000		1.000		1.000		1.000	

A.2.		200 nM		100 nM		50 nM		25 nM	
		01	02	03	04	05	06	07	08	09	10	11	12
ON-5.13-1(lpl)	A	0.295		0.338		0.591		1.054	
ON-5.14-2(lpl)	B	0.774		0.969		1.451		1.364	
ON-5.15-4(lpl)	C	0.983		2.976		1.182		2.609	
ON-5.10-1(II)	D	1.977		2.760		6.800		5.262	
ON-5.11-2(II)	E	1.609		2.855		3.959		2.697	
ON-5.12-4(II)	F	1.563		2.658		4.139		3.495	
ON-4.1	G	1.000		1.000		1.000		1.000	

A.3		200 nM		100 nM		50 nM		25 nM	
		01	02	03	04	05	06	07	08	09	10	11	12
ON-5.13-1(lpl)	A	1.229		0.883		1.012		0.949	
ON-5.14-2(lpl)	B	2.163		1.336		1.521		1.235	
ON-5.15-4(lpl)	C	1.131		1.227		1.500		1.177	
ON-5.10-1(II)	D	0.647		0.499		0.682		0.725	
ON-5.11-2(II)	E	3.585		2.357		2.707		1.283	
ON-5.12-4(II)	F	2.608		1.896		1.404		1.421	
ON-4.1	G	1.000		1.000		1.000		1.000	

B. OMe

B.1.		200 nM		100 nM		50 nM		25 nM	
		01	02	03	04	05	06	07	08	09	10	11	12
ON-5.16-1(I.I)	A	0.150		0.164		0.223		0.434	
ON-4.1	B	1.000		1.000		1.000		1.000	

B.2.		200 nM		100 nM		50 nM		25 nM	
		01	02	03	04	05	06	07	08	09	10	11	12
ON-5.16-1(I.I)	A	0.142		0.194		0.161		0.367	
ON-4.1	B	1.000		1.000		1.000		1.000	

B.3.		200 nM		100 nM		50 nM		25 nM	
		01	02	03	04	05	06	07	08	09	10	11	12
ON-5.16-1(I.I)	A	0.154		0.156		0.138		0.181	
ON-4.1	B	1.000		1.000		1.000		1.000	

Figure 8.22: Data for oligonucleotides ON-4.1 and ON-5.10 to ON-5.16 transfected with Lipofectamine3000. Rows of the table are arranged in Groups A and B with replicate plates displayed side by side. Plates were done in triplicate with replicates arranged into columns 1-3. Rows of each plate were treated with the same oligonucleotide as noted to the left of the values. Columns of each plate were treated with four different concentrations of a given oligonucleotide. Concentrations were dosed three times each. Values displayed are the total luminescence of a well divided by the total protein amount in that well relative to either untreated wells (indicated as row **A. Untreated** and **B. Untreated**) or to untreated wells and the activity over untreated of the 2´OMe-phosphorothioate control ON-4.1 at the same dose (indicated as row **A. OMe** and **B. OMe**). Each value is the average of the three replicate dosings of an oligonucleotide.

Replicate 1 **Replicate 2** **Replicate 3**

A. Untreated

A.1.		20 uM		10 uM		5 uM		2.5 uM	
		01	02	03	04	05	06	07	08	09	10	11	12
ON-5.13-1(lpl)	A	2.220		1.623		1.126		1.739	
ON-5.14-2(lpl)	B	7.821		5.349		2.725		1.771	
ON-5.15-4(lpl)	C	4.396		2.454		1.492		0.915	
ON-5.10-1(II)	D	0.322		0.230		0.226		0.453	
ON-5.11-2(II)	E	2.241		1.327		0.992		0.716	
ON-5.12-4(II)	F	2.819		1.783		0.986		0.721	
ON-4.1	G	2.746		1.764		1.041		0.819	

A.2.		20 uM		10 uM		5 uM		2.5 uM	
		01	02	03	04	05	06	07	08	09	10	11	12
ON-5.13-1(lpl)	A	5.708		1.641		0.921		0.971	
ON-5.14-2(lpl)	B	8.572		6.085		3.158		1.811	
ON-5.15-4(lpl)	C	2.205		4.024		1.905		0.888	
ON-5.10-1(II)	D	0.384		0.328		0.341		0.423	
ON-5.11-2(II)	E	2.673		1.907		1.221		0.815	
ON-5.12-4(II)	F	3.281		2.326		1.424		0.840	
ON-4.1	G	3.544		2.186		1.501		0.852	

A.3.		20 uM		10 uM		5 uM		2.5 uM	
		01	02	03	04	05	06	07	08	09	10	11	12
ON-5.13-1(lpl)	A	2.169		1.171		0.712		0.696	
ON-5.14-2(lpl)	B	4.389		2.878		1.676		0.616	
ON-5.15-4(lpl)	C	2.841		1.146		1.011		0.126	
ON-5.10-1(II)	D	0.248		0.178		0.141		0.174	
ON-5.11-2(II)	E	1.737		0.929		0.546		0.341	
ON-5.12-4(II)	F	2.133		0.837		0.544		0.353	
ON-4.1	G	2.125		0.939		0.613		0.389	

A. OMe

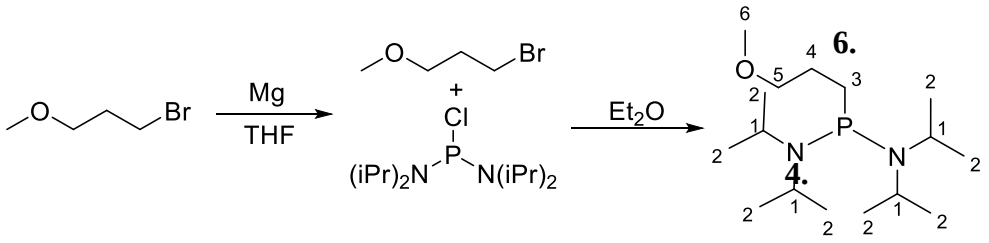
A.1.		20 uM		10 uM		5 uM		2.5 uM	
		01	02	03	04	05	06	07	08	09	10	11	12
ON-5.13-1(lpl)	A	0.808		0.920		1.082		2.124	
ON-5.14-2(lpl)	B	2.848		3.032		2.619		2.163	
ON-5.15-4(lpl)	C	1.601		1.391		1.434		1.118	
ON-5.10-1(II)	D	0.117		0.130		0.217		0.554	
ON-5.11-2(II)	E	0.816		0.752		0.953		0.874	
ON-5.12-4(II)	F	1.026		1.011		0.948		0.880	
ON-4.1	G	1.000		1.000		1.000		1.000	

A.2.		20 uM		10 uM		5 uM		2.5 uM	
		01	02	03	04	05	06	07	08	09	10	11	12
ON-5.13-1(lpl)	A	1.611		0.751		0.613		1.139	
ON-5.14-2(lpl)	B	2.419		2.784		2.103		2.125	
ON-5.15-4(lpl)	C	0.622		1.841		1.269		1.042	
ON-5.10-1(II)	D	0.108		0.150		0.227		0.496	
ON-5.11-2(II)	E	0.754		0.873		0.813		0.956	
ON-5.12-4(II)	F	0.926		1.064		0.948		0.985	
ON-4.1	G	1.000		1.000		1.000		1.000	

A.3.		20 uM		10 uM		5 uM		2.5 uM	
		01	02	03	04	05	06	07	08	09	10	11	12
ON-5.13-1(lpl)	A	1.021		1.247		1.160		1.789	
ON-5.14-2(lpl)	B	2.066		3.065		2.733		1.584	
ON-5.15-4(lpl)	C	1.337		1.221		1.649		0.323	
ON-5.10-1(II)	D	0.117		0.190		0.229		0.447	
ON-5.11-2(II)	E	0.818		0.990		0.890		0.876	
ON-5.12-4(II)	F	1.004		0.892		0.887		0.908	
ON-4.1	G	1.000		1.000		1.000		1.000	

Figure 8.23: Data for oligonucleotides ON-4.1 and ON-5.10 to ON-5.15 dosed gymnotically. Rows of the table are arranged into Group A with replicate plates displayed side by side. Plates were done in triplicate with replicates arranged into columns 1-3. Rows of each plate were treated with the same oligonucleotide as noted to the left of the values. Columns of each plate were treated with four different concentrations of a given oligonucleotide. Concentrations were dosed three times each. Values displayed are the total luminescence of a well divided by the total protein amount in that well relative to either untreated wells (indicated as row **A. Untreated**) or to untreated wells and the activity over untreated of the 2´OMe-phosphorothioate control ON-4.1 at the same dose (indicated as row **A. OMe**). Each value is the average of the three replicate dosings of an oligonucleotide.

8.8.3 Organic Chemistry for Compounds of Chapter 5
Synthesis of Methoxypropyl Phosphitylation Reagent (Compound 6)



Magnesium metal (360 mg) was suspended in dry THF (25 mL) in a dry round bottom flask with iodine crystals and purged with argon. 1-bromo-3-methoxypropane (840 µL) was added in portions via syringe over 20 minutes, and allowed to stir until returning to room temperature. In a separate round bottom flask, bis(diisopropylamino)chlorophosphine (1 g) was suspended in dry diethyl ether (20 mL) and cooled to 0°C while stirring under argon. The grignard was transferred in via cannula and the reaction was allowed to come to RT and stirred for 1 hour. The mixture was filtered through celite, the solids washed with diethyl ether and the solvent removed in vacuo. The filtrates were suspended in dry ACN (10 mL), and transferred to a sep funnel. The ACN was extracted with hexanes (20 mL) which were then washed with ACN (2 x 10 mL). The hexane layer was passed through a cotton plug and concentrated under vacuum before being passed briefly on a hi-vac line. The workup and evaporations were all performed under atmospheric conditions, and the product was isolated as a colorless oil with a density of 0.807 g/mL (65% yield). The oil was placed under argon and stored at -20°C until use.

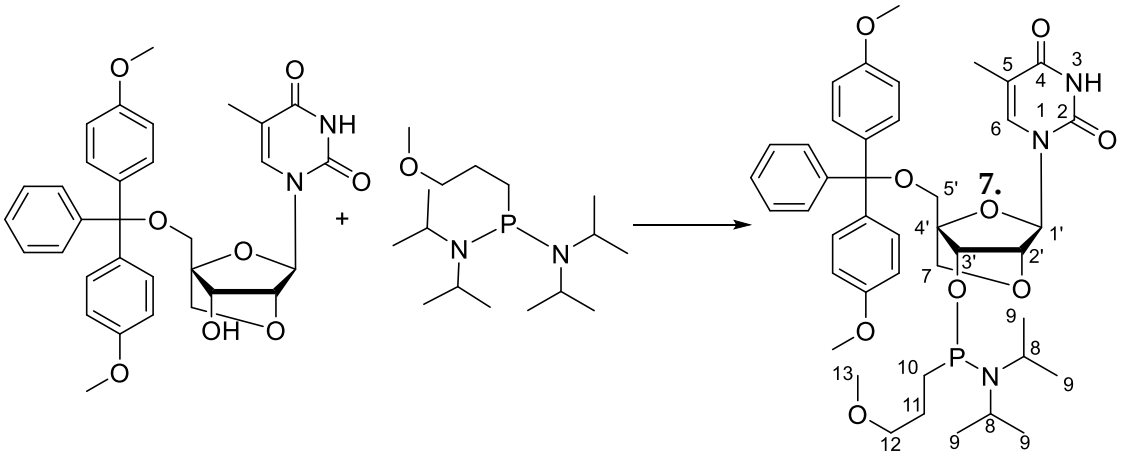
^{1}H NMR (400 MHz, $CDCl_3$) δ 3.54-3.07 (m, 9H, H-3, H-4, H-5, H-6), 1.79-1.46 (m, 4H, H1), 1.07 (dd, *J* = 40 Hz, 12 Hz, 24H, H-2)

^{31}P NMR (162 MHz, $CDCl_3$) δ 47.38

HR-MS : Measured 305.2718 , Calculated 305.2716

LR-LCMS : Found 305.28, Calculated 305

MOP Phosphitylation of LNA Thymidine



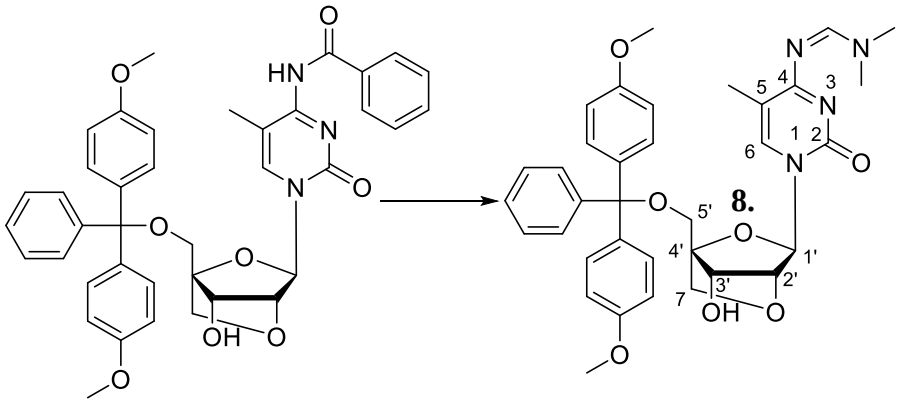
5´-DMT-LNA-T (500 mg) was dissolved in DCM (10 mL) and 1-methyl imidazole (70 µL) and tetrazole (154 µL) were added while stirring under argon. To this solution, bis(diisopropylamino)-3-methoxypropylphosphine (629 µL) was added from its storage vessel (see experiment 5.4) and stirred overnight at room temperature. The solution was removed in vacuo, the residue was diluted with ethyl acetate (10 mL) and transferred to a separatory funnel under inert atmosphere. Under atmospheric conditions, the ethyl acetate was worked up with 1:1 saturated sodium bicarbonate:water. 1:1 brine:water, and brine. The organic layer was dried over magnesium sulfate and removed in the argon rotavap again. The residue was purified on a silica gel column (0-3% MeOH in DCM w/ 1% TEA added) and characterized on 31P NMR (65% yield).

^{1}H NMR (400 MHz, $CDCl_3$) δ 7.85 (d, *J* = 12 Hz, 1H, Thymidine H-N), 7.40 (dd, *J* = 24 Hz, 4 Hz, 2H, H-Ar), 7.30-7.16 (m, 10H, H-Ar), 5.61 (s, 1H, H-1´), 4.31 (s, 1H, H-2´), 4.15-4.01 (m, 1H, H-4´), 3.83-3.62 (m, 8H, DMT-OMe, H-5´), 3.48 (dd, *J* = 28 Hz, 12 Hz, 2H, H-7), 3.36-3.04 (m, 7H, H-10 H-12 H-13), 1.64 (s, 3H, Thymidine CH3), 1.45-1.17 (m, 4H, H-8 H-11), 1.16-0.72 (m, 12H, H-9)

^{31}P NMR (162 MHz, $CDCl_3$) δ 135.04, 127.65

HR-MS : Measured 776.3672, Calculated 776.3671

Benzoyl Protected LNA-5Me-C to dimethylformamidine(DMF)-protected LNA 5Me-C (Compound 8).



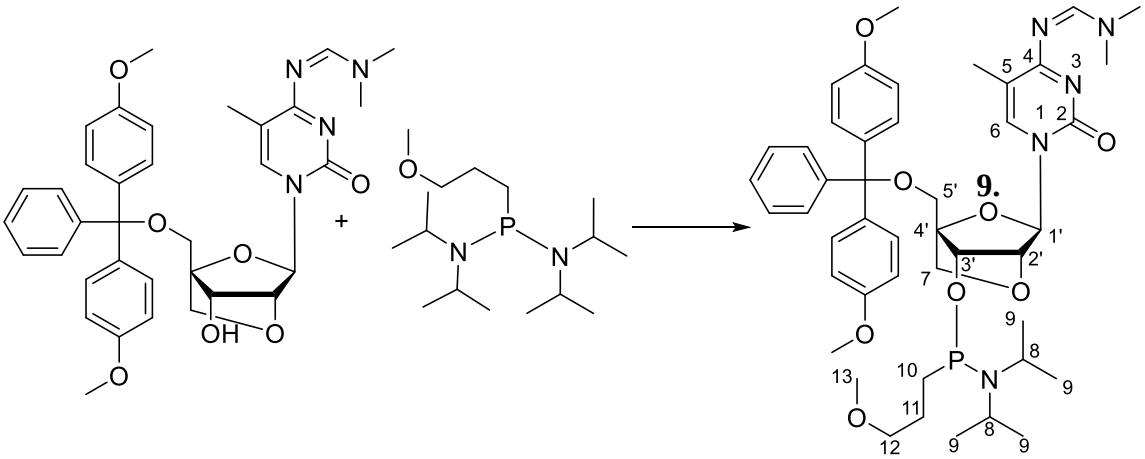
A 0.1 M solution of K2CO3 was made in methanol (30 mL). 500 mg of DMT-LNA-BzMeC was added and stirred at RT overnight. The solvent was removed and the product was columned (0-10% MeOH in DCM w/ 0.1% TEA added) to give a white solid. This was dissolved in DMF (10 mL) and DMF-DMA was added (330 µL) and stirred at RT overnight. The product was purified on silica (0-5% MeOH in DMF w/ 0.1% TEA added) to give a white foam (388 mg, 82%).

^{1}H NMR (400 MHz, $CDCl_3$) δ 8.68 (s, 1H, DMF-C-H), 7.49-7.06 (m, 10H, H-Ar), 6.78 (d, *J* = 8 Hz, 4H, H-Ar), 5.69 (s, 1H, H-1´), 5.23 (s, 1H, H-2´), 4.49 (s, 1H, H-3´), 4.18 (d, *J* = 8 Hz, 1H, H-4´), 3.79 (d, *J* = 8 Hz, 2H, H-5´), 3.72 (s, 6H, DMT-OMe), 3.43 (dd, *J* = 36 Hz, 12 Hz, 2H, H-7), 3.06 (d, *J* = 8 Hz, 6H, DMF-N-$(CH_3)_2$), 1.82 (s, 3H, Cytosine CH_3).

^{13}C NMR (101 MHz, CDCl3) δ 171.20 (C-DMF), 158.65 (C-Ar), 158.00 (C-Ar), 156.03 (C-Ar), 144.61 (C-Ar), 137.62 (C-Ar), 135.61 (C-Ar), 130.08 (C-Ar), 128.11 (C-Ar), 128.04 (C-Ar), 127.01 (C-Ar), 113.33 (C-Ar), 110.26 (C-Ar), 87.75 (C-1´), 86.63(C-2´), 79.38(C-3´), 71.67 (C-4´), 70.48 (C-9), 58.65 (C-5´), 55.26 (DMT-OMe), 35.03 (DMF-N-CH3), 14.26 (Cytosine CH_3).

HR-MS : Measured 627.2806, Calculated 627.2813

MOP Phosphitylation of DMF-LNA-5Me-C



5´-DMT-DMF-LNA-5MeC (160 mg) was dissolved in DCM (5 mL) and 1-methyl imidazole (40 µL) and tetrazole (1.7 mL of 0.45 M Soln. in ACN) were added while stirring under argon. To this solution, bis(diisopropylamino)-3-methoxypropylphosphine (190 µL) was added from its storage vessel (see experiment 5.5) and stirred overnight at room temperature. The solution was removed in vacuo, the residue was diluted with DCM (10 mL) and transferred to a separatory funnel. Under atmospheric conditions, the ethyl acetate was worked up with 1:1 saturated sodium bicarbonate:water. 1:1 brine:water, and brine. The organic layer was dried over magnesium sulfate and removed. The residue was purified on a silica gel column (0-5% MeOH in DCM w/ 1% TEA added) and characterized on 31P NMR (61% yield).

1H NMR (400 MHz, CDCl3) δ 8.57 (s, 1H, DMF-C-H), 7.73 (s, 1H, H-Ar), 7.46-7.10 (m, 9H, H-Ar), 6.91-6.73 (m, 4H, H-Ar), 6.26 (t, *J* = 2 Hz, 1H, H-1´), 5.44 (t, *J* = 28 Hz, 1H, H-2´), 4.25 (t, *J* = 12 Hz, 2H, H-5´), 4.06-3.93 (m, 1H, H-4´), 3.70 (s, 6H, DMT-OMe), 3.63 (d, *J* = 2 Hz, 2H, H-7), 3.57 (s, 3H, H-13), 3.33-3.27 (m, 4H, H-10, H-12), 3.08 (t, *J* = 24 Hz, 6H, DMF-N-$(CH_3)_2$),.11 (s, 3H, Cytosine CH_3), 1.50-1.31 (m, 4H, H-8, H-11), 1.07-0.84 (m, 12H, H-9)

^{31}P NMR (162 MHz, $CDCl_3$) δ 133.73, 125.52

HR-MS : Measured 881.4166 , Calculated 881.4249

8.9 Data for Chapter 6

8.9.1 LC-MS Data for Oligonucleotides ON-6.1 to ON-6.13

Oligo	Sequence	Calc. Mass (Da)	Found Mass (Da)
ON-6.1	*ggccaaaccucggcuuaccu*	6887.5	6887.0

Table 8.8: Sequence along with calculated and found mass for ON-6.1. Lower case letters indicate phosphorothioate linkages and *2´-OMe* is indicated by italics.

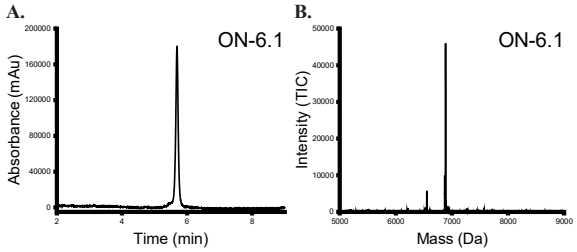


Figure 8.24 A. UV at A_{260} LC trace and **B.** MS-TIC trace for ON-6.1. MS-TIC is of the main peak as shown in **A.** Calculated and found masses can be found in Table 8.8

Oligo	Sequence (5´-3´)	Base Mass (Da)	Dye Mass (Da)	Calc. Mass (Da)	Found Mass (Da)	Dye Wt %
ON-6.2-oOH	***ttaat*** catactccag***tcgtt***	7100.4	-	7100.4	7099.9	-
ON-6.3-Cy3	Cy3+***ttaat*** catactccag***tcgtt***	7125.4	764	7889.4	7891.4	10.72
ON-6.4-Cy5	Cy5:***ttaat*** catactccag***tcgtt***	7125.4	942.2	8067.5	8070.3	13.22
ON-6.5-488	AF488:***ttaat*** catactccag***tcgtt***	7125.4	792.1	7917.5	7919	11.12
ON-6.6-546	AF546:***ttaat*** catactccag***tcgtt***	7125.4	1106.5	8231.9	8232.8	15.53
ON-6.7-594	AF594:***ttaat*** catactccag***tcgtt***	7125.4	981.1	8106.5	8106.7	13.77
ON-6.8-647	AF647:***ttaat*** catactccag***tcgtt***	7125.4	1117.3	8242.7	8243.5	15.68
ON-6.9-oN_3	N_3-***ttaat*** catactccag***tcgtt***	-	-	7125.4	7127.9	-

Table 8.9: Sequences along with calculated and found masses for ON-6.2 to ON-6.9. For oligonucleotides conjugated to dyes the base mass, dye mass and percentage by molecular weight of the dye compared to the base sequence. Lower case letters indicate phosphorothioate linkages. Ribose chemistries are denoted as DNA and ***2´-MOE***,. Dyes were conjugated to a 5´ azide on an oligonucleotide using SPAAC. + indicates a triazole formed with a BCN group, : indicates a triazole formed by a DBCO group.

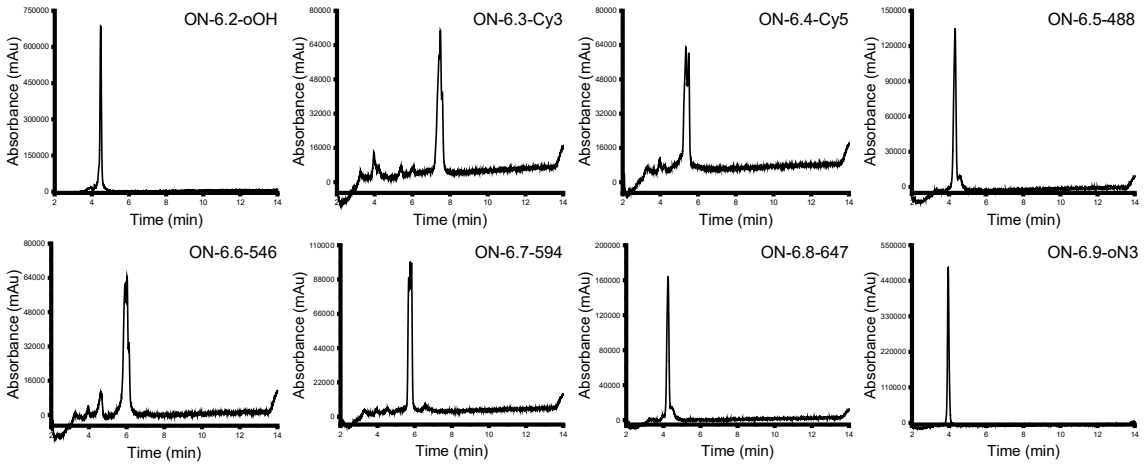


Figure 8.25: UV at A_{260} LC traces for oligonucleotides ON-6.2 to ON-6.9. Oligonucleotides ON-6.2-oOH and ON-6.9 were HPLC purified. For oligonucleotides ON-6.3 to ON-6.8 the base azide sequence was HPLC purified and after SPAAC conjugation excess dye was removed with molecular weight cut-off centrifuge filtration but the sequences were not re-HPLC purified.

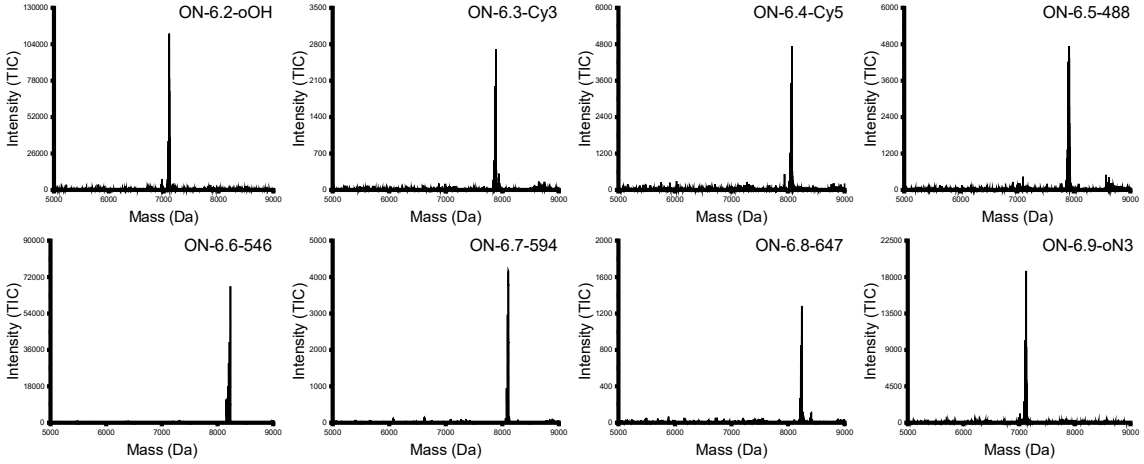


Figure 8.26: MS-TIC traces for the main peaks of ON-6.2 to ON-6.9 as shown in Figure 8.25. Calculated and observed masses can be seen in Table 8.9.

8.9.2 Data for Assays of Chapter 6

PCR data for both the H2K exon skipping assays and for MALAT-1 knockdown assays is shown in this section. For H2K exon skipping, the starting concentration of mRNA was determined via extrapolation using Cq value (cycle at which the threshold of detection is passed) of the unknown and the calibration curve constructed with the Cq values of the standards. For the MALAT-1 knockdown assays the fold change over untreated was calculated using the delta delta Cq method with the housekeeping gene GAPDH as a control. The fold change is calculated as 2^(-(Sample MALAT1 Cq- Sample GAPDH Cq)-(Untreated MALAT1 Cq- Untreated GAPDH Cq)).

qPCR Data:

A.

Condition	Rep 1 (M)	Rep 2 (M)	Rep 3 (M)	Average (M)	Std Dev (M)	Cq Rep 1	Cq Rep 2	Cq Rep 3
Std-1	2.50E-11	2.50E-11	2.50E-11	-	-	11.843	11.912	11.853
Std-2	2.50E-12	2.50E-12	2.50E-12	-	-	15.370	15.256	15.515
Std-3	2.50E-13	2.50E-13	2.50E-13	-	-	19.620	19.616	19.817
Std-4	2.50E-14	2.50E-14	2.50E-14	-	-	23.010	22.938	22.839
Std-5	2.50E-15	2.50E-15	2.50E-15	-	-	26.170	26.964	26.217
ON-6.1	3.55E-17	3.40E-17	3.00E-17	3.32E-17	2.84E-18	33.387	33.458	33.656
Untreated	1.95E-17	2.14E-17	1.73E-17	1.94E-17	2.05E-18	34.346	34.193	34.535

B.

Condition	Rep 1 (M)	Rep 2 (M)	Rep 3 (M)	Average (M)	Std Dev (M)	Cq Rep 1	Cq Rep 2	Cq Rep 3
Std-1	2.50E-11	2.50E-11	2.50E-11	-	-	11.752	11.809	11.688
Std-2	2.50E-12	2.50E-12	2.50E-12	-	-	15.278	15.086	15.367
Std-3	2.50E-13	2.50E-13	2.50E-13	-	-	19.155	19.165	19.505
Std-4	2.50E-14	2.50E-14	2.50E-14	-	-	22.799	22.887	22.812
Std-5	2.50E-15	2.50E-15	2.50E-15	-	-	26.523	26.332	26.836
ON-6.1	6.84E-18	5.80E-18	6.03E-18	6.22E-18	5.46E-19	36.271	36.271	36.271
Untreated	1.56E-18	2.27E-18	Na	1.92E-18	5.02E-19	38.200	38.200	-

Figure 8.27: One step RT-qPCR data for H2K Exon skipping assays. Samples were amplified with probes corresponding to skipped and unskipped sequences in one PCR reaction. Condition refers to either a known concentration stand are (Std 1-5), wells treated with oligonucleotide (ON-6.1) or untreated wells. Three replicates of each condition were performed with the Cq value for each as well as the calculated initial concentration of a sample or the known initial concentration of a standard. **A.** shows data for the unskipped transcript, **B.** for the skipped transcript.

A.

Condition	Rep 1 (M)	Rep 2 (M)	Rep 3 (M)	Average (M)	Std Dev (M)	Cq Rep 1	Cq Rep 2	Cq Rep 3
Std-1	2.50E-11	2.50E-11	2.50E-11	-	-	9.103	9.401	9.524
Std-2	2.50E-12	2.50E-12	2.50E-12	-	-	13.223	13.056	13.039
Std-3	2.50E-13	2.50E-13	2.50E-13	-	-	16.466	16.434	16.370
Std-4	2.50E-14	2.50E-14	2.50E-14	-	-	21.443	21.445	21.629
Std-5	2.50E-15	2.50E-15	2.50E-15	-	-	23.548	23.451	23.704
ON-6.1 (25 Cycles)	1.03E-10	5.81E-11	1.10E-10	9.05E-11	2.83E-11	7.151	8.069	7.045
Untreated (25 Cycles)	1.26E-10	1.58E-10	1.21E-10	1.35E-10	2.01E-11	6.828	6.465	6.889
NTC (25 Cycles)	1.69E-10	1.61E-10	-	1.65E-10	5.59E-12	6.358	6.434	-
ON-6.1 (20 Cycles)	1.29E-11	1.11E-11	1.61E-11	1.34E-11	2.53E-12	10.478	10.716	10.123
Untreated (20 Cycles)	2.00E-11	1.79E-11	1.84E-11	1.88E-11	1.11E-12	9.774	9.952	9.913
NTC (20 Cycles)	1.34E-11	8.98E-12	-	1.12E-11	3.10E-12	10.422	11.057	-
ON-6.1 (15 Cycles)	1.42E-12	1.36E-12	1.79E-12	1.52E-12	2.33E-13	14.007	14.082	13.639
Untreated (15 Cycles)	1.58E-12	2.12E-12	1.60E-12	1.77E-12	3.08E-13	13.837	13.365	13.820
NTC (15 Cycles)	2.10E-12	9.70E-13	-	1.53E-12	7.97E-13	13.385	14.619	-

B.

Condition	Rep 1 (M)	Rep 2 (M)	Rep 3 (M)	Average (M)	Std Dev (M)	Cq Rep 1	Cq Rep 2	Cq Rep 3
Std-1	2.50E-11	2.50E-11	2.50E-11	-	-	11.186	11.205	11.358
Std-2	2.50E-12	2.50E-12	2.50E-12	-	-	14.914	14.832	14.752
Std-3	2.50E-13	2.50E-13	2.50E-13	-	-	18.147	18.358	18.290
Std-4	2.50E-14	2.50E-14	2.50E-14	-	-	22.723	22.806	22.913
Std-5	2.50E-15	2.50E-15	2.50E-15	-	-	24.950	24.552	25.196
ON-6.1 (25 Cycles)	1.45E-10	9.75E-11	1.34E-10	1.26E-10	2.49E-11	8.663	9.271	8.779
Untreated (25 Cycles)	1.30E-10	2.35E-10	1.51E-10	1.72E-10	5.57E-11	8.827	7.920	8.601
NTC (25 Cycles)	1.74E-10	1.56E-10	-	1.65E-10	1.27E-11	8.387	8.555	-
ON-6.1 (20 Cycles)	1.45E-11	1.29E-11	1.62E-11	1.45E-11	1.62E-12	12.190	12.365	12.022
Untreated (20 Cycles)	1.64E-11	2.79E-11	1.74E-11	2.05E-11	6.35E-12	12.004	11.191	11.910
NTC (20 Cycles)	1.25E-11	1.32E-11	-	1.29E-11	4.97E-13	12.418	12.334	-
ON-6.1 (15 Cycles)	1.63E-12	1.49E-12	1.83E-12	1.65E-12	1.74E-13	15.541	15.680	15.360
Untreated (15 Cycles)	1.49E-12	3.30E-12	1.64E-12	2.14E-12	1.00E-12	15.676	14.461	15.531
NTC (15 Cycles)	1.67E-12	1.22E-12	-	1.45E-12	3.19E-13	15.500	15.983	-

C.

Condition	Rep 1 (%)	Rep 2 (%)	Rep 3 (%)	Average (%)
ON-6.1 (25 Cycles)	58.43	62.64	54.95	58.12
Untreated (25 Cycles)	50.80	59.79	55.41	56.00
NTC (25 Cycles)	50.62	49.08	-	49.88
ON-6.1 (20 Cycles)	52.92	53.79	50.13	52.09
Untreated (20 Cycles)	44.99	60.84	48.67	52.26
NTC (20 Cycles)	48.35	59.53	-	53.51
ON-6.1 (15 Cycles)	53.38	52.28	50.60	51.99
Untreated (15 Cycles)	48.52	60.81	50.62	54.78
NTC (15 Cycles)	44.35	55.71	-	48.53

Figure 8.28: Nested RT-PCR-qPCR data for H2K exon skipping assays. Condition refers to either a known concentration standard (Std 1-5), wells treated with oligonucleotide (ON-6.1), untreated wells or a non-targeting control (NTC) where PCR was performed without loading any mRNA. Cycle numbers refer to the number of PCR cycles performed in the first RT-PCR step before performing the qPCR step. Three replicates were performed and the Cq value of each as well as the calculated initial concentration of samples based on the curve constructed from Std 1-5. **A.** shows data for unskipped transcripts, **B.** for skipped transcripts and **C.** the exon skipping percentages calculated from the values in **A.** and **B.**

A.

Oligo	Replicate	Cq(MALAT1)	Cq(GAPDH)	Delta Cq	Delta Delta Cq	Fold Change
ON-6.2-oOH	1	16.721	14.413	2.308	0.595	0.662
ON-6.2-oOH	2	16.722	14.346	2.376	0.664	0.631
ON-6.2-oOH	3	16.925	14.544	2.382	0.669	0.629
Untreated	1	16.007	14.262	1.746	0.034	0.977
Untreated	2	15.862	14.271	1.591	-0.121	1.087
Untreated	3	16.054	14.373	1.681	-0.031	1.022
Untreated	4	16.015	14.418	1.597	-0.115	1.083
Untreated	5	16.171	14.241	1.930	0.218	0.860
Untreated	6	16.238	14.510	1.729	0.016	0.989
ON-6.3-Cy3	1	16.654	14.366	2.288	0.898	0.537
ON-6.3-Cy3	2	16.652	14.537	2.116	0.726	0.605
ON-6.3-Cy3	3	16.900	14.520	2.379	0.990	0.504
ON-6.4-Cy5	1	17.094	14.553	2.541	1.151	0.450
ON-6.4-Cy5	2	17.015	14.394	2.621	1.231	0.426
ON-6.4-Cy5	3	17.058	14.557	2.501	1.111	0.463
ON-6.5-488	1	16.591	14.357	2.234	0.844	0.557
ON-6.5-488	2	16.449	14.535	1.914	0.524	0.695
ON-6.5-488	3	16.642	14.412	2.230	0.840	0.558
ON-6.6-546	1	17.436	14.698	2.739	1.349	0.393
ON-6.6-546	2	17.163	14.603	2.560	1.170	0.444
ON-6.6-546	3	17.229	14.695	2.534	1.144	0.452
ON-6.7-594	1	16.787	14.528	2.259	0.869	0.547
ON-6.7-594	2	16.614	14.539	2.075	0.685	0.622
ON-6.7-594	3	16.684	14.624	2.060	0.670	0.629
ON-6.8-647	1	17.333	14.549	2.784	1.394	0.380
ON-6.8-647	2	17.366	14.634	2.733	1.343	0.394
ON-6.8-647	3	17.781	14.964	2.817	1.427	0.372
Untreated	1	15.702	14.376	1.327	-0.063	1.045
Untreated	2	15.697	14.328	1.369	-0.021	1.015
Untreated	3	15.797	14.403	1.394	0.005	0.997
Untreated	4	15.828	14.494	1.334	-0.055	1.039
Untreated	5	16.000	14.475	1.525	0.135	0.910

B.

Oligo	Replicate	Cq(MALAT1)	Cq(GAPDH)	Delta Cq	Delta Delta Cq	Fold Change
ON-6.2-oOH	1	15.580	14.760	0.820	0.646	0.639
ON-6.2-oOH	2	15.570	14.977	0.592	0.419	0.748
ON-6.2-oOH	3	15.673	15.106	0.567	0.394	0.761
ON-6.9-oN_3	1	15.729	15.086	0.642	0.469	0.722
ON-6.9-oN_3	2	15.943	14.903	1.040	0.867	0.548
ON-6.9-oN_3	3	15.543	14.884	0.659	0.485	0.714
Untreated	1	16.170	15.080	1.090	0.917	0.530
Untreated	2	15.358	15.130	0.228	0.055	0.962
Untreated	3	15.279	15.071	0.208	0.035	0.976
Untreated	4	15.446	15.239	0.207	0.034	0.977
Untreated	5	15.504	15.454	0.049	-0.124	1.090

Figure 8.29: RT-qPCR data for MALAT-1 knockdown assays. Oligo column refers to the ASO used in the well (200nM with Lipofectamine 3000 transfection). Cq values for both MALAT-1 and GAPDH are shown as averages of two techical replicates each. Delta Cq is calculated as $\Delta=(Cq_{MALAT1})-(Cq_{GAPDH})$. Delta Delta Cq is calculated as $\Delta\Delta=(\Delta_{Oligo})-(\Delta_{Untreated})$. Fold change is calculated as $2^{-(\Delta\Delta Oligo)}$. **A.** shows data for dye-conjugated oligonucleotides (ON-6.2 to ON-6.8). A note is that all conditions displayed are from the same cell culture plate, however, with technical replicates a total of 104 PCR reactions were performed meaning they had to be split into two PCR plates amplified immediately after one another. The bold line indicates the PCR plate split. **B.** shows data for comparison of 5´ azide and 5´ alcohol oligonucleotides (ON-6.2-oOH and ON-6.9-oN_3)

8.9.3 Click Background Data Collection Parameters

Fixation and Staining: Cells were fixed with 4% formaldehyde in PBS for 15 minutes at room temperature then permeabilised with 0.1% Triton-X-100 in PBS for 30 minutes at room temperature. Samples were then blocked with either PBS (control), 3% BSA in PBS for 1 hour at room temperature, 0.5% Casein in PBS for 1 hour at room temperature or 100 mM iodocatemide for 1 hour at room temperature in PBS followed by 3% BSA in PBS for 1 hour at room temperature. Staining was then done with different concentrations of AF488 dye (either alkyne or DBCO) in blocking buffer for 1 hour at room temperature. Staining was then done with CellTracker Deep Red for 15 minutes at room temperature according to the manufacturer's instructions. Three PBS washes were performed between each step.

Imaging: Cells were cultured in a glass bottomed 96-well plate coated in Poly-D lysine for adherence and mounted with ProLong Diamond antifade according to the manufacturers instructions. Cells were then imaged on an EVOSM7000 automated benchtop system using the GFP (excitation 470 nm, emission 525 nm) channel to view AF488 background and the Cy5 (excitation 628 nm, emission 692 nm) channel for view the CellTracker stain.

Image Processing: Automated image processing was done using the CellProfiler software using a pipeline of Threshold→IdentifyPrimaryObjects→MeasureObjectIntensity. Thresholding was done using the Cy5 channel with a global minimum cross-entropy approach with a threshold smoothing scale of 0.0 and a threshold correction factor of 1.0, lower and upper bound of 0.0 and 1.0 respectively and no log transform. Using the threshold as input objects were identified with a typical diameter of 20 to 200 pixel units discarding objects outside this range and objects touching the border of the image. A global, Otsu, Two-Class strategy was used with a threshold smoothing scale of 1.3488 and a threshold

correction factor of 1.0 with and upper and lower threshold bound of 0.0 and 1.0 respectively. Using the objects identified the integrated fluorescence intensity of the GFP channel was calculated.

9. References

(1) Nikolova, E. N.; Goh, G. B.; Brooks, C. L., 3rd; Al-Hashimi, H. M. Characterizing the protonation state of cytosine in transient G.C Hoogsteen base pairs in duplex DNA. *J Am Chem Soc* **2013**, *135* (18), 6766–6769. DOI: 10.1021/ja400994e.
(2) Nikolova, E. N.; Kim, E.; Wise, A. A.; O'Brien, P. J.; Andricioaei, I.; Al-Hashimi, H. M. Transient Hoogsteen base pairs in canonical duplex DNA. *Nature* **2011**, *470* (7335), 498–502. DOI: 10.1038/nature09775.
(3) Altona, C.; Sundaralingam, M. Conformational analysis of the sugar ring in nucleosides and nucleotides. A new description using the concept of pseudorotation. *J Am Chem Soc* **1972**, *94* (23), 8205–8212. DOI: 10.1021/ja00778a043.
(4) Nowotny, M.; Gaidamakov, S. A.; Ghirlando, R.; Cerritelli, S. M.; Crouch, R. J.; Yang, W. Structure of human RNase H1 complexed with an RNA/DNA hybrid: insight into HIV reverse transcription. *Mol Cell* **2007**, *28* (2), 264–276. DOI: 10.1016/j.molcel.2007.08.015.
(5) Drew, H. R.; Samson, S.; Dickerson, R. E. Structure of a B-DNA dodecamer at 16 K. *Proc Natl Acad Sci U S A* **1982**, *79* (13), 4040–4044. DOI: 10.1073/pnas.79.13.4040.
(6) Schrodinger, LLC. The PyMOL Molecular Graphics System, Version 1.8. 2015.
(7) Egli, M.; Flavell, A.; Pyle, A. M.; Wilson, W. D.; Haq, S. I.; Luisi, B.; Fisher, J.; Laughton, C.; Allen, S.; Engels, J.; et al. DNA and RNA Structure. In *Nucleic Acids in Chemistry and Biology*, Blackburn, G. M., Gait, M. J., Loakes, D., Williams, D. M. Eds.; The Royal Society of Chemistry, 2006; p 0.
(8) Michelson, A. M.; Todd, A. R. Nucleotides part XXXII. Synthesis of a dithymidine dinucleotide containing a 3′: 5′-internucleotidic linkage. *Journal of the Chemical Society (Resumed)* **1955**, (0), 2632–2638, 10.1039/JR9550002632. DOI: 10.1039/JR9550002632.
(9) Letsinger, R. L.; Mahadevan, V. Stepwise synthesis of oligodeoxyribonucleotides on an insoluble polymer support. *J Am Chem Soc* **1966**, *88* (22), 5319–5324. DOI: 10.1021/ja00974a053.
(10) Beaucage, S. L.; Caruthers, M. H. Deoxynucleoside phosphoramidites—A new class of key intermediates for deoxypolynucleotide synthesis. *Tetrahedron Letters* **1981**, *22* (20), 1859–1862. DOI: https://doi.org/10.1016/S0040-4039(01)90461-7.
(11) Brown, T. *Nucleic Acids Book, Chapter 5: Solid Phase Oligonucleotide Synthesis.* ATDbio,
(12) *Custom DNA Oligos*. Integrated DNA Technologies, 2025. https://eu.idtdna.com/pages/products/custom-dna-rna/dna-oligos/custom-dna-oligos.
(13) *OligoPilot oligonucleotide synthesizer*. Cytiva, 2025. https://www.cytivalifesciences.com/en/us/shop/oligonucleotide-synthesis/synthesizers/oligopilot-oligonucleotide-synthesizer-p-28018?srsltid=AfmBOort_DELLjRjTa7B93edX8rc3zO9C7-pCRusOfazK0NAhAm1jRC-.
(14) *Products*. Glen Research, 2025. https://www.glenresearch.com/browse/products.
(15) *Oligonucleotide Synthesis Products*. Hongene Biotech, 2025. https://www.hongene.com/products?category=o.
(16) Dias, N.; Stein, C. A. Antisense oligonucleotides: basic concepts and mechanisms. *Mol Cancer Ther* **2002**, *1* (5), 347–355.
(17) Cheng, X.; Wang, Y.; Zhang, T. T.; Cao, Y. N.; Cheng, H. B.; Du, Y.; Ge, X.; Ren, B.; Lu, J.; Li, L. Y. Emergence of Small Nucleic Acids as Drugs in Precision Medicine. *Clin Pharmacol Ther* **2025**. DOI: 10.1002/cpt.3678.
(18) Dominski, Z.; Kole, R. Restoration of correct splicing in thalassemic pre-mRNA by antisense oligonucleotides. *Proc Natl Acad Sci U S A* **1993**, *90* (18), 8673–8677. DOI: 10.1073/pnas.90.18.8673.
(19) Mann, C. J.; Honeyman, K.; Cheng, A. J.; Ly, T.; Lloyd, F.; Fletcher, S.; Morgan, J. E.; Partridge, T. A.; Wilton, S. D. Antisense-induced exon skipping and synthesis of

dystrophin in the mdx mouse. *Proc Natl Acad Sci U S A* **2001**, *98* (1), 42–47. DOI: 10.1073/pnas.98.1.42.
(20) Sabrina Haque, U.; Kohut, M.; Yokota, T. Comprehensive review of adverse reactions and toxicology in ASO-based therapies for Duchenne Muscular Dystrophy: From FDA-approved drugs to peptide-conjugated ASO. *Curr Res Toxicol* **2024**, *7*, 100182. DOI: 10.1016/j.crtox.2024.100182.
(21) Crooke, S. T. *Antisense Drug Technology: Principles, Strategies, and Applications, Second Edition: Chapter 2 The RNase H Mechanism*; CRC Press, 2007.
(22) Wong, E.; Goldberg, T. Mipomersen (kynamro): a novel antisense oligonucleotide inhibitor for the management of homozygous familial hypercholesterolemia. *P T* **2014**, *39* (2), 119–122.
(23) Cuchel, M.; Bruckert, E.; Ginsberg, H. N.; Raal, F. J.; Santos, R. D.; Hegele, R. A.; Kuivenhoven, J. A.; Nordestgaard, B. G.; Descamps, O. S.; Steinhagen-Thiessen, E.; et al. Homozygous familial hypercholesterolaemia: new insights and guidance for clinicians to improve detection and clinical management. A position paper from the Consensus Panel on Familial Hypercholesterolaemia of the European Atherosclerosis Society. *Eur Heart J* **2014**, *35* (32), 2146–2157. DOI: 10.1093/eurheartj/ehu274.
(24) Mullick, A. E.; Fu, W.; Graham, M. J.; Lee, R. G.; Witchell, D.; Bell, T. A.; Whipple, C. P.; Crooke, R. M. Antisense oligonucleotide reduction of apoB-ameliorated atherosclerosis in LDL receptor-deficient mice. *J Lipid Res* **2011**, *52* (5), 885–896. DOI: 10.1194/jlr.M011791.
(25) Ou, K.; Jia, Q.; Li, D.; Li, S.; Li, X. J.; Yin, P. Application of antisense oligonucleotide drugs in amyotrophic lateral sclerosis and Huntington's disease. *Transl Neurodegener* **2025**, *14* (1), 4. DOI: 10.1186/s40035-025-00466-9.
(26) Kilanowska, A.; Studzinska, S. In vivo and in vitro studies of antisense oligonucleotides - a review. *Rsc Adv* **2020**, *10* (57), 34501–34516. DOI: 10.1039/d0ra04978f.
(27) Shaw, J. P.; Kent, K.; Bird, J.; Fishback, J.; Froehler, B. Modified Deoxyoligonucleotides Stable to Exonuclease Degradation in Serum. *Nucleic Acids Research* **1991**, *19* (4), 747–750. DOI: DOI 10.1093/nar/19.4.747.
(28) Monia, B. P.; Johnston, J. F.; Sasmor, H.; Cummins, L. L. Nuclease resistance and antisense activity of modified oligonucleotides targeted to Ha-ras. *Journal of Biological Chemistry* **1996**, *271* (24), 14533–14540. DOI: DOI 10.1074/jbc.271.24.14533.
(29) Eckstein, F. Nucleoside Phosphorothioates. *J Am Chem Soc* **1966**, *88* (18), 4292–&. DOI: DOI 10.1021/ja00970a054.
(30) Eckstein, F. Nucleoside Phosphorothioates. *J Am Chem Soc* **1970**, *92* (15), 4718–+. DOI: DOI 10.1021/ja00718a039.
(31) Brautigam, C. A.; Steitz, T. A. Structural principles for the inhibition of the 3'-5' exonuclease activity of Escherichia coli DNA polymerase I by phosphorothioates. *J Mol Biol* **1998**, *277* (2), 363–377. DOI: 10.1006/jmbi.1997.1586.
(32) Matsukura, M.; Shinozuka, K.; Zon, G.; Mitsuya, H.; Reitz, M.; Cohen, J. S.; Broder, S. Phosphorothioate analogs of oligodeoxynucleotides: inhibitors of replication and cytopathic effects of human immunodeficiency virus. *Proc Natl Acad Sci U S A* **1987**, *84* (21), 7706–7710. DOI: 10.1073/pnas.84.21.7706.
(33) Agrawal, S.; Goodchild, J.; Civeira, M. P.; Thornton, A. H.; Sarin, P. S.; Zamecnik, P. C. Oligodeoxynucleoside phosphoramidates and phosphorothioates as inhibitors of human immunodeficiency virus. *Proc Natl Acad Sci U S A* **1988**, *85* (19), 7079–7083. DOI: 10.1073/pnas.85.19.7079.
(34) Kim, Y. Drug Discovery Perspectives of Antisense Oligonucleotides. *Biomol Ther (Seoul)* **2023**, *31* (3), 241–252. DOI: 10.4062/biomolther.2023.001.
(35) Crooke, S. T. Progress in antisense technology: the end of the beginning. *Methods Enzymol* **2000**, *313*, 3–45. DOI: 10.1016/s0076-6879(00)13003-4.

(36) Crooke, S. T.; Vickers, T. A.; Liang, X. H. Phosphorothioate modified oligonucleotide-protein interactions. *Nucleic Acids Res* **2020**, *48* (10), 5235–5253. DOI: 10.1093/nar/gkaa299.
(37) Crooke, S. T.; Wang, S.; Vickers, T. A.; Shen, W.; Liang, X. H. Cellular uptake and trafficking of antisense oligonucleotides. *Nat Biotechnol* **2017**, *35* (3), 230–237. DOI: 10.1038/nbt.3779.
(38) Laurent, Q.; Martinent, R.; Moreau, D.; Winssinger, N.; Sakai, N.; Matile, S. Oligonucleotide Phosphorothioates Enter Cells by Thiol-Mediated Uptake. *Angew Chem Int Ed Engl* **2021**, *60* (35), 19102–19106. DOI: 10.1002/anie.202107327.
(39) Levin, A. A. A review of the issues in the pharmacokinetics and toxicology of phosphorothioate antisense oligonucleotides. *Biochim Biophys Acta* **1999**, *1489* (1), 69–84. DOI: 10.1016/s0167-4781(99)00140-2.
(40) Henry, S. P.; Templin, M. V.; Gillett, N.; Rojko, J.; Levin, A. A. Correlation of toxicity and pharmacokinetic properties of a phosphorothioate oligonucleotide designed to inhibit ICAM-1. *Toxicol Pathol* **1999**, *27* (1), 95–100. DOI: 10.1177/019262339902700117.
(41) Pezeshki, G.; Schobitz, B.; Pohl, T.; Reul, J. M. Intracerebroventricular administration of missense oligodeoxynucleotide induces interleukin-6 mRNA expression in brain and spleen of rats. *Neurosci Lett* **1996**, *217* (2-3), 97–100.
(42) Schobitz, B.; Pezeshki, G.; Probst, J. C.; Reul, J. M.; Skutella, T.; Stohr, T.; Holsboer, F.; Spanagel, R. Centrally administered oligodeoxynucleotides in rats: occurrence of non-specific effects. *Eur J Pharmacol* **1997**, *331* (2-3), 97–107. DOI: 10.1016/s0014-2999(97)01014-5.
(43) Henry, S. P.; Bolte, H.; Auletta, C.; Kornbrust, D. J. Evaluation of the toxicity of ISIS 2302, a phosphorothioate oligonucleotide, in a four-week study in cynomolgus monkeys. *Toxicology* **1997**, *120* (2), 145–155. DOI: 10.1016/s0300-483x(97)03661-5.
(44) Peng Ho, S.; Livanov, V.; Zhang, W.; Li, J.; Lesher, T. Modification of phosphorothioate oligonucleotides yields potent analogs with minimal toxicity for antisense experiments in the CNS. *Brain Res Mol Brain Res* **1998**, *62* (1), 1–11. DOI: 10.1016/s0169-328x(98)00185-5.
(45) Jahns, H.; Taneja, N.; Willoughby, J. L. S.; Akabane-Nakata, M.; Brown, C. R.; Nguyen, T.; Bisbe, A.; Matsuda, S.; Hettinger, M.; Manoharan, R. M.; et al. Chirality matters: stereo-defined phosphorothioate linkages at the termini of small interfering RNAs improve pharmacology in vivo. *Nucleic Acids Res* **2022**, *50* (3), 1221–1240. DOI: 10.1093/nar/gkab544.
(46) Nukaga, Y.; Yamada, K.; Ogata, T.; Oka, N.; Wada, T. Stereocontrolled solid-phase synthesis of phosphorothioate oligoribonucleotides using 2'-O-(2-cyanoethoxymethyl)-nucleoside 3'-O-oxazaphospholidine monomers. *J Org Chem* **2012**, *77* (18), 7913–7922. DOI: 10.1021/jo301052v.
(47) Oka, N.; Wada, T.; Saigo, K. Diastereocontrolled synthesis of dinucleoside phosphorothioates using a novel class of activators, dialkyl(cyanomethyl)ammonium tetrafluoroborates. *J Am Chem Soc* **2002**, *124* (18), 4962–4963. DOI: 10.1021/ja017275e.
(48) Moulds, C.; Lewis, J. G.; Froehler, B. C.; Grant, D.; Huang, T.; Milligan, J. F.; Matteucci, M. D.; Wagner, R. W. Site and mechanism of antisense inhibition by C-5 propyne oligonucleotides. *Biochemistry* **1995**, *34* (15), 5044–5053. DOI: 10.1021/bi00015a015.
(49) Monia, B. P.; Lesnik, E. A.; Gonzalez, C.; Lima, W. F.; McGee, D.; Guinosso, C. J.; Kawasaki, A. M.; Cook, P. D.; Freier, S. M. Evaluation of 2'-modified oligonucleotides containing 2'-deoxy gaps as antisense inhibitors of gene expression. *J Biol Chem* **1993**, *268* (19), 14514–14522.

(50) Cummins, L. L.; Owens, S. R.; Risen, L. M.; Lesnik, E. A.; Freier, S. M.; McGee, D.; Guinosso, C. J.; Cook, P. D. Characterization of fully 2'-modified oligoribonucleotide hetero- and homoduplex hybridization and nuclease sensitivity. *Nucleic Acids Res* **1995**, *23* (11), 2019–2024. DOI: 10.1093/nar/23.11.2019.
(51) Sproat, B. S.; Lamond, A. I.; Beijer, B.; Neuner, P.; Ryder, U. Highly efficient chemical synthesis of 2'-O-methyloligoribonucleotides and tetrabiotinylated derivatives; novel probes that are resistant to degradation by RNA or DNA specific nucleases. *Nucleic Acids Res* **1989**, *17* (9), 3373–3386. DOI: 10.1093/nar/17.9.3373.
(52) Freier, S. M.; Altmann, K. H. The ups and downs of nucleic acid duplex stability: structure-stability studies on chemically-modified DNA:RNA duplexes. *Nucleic Acids Res* **1997**, *25* (22), 4429–4443. DOI: 10.1093/nar/25.22.4429.
(53) Lubini, P.; Zurcher, W.; Egli, M. Stabilizing effects of the RNA 2'-substituent: crystal structure of an oligodeoxynucleotide duplex containing 2'-O-methylated adenosines. *Chem Biol* **1994**, *1* (1), 39–45. DOI: 10.1016/1074-5521(94)90039-6.
(54) Lamond, A. I.; Sproat, B. S. Antisense oligonucleotides made of 2'-O-alkylRNA: their properties and applications in RNA biochemistry. *FEBS Lett* **1993**, *325* (1-2), 123–127. DOI: 10.1016/0014-5793(93)81427-2.
(55) Altmann, K. H.; Fabbro, D.; Dean, N. M.; Geiger, T.; Monia, B. P.; Muller, M.; Nicklin, P. Second-generation antisense oligonucleotides: structure-activity relationships and the design of improved signal-transduction inhibitors. *Biochem Soc Trans* **1996**, *24* (3), 630–637. DOI: 10.1042/bst0240630.
(56) Wagner, R. W.; Matteucci, M. D.; Lewis, J. G.; Gutierrez, A. J.; Moulds, C.; Froehler, B. C. Antisense gene inhibition by oligonucleotides containing C-5 propyne pyrimidines. *Science* **1993**, *260* (5113), 1510–1513. DOI: 10.1126/science.7684856.
(57) Lim, K. R. Q.; Yokota, T. Invention and Early History of Gapmers. *Methods Mol Biol* **2020**, *2176*, 3–19. DOI: 10.1007/978-1-0716-0771-8_1.
(58) Koshkin, A. A.; Singh, S. K.; Nielsen, P.; Rajwanshi, V. K.; Kumar, R.; Meldgaard, M.; Olsen, C. E.; Wengel, J. LNA (Locked Nucleic Acids): Synthesis of the adenine, cytosine, guanine, 5-methylcytosine, thymine and uracil bicyclonucleoside monomers, oligomerisation, and unprecedented nucleic acid recognition. *Tetrahedron* **1998**, *54* (14), 3607–3630. DOI: https://doi.org/10.1016/S0040-4020(98)00094-5.
(59) Seth, P. P.; Siwkowski, A.; Allerson, C. R.; Vasquez, G.; Lee, S.; Prakash, T. P.; Kinberger, G.; Migawa, M. T.; Gaus, H.; Bhat, B.; et al. Design, synthesis and evaluation of constrained methoxyethyl (cMOE) and constrained ethyl (cEt) nucleoside analogs. *Nucleic Acids Symp Ser (Oxf)* **2008**, (52), 553–554. DOI: 10.1093/nass/nrn280.
(60) Vester, B.; Wengel, J. LNA (locked nucleic acid): high-affinity targeting of complementary RNA and DNA. *Biochemistry* **2004**, *43* (42), 13233–13241. DOI: 10.1021/bi0485732.
(61) Wengel, J.; Alexei, K.; K., S. S.; Poul, N.; Michael, M.; K., R. V.; Ravindra, K.; Jan, S.; B., N. C.; Peter, J. J.; et al. Lna (Locked Nucleic Acid). *Nucleosides and Nucleotides* **1999**, *18* (6-7), 1365–1370. DOI: 10.1080/07328319908044718.
(62) Kaur, H.; Babu, B. R.; Maiti, S. Perspectives on chemistry and therapeutic applications of Locked Nucleic Acid (LNA). *Chem Rev* **2007**, *107* (11), 4672–4697. DOI: 10.1021/cr050266u.
(63) Petersen, M.; Wengel, J. LNA: a versatile tool for therapeutics and genomics. *Trends Biotechnol* **2003**, *21* (2), 74–81. DOI: 10.1016/S0167-7799(02)00038-0.
(64) Swayze, E. E.; Siwkowski, A. M.; Wancewicz, E. V.; Migawa, M. T.; Wyrzykiewicz, T. K.; Hung, G.; Monia, B. P.; Bennett, C. F. Antisense oligonucleotides containing locked nucleic acid improve potency but cause significant hepatotoxicity in animals. *Nucleic Acids Res* **2007**, *35* (2), 687–700. DOI: 10.1093/nar/gkl1071.

(65) Burdick, A. D.; Sciabola, S.; Mantena, S. R.; Hollingshead, B. D.; Stanton, R.; Warneke, J. A.; Zeng, M.; Martsen, E.; Medvedev, A.; Makarov, S. S.; et al. Sequence motifs associated with hepatotoxicity of locked nucleic acid--modified antisense oligonucleotides. *Nucleic Acids Res* **2014**, *42* (8), 4882–4891. DOI: 10.1093/nar/gku142.
(66) Kakiuchi-Kiyota, S.; Koza-Taylor, P. H.; Mantena, S. R.; Nelms, L. F.; Enayetallah, A. E.; Hollingshead, B. D.; Burdick, A. D.; Reed, L. A.; Warneke, J. A.; Whiteley, L. O.; et al. Comparison of hepatic transcription profiles of locked ribonucleic acid antisense oligonucleotides: evidence of distinct pathways contributing to non-target mediated toxicity in mice. *Toxicol Sci* **2014**, *138* (1), 234–248. DOI: 10.1093/toxsci/kft278.
(67) Kamola, P. J.; Kitson, J. D.; Turner, G.; Maratou, K.; Eriksson, S.; Panjwani, A.; Warnock, L. C.; Douillard Guilloux, G. A.; Moores, K.; Koppe, E. L.; et al. In silico and in vitro evaluation of exonic and intronic off-target effects form a critical element of therapeutic ASO gapmer optimization. *Nucleic Acids Res* **2015**, *43* (18), 8638–8650. DOI: 10.1093/nar/gkv857.
(68) Kasuya, T.; Hori, S.; Watanabe, A.; Nakajima, M.; Gahara, Y.; Rokushima, M.; Yanagimoto, T.; Kugimiya, A. Ribonuclease H1-dependent hepatotoxicity caused by locked nucleic acid-modified gapmer antisense oligonucleotides. *Sci Rep* **2016**, *6*, 30377. DOI: 10.1038/srep30377.
(69) Burel, S. A.; Hart, C. E.; Cauntay, P.; Hsiao, J.; Machemer, T.; Katz, M.; Watt, A.; Bui, H. H.; Younis, H.; Sabripour, M.; et al. Hepatotoxicity of high affinity gapmer antisense oligonucleotides is mediated by RNase H1 dependent promiscuous reduction of very long pre-mRNA transcripts. *Nucleic Acids Res* **2016**, *44* (5), 2093–2109. DOI: 10.1093/nar/gkv1210.
(70) Kamola, P. J.; Maratou, K.; Wilson, P. A.; Rush, K.; Mullaney, T.; McKevitt, T.; Evans, P.; Ridings, J.; Chowdhury, P.; Roulois, A.; et al. Strategies for In Vivo Screening and Mitigation of Hepatotoxicity Associated with Antisense Drugs. *Mol Ther Nucleic Acids* **2017**, *8*, 383–394. DOI: 10.1016/j.omtn.2017.07.003.
(71) Pallan, P. S.; Allerson, C. R.; Berdeja, A.; Seth, P. P.; Swayze, E. E.; Prakash, T. P.; Egli, M. Structure and nuclease resistance of 2',4'-constrained 2'-O-methoxyethyl (cMOE) and 2'-O-ethyl (cEt) modified DNAs. *Chem Commun (Camb)* **2012**, *48* (66), 8195–8197. DOI: 10.1039/c2cc32286b.
(72) Seth, P. P.; Vasquez, G.; Allerson, C. A.; Berdeja, A.; Gaus, H.; Kinberger, G. A.; Prakash, T. P.; Migawa, M. T.; Bhat, B.; Swayze, E. E. Synthesis and biophysical evaluation of 2',4'-constrained 2'O-methoxyethyl and 2',4'-constrained 2'O-ethyl nucleic acid analogues. *J Org Chem* **2010**, *75* (5), 1569–1581. DOI: 10.1021/jo902560f.
(73) Kakiuchi-Kiyota, S.; Whiteley, L. O.; Ryan, A. M.; Mathialagan, N. Development of a Method for Profiling Protein Interactions with LNA-Modified Antisense Oligonucleotides Using Protein Microarrays. *Nucleic Acid Ther* **2016**, *26* (2), 93–101. DOI: 10.1089/nat.2015.0576.
(74) Nielsen, P. E.; Egholm, M.; Berg, R. H.; Buchardt, O. Sequence-selective recognition of DNA by strand displacement with a thymine-substituted polyamide. *Science* **1991**, *254* (5037), 1497–1500. DOI: 10.1126/science.1962210.
(75) Ray, A.; Norden, B. Peptide nucleic acid (PNA): its medical and biotechnical applications and promise for the future. *FASEB J* **2000**, *14* (9), 1041–1060. DOI: 10.1096/fasebj.14.9.1041.
(76) Nielsen, P. E. PNA Technology. *Mol Biotechnol* **2004**, *26* (3), 233–248. DOI: 10.1385/MB:26:3:233.
(77) Oh, S. Y.; Ju, Y.; Park, H. A highly effective and long-lasting inhibition of miRNAs with PNA-based antisense oligonucleotides. *Mol Cells* **2009**, *28* (4), 341–345. DOI: 10.1007/s10059-009-0134-8.

(78) Story, S.; Bhaduri, S.; Ganguly, S.; Dakarapu, R.; Wicks, S. L.; Bhadra, J.; Kwange, S.; Arya, D. P. Understanding Antisense Oligonucleotide Efficiency in Inhibiting Prokaryotic Gene Expression. *ACS Infect Dis* **2024**, *10* (3), 971–987. DOI: 10.1021/acsinfecdis.3c00645.
(79) Park, S.; Kim, S. H.; Dezhbord, M.; Lee, E. H.; Jeon, Y.; Jung, D.; Gu, S. H.; Yu, C.; Lee, S. H.; Kim, S. C.; et al. Cell-permeable peptide nucleic acid antisense oligonucleotide platform targeting human betacoronaviruses. *Front Microbiol* **2023**, *14*, 1258091. DOI: 10.3389/fmicb.2023.1258091.
(80) Koppelhus, U.; Awasthi, S. K.; Zachar, V.; Holst, H. U.; Ebbesen, P.; Nielsen, P. E. Cell-dependent differential cellular uptake of PNA, peptides, and PNA-peptide conjugates. *Antisense Nucleic Acid Drug Dev* **2002**, *12* (2), 51–63. DOI: 10.1089/108729002760070795.
(81) Kilk, K.; Langel, U. Cellular delivery of peptide nucleic acid by cell-penetrating peptides. *Methods Mol Biol* **2005**, *298*, 131–141. DOI: 10.1385/1-59259-877-3:131.
(82) Summerton, J. Morpholino antisense oligomers: the case for an RNase H-independent structural type. *Biochim Biophys Acta* **1999**, *1489* (1), 141–158. DOI: 10.1016/s0167-4781(99)00150-5.
(83) Sang, A.; Zhuo, S.; Bochanis, A.; Manautou, J. E.; Bahal, R.; Zhong, X. B.; Rasmussen, T. P. Mechanisms of Action of the US Food and Drug Administration-Approved Antisense Oligonucleotide Drugs. *BioDrugs* **2024**, *38* (4), 511–526. DOI: 10.1007/s40259-024-00665-2.
(84) Ghosh, A.; Banerjee, A.; Gupta, S.; Sinha, S. A Unified Phosphoramidite Platform for the Synthesis of Morpholino Oligonucleotides and Diverse Chimeric Backbones. *J Am Chem Soc* **2024**, *146* (48), 32989–33001. DOI: 10.1021/jacs.4c09510.
(85) Summerton, J.; Weller, D. Morpholino antisense oligomers: design, preparation, and properties. *Antisense Nucleic Acid Drug Dev* **1997**, *7* (3), 187–195. DOI: 10.1089/oli.1.1997.7.187.
(86) Maksudov, F.; Kliuchnikov, E.; Pierson, D.; Ujwal, M. L.; Marx, K. A.; Chanda, A.; Barsegov, V. Therapeutic phosphorodiamidate morpholino oligonucleotides: Physical properties, solution structures, and folding thermodynamics. *Mol Ther Nucleic Acids* **2023**, *31*, 631–647. DOI: 10.1016/j.omtn.2023.02.007.
(87) Kang, H.; Chou, P. J.; Johnson, W. C., Jr.; Weller, D.; Huang, S. B.; Summerton, J. E. Stacking interactions of ApA analogues with modified backbones. *Biopolymers* **1992**, *32* (10), 1351–1363. DOI: 10.1002/bip.360321009.
(88) Hudziak, R. M.; Barofsky, E.; Barofsky, D. F.; Weller, D. L.; Huang, S. B.; Weller, D. D. Resistance of morpholino phosphorodiamidate oligomers to enzymatic degradation. *Antisense Nucleic Acid Drug Dev* **1996**, *6* (4), 267–272. DOI: 10.1089/oli.1.1996.6.267.
(89) Frank, D. E.; Schnell, F. J.; Akana, C.; El-Husayni, S. H.; Desjardins, C. A.; Morgan, J.; Charleston, J. S.; Sardone, V.; Domingos, J.; Dickson, G.; et al. Increased dystrophin production with golodirsen in patients with Duchenne muscular dystrophy. *Neurology* **2020**, *94* (21), e2270–e2282. DOI: 10.1212/WNL.0000000000009233.
(90) Cirak, S.; Arechavala-Gomeza, V.; Guglieri, M.; Feng, L.; Torelli, S.; Anthony, K.; Abbs, S.; Garralda, M. E.; Bourke, J.; Wells, D. J.; et al. Exon skipping and dystrophin restoration in patients with Duchenne muscular dystrophy after systemic phosphorodiamidate morpholino oligomer treatment: an open-label, phase 2, dose-escalation study. *Lancet* **2011**, *378* (9791), 595–605. DOI: 10.1016/S0140-6736(11)60756-3.
(91) Crooke, S. T.; Liang, X. H.; Baker, B. F.; Crooke, R. M. Antisense technology: A review. *J Biol Chem* **2021**, *296*, 100416. DOI: 10.1016/j.jbc.2021.100416.

(92) Juliano, R. L. Intracellular Trafficking and Endosomal Release of Oligonucleotides: What We Know and What We Don't. *Nucleic Acid Ther* **2018**, *28* (3), 166–177. DOI: 10.1089/nat.2018.0727.
(93) Hafez, I. M.; Maurer, N.; Cullis, P. R. On the mechanism whereby cationic lipids promote intracellular delivery of polynucleic acids. *Gene Ther* **2001**, *8* (15), 1188–1196. DOI: 10.1038/sj.gt.3301506.
(94) Egli, M.; Manoharan, M. Chemistry, structure and function of approved oligonucleotide therapeutics. *Nucleic Acids Res* **2023**, *51* (6), 2529–2573. DOI: 10.1093/nar/gkad067.
(95) Steirer, L. M.; Park, E. I.; Townsend, R. R.; Baenziger, J. U. The asialoglycoprotein receptor regulates levels of plasma glycoproteins terminating with sialic acid alpha2,6-galactose. *J Biol Chem* **2009**, *284* (6), 3777–3783. DOI: 10.1074/jbc.M808689200.
(96) Mukherjee, P.; Aksamitiene, E.; Alex, A.; Shi, J.; Bera, K.; Zhang, C.; Spillman, D. R.; Marjanovic, M.; Fazio, M.; Seth, P. P.; et al. Differential Uptake of Antisense Oligonucleotides in Mouse Hepatocytes and Macrophages Revealed by Simultaneous Two-Photon Excited Fluorescence and Coherent Raman Imaging. *Nucleic Acid Ther* **2022**, *32* (3), 163–176. DOI: 10.1089/nat.2021.0059.
(97) Baker, Y. R.; Thorpe, C.; Chen, J.; Poller, L. M.; Cox, L.; Kumar, P.; Lim, W. F.; Lie, L.; McClorey, G.; Epple, S.; et al. An LNA-amide modification that enhances the cell uptake and activity of phosphorothioate exon-skipping oligonucleotides. *Nat Commun* **2022**, *13* (1), 4036. DOI: 10.1038/s41467-022-31636-2.
(98) Rostovtsev, V. V.; Green, L. G.; Fokin, V. V.; Sharpless, K. B. A stepwise huisgen cycloaddition process: copper(I)-catalyzed regioselective "ligation" of azides and terminal alkynes. *Angew Chem Int Ed Engl* **2002**, *41* (14), 2596–2599. DOI: 10.1002/1521-3773(20020715)41:14<2596::AID-ANIE2596>3.0.CO;2-4.
(99) Tornoe, C. W.; Christensen, C.; Meldal, M. Peptidotriazoles on solid phase: [1,2,3]-triazoles by regiospecific copper(i)-catalyzed 1,3-dipolar cycloadditions of terminal alkynes to azides. *J Org Chem* **2002**, *67* (9), 3057–3064. DOI: 10.1021/jo011148j.
(100) Agard, N. J.; Prescher, J. A.; Bertozzi, C. R. A strain-promoted [3 + 2] azide-alkyne cycloaddition for covalent modification of biomolecules in living systems. *J Am Chem Soc* **2004**, *126* (46), 15046–15047. DOI: 10.1021/ja044996f.
(101) Sun, H.; Peng, X. Template-directed fluorogenic oligonucleotide ligation using "click" chemistry: detection of single nucleotide polymorphism in the human p53 tumor suppressor gene. *Bioconjug Chem* **2013**, *24* (7), 1226–1234. DOI: 10.1021/bc4001678.
(102) Wang, F.; Li, Y.; Li, W.; Chen, J.; Zhang, Q.; Anjum Shahzad, S.; Yu, C. A fluorescence turn-on detection of copper(II) based on the template-dependent click ligation of oligonucleotides. *Talanta* **2015**, *132*, 72–76. DOI: 10.1016/j.talanta.2014.08.064.
(103) Kumar, R.; El-Sagheer, A.; Tumpane, J.; Lincoln, P.; Wilhelmsson, L. M.; Brown, T. Template-directed oligonucleotide strand ligation, covalent intramolecular DNA circularization and catenation using click chemistry. *J Am Chem Soc* **2007**, *129* (21), 6859–6864. DOI: 10.1021/ja070273v.
(104) Kollaschinski, M.; Sobotta, J.; Schalk, A.; Frischmuth, T.; Graf, B.; Serdjukow, S. Efficient DNA Click Reaction Replaces Enzymatic Ligation. *Bioconjug Chem* **2020**, *31* (3), 507–512. DOI: 10.1021/acs.bioconjchem.9b00805.
(105) Mack, S.; Fouz, M. F.; Dey, S. K.; Das, S. R. Pseudo-Ligandless Click Chemistry for Oligonucleotide Conjugation. *Curr Protoc Chem Biol* **2016**, *8* (2), 83–95. DOI: 10.1002/cpch.1.

(106) Kukwikila, M.; Gale, N.; El-Sagheer, A. H.; Brown, T.; Tavassoli, A. Assembly of a biocompatible triazole-linked gene by one-pot click-DNA ligation. *Nat Chem* **2017**, *9* (11), 1089–1098. DOI: 10.1038/nchem.2850.
(107) El-Sagheer, A. H.; Brown, T. Click nucleic acid ligation: applications in biology and nanotechnology. *Acc Chem Res* **2012**, *45* (8), 1258–1267. DOI: 10.1021/ar200321n.
(108) Jawalekar, A. M.; Malik, S.; Verkade, J. M.; Gibson, B.; Barta, N. S.; Hodges, J. C.; Rowan, A.; van Delft, F. L. Oligonucleotide tagging for copper-free click conjugation. *Molecules* **2013**, *18* (7), 7346–7363. DOI: 10.3390/molecules18077346.
(109) Meyer, A.; Spinelli, N.; Dumy, P.; Vasseur, J. J.; Morvan, F.; Defrancq, E. Oligonucleotide sequential bis-conjugation via click-oxime and click-Huisgen procedures. *J Org Chem* **2010**, *75* (11), 3927–3930. DOI: 10.1021/jo100599m.
(110) Yamada, T.; Peng, C. G.; Matsuda, S.; Addepalli, H.; Jayaprakash, K. N.; Alam, M. R.; Mills, K.; Maier, M. A.; Charisse, K.; Sekine, M.; et al. Versatile site-specific conjugation of small molecules to siRNA using click chemistry. *J Org Chem* **2011**, *76* (5), 1198–1211. DOI: 10.1021/jo101761g.
(111) Chan, D. P.; Deleavey, G. F.; Owen, S. C.; Damha, M. J.; Shoichet, M. S. Click conjugated polymeric immuno-nanoparticles for targeted siRNA and antisense oligonucleotide delivery. *Biomaterials* **2013**, *34* (33), 8408–8415. DOI: 10.1016/j.biomaterials.2013.07.019.
(112) Pourceau, G.; Meyer, A.; Vasseur, J. J.; Morvan, F. Synthesis of mannose and galactose oligonucleotide conjugates by bi-click chemistry. *J Org Chem* **2009**, *74* (3), 1218–1222. DOI: 10.1021/jo802536q.
(113) Khatwani, S. L.; Kang, J. S.; Mullen, D. G.; Hast, M. A.; Beese, L. S.; Distefano, M. D.; Taton, T. A. Covalent protein-oligonucleotide conjugates by copper-free click reaction. *Bioorg Med Chem* **2012**, *20* (14), 4532–4539. DOI: 10.1016/j.bmc.2012.05.017.
(114) von Matt, P.; Lochmann, T.; Altmann, K.-H. Replacement of the phosphodiester linkage in oligonucleotides by heterocycles: synthesis of thymidine dinucleotide analogs with triazole-modified backbones. *Bioorganic & Medicinal Chemistry Letters* **1997**, *7* (12), 1549–1552. DOI: https://doi.org/10.1016/S0960-894X(97)00269-2.
(115) von Matt, P.; Altmann, K.-H. Replacement of the phosphodiester linkage in oligonucleotides by heterocycles: the effect of triazole- and imidazole-modified backbones on DNA/RNA duplex stability. *Bioorganic & Medicinal Chemistry Letters* **1997**, *7* (12), 1553–1556. DOI: https://doi.org/10.1016/S0960-894X(97)00270-9.
(116) Varizhuk, A.; Chizhov, A.; Smirnov, I.; Kaluzhny, D.; Florentiev, V. Triazole-Linked Oligonucleotides with Mixed-Base Sequences: Synthesis and Hybridization Properties. *European Journal of Organic Chemistry* **2012**, *2012* (11), 2173–2179. DOI: https://doi.org/10.1002/ejoc.201101700.
(117) Varizhuk, A. M.; Kaluzhny, D. N.; Novikov, R. A.; Chizhov, A. O.; Smirnov, I. P.; Chuvilin, A. N.; Tatarinova, O. N.; Fisunov, G. Y.; Pozmogova, G. E.; Florentiev, V. L. Synthesis of triazole-linked oligonucleotides with high affinity to DNA complements and an analysis of their compatibility with biosystems. *J Org Chem* **2013**, *78* (12), 5964–5969. DOI: 10.1021/jo400651k.
(118) Fujino, T.; Suzuki, T.; Okada, K.; Kogashi, K.; Yasumoto, K. I.; Sogawa, K.; Isobe, H. Chimeric RNA Oligonucleotides Incorporating Triazole-Linked Trinucleotides: Synthesis and Function as mRNA in Cell-Free Translation Reactions. *J Org Chem* **2016**, *81* (19), 8967–8976. DOI: 10.1021/acs.joc.6b01618.
(119) Dysko, A.; Baker, Y. R.; McClorey, G.; Wood, M. J. A.; Fenner, S.; Williams, G.; El-Sagheer, A.; Brown, T. Covalently attached intercalators restore duplex stability and splice-switching activity to triazole-modified oligonucleotides. *RSC Chem Biol* **2022**, *3* (6), 765–772. DOI: 10.1039/d2cb00100d.

(120) Varizhuk, A.; Chizhov, A.; Florentiev, V. Synthesis and hybridization data of oligonucleotide analogs with triazole internucleotide linkages, potential antiviral and antitumor agents. *Bioorg Chem* **2011**, *39* (3), 127–131. DOI: 10.1016/j.bioorg.2011.03.002.
(121) Isobe, H.; Fujino, T.; Yamazaki, N.; Guillot-Nieckowski, M.; Nakamura, E. Triazole-linked analogue of deoxyribonucleic acid ((TL)DNA): design, synthesis, and double-strand formation with natural DNA. *Org Lett* **2008**, *10* (17), 3729–3732. DOI: 10.1021/ol801230k.
(122) Sharma, V. K.; Singh, S. K.; Krishnamurthy, P. M.; Alterman, J. F.; Haraszti, R. A.; Khvorova, A.; Prasad, A. K.; Watts, J. K. Synthesis and biological properties of triazole-linked locked nucleic acid. *Chem Commun (Camb)* **2017**, *53* (63), 8906–8909. DOI: 10.1039/c7cc04092j.
(123) Kumar, P.; Truong, L.; Baker, Y. R.; El-Sagheer, A. H.; Brown, T. Synthesis, Affinity for Complementary RNA and DNA, and Enzymatic Stability of Triazole-Linked Locked Nucleic Acids (t-LNAs). *ACS Omega* **2018**, *3* (6), 6976–6987. DOI: 10.1021/acsomega.8b01086.
(124) Miller, P. S.; Yano, J.; Yano, E.; Carroll, C.; Jayaraman, K.; Ts'o, P. O. Nonionic nucleic acid analogues. Synthesis and characterization of dideoxyribonucleoside methylphosphonates. *Biochemistry* **1979**, *18* (23), 5134–5143. DOI: 10.1021/bi00590a017.
(125) Agrawal, S.; Goodchild, J. Oligodeoxynucleoside methylphosphonates: synthesis and enzymic degradation. *Tetrahedron Letters* **1987**, *28* (31), 3539–3542. DOI: https://doi.org/10.1016/S0040-4039(00)95529-1.
(126) Gryaznov, S. M.; Letsinger, R. L. Selective O-phosphitilation with nucleoside phosphoramidite reagents. *Nucleic Acids Res* **1992**, *20* (8), 1879–1882. DOI: 10.1093/nar/20.8.1879.
(127) Ota, K.; Nagao, K.; Hata, D.; Sugiyama, H.; Segawa, Y.; Tokunoh, R.; Seki, T.; Miyamoto, N.; Sasaki, Y.; Ohmiya, H. Synthesis of tertiary alkylphosphonate oligonucleotides through light-driven radical-polar crossover reactions. *Nat Commun* **2023**, *14* (1), 6856. DOI: 10.1038/s41467-023-42639-y.
(128) Miller, P. S.; Agris, C. H.; Murakami, A.; Reddy, P. M.; Spitz, S. A.; Ts'o, P. O. Preparation of oligodeoxyribonucleoside methylphosphonates on a polystyrene support. *Nucleic Acids Res* **1983**, *11* (18), 6225–6242. DOI: 10.1093/nar/11.18.6225.
(129) Hogrefe, R. I.; Vaghefi, M. M.; Reynolds, M. A.; Young, K. M.; Arnold, L. J., Jr. Deprotection of methylphosphonate oligonucleotides using a novel one-pot procedure. *Nucleic Acids Res* **1993**, *21* (9), 2031–2038. DOI: 10.1093/nar/21.9.2031.
(130) Miller, P. S. Oligonucleoside Methylphosphonates as Antisense Reagents. *Bio/Technology* **1991**, *9* (4), 358–362. DOI: 10.1038/nbt0491-358.
(131) Kandimalla, E. R.; Jamal, T.; and Agrawal, S. Synthesis and Properties of 2′-O-Methylribonucleotide Methylphosphonate Containing Chimeric Oligonucleotides. *Nucleosides and Nucleotides* **1995**, *14* (3-5), 1031–1035. DOI: 10.1080/15257779508012527.
(132) Guo, M.; Dong, Y.; and Agrawal, S. Mixed-Backbone Oligonucleotides Containing Segments of Deoxynucleosides Phosphorothioate and 2'-O-Methylribonucleosides Methylphosphonate: Synthesis and Properties. *Phosphorus, Sulfur, and Silicon and the Related Elements* **1999**, *144* (1), 363–366. DOI: 10.1080/10426509908546256.
(133) Reynolds, M. A.; Hogrefe, R. I.; Jaeger, J. A.; Schwartz, D. A.; Riley, T. A.; Marvin, W. B.; Daily, W. J.; Vaghefi, M. M.; Beck, T. A.; Knowles, S. K.; et al. Synthesis and thermodynamics of oligonucleotides containing chirally pure R(P) methylphosphonate linkages. *Nucleic Acids Res* **1996**, *24* (22), 4584–4591. DOI: 10.1093/nar/24.22.4584.

(134) Marcus-Sekura, C. J.; Woerner, A. M.; Shinozuka, K.; Zon, G.; Quinnan, G. V., Jr. Comparative inhibition of chloramphenicol acetyltransferase gene expression by antisense oligonucleotide analogues having alkyl phosphotriester, methylphosphonate and phosphorothioate linkages. *Nucleic Acids Res* **1987**, *15* (14), 5749–5763. DOI: 10.1093/nar/15.14.5749.
(135) Morvan, F.; Porumb, H.; Degols, G.; Lefebvre, I.; Pompon, A.; Sproat, B. S.; Rayner, B.; Malvy, C.; Lebleu, B.; Imbach, J. L. Comparative evaluation of seven oligonucleotide analogues as potential antisense agents. *J Med Chem* **1993**, *36* (2), 280–287. DOI: 10.1021/jm00054a013.
(136) Agrawal, S. Importance of nucleotide sequence and chemical modifications of antisense oligonucleotides. *Biochimica et Biophysica Acta (BBA) - Gene Structure and Expression* **1999**, *1489* (1), 53–67. DOI: https://doi.org/10.1016/S0167-4781(99)00141-4.
(137) Gray, G. D.; Basu, S.; Wickstrom, E. Transformed and immortalized cellular uptake of oligodeoxynucleoside phosphorothioates, 3'-alkylamino oligodeoxynucleotides, 2'-O-methyl oligoribonucleotides, oligodeoxynucleoside methylphosphonates, and peptide nucleic acids. *Biochem Pharmacol* **1997**, *53* (10), 1465–1476. DOI: 10.1016/s0006-2952(97)82440-9.
(138) Zhao, Q.; Matson, S.; Herrera, C. J.; Fisher, E.; Yu, H.; Krieg, A. M. Comparison of Cellular Binding and Uptake of Antisense Phosphodiester, Phosphorothioate, and Mixed Phosphorothioate and Methylphosphonate Oligonucleotides. *Antisense Research and Development* **1993**, *3* (1), 53–66. DOI: 10.1089/ard.1993.3.53.
(139) Shen, W.; De Hoyos, C. L.; Migawa, M. T.; Vickers, T. A.; Sun, H.; Low, A.; Bell, T. A., 3rd; Rahdar, M.; Mukhopadhyay, S.; Hart, C. E.; et al. Chemical modification of PS-ASO therapeutics reduces cellular protein-binding and improves the therapeutic index. *Nat Biotechnol* **2019**, *37* (6), 640–650. DOI: 10.1038/s41587-019-0106-2.
(140) Migawa, M. T.; Shen, W.; Wan, W. B.; Vasquez, G.; Oestergaard, M. E.; Low, A.; De Hoyos, C. L.; Gupta, R.; Murray, S.; Tanowitz, M.; et al. Site-specific replacement of phosphorothioate with alkyl phosphonate linkages enhances the therapeutic profile of gapmer ASOs by modulating interactions with cellular proteins. *Nucleic Acids Res* **2019**, *47* (11), 5465–5479. DOI: 10.1093/nar/gkz247.
(141) Vasquez, G.; Migawa, M. T.; Wan, W. B.; Low, A.; Tanowitz, M.; Swayze, E. E.; Seth, P. P. Evaluation of Phosphorus and Non-Phosphorus Neutral Oligonucleotide Backbones for Enhancing Therapeutic Index of Gapmer Antisense Oligonucleotides. *Nucleic Acid Ther* **2022**, *32* (1), 40–50. DOI: 10.1089/nat.2021.0064.
(142) Buntz, A.; Killian, T.; Schmid, D.; Seul, H.; Brinkmann, U.; Ravn, J.; Lindholm, M.; Knoetgen, H.; Haucke, V.; Mundigl, O. Quantitative fluorescence imaging determines the absolute number of locked nucleic acid oligonucleotides needed for suppression of target gene expression. *Nucleic Acids Res* **2019**, *47* (2), 953–969. DOI: 10.1093/nar/gky1158.
(143) He, C.; Migawa, M. T.; Chen, K.; Weston, T. A.; Tanowitz, M.; Song, W.; Guagliardo, P.; Iyer, K. S.; Bennett, C. F.; Fong, L. G.; et al. High-resolution visualization and quantification of nucleic acid-based therapeutics in cells and tissues using Nanoscale secondary ion mass spectrometry (NanoSIMS). *Nucleic Acids Res* **2021**, *49* (1), 1–14. DOI: 10.1093/nar/gkaa1112.
(144) Lacroix, A.; Vengut-Climent, E.; de Rochambeau, D.; Sleiman, H. F. Uptake and Fate of Fluorescently Labeled DNA Nanostructures in Cellular Environments: A Cautionary Tale. *ACS Cent Sci* **2019**, *5* (5), 882–891. DOI: 10.1021/acscentsci.9b00174.
(145) Mazur, C.; Powers, B.; Zasadny, K.; Sullivan, J. M.; Dimant, H.; Kamme, F.; Hesterman, J.; Matson, J.; Oestergaard, M.; Seaman, M.; et al. Brain pharmacology of

intrathecal antisense oligonucleotides revealed through multimodal imaging. *JCI Insight* **2019**, *4* (20). DOI: 10.1172/jci.insight.129240.
(146) Kavoosi, S.; Dey, D.; Islam, K. Synthesis of 5-Dihydroxyboryluridine Phosphoramidite and Its Site-Specific Incorporation into Oligonucleotides for Probing Thymine DNA Glycosylase. *Organic Letters* **2019**, *21* (17), 6614–6618. DOI: 10.1021/acs.orglett.9b02042.
(147) Kvach, M. V.; Tsybulsky, D. A.; Shmanai, V. V.; Prokhorenko, I. A.; Stepanova, I. A.; Korshun, V. A. Non-nucleoside phosphoramidites of xanthene dyes (FAM, JOE, and TAMRA) for oligonucleotide labeling. *Curr Protoc Nucleic Acid Chem* **2013**, *Chapter 4*, 4 55 51–54 55 33. DOI: 10.1002/0471142700.nc0455s52.
(148) Lebedeva, N. A.; Anarbaev, R. O.; Kupryushkin, M. S.; Rechkunova, N. I.; Pyshnyi, D. V.; Stetsenko, D. A.; Lavrik, O. I. Design of a New Fluorescent Oligonucleotide-Based Assay for a Highly Specific Real-Time Detection of Apurinic/Apyrimidinic Site Cleavage by Tyrosyl-DNA Phosphodiesterase 1. *Bioconjugate Chem* **2015**, *26* (10), 2046–2053. DOI: 10.1021/acs.bioconjchem.5b00451.
(149) Meares, A.; Susumu, K.; Mathur, D.; Lee, S. H.; Mass, O. A.; Lee, J.; Pensack, R. D.; Yurke, B.; Knowlton, W. B.; Melinger, J. S.; et al. Synthesis of Substituted Cy5 Phosphoramidite Derivatives and Their Incorporation into Oligonucleotides Using Automated DNA Synthesis. *Acs Omega* **2022**, *7* (13), 11002–11016. DOI: 10.1021/acsomega.1c06921.
(150) Theisen, P.; Mccollum, C.; Upadhya, K.; Jacobson, K.; Vu, H. N.; Andrus, A. Fluorescent Dye Phosphoramidite Labeling of Oligonucleotides. *Tetrahedron Letters* **1992**, *33* (35), 5033–5036. DOI: Doi 10.1016/S0040-4039(00)61181-4.
(151) Li, G.; Moellering, R. E. A Concise, Modular Antibody-Oligonucleotide Conjugation Strategy Based on Disuccinimidyl Ester Activation Chemistry. *Chembiochem* **2019**, *20* (12), 1599–1605. DOI: 10.1002/cbic.201900027.
(152) Wang, Z.; Bian, N.; Qian, X.; Giese, R. W. N-hydroxysuccinimide ester labeling 5'-aminoalkyl DNA oligomers: reaction conditions and purification. *J Chromatogr A* **1998**, *806* (1), 93–95. DOI: 10.1016/s0021-9673(98)00093-4.
(153) Astakhova, I. K.; Hansen, L. H.; Vester, B.; Wengel, J. Peptide-LNA oligonucleotide conjugates. *Org Biomol Chem* **2013**, *11* (25), 4240–4249. DOI: 10.1039/c3ob40786a.
(154) Wang, Q.; Wang, W.; Peng, X. L.; Ge, G. R.; Li, W. H.; Zhu, C.; Chen, X.; Guo, S.; Li, N.; Yang, H. L.; et al. Engineering Peptide-Oligonucleotide Nano-Conjugates via Click Reaction as Self-Delivery System for Gene Therapy of Inflammatory Arthritis. *Adv Funct Mater* **2024**, *34* (41). DOI: 10.1002/adfm.202406503.
(155) Astakhova, I. K.; Wengel, J. Interfacing click chemistry with automated oligonucleotide synthesis for the preparation of fluorescent DNA probes containing internal xanthene and cyanine dyes. *Chemistry* **2013**, *19* (3), 1112–1122. DOI: 10.1002/chem.201202621.
(156) Doe, E.; Hayth, H. L.; Brumett, R.; Khisamutdinov, E. F. Effective, Rapid, and Small-Scale Bioconjugation and Purification of "Clicked" Small-Molecule DNA Oligonucleotide for Nucleic Acid Nanoparticle Functionalization. *Int J Mol Sci* **2023**, *24* (5). DOI: 10.3390/ijms24054797.
(157) Marks, I. S.; Kang, J. S.; Jones, B. T.; Landmark, K. J.; Cleland, A. J.; Taton, T. A. Strain-promoted "click" chemistry for terminal labeling of DNA. *Bioconjug Chem* **2011**, *22* (7), 1259–1263. DOI: 10.1021/bc1003668.
(158) Schwechheimer, C.; Doll, L.; Wagenknecht, H. A. Synthesis of Dye-Modified Oligonucleotides via Copper(I)-Catalyzed Alkyne Azide Cycloaddition Using On- and Off-Bead Approaches. *Curr Protoc Nucleic Acid Chem* **2018**, *72* (1), 4 80 81–84 80 13. DOI: 10.1002/cpnc.47.

(159) Seela, F.; Pujari, S. S. Azide-alkyne "click" conjugation of 8-aza-7-deazaadenine-DNA: synthesis, duplex stability, and fluorogenic dye labeling. *Bioconjug Chem* **2010**, *21* (9), 1629–1641. DOI: 10.1021/bc100090y.
(160) Gong, H. B.; Holcomb, I.; Ooi, A.; Wang, X. H.; Majonis, D.; Unger, M. A.; Ramakrishnan, R. Simple Method To Prepare Oligonucleotide-Conjugated Antibodies and Its Application in Multiplex Protein Detection in Single Cells. *Bioconjugate Chem* **2016**, *27* (1), 217–225. DOI: 10.1021/acs.bioconjchem.5b00613.
(161) Wiener, J.; Kokotek, D.; Rosowski, S.; Lickert, H.; Meier, M. Preparation of single- and double-oligonucleotide antibody conjugates and their application for protein analytics. *Sci Rep-Uk* **2020**, *10* (1). DOI: ARTN 1457 10.1038/s41598-020-58238-6.
(162) Jones, J. A.; McMahon, N. P.; Zheng, T.; Eng, J.; Chin, K.; Kwon, S. J.; Nederlof, M. A.; Gray, J. W.; Gibbs, S. L. Oligonucleotide conjugated antibody strategies for cyclic immunostaining. *Sci Rep-Uk* **2021**, *11* (1). DOI: ARTN 23844 10.1038/s41598-021-03135-9.
(163) *BaseClick DNA and RNA Experts*. BaseClick, 2025.
(164) Lietard, J.; Meyer, A.; Vasseur, J. J.; Morvan, F. New strategies for cyclization and bicyclization of oligonucleotides by click chemistry assisted by microwaves. *J Org Chem* **2008**, *73* (1), 191–200. DOI: 10.1021/jo702177c.
(165) Pourceau, G.; Meyer, A.; Vasseur, J. J.; Morvan, F. Azide solid support for 3'-conjugation of oligonucleotides and their circularization by click chemistry. *J Org Chem* **2009**, *74* (17), 6837–6842. DOI: 10.1021/jo9014563.
(166) Gerowska, M.; Hall, L.; Richardson, J.; Shelbourne, M.; Brown, T. Efficient reverse click labeling of azide oligonucleotides with multiple alkynyl Cy-Dyes applied to the synthesis of HyBeacon probes for genetic analysis. *Tetrahedron* **2012**, *68* (3), 857–864. DOI: 10.1016/j.tet.2011.11.041.
(167) Technologies, B. *5'-TFA-Amino Modifier C6 CE-Phosphoramidite*. 2026.
(168) Scientific, T. F. *NHS-Azide*. 2026.
(169) Kashyap, D.; Cadeddu, M.; Oliver, P. L.; Milne, T. A.; Booth, M. J. Harnessing BET-Bromodomain Assisted Nuclear Import for Targeted Subcellular Localization and Enhanced Efficacy of Antisense Oligonucleotides. *J Am Chem Soc* **2025**, *147* (32), 29478–29488. DOI: 10.1021/jacs.5c09544.
(170) Miller, G. P.; Kool, E. T. Versatile 5′-functionalization of oligonucleotides on solid support:: Amines, azides, thiols, and thioethers via phosphorus chemistry. *Journal of Organic Chemistry* **2004**, *69* (7), 2404–2410. DOI: DOI 10.1021/jo035765e.
(171) El-Sagheer, A. H.; Sanzone, A. P.; Gao, R.; Tavassoli, A.; Brown, T. Biocompatible artificial DNA linker that is read through by DNA polymerases and is functional in Escherichia coli. *Proc Natl Acad Sci U S A* **2011**, *108* (28), 11338–11343. DOI: 10.1073/pnas.1101519108.
(172) Paredes, E.; Das, S. R. Click chemistry for rapid labeling and ligation of RNA. *Chembiochem* **2011**, *12* (1), 125–131. DOI: 10.1002/cbic.201000466.
(173) Collotta, D.; Bertocchi, I.; Chiapello, E.; Collino, M. Antisense oligonucleotides: a novel Frontier in pharmacological strategy. *Front Pharmacol* **2023**, *14*. DOI: ARTN 1304342 10.3389/fphar.2023.1304342.
(174) Dellinger, D. J.; Timár, Z.; Myerson, J.; Sierzchala, A. B.; Turner, J.; Ferreira, F.; Kupihár, Z.; Dellinger, G.; Hill, K. W.; Powell, J. A.; et al. Streamlined Process for the Chemical Synthesis of RNA Using 2′-Thionocarbamate-Protected Nucleoside Phosphoramidites in the Solid Phase. *J Am Chem Soc* **2011**, *133* (30), 11540–11556. DOI: 10.1021/ja201561z.
(175) Rosemeyer, H.; Toth, G.; Golankiewicz, B.; Kazimierczuk, Z.; Bourgeois, W.; Kretschmer, U.; Muth, H. P.; Seela, F. Syn Anti-Conformational Analysis of Regular and Modified Nucleosides by 1d H-1 Noe Difference Spectroscopy - a Simple

Graphical-Method Based on Conformationally Rigid Molecules. *Journal of Organic Chemistry* **1990**, *55* (22), 5784–5790. DOI: DOI 10.1021/jo00309a024.
(176) Sokoloski, J. E.; Godfrey, S. A.; Dombrowski, S. E.; Bevilacqua, P. C. Prevalence of nucleobases in the active sites of functional RNAs. *Rna* **2011**, *17* (10), 1775–1787. DOI: 10.1261/rna.2759911.
(177) Egli, M.; Manoharan, M. Chemistry, structure and function of approved oligonucleotide therapeutics. *Nucleic Acids Research* **2023**, *51* (6), 2529–2573. DOI: 10.1093/nar/gkad067.
(178) Evich, M.; Spring-Connell, A. M.; Germann, M. W. Impact of modified ribose sugars on nucleic acid conformation and function. *Heterocycl Commun* **2017**, *23* (3), 155–165. DOI: 10.1515/hc-2017-0056.
(179) Koshkin, A. A.; Nielsen, P.; Meldgaard, M.; Rajwanshi, V. K.; Singh, S. K.; Wengel, J. LNA (locked nucleic acid):: An RNA mimic forming exceedingly stable LNA:LNA duplexes. *J Am Chem Soc* **1998**, *120* (50), 13252–13253. DOI: DOI 10.1021/ja9822862.
(180) Worrell, B. T.; Malik, J. A.; Fokin, V. V. Direct Evidence of a Dinuclear Copper Intermediate in Cu(I)-Catalyzed Azide-Alkyne Cycloadditions. *Science* **2013**, *340* (6131), 457–460. DOI: DOI 10.1126/science.1229506.
(181) Seela, F.; Sirivolu, V. R. Nucleosides and oligonucleotides with diynyl side chains: the huisgen-sharpless cycloaddition "click reaction" performed on DNA and their constituents. *Nucleosides Nucleotides Nucleic Acids* **2007**, *26* (6-7), 597–601. DOI: 10.1080/15257770701490308.
(182) Seela, F.; Sirivolu, V. R. DNA containing side chains with terminal triple bonds: Base-pair stability and functionalization of alkynylated pyrimidines and 7-deazapurines. *Chem Biodivers* **2006**, *3* (5), 509–514. DOI: 10.1002/cbdv.200690054.
(183) Gramlich, P. M.; Warncke, S.; Gierlich, J.; Carell, T. Click-click-click: single to triple modification of DNA. *Angew Chem Int Ed Engl* **2008**, *47* (18), 3442–3444. DOI: 10.1002/anie.200705664.
(184) Seo, T. S.; Li, Z.; Ruparel, H.; Ju, J. Click chemistry to construct fluorescent oligonucleotides for DNA sequencing. *J Org Chem* **2003**, *68* (2), 609–612. DOI: 10.1021/jo026615r.
(185) Honcharenko, D.; Druceikaite, K.; Honcharenko, M.; Bollmark, M.; Tedebark, U.; Stromberg, R. New Alkyne and Amine Linkers for Versatile Multiple Conjugation of Oligonucleotides. *ACS Omega* **2021**, *6* (1), 579–593. DOI: 10.1021/acsomega.0c05075.
(186) Wenska, M.; Alvira, M.; Steunenberg, P.; Stenberg, A.; Murtola, M.; Stromberg, R. An activated triple bond linker enables 'click' attachment of peptides to oligonucleotides on solid support. *Nucleic Acids Res* **2011**, *39* (20), 9047–9059. DOI: 10.1093/nar/gkr603.
(187) Epple, S.; Modi, A.; Baker, Y. R.; Wegrzyn, E.; Traore, D.; Wanat, P.; Tyburn, A. E. S.; Shivalingam, A.; Taemaitree, L.; El-Sagheer, A. H.; et al. A New 1,5-Disubstituted Triazole DNA Backbone Mimic with Enhanced Polymerase Compatibility. *J Am Chem Soc* **2021**, *143* (39), 16293–16301. DOI: 10.1021/jacs.1c08057.
(188) Kumar, P.; El-Sagheer, A. H.; Truong, L.; Brown, T. Locked nucleic acid (LNA) enhances binding affinity of triazole-linked DNA towards RNA. *Chem Commun (Camb)* **2017**, *53* (63), 8910–8913. DOI: 10.1039/c7cc05159j.
(189) El-Sagheer, A. H.; Brown, T. New strategy for the synthesis of chemically modified RNA constructs exemplified by hairpin and hammerhead ribozymes. *Proc Natl Acad Sci U S A* **2010**, *107* (35), 15329–15334. DOI: 10.1073/pnas.1006447107.
(190) Ora, M.; Peltomäki, M.; Oivanen, M.; Lönnberg, H. Metal-ion-promoted cleavage, isomerization, and desulfurization of the diastereomeric

phosphoromonothioate analogues of uridylyl(3′,5′)uridine. *Journal of Organic Chemistry* **1998**, *63* (9), 2939–2947. DOI: DOI 10.1021/jo972112n.
(191) Honcharenko, M.; Honcharenko, D.; Stromberg, R. Efficient Conjugation to Phosphorothioate Oligonucleotides by Cu-Catalyzed Huisgen 1,3-Dipolar Cycloaddition. *Bioconjug Chem* **2019**, *30* (6), 1622–1628. DOI: 10.1021/acs.bioconjchem.9b00217.
(192) Rich, A. The double helix: a tale of two puckers. *Nat Struct Biol* **2003**, *10* (4), 247–249. DOI: 10.1038/nsb0403-247.
(193) Herrero-Galán, E.; Fuentes-Perez, M. E.; Carrasco, C.; Valpuesta, J. M.; Carrascosa, J. L.; Moreno-Herrero, F.; Arias-Gonzalez, J. R. Mechanical Identities of RNA and DNA Double Helices Unveiled at the Single-Molecule Level. *J Am Chem Soc* **2013**, *135* (1), 122–131. DOI: 10.1021/ja3054755.
(194) Potaman VN, S. R. *DNA: Alternative Conformations and Biology*. Landes Bioscience, 2000–2013. https://www.ncbi.nlm.nih.gov/books/NBK6545/.
(195) Barchi, J. J.; Jeong, L. S.; Siddiqui, M. A.; Marquez, V. E. Conformational analysis of the complete series of 2' and 3' monofluorinated dideoxyuridines. *J Biochem Bioph Meth* **1997**, *34* (1), 11–29. DOI: Doi 10.1016/S0165-022x(96)00032-2.
(196) Manoharan, M.; Akinc, A.; Pandey, R. K.; Qin, J.; Hadwiger, P.; John, M.; Mills, K.; Charisse, K.; Maier, M. A.; Nechev, L.; et al. Unique Gene-Silencing and Structural Properties of 2′-Fluoro-Modified siRNAs. *Angew Chem Int Edit* **2011**, *50* (10), 2284–2288. DOI: 10.1002/anie.201006519.
(197) Pallan, P. S.; Greene, E. M.; Jicman, P. A.; Pandey, R. K.; Manoharan, M.; Rozners, E.; Egli, M. Unexpected origins of the enhanced pairing affinity of 2′-fluoro-modified RNA. *Nucleic Acids Research* **2011**, *39* (8), 3482–3495. DOI: 10.1093/nar/gkq1270.
(198) Zengin Kurt, B.; Dhara, D.; El-Sagheer, A. H.; Brown, T. Synthesis and Properties of Oligonucleotides Containing LNA-Sulfamate and Sulfamide Backbone Linkages. *Org Lett* **2024**, *26* (19), 4137–4141. DOI: 10.1021/acs.orglett.4c01232.
(199) Vinjamuri, B. P.; Pan, J. Y.; Peng, P. A Review on Commercial Oligonucleotide Drug Products. *J Pharm Sci-Us* **2024**, *113* (7), 1749–1768. DOI: 10.1016/j.xphs.2024.04.021.
(200) Koenig, M.; Hoffman, E. P.; Bertelson, C. J.; Monaco, A. P.; Feener, C.; Kunkel, L. M. Complete Cloning of the Duchenne Muscular-Dystrophy (Dmd) Cdna and Preliminary Genomic Organization of the Dmd Gene in Normal and Affected Individuals. *Cell* **1987**, *50* (3), 509–517. DOI: Doi 10.1016/0092-8674(87)90504-6.
(201) Kolwicz, S. C.; Hall, J. K.; Moussavi-Harami, F.; Chen, X. L.; Hauschka, S. D.; Chamberlain, J. S.; Regnier, M.; Odom, G. L. Gene Therapy Rescues Cardiac Dysfunction in Duchenne Muscular Dystrophy Mice by Elevating Cardiomyocyte Deoxy-Adenosine Triphosphate. *Jacc-Basic Transl Sc* **2019**, *4* (7), 778–791. DOI: 10.1016/j.jacbts.2019.06.006.
(202) Sun, C. M.; Shen, L. A.; Zhang, Z.; Xie, X. Therapeutic Strategies for Duchenne Muscular Dystrophy: An Update. *Genes-Basel* **2020**, *11* (8). DOI: ARTN 837 10.3390/genes11080837.
(203) Lim, K. R.; Maruyama, R.; Yokota, T. Eteplirsen in the treatment of Duchenne muscular dystrophy. *Drug Des Devel Ther* **2017**, *11*, 533–545. DOI: 10.2147/DDDT.S97635.
(204) Manzur, A. Y.; Kinali, M.; Muntoni, F. Update on the management of Duchenne muscular dystrophy. *Arch Dis Child* **2008**, *93* (11), 986–990. DOI: 10.1136/adc.2007.118141.
(205) Ricotti, V.; Ridout, D. A.; Scott, E.; Quinlivan, R.; Robb, S. A.; Manzur, A. Y.; Muntoni, F.; NorthStar Clinical, N. Long-term benefits and adverse effects of

intermittent versus daily glucocorticoids in boys with Duchenne muscular dystrophy. *J Neurol Neurosurg Psychiatry* **2013**, *84* (6), 698–705. DOI: 10.1136/jnnp-2012-303902.
(206) Gloss, D.; Moxley, R. T., 3rd; Ashwal, S.; Oskoui, M. Practice guideline update summary: Corticosteroid treatment of Duchenne muscular dystrophy: Report of the Guideline Development Subcommittee of the American Academy of Neurology. *Neurology* **2016**, *86* (5), 465–472. DOI: 10.1212/WNL.0000000000002337.
(207) Roberts, T. C.; Wood, M. J. A.; Davies, K. E. Therapeutic approaches for Duchenne muscular dystrophy. *Nature Reviews Drug Discovery* **2023**, *22* (11), 917–934. DOI: 10.1038/s41573-023-00775-6.
(208) Chwalenia, K.; Wood, M. J. A.; Roberts, T. C. Progress and prospects in antisense oligonucleotide-mediated exon skipping therapies for Duchenne muscular dystrophy. *J Muscle Res Cell Motil* **2025**. DOI: 10.1007/s10974-024-09688-2.
(209) Gemignani, F.; Sazani, P.; Morcos, P.; Kole, R. Temperature-dependent splicing of β-globin pre-mRNA. *Nucleic Acids Research* **2002**, *30* (21), 4592–4598. DOI: DOI 10.1093/nar/gkf607.
(210) Kang, S. H.; Cho, M. J.; Kole, R. Up-regulation of luciferase gene expression with antisense oligonucleotides: Implications and applications in functional assay developments. *Biochemistry* **1998**, *37* (18), 6235–6239. DOI: DOI 10.1021/bi980300h.
(211) Zhou, Z. X.; Liu, X. R.; Zhu, D. C.; Wang, Y.; Zhang, Z.; Zhou, X. F.; Qiu, N. S.; Chen, X. S.; Shen, Y. Q. Nonviral cancer gene therapy: Delivery cascade and vector nanoproperty integration. *Adv Drug Deliver Rev* **2017**, *115*, 115–154. DOI: 10.1016/j.addr.2017.07.021.
(212) Koynova, R.; Tenchov, B.; Wang, L.; MacDonald, R. C. Hydrophobic Moiety of Cationic Lipids Strongly Modulates Their Transfection Activity. *Mol Pharmaceut* **2009**, *6* (3), 951–958. DOI: 10.1021/mp8002573.
(213) Gangopadhyay, S.; Das, G.; Gupta, S.; Ghosh, A.; Bagale, S. S.; Roy, P. K.; Mandal, M.; Harikrishna, S.; Sinha, S.; Gore, K. R. 4′-Acetamidomethyl-2′-methoxyethyl Nucleic Acid Modifications Improve Thermal Stability, Nuclease Resistance, Potency, and hAgo2 Binding of Small Interfering RNAs. *Journal of Organic Chemistry* **2024**, *89* (6), 3747–3768. DOI: 10.1021/acs.joc.3c02506.
(214) Hill, A. C.; Hall, J. The MOE Modification of RNA: Origins and Widescale Impact on the Oligonucleotide Therapeutics Field. *Helv Chim Acta* **2023**, *106* (3). DOI: 10.1002/hlca.202200169.
(215) Cruz-León, S.; Vanderlinden, W.; Müller, P.; Forster, T.; Staudt, G.; Lin, Y. Y.; Lipfert, J.; Schwierz, N. Twisting DNA by salt. *Nucleic Acids Research* **2022**, *50* (10), 5726–5738. DOI: 10.1093/nar/gkac445.
(216) Valberg, L. S.; Holt, J. M.; Paulson, E.; Szivek, J. Spectrochemical Analysis of Sodium Potassium Calcium Magnesium Copper and Zinc in Normal Human Erythrocytes. *J Clin Invest* **1965**, *44* (3), 379–+. DOI: Doi 10.1172/Jci105151.
(217) Muses, S.; Morgan, J. E.; Wells, D. J. A New Extensively Characterised Conditionally Immortal Muscle Cell-Line for Investigating Therapeutic Strategies in Muscular Dystrophies. *Plos One* **2011**, *6* (9). DOI: ARTN e24826 10.1371/journal.pone.0024826.
(218) Doran, T. J.; Lu, P. J.; Vanier, G. S.; Collins, M. J.; Wu, B.; Lu, Q. L. Microwave irradiation enhances gene and oligonucleotide delivery and induces effective exon skipping in myoblasts. *Gene Therapy* **2009**, *16* (1), 119–126. DOI: 10.1038/gt.2008.144.
(219) Dowdy, S. F. Endosomal escape of RNA therapeutics: How do we solve this rate-limiting problem? *Rna* **2023**, *29* (4), 396–401. DOI: 10.1261/rna.079507.122.
(220) Wadia, J. S.; Stan, R. V.; Dowdy, S. F. Transducible TAT-HA fusogenic peptide enhances escape of TAT-fusion proteins after lipid raft macropinocytosis. *Nat Med* **2004**, *10* (3), 310–315. DOI: 10.1038/nm996.

(221) Lonn, P.; Kacsinta, A. D.; Cui, X. S.; Hamil, A. S.; Kaulich, M.; Gogoi, K.; Dowdy, S. F. Enhancing Endosomal Escape for Intracellular Delivery of Macromolecular Biologic Therapeutics. *Sci Rep* **2016**, *6*, 32301. DOI: 10.1038/srep32301.
(222) Brown, C. R.; Gupta, S.; Qin, J.; Racie, T.; He, G.; Lentini, S.; Malone, R.; Yu, M.; Matsuda, S.; Shulga-Morskaya, S.; et al. Investigating the pharmacodynamic durability of GalNAc-siRNA conjugates. *Nucleic Acids Res* **2020**, *48* (21), 11827–11844. DOI: 10.1093/nar/gkaa670.
(223) Juliano, R. L. Chemical Manipulation of the Endosome Trafficking Machinery: Implications for Oligonucleotide Delivery. *Biomedicines* **2021**, *9* (5). DOI: 10.3390/biomedicines9050512.
(224) Dowdy, S. F.; Setten, R. L.; Cui, X. S.; Jadhav, S. G. Delivery of RNA Therapeutics: The Great Endosomal Escape! *Nucleic Acid Ther* **2022**, *32* (5), 361–368. DOI: 10.1089/nat.2022.0004.
(225) Li, J.; Dhilipkannah, P.; Holden, V. K.; Sachdeva, A.; Todd, N. W.; Jiang, F. Dysregulation of lncRNA MALAT1 Contributes to Lung Cancer in African Americans by Modulating the Tumor Immune Microenvironment. *Cancers (Basel)* **2024**, *16* (10). DOI: 10.3390/cancers16101876.
(226) Mazarei, M.; Shahabi Rabori, V.; Ghasemi, N.; Salehi, M.; Rayatpisheh, N.; Jahangiri, N.; Saberiyan, M. LncRNA MALAT1 signaling pathway and clinical applications in overcome on cancers metastasis. *Clin Exp Med* **2023**, *23* (8), 4457–4472. DOI: 10.1007/s10238-023-01179-x.
(227) Arun, G.; Aggarwal, D.; Spector, D. L. MALAT1 Long Non-Coding RNA: Functional Implications. *Noncoding RNA* **2020**, *6* (2). DOI: 10.3390/ncrna6020022.
(228) Schmidt, L. H.; Spieker, T.; Koschmieder, S.; Schaffers, S.; Humberg, J.; Jungen, D.; Bulk, E.; Hascher, A.; Wittmer, D.; Marra, A.; et al. The long noncoding MALAT-1 RNA indicates a poor prognosis in non-small cell lung cancer and induces migration and tumor growth. *J Thorac Oncol* **2011**, *6* (12), 1984–1992. DOI: 10.1097/JTO.0b013e3182307eac.
(229) Dizaji, B. F. Strategies to target long non-coding RNAs in cancer treatment: progress and challenges. *Egyptian J Med Human* **2020**, *21* (1). DOI: ARTN 41 10.1186/s43042-020-00074-4.
(230) Arun, G.; Diermeier, S.; Akerman, M.; Chang, K. C.; Wilkinson, J. E.; Hearn, S.; Kim, Y.; MacLeod, A. R.; Krainer, A. R.; Norton, L.; et al. Differentiation of mammary tumors and reduction in metastasis upon Malat1 lncRNA loss. *Genes Dev* **2016**, *30* (1), 34–51. DOI: 10.1101/gad.270959.115.
(231) Adewunmi, O.; Shen, Y.; Zhang, X. H.; Rosen, J. M. Targeted Inhibition of lncRNA Malat1 Alters the Tumor Immune Microenvironment in Preclinical Syngeneic Mouse Models of Triple-Negative Breast Cancer. *Cancer Immunol Res* **2023**, *11* (11), 1462–1479. DOI: 10.1158/2326-6066.CIR-23-0045.
(232) Gutschner, T.; Hammerle, M.; Eissmann, M.; Hsu, J.; Kim, Y.; Hung, G.; Revenko, A.; Arun, G.; Stentrup, M.; Gross, M.; et al. The noncoding RNA MALAT1 is a critical regulator of the metastasis phenotype of lung cancer cells. *Cancer Res* **2013**, *73* (3), 1180–1189. DOI: 10.1158/0008-5472.CAN-12-2850.
(233) Pirie, E.; Ray, S.; Pan, C.; Fu, W.; Powers, A. F.; Polikoff, D.; Miller, C. M.; Kudrna, K. M.; Harris, E. N.; Lusis, A. J.; et al. Mouse genome-wide association studies and systems genetics uncover the genetic architecture associated with hepatic pharmacokinetic and pharmacodynamic properties of a constrained ethyl antisense oligonucleotide targeting Malat1. *PLoS Genet* **2018**, *14* (10), e1007732. DOI: 10.1371/journal.pgen.1007732.

(234) Xiao, W.; Halabi, R.; Lin, C. H.; Nazim, M.; Yeom, K. H.; Black, D. L. The lncRNA Malat1 is trafficked to the cytoplasm as a localized mRNA encoding a small peptide in neurons. *Genes Dev* **2024**, *38* (7-8), 294–307. DOI: 10.1101/gad.351557.124.
(235) Zhang, C. L.; Qin, Y.; Wu, Y.; Xu, H.; Shu, Y. Long non-coding RNA in hematological malignancies and its clinical applications. *Chinese Med J-Peking* **2024**, *137* (10), 1151–1159. DOI: 10.1097/Cm9.0000000000003090.
(236) El Bassit, G.; Patel, R. S.; Carter, G.; Shibu, V.; Patel, A. A.; Song, S. J.; Murr, M.; Cooper, D. R.; Bickford, P. C.; Patel, N. A. MALAT1 in Human Adipose Stem Cells Modulates Survival and Alternative Splicing of PKCδII in HT22 Cells. *Endocrinology* **2017**, *158* (1), 183–195. DOI: 10.1210/en.2016-1819.
(237) Li, G. Z.; Meng, G. X.; Pan, G. Q.; Zhang, X.; Yan, L. J.; Li, R. Z.; Ding, Z. N.; Tan, S. Y.; Wang, D. X.; Tian, B. W.; et al. MALAT1/ mir-1-3p mediated BRF2 expression promotes HCC progression via inhibiting the LKB1/AMPK signaling pathway (vol 23, 188, 2023). *Cancer Cell Int* **2024**, *24* (1). DOI: ARTN 260 10.1186/s12935-024-03399-x.
(238) Amodio, N.; Stamato, M. A.; Juli, G.; Morelli, E.; Fulciniti, M.; Manzoni, M.; Taiana, E.; Agnelli, L.; Cantafio, M. E. G.; Romeo, E.; et al. Drugging the lncRNA MALAT1 via LNA gapmeR ASO inhibits gene expression of proteasome subunits and triggers anti-multiple myeloma activity. *Leukemia* **2018**, *32* (9), 1948–1957. DOI: 10.1038/s41375-018-0067-3.
(239) Iwashita, S.; Shoji, T.; Koizumi, M. Evaluating the Knockdown Activity of MALAT1 ENA Gapmers In Vitro. *Gapmers* **2020**, *2176*, 155–161. DOI: 10.1007/978-1-0716-0771-8_11.
(240) Harding, P. L.; Fall, A. M.; Honeyman, K.; Fletcher, S.; Wilton, S. D. The influence of antisense oligonucleotide length on dystrophin exon skipping. *Mol Ther* **2007**, *15* (1), 157–166. DOI: 10.1038/sj.mt.6300006.
(241) Le, B. T.; Hornum, M.; Sharma, P. K.; Nielsen, P.; Veedu, R. N. Nucleobase-modified antisense oligonucleotides containing 5-(phenyltriazol)-2′-deoxyuridine nucleotides induce exon-skipping. *Rsc Adv* **2017**, *7* (86), 54542–54545. DOI: 10.1039/c7ra10964d.
(242) Le, B. T.; Murayama, K.; Shabanpoor, F.; Asanuma, H.; Veedu, R. N. Antisense oligonucleotide modified with serinol nucleic acid (SNA) induces exon skipping in myotubes. *Rsc Adv* **2017**, *7* (54), 34049–34052. DOI: 10.1039/c7ra06091b.
(243) Lehto, T.; Alvarez, A. C.; Gauck, S.; Gait, M. J.; Coursindel, T.; Wood, M. J. A.; Lebleu, B.; Boisguerin, P. Cellular trafficking determines the exon skipping activity of Pip6a-PMO in skeletal and cardiac muscle cells. *Nucleic Acids Research* **2014**, *42* (5), 3207–3217. DOI: 10.1093/nar/gkt1220.
(244) Hoffman, E. P.; Brown, R. H.; Kunkel, L. M. Dystrophin - the Protein Product of the Duchenne Muscular-Dystrophy Locus. *Cell* **1987**, *51* (6), 919–928. DOI: Doi 10.1016/0092-8674(87)90579-4.
(245) Muntoni, F.; Strong, P. N. Transcription of the Dystrophin Gene in Duchenne Muscular-Dystrophy Muscle. *Febs Letters* **1989**, *252* (1-2), 95–98. DOI: Doi 10.1016/0014-5793(89)80896-8.
(246) Tennyson, C. N.; Shi, Q. W.; Worton, R. G. Stability of the human dystrophin transcript in muscle. *Nucleic Acids Research* **1996**, *24* (15), 3059–3064. DOI: DOI 10.1093/nar/24.15.3059.
(247) Hildyard, J. C. W.; Rawson, F.; Wells, D. J.; Piercy, R. J. Multiplex hybridization within a single transcript: RNAscope reveals dystrophin mRNA dynamics. *Plos One* **2020**, *15* (9). DOI: ARTN e0239467 10.1371/journal.pone.0239467.

(248) Livak, K. J.; Schmittgen, T. D. Analysis of relative gene expression data using real-time quantitative PCR and the 2(-Delta Delta C(T)) Method. *Methods* **2001**, *25* (4), 402–408. DOI: 10.1006/meth.2001.1262.
(249) Manoharan, M. Oligonucleotide conjugates as potential antisense drugs with improved uptake, biodistribution, targeted delivery, and mechanism of action. *Antisense Nucleic Acid Drug Dev* **2002**, *12* (2), 103–128. DOI: 10.1089/108729002760070849.
(250) Zharkov, T. D.; Markov, O. V.; Zhukov, S. A.; Khodyreva, S. N.; Kupryushkin, M. S. Influence of Combinations of Lipophilic and Phosphate Backbone Modifications on Cellular Uptake of Modified Oligonucleotides. *Molecules* **2024**, *29* (2). DOI: 10.3390/molecules29020452.
(251) Löschberger, A.; Niehörster, T.; Sauer, M. Click chemistry for the conservation of cellular structures and fluorescent proteins: ClickOx. *Biotechnol J* **2014**, *9* (5), 693–697. DOI: 10.1002/biot.201400026.
(252) Uttamapinant, C.; Tangpeerachaikul, A.; Grecian, S.; Clarke, S.; Singh, U.; Slade, P.; Gee, K. R.; Ting, A. Y. Fast, Cell-Compatible Click Chemistry with Copper-Chelating Azides for Biomolecular Labeling. *Angew Chem Int Edit* **2012**, *51* (24), 5852–5856. DOI: 10.1002/anie.201108181.
(253) Cappella, P.; Gasparri, F.; Pulici, M.; Moll, J. A novel method based on click chemistry, which overcomes limitations of cell cycle analysis by classical determination of BrdU incorporation, allowing multiplex antibody staining. *Cytom Part A* **2008**, *73a* (7), 626–636. DOI: 10.1002/cyto.a.20582.
(254) Jao, C. Y.; Salic, A. Exploring RNA transcription and turnover in vivo by using click chemistry. *Proc Natl Acad Sci U S A* **2008**, *105* (41), 15779–15784. DOI: 10.1073/pnas.0808480105.
(255) Cañeque, T.; Müller, S.; Rodriguez, R. Visualizing biologically active small molecules in cells using click chemistry. *Nat Rev Chem* **2018**, *2* (9), 202–215. DOI: 10.1038/s41570-018-0030-x.
(256) Zhang, C.; Dai, P.; Vinogradov, A. A.; Gates, Z. P.; Pentelute, B. L. Site-Selective Cysteine-Cyclooctyne Conjugation. *Angew Chem Int Edit* **2018**, *57* (22), 6459–6463. DOI: 10.1002/anie.201800860.
(257) Ando, T.; Takamori, Y.; Yokoyama, T.; Yamamoto, M.; Kawakami, T. Directed evolution of dibenzocyclooctyne-reactive peptide tags for protein labeling. *Biochem Bioph Res Co* **2021**, *534*, 27–33. DOI: 10.1016/j.bbrc.2020.12.002.
(258) Stirling, D. R.; Swain-Bowden, M. J.; Lucas, A. M.; Carpenter, A. E.; Cimini, B. A.; Goodman, A. CellProfiler 4: improvements in speed, utility and usability. *BMC Bioinformatics* **2021**, *22* (1), 433. DOI: 10.1186/s12859-021-04344-9.
(259) *CellTracker™ Fluorescent Probes*. Thermo Fisher Scientific, 2025. https://www.thermofisher.com/order/catalog/product/C34565.